School of Civil and Mechanical Engineering

Department of Civil Engineering

Low Calcium Fly Ash Based Geopolymer Concrete: Long Term Durability Properties

Didar Singh Cheema

This thesis is presented for the Degree of
Doctor of Philosophy
of
Curtin University

December 2014

DECLARATION

To the best of knowledge and beliefs this thesis contains no material published previously by any other person except where due acknowledge has been made.

This thesis contains no material which has been accepted for the award of any other degree or diploma in any university.

Signature:
Didar Singh Cheema
December 2014

ABSTRACT

Geopolymer concrete is a relatively new material, its widespread acceptance is hindered by a lack of its long term durability properties and limited knowledge about its limitations as an alternative to Ordinary Portland Cement (OPC) concrete. The need to reduce the environmental impacts associated with the production of OPC concrete is widely recognised by the cement and concrete industries. Past research has shown that a low calcium fly ash-based geopolymer (LCFG) concrete has good mechanical properties with the potential for a reduced carbon footprint resulting from the zero-cement content. As such it may be a potential construction material as a greener alternative to OPC concrete.

Low calcium fly ash has a typical composition of silicate varying between 48-54% and of aluminate varying between 26-29%. Silica to alumina ratio of low calcium fly ash from Collie Power Plant, Western Australia is approximately close to 2, which normally is the typical Si/Al elemental ratio for geopolymer binder. Geopolymer binder in LCFG concrete is an inorganic material that results from the reaction of source materials rich in silica and alumina and alkaline solution of high alkalinity as a polymeric reaction rather than a calcium- silicate - hydrate (C-H-S) gel structure as found in OPC concrete. Due to the different chemical reaction nature in LCFG concrete, it is likely that its microstructure will be different to OPC concrete.

Very limited research is available in terms of LCFG's long term durability properties. That is, its potential to perform satisfactorily with minimal maintenance over the anticipated design life under environmental actions is unknown. Environmental actions may range from non- aggressive to severe. LCFG concrete was investigated in this research to determine the long term durability properties. Laboratory and field-placed culvert specimens were investigated. Laboratory reinforced samples of size 300mm x 300mm x 120mm in thickness (approximately) depending on the cover to the reinforcement and cylinder specimens of size 100 x 200 mm were prepared. For comparison, OPC concrete samples & specimens of equivalent strength were prepared.

Prior to this research, a feasibility study was undertaken in co-operation with local pre-cast industry in 2007 for the manufacturing of pre-cast LCFG concrete box culverts. The LCFG concrete box culverts of size 1200 x 1200 x 600 mm from the feasibility study together with OPC concrete box culverts of the same specification were used to assess the long term durability properties in aggressive and non-aggressive field environments in this research.

One set of box culvert (comprising of LCFG concrete box culvert and one OPC concrete box culvert) was subjected to severe field environmental exposures and one set was subjected to non- aggressive field environment. Laboratory specimens of both types of concretes were tested for strength before subjecting to simulated severe laboratory exposure mimicking the severe field environmental conditions. The average compressive strength of geopolymer concrete representing was 54MPa. For OPC concrete, the average compressive strength was 55MPa to 58MPa. For an OPC concrete with pore blocking additive, the average compressive strength was 56MPa.

Relevant properties of LCFG reinforced concrete in comparison with OPC reinforced concrete were evaluated from long term durability perspective on the basis of experimental testing in this research. Experimental research program included the set-up of laboratory model simulated to severe field conditions and follow on testing work. The testing work included compressive strength and its regression under environmental action, volume of permeable voids before & after severe exposure of three years, assessment of moisture transport process & its porosity (capillary suction, absorption, permeation & diffusion), assessment of microstructure & pore structure (using 3-D micro-tomography technique), assessment of chloride ingress mainly responsible for the corrosion of embedded steel (using NT Build 443 diffusion & chloride profile testing) and the assessment of pH & carbonation. Electrochemical testing work included – concrete resistivity, half cell potential, corrosion current density and corrosion rate for the concomitant integrity of the embedded steel using electrochemical techniques (Wenner Probe, Half Cell Potential and Galvanostatic Pulse & silicate passivation measurement techniques) in this research.

Various properties that were investigated in this research as detailed above assisted in understanding the factors and processes deteriorating LCFG concrete and its resistance to deterioration compared to OPC concrete.

An evaluation of majority of the properties under severe environmental exposure indicated that LCFG concrete possible applications may be limited to non –aggressive to mild environmental exposure scenarios. Test results further assisted in developing the Half Cell Potential criteria and Chloride Threshold criteria appropriate for LCFG concrete. Also low pH environments particularly observed for LCFG concrete under severe exposures scenarios in this research prompted to investigate a modified mix, which should enhance its in-situ applications from ambient curing perspective.

A mix with small proportion of slag was developed and investigated for compressive strength and short term durability properties. This was termed as blended LCFG concrete in this research and showed its suitability for gaining adequate early strength under ambient curing with relatively improved pH values when tested after seawater exposure of one year.

Based on these short term durability properties of blended LCFG concrete investigated in this research, it was concluded that it could be a preferred potential construction material for low risk in-situ applications, such as: dual use path, concrete crash barrier, curtain walls, noise abatement walls and traffic island in –fills. For precast components both LCFG concrete and blended LCFG concrete may be the potential construction material.

ACKNOWLEDGEMENTS

The research work was carried out at the Material Engineering Branch (MEB), Main Roads Western Australia (MRWA) with financial support of the Structural Branch MRWA and in conjunction with the co-operation of local Precast Industry (ROCLA) and Science and Engineering Faculty (Civil) of Curtin University Western Australia as a research and development initiative. This research study acknowledges the support from others, including but not limited to, on a co-operative basis from Department of Imaging and Applied Physics, Western Australian Corrosion Research Group, Department of Chemistry Curtin University, Savcor Finn Pty Ltd , Multi-scale Earth System Dynamics Western Australian Geothermal Centre of Excellence for specialised testing and support from the Australian Road Research Board (ARRB) Victoria, SGS (WA), Fly Ash Australia Pty Ltd, Cockburn Cement and local chemical suppliers (SWIFT, SIGMA).

The research was supervised by Emeritus Professor B Vijay Rangan and Dr Natalie Lloyd. The author acknowledges the consistent guidance and support throughout the research duration of Prof Rangan and Dr Natalie Lloyd. Prof Rangan's and Dr Natalie Lloyd's special efforts in many ways, including their valuable comments and suggestions, were encouraging to achieve the objective of my research work.

The author thanks his colleagues RF Scanlon, Les Marchant, David Harris, Ross Keeley, Firoz Chowdhury and Adam Lim for their support through the research work.

Special thanks are extended to Mike Trew from ROCLA, Dr Liam Halloway from SAVCOR Finn Pty Ltd, Dr Florian Fusseis, Multi-scale Earth System Dynamics Western Australian Geothermal Centre of Excellence, Lomas Capelli from Western Australian Corrosion Research Group & William Rickard from the Department of Imaging and Applied Physics - Curtin University, Dr Ahmad Shayan and Dr Amin Xu from ARRB Victoria, MEB laboratory technical officers Phil Brittan, Chester Gibson, Greg Healy, Curtin University Laboratory Manager Mr. Ashley Hughes, Mr. Robert Cutter & Mr. Michael Ellis and Administrative Manager Ms Dianne Garth and Technical Manager Nhu Nguyen from SGS Western Australia.

Finally and importantly, the author thanks his wife Jaskiranjit Cheema for her patience in many ways and devoted family members – Mona, Satpal, Reshem & Nehaal Gill, Harpreet, Simeran & Arjun Cheema and wonderful support from friends locally & overseas.

List of Publications

Following publications produced during the course of PhD research.

1. **Cheema, DS**., Lloyd, NA., & Rangan, BV., 2008. Durability of Geopolymer Concrete Box Culverts- A Green Alternative, 34th Conference on Our World in Concrete and Structure 09, Singapore
2. **Cheema, DS.** , 2011. Durability of Steel in Geopolymer Concrete, 18th international Corrosion Congress, 2011, Perth, Australia
3. **Cheema, DS**., 2012 Low Calcium Fly Ash Geopolymer Concrete – A Promising Sustainable Alternative for Rigid Concrete Road Furniture, 25th ARRB Conference, Perth Australia
4. **Cheema, DS.**, Lloyd, NA., & Rangan, BV., 2012. **'**Geopolymer Concrete Sustainability Potential', Presented as Poster Paper at Twelfth International Conference on Recent Advances in Concrete Technology and Sustainability Issues, Prague, Czech Republic.
5. **Cheema, DS**. , 2012. **'**Fly Ash-A Greener Construction Material Alternative', International Conference on Advancements in Mechanical and Materials Engineering (AFTMME-2012), Punjab Technical University, Kapurthala Jallandhar, India, Presented Paper.
6. **Cheema, D.S**., Lloyd, NA., 2012. **'**Low Calcium Fly Ash Geopolymer Concrete Sustainability and Durability Potential', First International Conference on concrete Sustainability, 27-29 May, Tokyo, Japan.
7. **Cheema, DS**., Lloyd, NA., 2014.Blended Low Calcium Fly Ash Geopolymer Concrete - Environment Friendly Construction Material, International Conference on Geological and Civil Engineering, Macau. IPVBEE vol, 62(2014) IACSIT Press, Singapore. DOI: 10.7763/IPCBEE.2014. V62.13

NOMENCLATURE AND DEFINITION

Aluminate: A compound containing aluminium and oxygen

Silicate: A compound containing silicon and oxygen

Aluminosilicate: A combined silicate and aluminate also referred as sialate (Poly sialates is with Si/Ai ratio = 1, poly sialate- siloxo is with Si/Al ratio =2 and poly sialate disiloxo is with Si/Al ratio = 3)

Monomer: A molecule that combines with other molecules to form a polymer.

Polymer: A large molecule composed of repeating structural units (monomers).

Polycondensation: A chemical condensation leading to the formation of a polymer by linking together molecules of a monomer and the releasing of water.

Polymerisation: The chemical process by which monomers bond together to form polymers.

Amorphous: Solid substances with no definite geometric internal structure but have definite external form and get destroyed when pulverised.

Zeolites: A group of minerals, typically forming in the vesicles of volcanic rocks as a result of metamorphism, characterized by silicates framework consisting of interlocked tetrahedrons of SiO_4 and AlO_4 linked together by shared oxygen atoms and with highly crystalline microstructure.

C-S-H: Calcium Silicate Hydrate

C-A-S- H: Aluminate substituted Calcium Silicate Hydrate

N-C-A-S- H: Sodium Calcium Aluminate substituted Silicate Hydrate

LCFG Concrete: Low Calcium Fly Ash Geopolymer (LCFG) concrete

OPC Concrete: Ordinary Port land Cement (OPC) concrete/ conventional concrete

G40: Low Calcium Fly Ash Geopolymer (LCFG) concrete laboratory samples & cylinder specimens of 40 MPa average target compressive strength.

G50: Low Calcium Fly Ash Geopolymer (LCFG) concrete laboratory samples & cylinder specimens of 50 MPa average target compressive strength.

S40: Ordinary Portland Cement (OPC) concrete laboratory samples & cylinder specimens of S40 MPa average target compressive strength.

Sx40: Ordinary Portland Cement (OPC) concrete laboratory samples & cylinder specimens of S40 MPa average target compressive strength with pore blocking additive.

S50: Ordinary Portland Cement (OPC) concrete laboratory samples & cylinder specimens of 50 MPa target compressive strength.

LCFG Concrete Box Culvert: LCFG concrete box culvert sample from feasibility study of manufacturing pre-cast LCFG concrete structure component using pre-cast industry plant facilities usually meant for manufacturing pre-cast OPC concrete structure.

OPC Concrete Box Culvert: OPC concrete box culvert from pre-cast industry (ROCLA).

VPV: Volume of Permeable Voids

A: Mass of oven dried sample (g)

B: Mass of surface-dry sample after immersion (g)

C: Mass of surface-dry sample after immersion and boiling (g)

D: Apparent mass of sample in water after immersion and boiling (g)

P: Density of water = $1g/cm^3$

C_{cr}/C_{th}: The chloride threshold limit for different exposures.

C_0: The background chloride concentration of concrete matrix, assumed as 0-0.005% by weight of concrete.

Cs: Concrete surface chloride concentration.

C_b: Concrete bound chloride

C_f: Concrete free chloride

Erfc: The complementary error function.

D_{ap}: Apparent diffusion coefficient (m^2/s). Derived from total soluble salts.

D_{ap0}: The diffusion measurement at some known reference time 't_0.

m: An index quantifying the reduction in diffusivity which ranges from 0 signifying constant diffusivity with time, to 1.

D_t: Time dependant diffusion coefficient (m^2/s).

T_{corr}: Corrosion initiation time

σ*: Surface tension (N/M)

r: Pore radius (in voxels). One voxel is 1.3μm.

nm: Nano meter

Isotropy Index: Ratio of pore orthogonal radius

RH: Relative Humidity

HCP: Half Cell Potential in Volts

ρ*: Resistivity in Ohm-m or Ohm-cm or k Ohm.cm

σ: Conductivity (Reciprocal of resistivity)

R: Gas constant R=8.3143 J/(mol*K)

T: Temperature, ^oK

n: Number of electrons transferred

F: Faraday constant F=96500 C/mol (C-coulombs)

pH: Molar concentration of hydrogen ions

I: Current in Ampere

ΔI: Change in Current

Icorr: Corrosion Current

E: Potential in Volt

ΔE: Change in Potential

R: Resistance in Ohm

Rp: Polarisation Resistance in Ohm

RΩ: Ohmic Resistance in Ohm

Rct: Resistance of Charge Transfer at the Interface in Ohm

Rs: Concrete Cover Resistance in Ohm

Cdl: Double Layer Capacitance

E0/Ecorr, Open Circuit: Techniques which does not apply any voltage or current and simply measure the voltage difference between the working electrode and reference electrodes. Used in corrosion applications to determine the state of equilibration between anodic and catholic reaction, also known as E corr.

LPR, Linear Polarisation: Corrosion technique that uses a single voltage scan or ramp programmed from an initial potential to final potential (range generally limited to +/- 20mV vs. open circuit at Ecorr) that progresses at a defined step height per step time. The technique provides capability to calculate the corrosion rate.

Galvanostatic: Corrosion technique that applies a constant current through the working electrode of an electrochemical cell, with potential of the working electrode measured as a function of time relative to the reference electrode. Technique is used to break down the passive film with a constant current.

Potentiostatic: Corrosion technique that applies a constant potential on the working electrode of an electrochemical cell, with the current flowing through the electrode measured as a function of time relative to the reference electrode. Technique is used to break down the passive film with a constant current.

CONTENT

LIST OF FIGURES

List of Tables

APPENDICES:

CHAPTER 1 INTRODUCTION

1 INTRODUCTION

1.1 BACKGROUND

This chapter presents the thesis structure of low calcium fly ash geopolymer (LCFG) concrete for its long term durability properties in combination with severe and non-aggressive environmental exposures.

Source materials for geopolymer are mostly calcined one, rich in silica & alumina. Silica being the second most abundant element on earth is of great interest to engineers, geologists and chemists. In 1978, Davidovits (1988; 1994) discovered its ability to form paste with alkaline solution (Sodium Silicate solution catalysed by Sodium or Potassium Hydroxide solution of different molarity) and coined its polymer structure as 'Geopolymer'.

Geopolymer binder paste can be used similar to Ordinary Portland Cement (OPC) paste, that is, its combination with fine aggregate can be used as a mortar and in combination with both fine and coarse aggregates can be used as a concrete.

Thus LCFG concrete can also be the potential material for the construction of variety of structures associated with roads, buildings & drainage infrastructure similar to OPC concrete.

Geopolymer has wide range of other applications, which may include automobile, aerospace, nonferrous foundries and metallurgy (Davidovits, 2008).

Davidovits (1999) used alkaline activated calcined kaolin (at 750^{o}C for 6 hours) as a source material for making geopolymer binder. Davidovits proposed the following areas of its applications based on elemental ratio of Si to Al of source material, as summarised in Table 1.1 below.

Table 1-1 Geopolymer Source Material Si & Al Elemental Ratio (Davidovits, 1999)

Si/Al	Applications
1	Bricks, ceramics, fire protection
2	Low CO_2 cements, concrete, radioactive & toxic waste encapsulation
3	Heat resistance composites, foundry equipment, fibre glass composites
>3	Sealants for industry
20<Si/Al<35	Fire resistance and heat resistance fibre composites

Follow on research works extended its development using other source materials, such as, low calcium fly ash, slag (Palomo et al, 1999; Fernandez-Jimenez et al, 2003), mine tailings and naturally occurring mineral (Barbosa et al. 2000)). Fly ash being an industrial by-product of coal fired power plants is viewed as the most appropriate material due to its environmental benefits (Hardjito & Rangan, 2005).

Currently OPC (Ordinary Portland Cement) concrete is the prevalent construction material to meet the growing demand of transport, buildings and drainage infrastructure development. Concrete manufacturers are the fourth largest contributors to global carbon emission trailing behind oil, coal and natural gas (Sanjayan, 2012). Continually increasing demand for OPC concrete and its likely impacts on the environments & climate change are in the lime light over a past decade or so. OPC is the dominant source of carbon emission in OPC concrete, which produces approximately one tonne of CO_2 emission with the production of one tonne of OPC (Davidovits, 1994c; McCaffrey, 2002). OPC production constitutes approximately 7% of the global CO_2 emission (Meyer, 2009).

So one way of attaining the long term goal of reducing the negative footprint of OPC concrete is through the minimisation of virgin material and making use of industrial waste by-products (Mehta, 2001 & Mehta, 2002). Fly ash industrial by-product in Australia was approximately 1.46 million tonnes in year 2008 and only 35% of it was in use for various applications (ADAA Statistics, 2009). Chemical composition of various Australian sources producing fly ash (Aynsley et al, 2003) is detailed in Appendix B. The partial use of fly ash from coal fired power plants, ground granulated blast furnace slag from iron ore production and silica fume are already in use as a supplementary cementitious material (SCM) for OPC concrete because of their long track records. SCM use in OPC concrete ameliorates its negative impacts to some extent.

Fly ash being a by- product of coal fired energy production process, its assigned CO_2 emission may be treated as zero. This is because of fact that thermal power plants are not for the production of fly ash, rather are for the production of energy (Sanjayan, 2012). In LCFG concrete fly ash can replace the Ordinary Portland Cement (OPC) in total and can result considerable saving of CO_2 emission, which otherwise will be from the use of Ordinary Portland Cement.

One tonne of LCFG binder is capable of producing 3 m^3 of concrete approximately. Other factors contributing CO_2 emission are generally associated with transport of an alkaline solution, fly ash and its heat curing requirement. According to Davidovits (1994c), resulting CO_2 emission from these operations is in the order of 0 .18 tonne per tonne of geopolymer cement. As such low calcium fly ash based geopolymer (LCFG) concrete on the basis of its low CO_2 emission is attracting a wide spread attention. Reduced carbon foot print is due to its zero cement content.

Past research has reported that LCFG concrete has good engineering properties, which are comparable to OPC concrete or even superior to OPC concrete. That is, it is durable for some aggressive environments such acid, sulphate (Wallah and Rangan, 2006; Bakharev, 2005) and heat (Kong & Sanjayan, 2007). These durable properties of LCFG concrete could potentially be from low calcium content of its fly ash binder. Nevertheless, the composite nature of reinforced concrete poses challenges both for concrete and reinforcement that are subject to separate but interrelated deterioration processes.

Therefore, the integrity of reinforced concrete depends upon the deterioration of either material or both in unison from durability prospective. It is important to know that reinforced LCFG concrete has adequate resistance to deteriorating processes over a long term under environmental actions.

But LCFG concrete being a relatively new material, its dependence on variety of variables influencing the development of its final microstructure and resulting durability needs to be established. These variables may include: composition variability of source material, combined modulus of alkaline solution composition comprising of Sodium Silicate Solution modulus and Sodium Hydroxide solution of different molarity, alkaline solution/fly ash ratio, aggregate/ binder ratio, water to geopolymer solid ratio, mixture constituents and heat curing.

1.2 DETERIORATING PROCESSES & MECHANISMS

Deterioration mechanisms impacting on the durability performance of reinforced concrete structures are broadly associated with harmful soluble salts, which are carried by liquid or gases (transport medium) through concrete interconnected pores setting initiation and propagation of deterioration processes. Chloride ingress, carbonation & sulphate chemical attack are the main deterioration processes, which are responsible for degrading concrete and depassivating its embedded steel from corrosion perspective (Roy, 1986).

Like conventional concrete, the durability of the LCFG concrete is related to its initial microstructure development and the factors controlling its microstructure intactness for eventual durability. While mechanical strength of cementitious material is an indirect indicator of its resistance to degradation, strong materials do not always resist chemical attack and disintegrative forces under certain environmental exposures (Roy, 1986). Thus the development of concrete microstructure and its least deteriorating performance under environmental action reflects its durability (Mehta and Manmohan, 1980; Roy 1986).

From a long term durability perspective of LCFG concrete in comparison with OPC concrete, research information and data in this research will base on laboratory testing and field testing of samples and specimens exposed to severe environments and as well under non- aggressive exposure. This will require the set-up of a laboratory model mimicking the severe field exposure, preparation of samples & specimens and experimental testing as detailed subsequently under the objectives of research.

1.3 RESEARCH OBJECTIVES

The objectives of this research are to study the long term durability properties of low calcium fly ash based geopolymer concrete produced using optimised mix proportion from previous research (Hardjito & Rangan, 2005) under laboratory simulated and field environmental actions (non-aggressive to severe exposure with possible scenarios - buried, immersed and exposed). Parameters supporting the durability of LCFG concrete in comparison with OPC concrete will be assessed , which will include: strength, volume of permeable voids, moisture transport processes, porosity, micro-structural & pore structure properties, diffusion of chloride ions to inner regions, scaling resistance to chemical attack, carbonation, pH and electrochemical properties indicating the stability of embedded steel (concrete resistivity, half cell potential and linear polarisation resistance measured galvano-statically ascertaining the active corrosion and corrosion rate of embedded steel).

To ascertain these parameters in this research, set-up of two parallel experimental set-ups will be aimed at. These experimental set-ups will include selection of field severe environmental exposure to which laboratory exposure will be simulated. Having established these experimental set –ups, follow on aim will be to prepare samples and specimen for both field and laboratory experimental set-ups from LCFG concrete and OPC concrete of equivalent strength grade. The next aim of the research will then be to establish base line properties (such as compressive strength, volume of permeable void, diffusion coefficient and Half Cell Potential- electrochemical property) before exposing these samples and specimen to severe exposure. Having established the base line parameters, monitoring of the durability performance over the research duration of three years will be undertaken. This will include the study of strength reduction trend, qualitative and quantitative visual assessment externally, chloride and salt ingress ability of each type of concrete, moisture transport processes assessment for each type of concrete, passivation status of embedded steel (relying on pH, carbonation and electrochemical properties), volume of permeable voids after three year exposures and finally breaking the samples & specimens to assess the corrosion status of embedded steel visually. Based on the combined analysis of these properties, durability status of the LCFG concrete compared to OPC concrete will be assessed.

Field samples will be pre-cast LCFG concrete box culvert from a previous feasibility study (Siddiqui, 2007; Cheema et al, 2009) along with OPC concrete box culvert of equivalent strength, which will be exposed to severe field environmental exposures in this research. Mix proportions of these LCFG concrete box culverts were also from previous research (Hardjito & Rangan, 2005) and were manufactured using local pre-cast industry (ROCLA) plant facility.

These laboratory & field samples will also be assessed visually and electrochemically for non –aggressive exposure to assess the improved extent of their durable performance.

1.4 SCOPE OF WORK

Therefore to meet the research objectives as detailed above, scope of work of this research included the following activities;

- Selection of field severe model,
- Set-up of laboratory model simulating the selected field severe model,
- Manufacturing laboratory samples and specimens of both LCFG concrete and OPC concrete.

- Exposing laboratory samples and specimens to laboratory simulated model and box culvert samples to field severe exposure and as well to field non –aggressive exposure.
- Monitoring strength regression trend of both type of concrete over three year severe exposure.
- Assessing volume of permeable voids before and after the long term severe exposure of three years.
- Assessment of moisture transport processes (capillary, absorptions, permeation & diffusion) carrying invading agents from the environments and resistance to chemical attack from scaling perspective.
- Assessment of chloride migration to the interior using diffusion coefficient testing.
- Extracting core specimens for micro-structural & pore structure (using 3-D Microtomography), pH & chloride ingress profile testing from laboratory samples and from field box culvert samples
- Assessing electrochemical properties of embedded steel from corrosion perspective together with qualitative visual assessment. The electrochemical properties will include measuring of pH, concrete resistivity, half cell potential, galvano-static pulse measurement based on linear polarisation resistance principle and the assessment of silicate passivation effect to embedded steel in LCFG concrete using SEM, EDX and XRD techniques.

The testing work scoped will characterise the engineering properties from a durability perspective, as an extension to properties of LCFG concrete reported elsewhere (Hardjito & Rangan,2005) and (Wallah and Rangan, 2006).

The source material (low calcium fly ash) for LCFG concrete in this research used was from Collie Power Plant, Western Australia, which was the source for previous research geopolymer mixtures (Hardjito & Rangan, 2005) as well. This was to minimise any adverse impact which may result from the significant variation of chemical composition because of different material source.

Given the variability of source material even from the same source, possible impacts of source material composition's variability from the past research studies (Hardjito & Rangan, 2005 and Olivia, 2011) will be analysed in this research to deduce any new interpretation in line with the test outputs of this research.

1.5 THESIS STRUCTURE

Based on the above detailed work of this research, the thesis is structured as:

Chapter 1 gives the background, objectives and thesis structure.

Chapter 2 presents a review of existing knowledge which informed the mixture design and curing regime adopted. This includes geopolymer chemistry, chemical structure, alkaline solution chemical composition, binder mix synthesis chemistry, LCFG concrete processing techniques and the possible exposures classes from durability perspective in this research.

Chapter 3 presents a literature review of conventional concrete pertaining to deteriorating processes and its durability criteria. These deteriorating processes may affect durability of low calcium fly ash based geopolymer (LCFG) concrete as well and will inform the development of the research methodology to study its long term durability properties.

Chapter 4 presents the specimen preparations of LCFG concrete & OPC concrete and a brief description of experiments and experimental method supporting the informed research methodology from literature review in Chapter 3.

Chapter 5 presents the results of the experimental program on properties of LCFG concrete compared to OPC concrete from durability perspective from variety of experimental results detailed in the scope and LCFG concrete synthesis analysis, interpretation & discussion.

This chapter also cover the assessment of short term durable properties of modified mix as a blended LCFG concrete coupled with the construction suitability requirements of in-situ applications under ambient curing conditions, which prompted from LCFG concrete test outputs in this research.

Chapter 6 presents the source material and alkaline solution composition synthesis analysis, OPC concrete analogy, interpretive results and discussion

Chapter 7 presents the conclusions

Chapter 8 presents the recommendations.

CHAPTER 2 BACKGROUND TO GEOPOLYMER

2 GEOPOLYMER BINDER MIX CONSTITUENTS CHEMISTRY

2.1 INTRODUCTION

This chapter presents the basic understanding of the chemical reactants, reaction products of geopolymer binder responsible for the eventual development of LCFG concrete microstructure and pore structure. This concomitant development of micro structural and pore structure have significant bearing on long term durability properties. While subsequent subsections describe the basic chemistry of these reactants, this chapter also presents the guidance from applicable Australian Standards relevant to concrete class, concrete strength, cover to embedded reinforcement and the environmental exposure category from design life considerations of the concrete structure will be exposed to.

2.1.1 Mineral Structure of Geopolymer Binder Reactants (Silicate)

The earth crustal minerals are mainly a combination of two elements, that is, oxygen and silicon. Silicon together with oxygen is silicon dioxide (silica). Silica when combined with oxides of aluminium, calcium and iron it forms silicate minerals in our rocks and soils (Bergna & Roberts, 2006) and is abundantly available in our earth's crust.

Also because of small size of silicon ion relative to the oxygen ions, the silicon ion fits between four oxygen ions that are arranged like a triangular pyramid as shown in Figure 2.1 below (a- ball and stick model, b- solid tetrahedron, c-skeletal tetrahedron and d- spaced filling model based on packed sphere).

Nearly all of the silicates have structures based on $[SiO_4]^{-4}$ tetrahedron, which is the building block of silica and silicate structure. All form of silica contain Si-O bond, which is the most stable of all Si-X elements bond.

The bond length is about 0.162 nm which is considerably smaller than the sum of covalent radii of silicon and oxygen (0.191 nm). This shorter bond length accounts for partial ionic character of siloxane bond and is responsible for its relatively high stability (Unger, 1979).

Each oxygen atom in a $[SiO_4]^{-4}$tetrahedron has only half of its negative charge satisfied by the Si-O bond (bond strength = 1) and for charge balancing, must bond to other cations.

If oxygen is bonded to two Si atoms, the co-ordination polyhedra of oxygen around those two Si atoms will share corners and the oxygen in common will have its charge fully balanced by the two Si-O bonds.

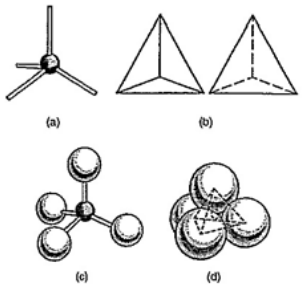

Figure 2-1 - Chemical Structure of Silica (Bergna, H.E., et al. 2006, Page 10)

In practice two different SiO_4 groups may share only one oxygen atom, but any or all four atoms of SiO_4 group may be shared with adjacent groups.

Due to this fact that $[SiO_4]^{-4}$ tetrahedra can share corners and fully balance oxygen charges locally. As such number of silicate structures are possible which can be classified on the basis of their degree of polymerization of the $[SiO_4]^{-4}$ tetrahedra.

Sharing of two oxygen per unit yields chain, three atoms a sheet and four atoms a three dimensional (3D) network (Gould, 1957). Familiarity of the crystalline structure of silica helps in understanding the bulk and surface structure of amorphous silica. Natural silica can be crystalline as in quartz, cristobalite, tridymite, coesite and stishovite or amorphous as in opal (Bergna, et al. 2006).

Similar to three-dimensional crystalline zeolite formation based on aluminosilicate framework of inorganic polymers, which requires high pH and concentrated alkali to result amorphous aluminosilicate gel followed by crystallization at high temperature between 100-180 (Ray, 1978 and Bell, 1999), Davidovits developed amorphous to semi- crystalline aluminosilicate inorganic polymer from aluminosilicate source material (metakaolin) comprising of SiO_2 and Al_2O_3 at low temperature and termed it as geopolymer of which reaction product is a polymer incorporating Al, Si and O.

Thus geopolymer binder is chemically different than the hardened OPC, in which the reaction products are calcium silicate hydrate (C-S-H) and calcium hydroxides as detailed in the subsequent section.

2.2 GEOPOLYMER CHEMICAL STRUCTURE

In the early stage of development, Davidovits (1982) synthesised geopolymer using calcined kaolin clay heated at 750^{o}C for 6 hours, known as metakaolin. Metakaolin is a dehydroxylated form of clay mineral (kaolinite) and is naturally available in abundance. An alkali activation of this source material results three- dimensional geopolymer structures in term of polysialates, in which sialate refers to aluminosilicate.

Geopolymerisation that results from the chemical reaction between aluminosilicate and silicate under high alkaline conditions gives polymeric –Si-O-Al-O- bonds (Davidovits 1982; 1991, 1994, 2002). Davidovits (1991) described that several polysialates units are possible for geopolymer resulting from the polymerisation reaction. Common polysialates, which link together via polycondensation to form long polymer chains with final three dimensional microstructure, are as shown below in Figure 2.2.

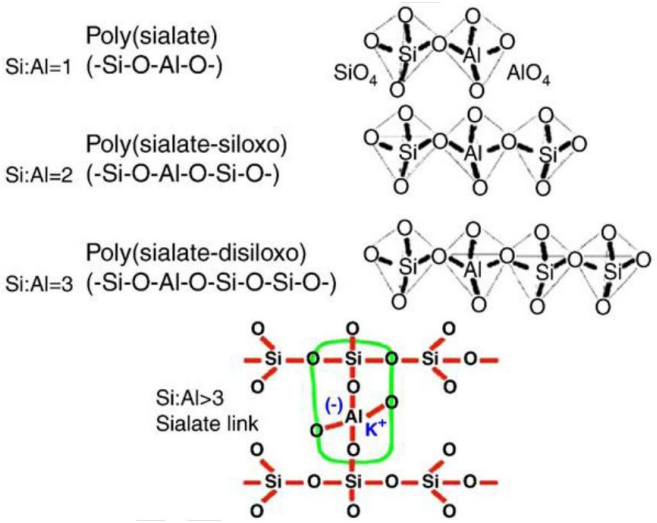

Figure 2-2 Geopolymeric molecular networks (Davidovits 2002)

Polysialate general formula is as below (Davidovits, 1991).

Mn [-(SiO_2) z–AlO_2] n. wH_2O

Where: M = the alkaline element or cation such as potassium, sodium or calcium; the symbol – indicates the presence of a bond, n is the degree of polycondensation or polymerisation; w is ≤ 3 and z is1, 2 or 3 as shown above for geopolymeric molecular network and could be higher up to 32.

Davidovits (1994, 1999) proposed that geopolymer binder being a polymeric reaction of alkaline liquids and source material, can be produced from a material of geological origin (such as reactive clay; metakaolin, neokaolinite, parakaolinite, halloysite and milanite) or by-product material (fly ash, blast furnace slag, mine tailings and rice husk) rich in silicon and the aluminium. So since its inception a wide variety of aluminosilicate mineral source have been utilised to develop environmentally friendly geopolymer binders such as fly ash, slag, pozzolan material and a mixture of metakaolinite by various researchers (Van Jaarsveld & van Deventer, 1999; Palomo et al 1999; Brough & Atkinson, 2002; Barbosa et al. 2000).

An alkaline activated source material produce aluminosilicate and result inorganic polymers known as polysialates in geopolymer. These are comprised of $[SiO_4]^{-4}$ and $[AlO_4]^{-5}$ tetrahedron network linked alternatively and sharing oxygen in common, which give an amorphous or semi crystalline geopolymer structure.

In geopolymer, aluminium tetrahedron $(ALO_4)^{-5}$ in the network being four coordinated with respect to oxygen results negative charge imbalance, which needs to be balanced by the presence of cation in the mix to maintain the neutrality. The charge balancing cations such as Na, K, Ca and Li in the matrix will thus be of value that assists in bringing the reaction neutrality. The source of these charge balancing cations could be either from the feedstock or from alkaline solution used in the synthesisation of geopolymer binder. The tetrahedron network configuration is shown in Figure 2.3 (Davidovits, 2008) below.

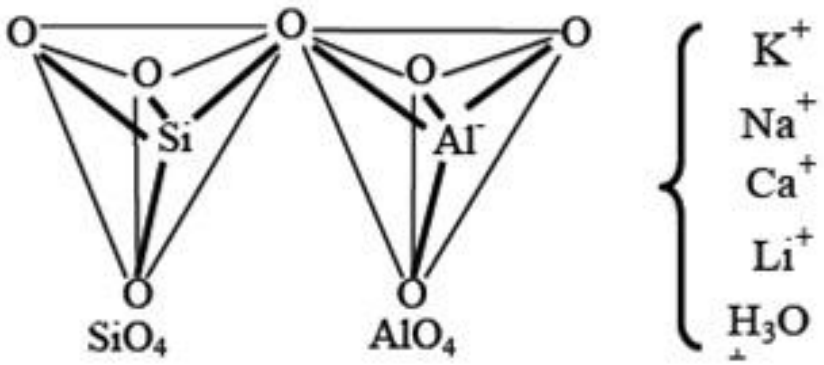

Figure 2-3 Tetrahedron Configuration of Sialate (Davidovits, 2008)

The by-product of geopolymerisation reaction that takes place between alkaline activated aluminium and silicon rich source material is water.

The schematic formation of geopolymer material can be shown as described by Equations (2.1) and (2.2) below (Van Jaarsveld et al, 1997; Davidovits, 1999):

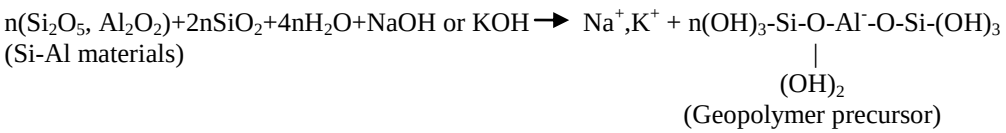

Equation 2.1

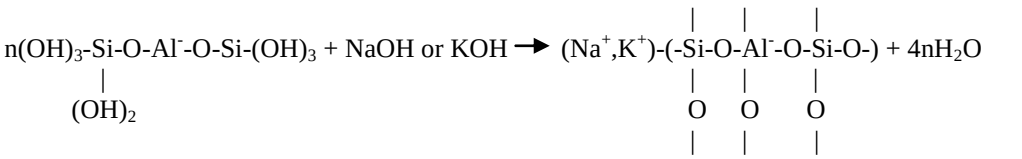

Equation 2.2

Anhydrous sodium silicate contains a chain polymeric anion composed of corner shared (SiO_4) tetrahedra, and not a discrete SiO_3^{2-} ion (Greenwood et al, 1997). Many researchers in the past have attempted to describe its possible phases of reactants during the chemical reaction (Fernandez-Jimenez et al, 2005; Duxson et al, 2007; Jo et al, 2007) and its final three dimensional geopolymer structure, which has properties similar to OPC binder. Reference in the literature also points its final structure as two - up - three dimensional (Skvara et al, 2006).

In an alkaline solution aluminosilicate undergo dissolution and polycondensation to form inorganic polymer (Sofi et al, 2007). Progressive research refined the terminology further. Van Deventer et al (2010) redefined boundaries' distinction between inorganic geopolymer and inorganic polymers on the basis of source material nature, alkali activator and final product within the broader spectrum of alkali activated material (AAM).

The schematic distinction of the terminology is shown in Figure 2.4 below. Such as activation of slag by low to mild alkaline solution can also be a sole binder. Alkali activated slag inorganic polymers contain CSH gel structure with lower Ca/Si ratio (7-10) similar to OPC , but not like fly ash based geopolymer which require high alkaline solution (Adam et al, 2009), while source material activated by anhydrous- alkaline as an AAM family as shown in Figure 2.4 below.

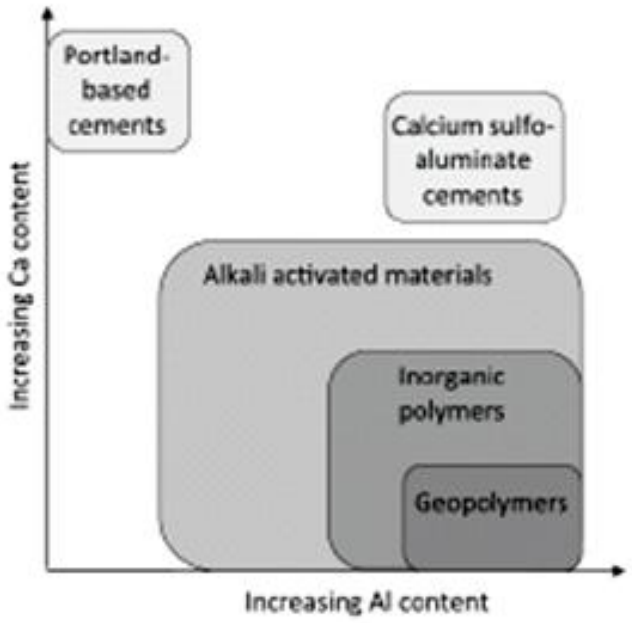

Figure 2-4 Geopolymers and Inorganic Polymer Boundaries in Alkali Activated Materials (Van Deventer Van Deventer et al 2010)

Past research has shown that correctly manufactured heat cured geopolymer concrete performs well with respect to mechanical properties such compressive strength, low creep, drying shrinkage, acid attack (Hardjito & Rangan, 2005) and heat resistant (Kong & Sanjayan, 2007).

So the second most component of geoloymer binder is its alkaline solution components. Following section provides their brief detail.

2.3 ALKALINE COMPONENTS' CHEMISTRY

2.3.1 Soluble Sodium Silicate

There are two different type of manufacturing process for sodium silicate production (Stengel et al, 2009).

One involves the fusion of silica sand and appropriate carbonate at high temperatures (Stengel et al, 2009 and Asrar et al, 1998) in a furnace at 1400^{o}C to produce a water soluble glass. The reaction that takes place in the furnace is given by the equation 2.3 below (Asrar et al, 1998)

$$Me_2CO_3 + x\ SiO_2 \longrightarrow Me_2O\ .\ xSiO_2 + CO_2 \qquad \ldots \text{Equation 2.3}$$

Where, Me is either sodium or potassium and x is the weight ratio.

Sodium silicate has the general chemical formulation of $Na_2O.xSiO_2$, being a mixture of varying proportions of SiO_2 and Na_2O, and it is also known as water glass. Silicate products with weight ratios of silica (SiO_2) to alkali (Na_2O) up to 4.0 approximately can be produced.

The highest practical ratio is about 3.8. The fused glasses are dissolved in water to produce syrupy solutions, with solid contents about 30 to 50 % (Asrar et al, 1998). The SiO_2/Na_2O ratio can be reduced by adding sodium hydroxide and gives a series of liquid products. A wide range of liquid forms are available, with SiO_2:Na_2O ratios from 3.8 to 1.6, and a solid content from about 25 to 55%, or in the low ratio range, a number of solid hydrous or anhydrous materials.

The most common sodium silicate commercial liquid is of weight ratio of silica to alkali (Na_2O) as 3.22 with 37 to 38% solids (Asrar et al, 1998). The term sodium silicate or soluble silicate, or water glass is not explicit enough, because of the variation of its properties over the range of products. So specifying the silicate ratio and its concentration are of significance when looking at its application (Asrar et al, 1998). This process is expected to expend energy 4.58 MJ/kg (Stengel et al, 2009).

The second process is the hydrothermal process, where the sand is dissolved in sodium hydroxide under high pressure and temperature in an autoclave. It is manufactured through the hydrothermal dissolution of silica sand in sodium hydroxide to produce a sodium silicate solution of 48% solid and a weight ratio of 2 (2 parts SiO_2 to 1 part Na_2O). The energy requirement for the production of this hydrothermal liquor is 500 MJ per tonne of output (Fawer, 1999) or 0.5MJ/kg. This is significantly lower than OPC production, which requires about 4,400 MJ per tonne (International Energy Agency, 2007).

Sodium silicate manufacturing process by infusion process as detailed above is more energy intensive than OPC production/ tonne. However by hydrothermal process sodium silicate production requires lower energy, that is, almost 9 times less than OPC. Secondly its usage in LCFG concrete equates to about 10-12% of OPC per cubic metre of concrete, as such resulting LCFG concrete is still offers a considerable saving on CO_2 emission (Cheema & Llyod, 2014).

Sodium silicate solution of A53 grade with SiO_2/Na_2O ratio of 2 (also called silica modulus) has been used in this research study has been sourced from a commercial supplier in Australia. Its chemical composition was; SiO_2 = 29.4% , Na_2O = 14.7% and H_2O = 55.9% by mass.

2.3.2 Sodium Hydroxide

Sodium hydroxide is produced from the chloro-alkali process which is an electrolysis process of salt water producing both Sodium hydroxide and chlorine gas (Sanjayan, 2012). Sodium hydroxide in alkaline solution act as an activator in the synthesisation of LCFG concrete binder with its molar concentration ranging between 8 M to 16M. Usage of NaOH solid in LCFG concrete is about 3% of OPC per cubic metre of concrete and due to this meagre component, its component of CO_2 emission is very insignificant (Cheema & Llyod 2014).

Sodium hydroxide (NaOH) of technical grade of purity 98% in flake form obtained from commercial supplier in Australia was used in the alkaline solution, which comprised of 26.2% by mass and 68.6% water (Hardjito & Rangan, 2005) for 8M concentration. Because of significantly lower solid proportion of alkaline solution in LCFG concrete per cubic metre compared to OPC proportion for one cubic metre of conventional concrete, CO_2 emission associated with combined alkaline solution for one cubic metre of LCFG concrete will be substantially lower than one cubic metre of conventional OPC concrete. Although some researchers refer that the environmental benefits of CO_2 emission saving with LCFG concrete is not great compared to OPC concrete (Stengel et al, 2009; McLellan et al, 2011; Habert et al, 2011).

2.4 LCFG CONCRETE MIX CONSTITUENTS & MIX PROPORTIONS

LCFG concrete mechanical properties, being similar to OPC concrete, that is, its plain and reinforced one may have the potential like OPC plain and reinforced concrete for non-structural and structural purpose. LCFG concrete mixture parameters used in this research are on the basis of past research (Hardjito & Rangan, 2005) as detailed in the following sub-sections.

2.4.1 Mix Synthesising Parameters Background

Hardjito and Rangan (2005) found that Na_2O/SiO_2 mix molar ratios are not workable for low calcium fly ash source material (ASTM Class-F), as developed for calcined kaolin source material.

Using calcined kaolin as source material Davidovits (1982) proposed the alkaline oxide mix molar ratios' range as $0.2 < Na_2O/SiO_2 < 0.28$ (Barbosa et al, 2000 optimised this Na_2O/SiO_2 mix molar ratio to 0.25) and SiO_2/Al_2O_3 oxide mix molar ratio between 3.5-4.5.

According to Hardjito & Rangan (2005) research suitable Na_2O/SiO_2 mix molar ratio for low calcium fly ash source material ranges between 0.098 - 0.120. This Na_2O/SiO_2 mix molar ratio in Hardjito & Rangan (2005) research was from source material composition represented by Batch 1 of low calcium fly ash out of three batches in their research. Respective composition of these batches is detailed in the subsequent section.

Batch 1 resulted constant value of SiO_2/Al_2O_3 mix molar ratio, which was 3.89. This SiO_2/Al_2O_3 mix molar ratio was close to the upper value optimised by Sagoe-Crentsil and Brown (2006) research, which showed the SiO_2/Al_2O_3 mix molar ratio range as 3.5-3.8.

Hardjito & Rangan (2005) research showed the impact of H_2O/Na_2O mix molar ratio (which varied between 10-12.5) on compressive strength and further stated that as long as Na_2O/SiO_2 mix molar ratio is kept constant by using different molarity NaOH & extra water content, the compressive strength remains unaffected. This was shown by maintaining the constant value of Na_2O/SiO_2 mix molar ratio as 0.115.

From Hardjito & Rangan (2005) research, these oxides' mix molar ratios parameters were as below using Batch 1 composition (as summarised in Table 2.1 below) of a source material from Collie Power Plant, Western Australia.

- Na_2O/SiO_2 - 0.098-0.115
- SiO_2/Al_2O_3 - 3.89
- H_2O/Na_2O - 10-12.5

Low calcium fly ash material being from the same source, its mix synthesisation parameters in term of oxides' mix molar ratios resulting LCFG concrete are assumed to be repeatable In this research.

2.4.2 LCFG Concrete Mix Constituents Composition and Proportions of this Research Study

- *Fly Ash*

Table 2.1 below summarises the composition of low calcium fly ash from Collie Power Station in the past research studies. Batches 1 to 3 were from Hardjito & Rangan, (2005) and batch 4-5 were from Olivia (2011).

Table 2-1 Fly Ash Components as determined by XRF (mass %)

Oxides	Batch 1 (1)	Batch 2 (1)	Batch 3 (1)	Batch 4 (2)	Batch 5 (2)
SiO_2	53.36	47.80	48.00	50.20	50.50
Al_2O_3	26.49	24.40	29.00	26.30	26.57
Fe_2O_3	10.86	17.40	12.70	14.40	13.77
CaO	1.34	2.42	1.78	2.27	2.13
Na_2O	0.37	0.31	0.39	0.36	0.45
K_2O	0.80	0.55	0.55	0.58	0.77
TiO_2	1.47	1.33	1.67	1.67	1.67
MgO	0.77	1.19	0.89	1.48	1.54
P_2O_5	1.43	2	1.69	1.57	1.00
SO_3	1.70	0.29	0.50	0.32	0.41
ZrO_2	-	-	0.06	-	-
Cr	-	0.01	0.016	-	-
MnO	-	0.12	0.06	-	-
*LOI (3)	1.39	1.10	0.61	0.58	0.60

Note s: (1)- Chemical Composition of Fly Ash Batch 1 to 3 (Hardjito & Rangan, 2005)

(2)- Batch 4 & 5 (Olivia, 2011)

(3)- Loss on Ignition

For optimal geopolymer binding 80-90% passing 45µm may be required (Fernandez-Jimenez, et al 2005). Australian Standards (AS 3582) requires 75% passing 45µm. Figure 2.5 shows the SEM image of fly ash from Collie Power Plant. Fly ash particular size distribution analysis is included in Appendix B.

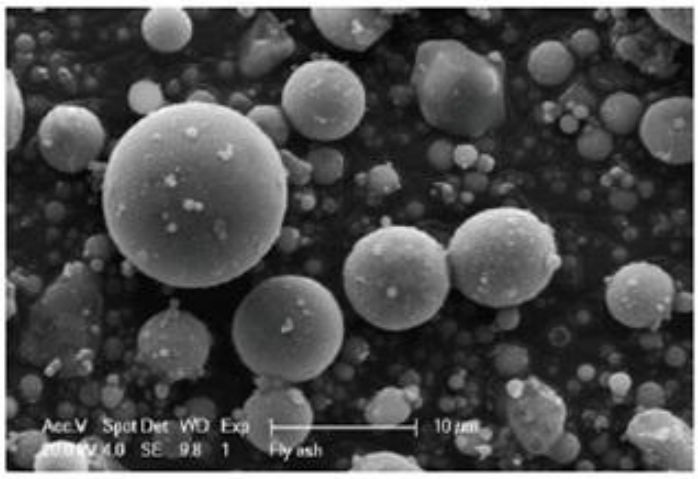

Figure 2-5 Collie Fly Ash Particles (Temuujin et al, 2009)

The particular size, CaO and glassy phase content of the source material influence the final geopolymer product. Finer particles and high content of glassy phase increase the reaction activity resulting higher degree of polymerisation and higher compressive strength (Diaz et al, 2010) and consequential micro-structural properties. Low calcium fly ash is the main component of LCFG concrete and its ratio with reference to alkaline solution was kept as 0.35 (alkaline solution/Fly ash) in this research. This was on the basis of Hardjito & Rangan (2005) research findings.

The past research has shown that fly ash from various sources has different mineralogy and solubility affecting the ability of fly ash to react in the geopolymer mixture. The material from the same source may give different results because of variability in the mineral content (Van Jaarsveld *et al*, 2002). Geopolymer concrete mixture compositional parameters and manufacturing processes can result its variable performance (Duxson et al, 2005 & 2007; van Deventer et al, 2007 & 2012; Stevenson & Sagoe-Crentsil, 2005a & 2005b).

Other factors: alkaline modulus, alkaline oxide mix molar ratio translating to water/geopolymer solid ratio (Hardjito & Rangan, 2005) and curing temperature regimes influence the formation of final structure. Given the variability of the source material composition as summarised in Table 2.1 above, Batch 1 composition has been assumed as the base composition from analysis perspective in this research and from consistency perspective with Hardjito & Rangan (2005) research findings. Final mixture designs' compositions are detailed in Chapter 4 (Section 4.3).

Also possible impacts of fly ash composition variability from Collie Power Plant in the past research have been analysed in Chapter 6 (Section 6.1) on mix molar ratios and their influence on microstructure.

- *Sodium Silicate Alkaline Solution*

As detailed in Section 2.3.1, the second most constituent of LCFG concrete binder is alkaline solution, which is comprised of sodium silicate solution of modulus 2 and NaOH solution of 8M for 40MPa and 14 M molarity for 50MPa geopolymer concrete samples and specimens. The mix proportion of alkaline solution in this research was 2.5 (Na_2SiO_3/ NaOH ratio) and was in line with previous research (Hardjito & Rangan, 2005).

- *Fine and coarse aggregate*

This is the third most component of the LCFG concrete. It was 77% (Hardjito & Rangan, 2005) of the entire mixture by mass resulting binder aggregate ratio of 3.35.

- *Super plasticiser*

Super plasticiser (sulphonated – naphthalene based) at the rate of 1.5% of fly ash by mass used in this research was also as per Hardjito & Rangan (2005) research findings.

Table 2.2 below summarise the main salient features of OPC concrete and LCFG concrete chemical reaction by which they differ.

Table 2-2 Chemical Reaction of OPC Concrete and LCFG Concrete

OPC Concrete Mix Reaction	**LCFG Concrete Mix Reaction**
Binder Typical Composition: Silica(SiO_2) – 17-25% Alumina (Al_2O_3) – 3-8% Sodium Oxide(Na_2O) – 0.5-1.3 Iron Oxide(Fe_2O_3) – 3-8% Calcium Oxide (CaO) – 60-67% **Reactant**- Water **Catalyst**- None **De-catalysing agent** - Gypsum ($CaSO_3$) **Reaction Products:** Calcium Silicate Hydrate (CSH) gel + Free Lime [CaO.2 SiO_2.H_2O + $Ca(OH)_2$], Calcium Aluminate Hydrate (CaO.2 Al_2O_3.H_2O) causing early setting and Ettringite Needles – (C_3A+ Gypsum), which further converts into monosulphate and hexagonal solid plate solution (C_4AH_{13}).	Binder Typical Composition: Silica(SiO_2) – 60% Alumina (Al_2O_3) – 30% Sodium Oxide(Na_2O) – 0.1-1 Iron Oxide(Fe_2O_3) – 5% Calcium Oxide (CaO) – 2% **Reactant** - Alkaline Solution [Sodium Silicate Solution + (Sodium Hydroxide flake+ water) + water as required] **Catalyst** – Sodium Hydroxide **Reaction Products**: Poly sialate(Si-O-Al-O) with Si:Al=1 or Poly sialate – silixo (-Si-O-Al-O-Si-O-) with Si:Al=2 or Poly sialate – disilixo(-Si-O-Al-O-Si-O- Si-O-) with Si:Al=3 and water as a by-product. The generalised formula of poly sialate is as Mn [-(SiO2) z–AlO2] n . wH_2O (Davidovits, 1991) Alkalinity of alkaline solution depletes as the reaction proceeds which involve partial dissolution of silica & aluminates species of source material, a charging balancing of aluminate and polycondensation of above reaction products. The multiple gel formation phases produced during the polycondensation of aluminosilicate get denser and denser expelling by- product water as result of the reaction.
Alkalinity: Free lime produced is the source of high alkalinity in OPC concrete, secondly form impermeable calcium silicate and calcium aluminate hydrate with or without pozzolanic material and hydrates over a longer period. Reaction is exothermic.	**Alkalinity:** Alkalinity depletes due to the nature of the chemical reaction in LCFG concrete and is not compensated due to limited CaO source material constituent in LCFG concrete. Reaction is exothermic with no adverse impact on compressive strength.
Water: Water present comprised of non-evaporative and evaporative components.	**Water**: water present is free water, which is subject to evaporation.
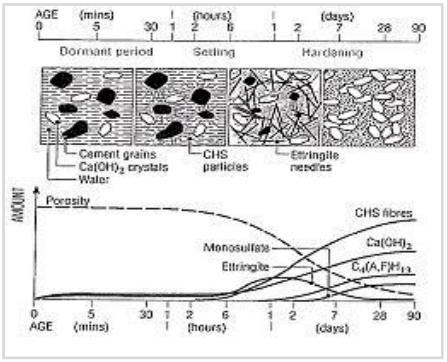 Source: C&CAA, 1994	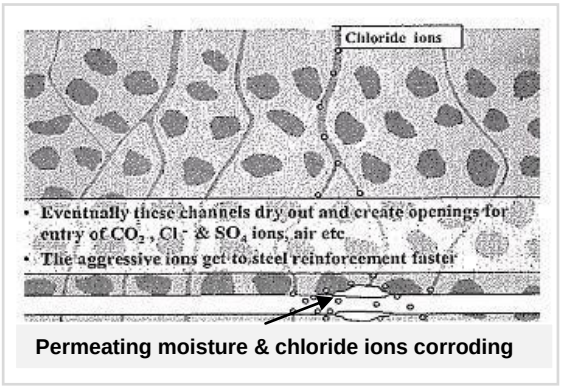 Source: www.cementandconcrete.com
Hydration Products: Hydration over longer period approximately up to a year or so results discontinuous pore structure with decreased porosity. **Strength:** Target strength gain period is 28days and require at least 7 -14 days wet curing in majority of scenarios or its equivalent curing method.	Pore blocking process resulting discontinuous pore structure is unknown in LCFG concrete yet. **Strength:** Target strength gain period is 24 hours and require heat curing at 60 ^oC or above either by steam or by oven dry heat unless some reagent is used in the mix to offset the heat curing requirements.

Environmental exposure class relative to the concrete strength and reinforcement cover requirement are described in the subsequent section. These are based on relevant Australian Standards from durability perspective and are as guiding principles.

2.5 ENVIRONMENTAL EXPOSURE CONDITIONS & CONCRETE REQUIREMENTS AS PER AUSTRALIAN STANDARDS (AS)

For long term durability study as detailed in the research objectives (Section 1.3), laboratory samples & cylinder specimen prepared under this research and LCFG concrete box culvert samples from the previous feasibility study were to be exposed to environmental conditions of severe and non-aggressive nature. Field and laboratory simulated severe exposure scenario and as well non –aggressive field scenario are detailed in Chapter 4 (Section 4.2).

Relevant Australian Standards providing guidance on environmental exposure class, compatible requirements of concrete strength and concrete cover to the reinforcement are AS3600-2009, 2159-2009, 5100-2004 and 3735-2001. Following tables extracted from these common applicable Australian Standards for concrete structures detail the severity class of these environmental scenarios.

Applicable Australian Standard including attached conditions imply an indicative minimum requirements of concrete strength and cover to the reinforcement for OPC concrete that will be able to meet the specified durability requirements over the design life of the structure under listed environmental exposure scenarios. Each Australian Standard (AS) however has minor distinctions in defining their applicable terms for concrete structures.

For example, AS 2159 -2009 provides sulphates, pH and chloride content criteria similar to AS 3735, however it does not use the exposure designations as A, B & C. AS 3600-2009 does not state the exposure class based on chloride content. For guidance on such exposure class (designated as U) it refers to AS 3735.

So Tables 2.3 to 2.13 are included in this research thesis. These tables summarise the requirement of concrete strength and reinforcement covers suiting to specific exposure class for guidance purpose from durability perspective. The bracketed number of these tables is from relevant Australian Standards.

2.5.1 Environmental Exposure Classifications

Following Tables (2.3 to 2.7) from Australian Standards summarise the possible environmental exposure class as per AS 3600-09 (Concrete Structures) & AS2159-09 - Pile Foundations.

AS 3600-09 (Concrete Structures)

- Surfaces of members in water

Table 2-3 Environmental Exposure Class (Table 4.3)

Exposure Conditions	Exposure Classification
Fresh Water	B1
Sea water- Submerged	B2
In Spray Zone (1m above the wave crest level)	C1
Sea water – Tidal/Splash Zone (1m above lowest astronomical tide (LAT) 1m below highest astronomical tide (HAT)	C2
In soft or running water	U

- Surfaces of members in exterior environments above ground.

Table 2-4 Environmental Exposure Class (Table 4.3)

Exposure Conditions	Exposure Classification
Near- coastal (1-50km) any climatic zone	B1
Coastal (up to 1km from coast line) any climatic zone	B2

- Surfaces of members in ground and groundwater

Table 2-5 Environmental Exposure Class (Table 4.8.1)

Exposure Conditions				Exposure Classification	
Sulphate (expressed as SO_4^*)		pH	Chlorides in groundwater ppm*	Soil Conditions A	Soil Conditions B
In Soil ppm	In groundwater ppm				
<5000	<1000	>5.5	<6000	A2	A1
5000-10000	1000-3000	4.5-5.5	6000-12000	B1	A2
10000-20000	3000-10000	4-4.5	12000-30000	B2	B1
>20000	>10000	<4	>30000	C	B2

* Approximately 100ppm of SO_4 = 80ppm of SO_3

A High permeability soils (e.g. sands and gravels) which are in ground water

B Low permeability soils (e.g. silts and clay) or all soils above groundwater.

* For chloride in groundwater it requires reference to AS 2159 & 3735

SR type cement is recommended for B1, B2, C1 or C2 and Protective coating for B2, or C1 or C2 in acid sulphate soils (ASS).

AS2159-09 - Pile Foundations

Table 2-6 Environmental Exposure Class (Table 6.4.2-A)

Exposure Conditions	Exposure Classification
Sea water- Submerged	Moderate
Sea water – Tidal/Splash Zone	Severe
Fresh water	Mild

Table 2-7 Environmental Exposure Class (Table 6.4.2(c) Exposure Classification for concrete Piles-Piles in Soil)

Exposure Conditions				Exposure Classification	
Sulphate (expressed as SO_4^*)		pH	Chlorides in groundwater ppm	Soil Conditions A (Soil High Permeability)	Soil Conditions B(Soil Low Permeability)
In Soil ppm	In groundwater ppm				
<5000	<1000	>5.5	<6000	Mild	Non-Aggressive
5000-10000	1000-3000	4.5-5.5	6000-12000	Moderate	Mild
10000-20000	3000-10000	4-4.5	12000-30000	Severe	Moderate
>20000	>10000	<4	>30000	Very Severe	Severe

* Approximately 100ppm of SO_4 = 80ppm of SO_3

A High permeability soils (e.g. sands and gravels) which are in ground water

B Low permeability soils (e.g. silts and clay) or all soils above groundwater.

AS 5100-2004 specifies the same exposure classification as AS3600-09 with the exception that *it designates exposure class as A &C* which are A1 &A2 and C1 & C2 in AS3600-2009. In addition it specifies 100 years design life criteria while does not specify soil and groundwater conditions regarding which it refers to other ASs.

2.5.2 Reinforcement Cover Requirement from Corrosion Protection

Following Tables (2.8- 2.13) summarise reinforcement cover requirements for various exposure class, concrete strength and design life of the structure.

AS 2159 -2009 has provisions of both 50 years and 100 years design life but for 50 years design life criteria, it specifies concrete for precast and prestressed components not below 50MPa and minimum cover requirement for steel as detailed in Table 2.8 below in blue.

Table 2-8 Reinforcement Cover and Exposure Classification (Concrete Strength and Reinforcement Cover in Piles (Table 6.4.3)

Exposure Classification	Min Concrete Strength(fc') MPa		Min Cover to reinforcement, mm			
	Precast & Prestressed	Cast in Place	50 Year Design Life		100 year Design Life	
			Precast & Prestressed	Cast in Place	Precast & Prestressed	Cast in Place
Non-Aggressive	50	25*	20	45	25	65
Mild	50	32	20	60	30	75
Moderate	50	40	25	65	40	85
Severe	50	50	40	70	50	100
Very Severe	>50	>50	40	75	50	120

* For reinforced piles fc' = 32MPa minimum

1 coating for very severe condition

2 fc' to be specified at age greater than 28 days where concrete contains SCM.

3 Precast pile has cover limits – excessive cover will lead to spalling during pile driving.

Table 2.9 to 2.10 below summarise the minimum cover requirements as per AS3600-2009 – Concrete Structures

Table 2-9 Reinforcement Cover and Exposure Classification (Table 4.10.3.2)

Exposure Classification	*Required Cover , mm				
	Characteristic Strength (fc')				
	20MPa	25MPa	32MPa	40MPa	≥50MPa
A1	20	20	20	20	20
A2	(50)	30	25	20	20
B1		(60)	40	30	25
B2			(65)	45	35
C1				(70)	50
C2					65

*Required Cover where standard formwork and compaction are used

Table 2-10 Reinforcement Cover and Exposure Classification (Table 4.10.3 B)

Exposure Classification	*Required Cover , mm				
	Characteristic Strength (fc')				
	20MPa	25MPa	32MPa	40MPa	≥50MPa
A1	20	20	20	20	20
A2	(45)	30	20	20	20
B1		(45)	30	25	20
B2			(50)	35	25
C1				(60)	45
C2					60

*Nominal Cover where repetitive procedures and intense compaction or self-compacting concrete are used in rigid formwork

In Table 2.9 and 2.10 above, cover thickness in brackets are the appropriate minimum cover when concession given in Clause 4.3.2 relating to the strength grade for particular exposure classification, is applied. AS 3600-2009 specifies design the life as 50 ± 20% with required cover for steel as per AS- Table 4.10.3(B) above where rigid formwork and intense compaction are used. It specifies the use of 40MPa concrete with 35mm cover for B2 (moderate exposure condition) and 60mm cover for C1 (severe exposure condition). *Both AS2159 and 3600 require strength and slightly varying cover requirements for 50 years design life.*

- AS5100.5-04 Bridge Design

Table 2-11 Reinforcement Cover and Exposure Classification (Table 4.10.3 A)

Exposure Classification	*Required Cover, mm			
	Characteristics Strength (fc')			
	25MPa	32MPa	40MPa	≥50MPa
A1	35	30	25	25
B1		45	35	35
B2			55	45
C				70

*Nominal Cover where standard formwork and compaction are used

Table 2-12 Reinforcement Cover and Exposure Classification (Table 4.10.3 B)

Exposure Classification	*Required Cover, mm			
	Characteristics Strength (fc')			
	25MPa	32MPa	40MPa	≥50MPa
A1	25	25	25	25
B1		35	30	25
B2			45	35
C				50

*Nominal Cover where rigid formwork and intense compaction are used

Where rigid formwork and intense compaction are used, AS 5100 specifies the use of 40MPa concrete with 45mm cover for B2 (moderate exposure condition) and does not specify its application for C (severe exposure condition). This distinction between AS5100 and AS 3600 is that AS5100 specifies 100 years design life criteria, while AS 3600 specifies design life criteria up to 50 years. Cover requirement of 40MPa concrete for B2 conditions in both ASs is not comparable. However AS5100 implies that only 10mm extra cover for

40MPa concrete is required for B2 exposure conditions and 5mm extra cover is required for 50MPa concrete for C exposure conditions to extend the design life to 100 years.

Again both AS2159 (for precast and prestressed component) and AS5100 require slightly different cover requirement for B2 exposure conditions against 100 design life criteria. AS2159 requires 50MPa concrete for all scenarios with minimum 40mm cover to steel for B2 exposure conditions while AS5100 specifies the use of 40MPa with nominal 45mm cover to steel for B2 scenario.

2.5.3 Summary and Adopted Reinforcement Cover in this Research

Table 2.13 provides the summary of exposure class, required strength and cover thickness to the reinforcement for various exposure classes as per AS2159 and AS3600. Required cover thickness in red are the minimum cover requirements as per AS2159 in comparison with AS3600 for 50MPa concrete, while AS 3600 requires 35mm cover for B2 scenario and concessional cover of 60mm for C1 scenario for 40 MPa concrete.

Table 2-13 Reinforcement Cover and Exposure Classification

Exposure Classification				**Required Cover (AS3600)/ Min Cover (AS2159), mm**				
AS2159		**AS3600**		**Characteristic Strength (fc')**				
Soil Type		**Soil Type**		**20 MPa**	**25 MPa**	**32 MPa**	**40 MPa**	**≥50 MPa**
A	**B**	**A**	**B**					
Mild	Non - Aggressive	A2	A1					
Moderate	Moderate	B1	B1				25	20/25
Severe	Severe	B2	B2				35	25/40
Very Severe	Very Severe	C1	C1				(60)	45/40
		C2	C2					60

Analysis of various applicable Australian Standards has shown minor distinctions in their cover requirements to reinforcement as a guide for moderate to severe exposures. So for the purpose of long term durability study of LCFG concrete up to 50 year design life in this research, reinforced laboratory samples were prepared with 25mm, 35mm and 50mm cover for respective concretes of 40MPa and 50MPa. These are detailed in Chapter 4 (Section 4.3). LCFG concrete box culvert samples' cover reinforcement was 25mm as per specifications of the pre- cast industry for small OPC concrete box culvert and was governed by the standard steel mould's size.

CHAPTER 3 LITERATURE REVIEW

3 CONCRETE DURABILITY RELATED LITERATURE

3.1 INTRODUCTION

Very limited literature is available on processes and mechanisms characterising the long term durable properties of LCFG concrete in combination with environmental exposures. The analogous trend of LCFG concrete mechanical properties to OPC concrete suggests that its resistance to degrading deteriorating processes & mechanisms will be analogous too. As such this chapter presents the relevant durability literature review of OPC concrete to understand the validity or applicability of its various durability criteria for LCFG concrete from long term durability perspective. This chapter also presents the pertinent literature review of LCFG concrete available over the past two decades or so to support the findings of this research.

3.1.1 Background

Although the strength of concrete is an indicator of its properties encompassing structural adequacy and durability to some extent, the resistance to chemical attack & physical degradation of cementitious materials is indirectly related to mechanical strength of the material. That is, strong material may not resist chemical attack and disintegrative force from the environmental exposures (non- aggressive to severe). The porosity and pore structure of binder paste have significant roles in controlling the ingress of potential deleterious substances.

As such factors controlling the initial microstructure development of the concrete are strongly related to its eventual durability. The resistance of hardened binder paste to chemical attack and physical degradation is the result of combined effect of micro-structural factors, mechanism of moisture transport processes and environmental exposures conditions (Mehta & Manmohan, 1980; Roy, 1986).

Following sections detail these factors and moisture transport processes to understand how each type of concrete (that is, OPC concrete and LCFG concrete) behaves under such individual or combined effect in this research from comparative aspect.

3.2 DETERIORATION MECHANISMS AFFECTING DURABILITY PROPERTIES

3.2.1 Porosity and Pore Structure of Concrete Matrix

The eventual development of microstructure & pore structure is the major factor in controlling transport processes for the ingress of potentially harmful chemical compounds. The medium for species (chloride ions depassivating the protective layer of reinforcing steel, sulphate ions causing sulphate attack & acid attack and permeating gases - oxygen or CO_2 or H_2S) being transported through porous concrete is water (Roy, 1986). There are several mechanisms by which the chlorides ions can be transported into the concrete (Arup 1983, West & Hime, 1985; Azad, 1999; Hong et al, 2006). Following moisture transport processes support the penetration of deleterious substances into the concrete matrix to result deterioration and underpinning deteriorating mechanisms.

- Capillary flow or Absorption: This allow the suction of flow even against gravity into the structures due to surface tension forces which is increased by the loss of water through evaporation from the surface irrespective of the shape, size, length and tortuosities of capillary pores once the meniscus manifests. Pore connectivity may translocate the capillary moisture in any direction (Andrew Phaedonos, 2008; Cement Concrete Aggregate Australia (CA), 2009- Chloride Resistance of Concrete).
- Permeation: This allows flow under pressure gradient e.g. submerged structures constricting flow, holding water or retaining water (Andrew Phaedonos, 2008 & 2001 and Cement Concrete Aggregate Australia (CA), 2009).
- Diffusion: This allows the liquid, gas (CO_2, O_2, H_2, H_2S etc.) or ions transport due to concentration gradient. Chloride ions' diffusion to the inner region through water filled pathway is predominant where the structure or its components are saturated (Azad, 1999; Hong et al, 2006). Surface concentration, migrated chloride and water-filled pathway are instrumental in the development of concentration gradient for chloride ingress (Browne & Geoghegan, 1985; Tuutti, 1982; Azad, 1999; Andrew Phaedonos, 2008; Cement Concrete Aggregate Australia (CA), 2009).

Partially submerged or exposed structure components are subject to wetting and drying cycles (such as tidal/ splash zones) and are more prone to ingressing agents through absorption resulting from capillary suction (Azad, 1999, Andrew Phaedonos, 2008, CA 2009). Water vapour diffusion associated with drying cycles and differing relative humidity in combination with the drifting air borne contaminants influences the deterioration processes and their rate (Azad, 1999; Andrew Phaedonos, 2008).

So even for non- aggressive or mild scenarios, absorption on account of capillary action is the predominant transport mechanism (Azad, 1999).

Micro-structural characteristics, which develop as a results of chemical reaction of mix constituents (low calcium fly ash rich in silica and alumina activated by alkaline solution in case of LCFG concrete and GP cement with or without supplementary cementitious material (SCM) in case of OPC concrete activated by water) can influence these transport processes.

3.2.1.1 Liquid Phases of OPC Concrete and LCFG Concrete

Past research shows that the water is not consumed in the LCFG concrete chemical reaction, which is one of the major differences from OPC concrete (van Jaarsveld et al, 1997; Davidivits, 1999). In OPC concrete water gets consumed chemically in hydration phase resulting the formation of C-S-H products, which tend to fill up the capillary pores in the fresh paste of OPC concrete (Andrew Phaedonos, 2001). The resulting capillary pores' volume further depends on the water/binder ratio and the degree of hydration. Higher water/binder ratio will result higher capillary pore system supporting the porosity (Andrew Phaedonos, 2001).

In LCFG concrete, the hardened binder paste consists of sodium silicate and aluminosilicate gel, partially or unreacted fly ash silicate and aluminates particles, inert particles and capillary pores system. As the chemical reaction of LCFG concrete releases water as a by - product (Davidovits, 1994; Van Jaarsveld et al,1997) which along with any extra water added in mix synthesisation tend to escape to the surface during curing regime. This escaping process of bulk or free water may result the development of continuous capillary pore systems. Additionally sodium almino-silicate gel in geopolymer reaction may have interconnected interstitial voids as gel pores from water (water molecule size at approximately 4^{o}C is 0.310 nm- Patrick, 2010). These gel pores are also conduits for liquids and gases permeation (Andrew Phaedonos, 2001) and are significantly smaller than capillary pores.

The liquid phases which get developed from polymerisation and polycondensation of geopolymer reaction in combination with environmental actions may influence the hardened LCFG concrete and will be in the following forms:

- Hygroscopic film (single molecule or polymolecular layer of water) attached rigidly to unreacted silica or partially dissolved or polymerised framework in the geopolymer concrete matrix with an immense physical force (Jumikis, 1967).
- Film moisture that is held to the hygroscopic film with a considerable molecular force but not as large as in the case of hygroscopic film. Moisture in this phase is subjected to movement or migration under the application of external energy potential which could be electrical or thermal potential (Jumikis, 1967).
- Free or bulk water which is in excess of the amount of water the LCFG concrete matrix can retain (Jumikis, 1967).

These liquid phases are thus of evaporable and non-evaporable water (Sergi & Panteli, 2011). In OPC concrete the tendency of pore blocking due to hydration products continues over some time during the hardening phase. This aspect of pores' blocking tendency for LCFG concrete during its hardening phases is not known, which may influence the porosity of its matrix on similar line to OPC concrete over an extended period.

The connectivity of larger pores allows the transmission of liquid through the concrete matrix (Roy et al, 1993). However research study by The Pennsylvania State University indicates that finer gel pores do not to contribute to the transport rate of the various species significantly (Roy et al, 1993). The nature of chemical reaction that occurs in LCFG concrete producing by-product water may results concrete matrix of finer pore system of permeating nature, which may be more susceptible to adverse impact of capillary actions.

The absorption effect on account of capillary action gets exasperated where the occurrences of repeated wetting cycles after a prolonged dry spill are not uncommon (Azad, 1999). For partially submerged structure components, the extent of capillary water rise in finer pores' size could be more pronounced (Azad, 1999). Thus the various pore system of concrete (i.e. capillary, gel, air voids and micro crack) if interconnected represent the volume of permeable voids (VPV).

These voids may be comprised of entrapped air void (between 10-500μm), capillary pore (vary between 2nm-10 μm) and gel pore with diameter 1nm or less (Aldridge et al, 2008). The pore structures and the porosity of binder paste for both LCFG concrete and conventional concrete on account of these permeable voids have major control on the ingress of potentially deleterious substances.

The diffusion of ions and the rate of permeation of fluids across the porous cementitious material are related to volume of these pores and the interconnectivity of these pores in moist state (Kumar & Roy, 1986; Azad, 1999; Hong et al, 2006).

Past research studies also mention the use of wide variety of techniques for determining the pore size distribution and pore characteristics of OPC cement pastes (Kumar & Roy, 1986), such as, mercury intrusion porosimetry (MIP) for measuring the pores' number, their sizes and connectivity, which allow permeating fluids and ions through the concrete (Mehta et al 1980, Nyame & Illston, 1980; Kumar & Roy 1986; Li & Roy, 1986). Washburn equation below (Aldred, 2008) provides the relationship of pressure and pore size.

$$P = (-2\sigma.\cos\theta)/r$$

Where:

P = pressure head (m), σ = surface tension (N/M), θ = angle of contact in degree and r = pore radius in (m)

The maxima of function dV/dP on the basis of reciprocal relationship of pressure and pore radius provides the grouping of largest fraction of interconnected pores and their radius in the vicinity of the maxima. These largest fractions of interconnected pores control the transmissivity of the material (Nyame & Illston, 1980; Roy, 1986). So the deterioration processes such as chloride ingress, carbonation, chemical attack (sulphate and acid), alkali aggregate reaction, corrosion of steel reinforcement can be controlled by restricting the movement of moisture in the concrete i.e. by controlling penetrability (Andrew Phaedonos, 2001).

Although moisture transport processes appear same for these both type of concrete, but their manifesting mechanism may not be same, which gets influenced by many factors during reaction, curing & hardening stages. For example, correct mix parameters of LCFG concrete during the initial stages of mixing and mix synthesisation have the potential for denser micro-structural & pore structure development.

Micro-structural & pore structure can play a significant role in restricting such moisture movement coupled with due consideration to environmental exposure scenarios.

In the past studies, Mukhin et al (2007) showed the increasing trend of capillary water rise in LCFG concrete when it is ambiently cured compared to steam cured. Mukhin et al (2007) in their study described ambiently cured sample comprised of initial dry curing at 23^{o}C (time unspecified) followed by wet curing for 28 days at 23^{o}C. Steam cured specimens were for 12 hours at 90 ^{o}C followed by 4 hours cooling.

So above literature formed the basis to assess the respective concrete properties such as porosity, processes supporting moisture transport, microstructure and pore structure from durability aspect.

Tests used to assess these properties in this research included; Volume of Permeable Void (VPV) test, Capillary Pore Suction test, and 3-D Micro-tomography technique. While parameters and results of these tests as detailed in Chapter 5 enabled the assessment of porous characteristics & micro-structural characteristics of LCFG concrete compared to OPC, but from long term durability diffusion has also been investigated in this research using NT Build 443 test. This has been considered as a key indicator. Parameters, assumptions and theoretical background of diffusion based on Fick's Second Law are given in the subsequent section.

3.2.2 Theoretical Background of Diffusion and its Parameters

While majority of the fluid transport processes described in the preceding section (capillary flow, absorption and wicking) characterises the surface layer properties of porous concrete, but their role is significant in carrying the invading chloride & other harmful salts from the environment deeper into the concrete coupled with drying and wetting cycles. Concrete exposed to these cycles of capillary uptake and evaporation induce constant content of chloride, the thickness of which depend upon the severity of the environments, quality of concrete and the location of the concrete structure component (Hong et al, 2006).

Concentration gradient develops as a result of ingressing chloride, derive the chloride ions further to the interior through diffusion. It is the diffusion process which characterises the bulk concrete (Hong et al, 2006) properties from long term durability perspective. This is applicable for both OPC concrete and LCFG concrete, because concrete element extends across the zones (exterior and interior). If the outside chloride concentration is higher than the inside concentration of the concrete then the migration of the chloride ion will happen as a result of concentration gradient through pore water in concrete by diffusion (Azad, 1999; Andrew Phaedonos, 2008).

Therefore diffusion coefficient is considered as the relevant concrete resistance parameter from long term durability perspective. Thus diffusion is one of the most basic transport mechanisms of chloride ingress for reasonably moist conditions and follows the Fick's Second Law of Diffusion (Crank, 1975). Its assumption and theoretical description are briefly detailed as below. The process can be treated as happening in a semi-infinite space assuming the chloride ingress is not affected by the prevailing conditions at the surface. The Fick's Second Law of Diffusion mathematical equation is given by the equation 3.1 as below:

$$dC(x,t)/d\,t = D[d^2\,C(x,t)/d\,x^2] \qquad \text{…. Equation 3.1}$$

Where C(x,t) = concentration, t = time, x = distance from the boundary and D is the diffusion coefficient. The solution to equation 3.1 for a semi-infinite domain with a uniform concentration surface concentration Cs at the surface where x = 0 is given as below (Crank, 1975).

$$C(x,t) = (C_s - C_0)[1-Erf(x/\sqrt{4Dt})] \qquad \text{..... Equation 3.2}$$

Where C(x,t) = the concentration at distance x from the boundary and 'x' denotes the cover (distance in concrete from the diffusion surface) and 't' denotes the time of exposure in seconds and D is the diffusion coefficient in m^2/s. In term of threshold limit this equation is as below.

$$(C_{cr} - C_o)/(C_s - C_o) = erfc\,(x/\sqrt{4Dt}) \qquad \text{…… Equation 3.3}$$

C (0, t) defines the surface concentration (C_s) and C(x, 0) defines the initial chloride concentration in concrete (C_0).

Where:

- C_{cr} is the threshold limit, its indicative values for different exposure are detailed subsequently.
- C_0 is the background chloride concentration inside concrete and is assumed as 0.005% - 0.01% by weight of concrete.
- Cs is the concrete surface chloride concentration.
- Erfc is the complementary error function.

According to Nilsson (1993), diffusion coefficient is a function of the chloride binding capacity. The chloride binding is defined as the ability of a material to bind chloride ions further when the chloride concentration increases, and is denoted by $\partial C_b/\partial C_f$. The diffusion coefficient derived from the total soluble chloride profile accounts for both free and bound chloride and is the apparent diffusion coefficient (D_{ap}) given by expression below.

$$D_{ap} = D_0/ (1+\partial C_b/\partial C_f)$$

Where D_0 is the diffusion coefficient of the free ions. C_b is bound chloride and C_f is the free chloride.

For OPC concrete it has been seen that resistance to the chloride ions is seen to be improved with age according to the simple power function:

$$D_{ap} = D_{ap0} (t_0/t)^m$$

Where D_{ap0} is the diffusion measurement at some known reference time 't_0' and 'm' is the index quantifying the reduction in diffusivity which ranges from 0 signifying constant diffusivity with time, to 1. The implication of this decreasing apparent diffusion (D_{ap}) with time is that prediction based on the above expression at very early age will be overestimated than the real one. Therefore in term of time dependant diffusion coefficient the equation 3.3 will be as.

$$(C_{cr} – C_o)/(C_s-C_o) = \text{erfc} (x/\sqrt{4D_t t}) \quad \ldots\ldots \text{ Equation 3.4}$$

Based on equation 3.4, time required for thresh hold concrete to reach the reinforcement cover level is the corrosion initiation time T_{corr} and is given by the equation 3.5 below (Michael et al, 1999 and Stanish et al, 2003).

$$T_{corr} = x^2/4D_t [\text{erfc}^{-1} (C_{cr} – C_o)/ (C_s-C_o)]^{-2} \quad \ldots\ldots\ldots \text{ Equation 3.5}$$

From above equations, it follows that range of cover thickness that will provide an equivalent design life, further depends on the binder content, assumed or derived Cs value and initial chloride concentration C_o. As such the variables are concrete cover (x), the chloride concentration at the surface (Cs) and the concrete age factor for determining diffusion coefficient, which are equally relevant for LCFG concrete. Diffusion coefficient derived from the free chloride or water soluble chloride profile is effective diffusion (D_e).

The theoretical relationship provides the link between C_0 and D and allows the estimation of diffusion coefficient of free chloride in concrete. Sergi et al (1992) study showed that total and free chloride profiles could be interpolated to good approximation by Flick's Law.

So the mathematical diffusion model based on Fick's Second Law provides the service life indication for reinforced OPC concrete. Prediction relies on two broad phases (initiation time T_0 and propagation time T_1 totalling the serviceable time period to T_0+T_1 beyond which the damage can be unacceptable and renders the structure to be unserviceable. Figure 3.1 below shows the service life for two type of OPC concrete, one with early initiation time but lower rate of propagation while other with late initiation time but higher rate of propagation (Concrete Institution of Australia (CIA), 2001 & Tutti, 1982).

Similar service life prediction model appears to be probable for LCFG concrete. The corrosion initiation expressed in years is the time between the commencements of exposure of the concrete element to chloride and threshold chloride concentration level to initiate the reinforcement corrosion in the concrete. This depends on surface chloride ion concentration C_s, background chloride concentration C_0 inside the concrete and diffusion coefficient.

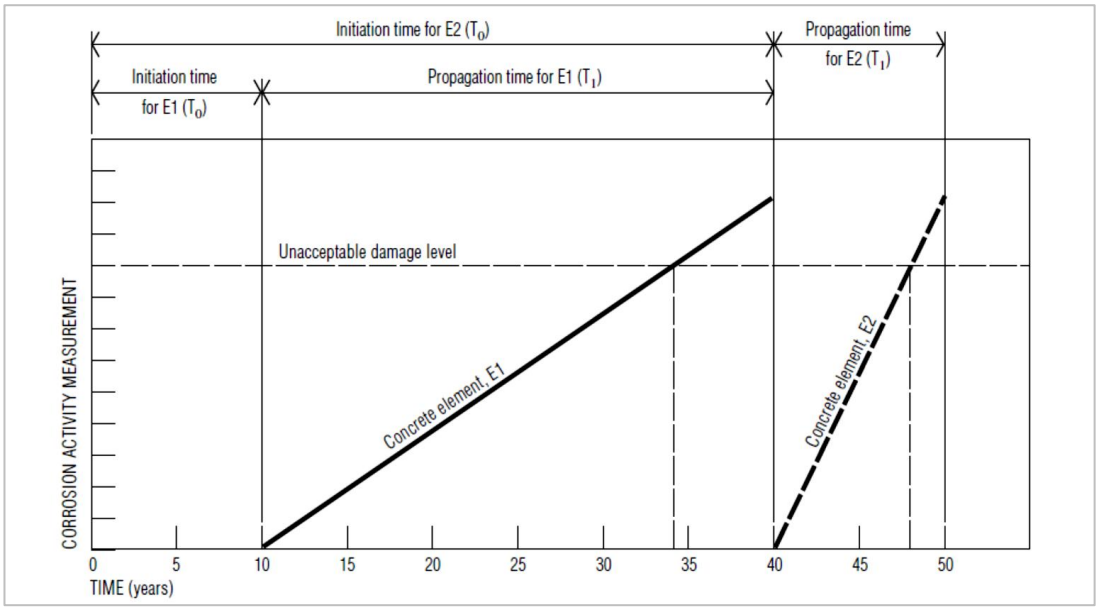

Figure 3-1 Deterioration Intervention Model (CIA, 2001)

For members which are inaccessible for maintenance during its design life, the corrosion initiation period governs the design life of the asset or asset component (CIA, 2001). Japanese Standard provides an indication of chloride surface concentration indication relevant to the distance from sea as shown in Figure 3.2 below.

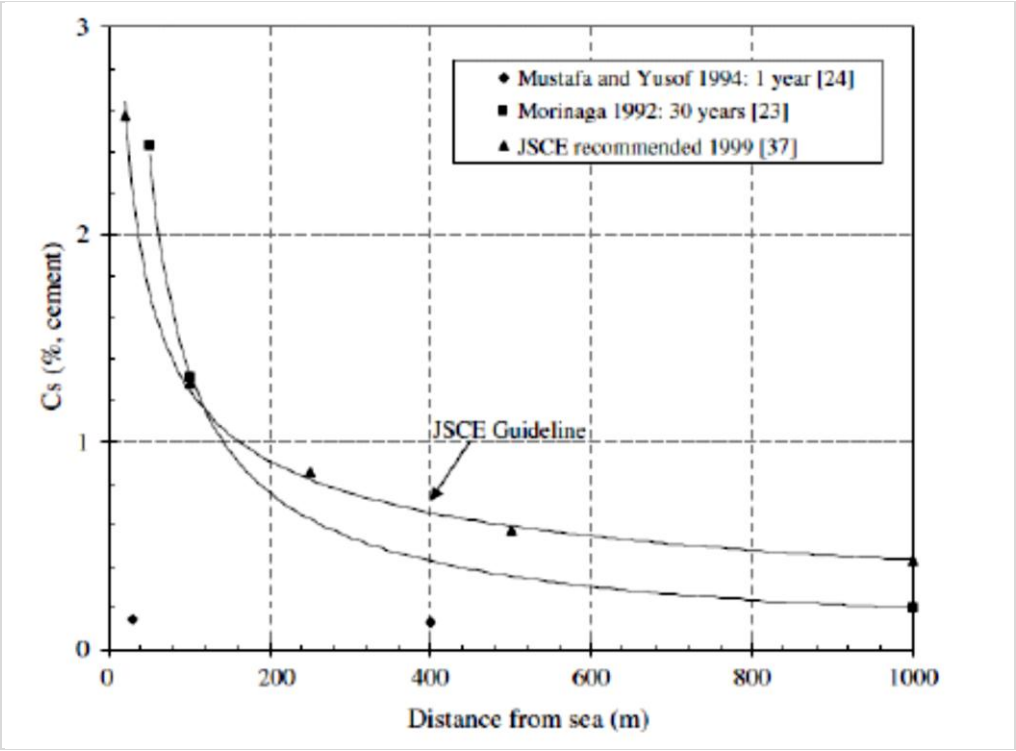

Figure 3-2 Surface Chloride Concentrations (Japanese Standard)

Micro-structural properties, such as, porosity and permeability affect the diffusion in exterior layers, while interior layers diffusion is affected by chloride ions exchange and is influenced by chloride binding (Gjorv & Vennesland, 1979; Collepardi et al, 1972). Once the chloride concentration at greater depth is established where pores are more likely to be saturated, migration of chloride ions to the inner regions through diffusion process will prevail.

Chloride induced corrosion of reinforcement is the major issue with OPC concrete durability especially in salt rich environment. Hot weather, humid climatic conditions and high level of airborne chlorides aggravate these environment further (Rasheeduzzafar et al, 1984).

For the integrity of reinforced OPC concrete the concentration of chloride in reinforced concrete at the reinforcement cover depth should not exceed the threshold limit. Green et al, 2010 details these threshold limits for reinforced OPC concrete described subsequently.

These chloride threshold limits has been assumed to be applicable for the assessment of corrosion initiation in LCFG concrete unless perceived otherwise based on the test outcomes of this research.

3.2.2.1 Chloride Threshold Limits

Despite significant research on the required threshold value of chloride concentration for corrosion initiation, the consensus on its universal value is far from close yet due to the complexity of the corrosion process which depends upon the number of interactive factors such as pH of concrete, ratio of Cl^-/OH^- in pore solution and binder content (Browne, 1982; Rasheeduzzafar et al, 1984; Hansson & Soresen, 1990; Hussain et al, 1996). Reported values of threshold level of chloride content vary from 0.6 -1.33 kg/m^3 of concrete. ACI (1989) recommended maximum limit of water soluble chloride is 0.3% by weight of cement for reinforced construction. Table 3.1 summarises the widely used chloride content criteria in Europe for existing concrete structures (Broomfield, 1997).

Table 3-1 Percentage Chloride Content by Mass of Cement or Concrete

% Chloride by mass of cement	% Chloride by mass of concrete	Risk
<0.2	<0.03	Negligible
0.2-0.4	0.03-0.06	Low
0.4-1	0.06-0.14	Moderate
>1	>0.14	High

Table 3.2 below summarise the chloride concentration threshold limits- Ccr or Ct (Green, et al 2010) - CIA typical values by weight of concrete for modelling purpose.

Table 3-2 Chloride Threshold Concentration (Ct) Values for Modelling Purpose

Type of reinforcement/ prestressing	Chloride threshold concentration
Plain steel reinforcement	0.06% by weight of concrete
Stainless steel reinforcement	0.5 % by weight of concrete
Pre-tensioned or post tensioned steel reinforcement	0.045% by weight of concrete

(Green, et al 2010 CIA Vol 36-Issue3)

Table 3.3 summarise the typical values of concrete surface chloride concentration- Cs for modelling purpose. C_0 is the background chloride ion concentration and is assumed as 0.005%- 0.01% by weight of concrete.

Table 3-3 Minimum Surface Chloride Concentration (Cs) for Modelling Purpose

Zone (Concrete Exposure Category)	Minimum Surface Chloride concentration, Cs (% by weight of concrete)
Continuously immersed or buried Plain steel reinforcement	0.4
High risk(tidal/splash)	0.8
Medium Risk(above +3m Chart Datum(CD) and no splash	0.55
Low Risk(atmospheric)	0.3

(Green, et al 2010 CIA Vol 36 Issue 3)

3.2.2.2 Chloride Binding

Capillary & absorption in outer region result chloride ingress more rapid than diffusion (Hong et al, 2006). In OPC concrete, blended cement with fly ash SCM has lower diffusion, which attribute to lesser amount of $Ca(OH)_2$, means lesser capacity for ion exchange and thus lesser penetration of chlorides (Gjorv & Vennesland, 1979). This is because of fly ash high aluminate (Al_2O_3) content of 17% compared to silica fumes (0.1%) and cement (4%), responsible for chloride binding. This may result chloroaluminate salt (Friedel Salt) and consequently the lower availability of free chloride to cause localised corrosion (Koulombi et al, 1993).

However limited literature is available on the chloride binding ability of LCFG concrete, even though its binder content accounts for 100% fly ash. This has been investigated by undertaking actual chloride profile tests in this research, detailed in Chapter 5.

3.2.2.3 Pore Structure Influence on Diffusion

There are indications in the literature that finer pore structure may be able to restrict the ion movement due to electric double layer effect. The double layer effect (Helmholttz' Electric Double Layer & Gouy Chapaman Electric Diffuse Double Layer Theory) coupled with finer structure assists in slowing the movement of sodium cations, which could result slow movement of negatively charged chloride ion owing to the charge neutrality. Also presence of hydroxyl ions in the diffused double layer further helps to restrict the movement of sodium ions and consequently the movement of chloride ions. This phenomenon retards the diffusion process (Sergi & Panteli, 2011). These phenomena may be present in LCFG concrete as such examining of its pore structure was considered imperative in this research.

There are also mixed opinions in the literature that smaller pores are associated with higher chloride ions exchange and alter the pore size distribution of hardened binder paste (Midgley & Illston, 1984). Chloride diffusion into OPC concrete is very slow process and takes many years before it causes the corrosion of the reinforcement (Shayan et al, 2008).

Midgley & Illston (1984) study showed that chloride penetration depth increases with higher water /binder ratio and concentration of chloride ions, which is dependent on exposure period, curing period, age of concrete at the commencement of exposure to chloride and the porosity & permeability properties of the OPC concrete and seems applicable for LCFG concrete.

So despite some mixed opinions in the literature about the high or low diffusion mechanism on account of fine pore structure, the detrimental effect of diffusion coupled with other mechanisms (such as capillary flow, permeation caused by pressure gradient) in aggressive environmental exposure with high chloride concentration can still be significant (Midgley & Illston, 1984; Azad, 1999).

Very little information is available for LCFG concrete, such as rate of chloride ingress over time in combination with environmental exposures scenarios (buried, immersed and exposed) for controlled concrete mixes. The impact of these mechanisms has been assessed experimentally in this research for LCFG concrete compared to both OPC concrete.

The comparative assessment of these factors and diffusion coefficient for LCFG concrete will assist in understanding its long term durable behaviour compared to OPC concrete in this research.

3.2.2.4 Permeable Voids & Long Term Diffusivity

An increase in water/binder ratio similar to OPC concrete (Rangan, 2008) influences the majority of the LCFG concrete physical properties and hence its deterring trend to deterioration mechanisms appears to be similar to OPC concrete.

But due to limited literature available on long term diffusion properties of LCFG concrete, it will be for some time yet for diffusion trend to be established for LCFG concrete on similar lines for OPC concrete as shown below in Figure 3.3 below. That is, diffusion coefficient values for OPC concrete from a short term exposure period (at least after 28days) is good indicator of long term diffusion coefficient.

Figure 3.3 (a) below show the reduction in D365 is one third of D28 and Figure 3.3 (b) below shows diffusion coefficient reducing trend over longer period (Cement and Concrete Aggregate, Australia (CA), 2009 - a Publication on Chloride Resistance of Concrete).

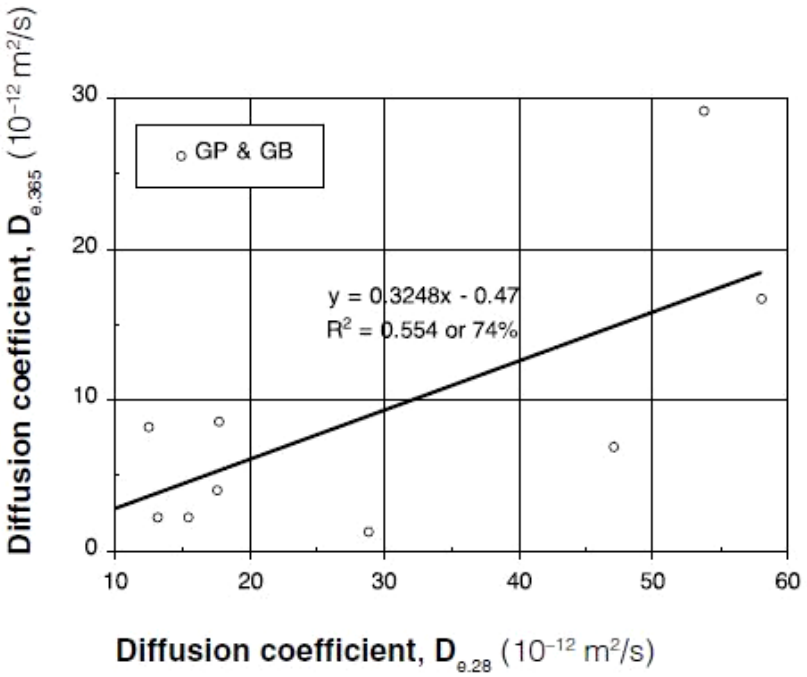

(a)

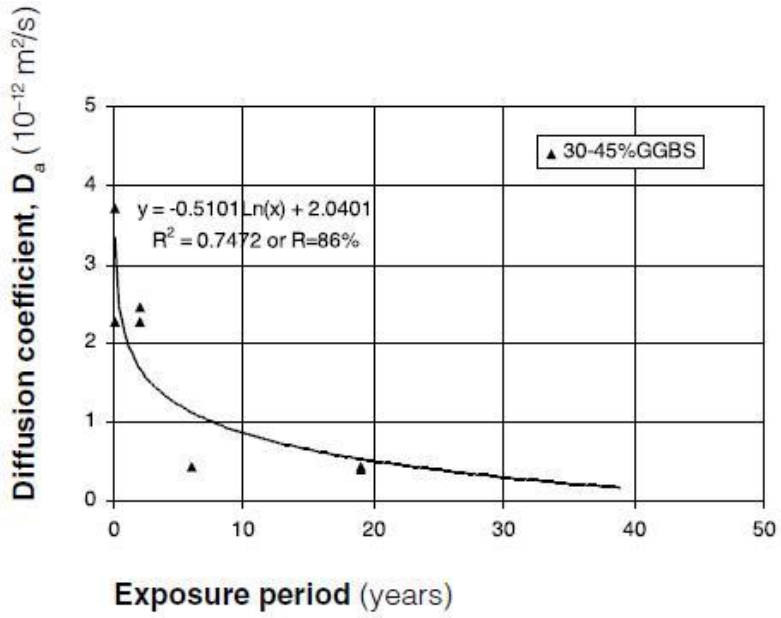

(b)

Figure 3-3 OPC Diffusion Coefficient Trend - Short Term and Long Term (CA 2009)

While low water/binder ratio improves the porosity, permeability properties and reduces the diffusion, for OPC concrete, but this is critical for polymerisation in LCFG concrete. This is because that lower water/ binder ratio tends to prevent the adequate mixing, which can restrict ionic transport and result unworkable mix while high water/binder ratio may dilute the reaction resulting concrete matrix of high porosity (Barbosa et al, 2000; Andrew Phaedonos, 2001; Skvara et al, 2006).

3.2.3 Oxide Passive Film and Depassivating Chloride

When reinforcing steel is exposed to the OPC concrete environment, the corrosion process occurs such that it produces a very thin and stable oxide layer often called a "passive film" (Page & Treadaway, 1982). Due to its complexity, various models that were suggested by previous researchers describing the passive film formation of iron, one is based on a three-dimensional crystalline oxide structure.

This has been suggested that the crystalline oxide film either consists of a layered structure with a Fe_3O_4 inner layer and a γFe_2O_3 outer layer, or a single layer consisting primarily of γFe_2O_3 (Nagayama & Cohen, 1962; Juanto et al, 1987). The other is model, which has been shown to be the more likely case, is the "hydrated amorphous polymeric model". The work by Murphy (1992) gave a schematic representation of this model as in Figure 3.4 below. Polymeric like oxide chains are bound together by water molecules creating the amorphous structure. The thickness of this passive film is often quoted to be in the order of 5 nm. Figure 3.4 below shows the schematic polymeric model of the passive film formed on iron showing the iron oxides bound together by water molecules (Murphy, 1992).

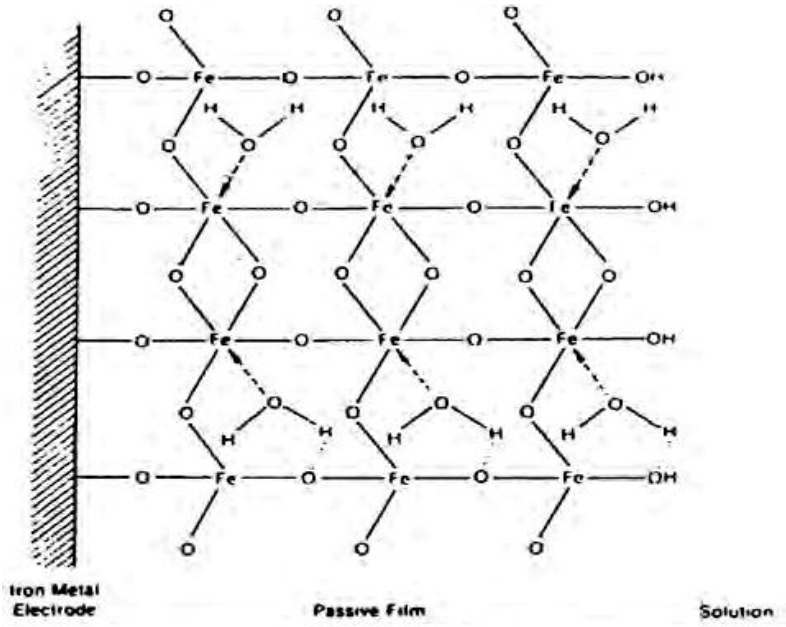

Figure 3-4 Passive Oxide Film Model (Murphy, 1992)

The passive film does not form immediately but starts to form as soon as the pH of the mixing water rises due to hydration of cement and stabilises over the first week to protect the steel from active corrosion (Hanson et al, 2007). Passivation layer remain intact under high pH environments (between 12-13) over the service life (Hansson et al, 2007).

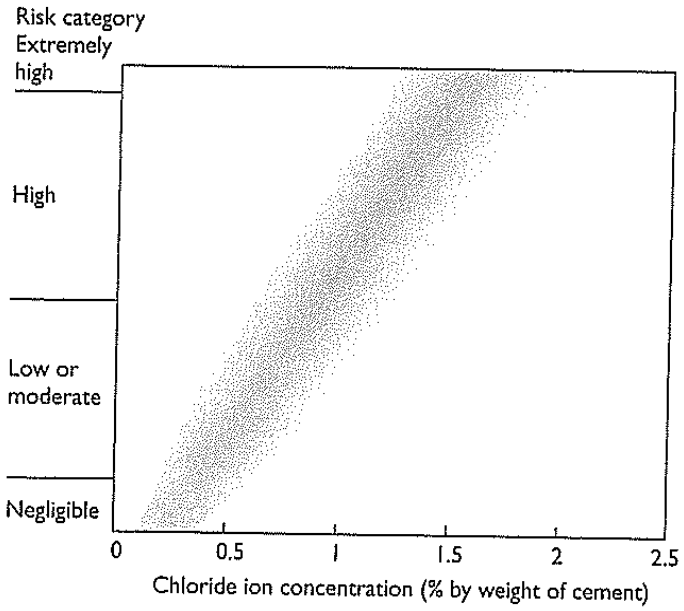

Figure 3-5 Reinforcement corrosion with ingressed chloride in the absence of carbonation (Broomfield, 2007)

As detailed above, past research by various authors has shown slightly different values for a critical chloride threshold to depassivate the passive oxide film layer. Figure 3.5 above shows the likely corrosion risk on account of chloride ion concentration (Broomfield, 2007). Chloride profile can be used along with estimation of the diffusion constant to estimate the future penetration rate and build-up of chloride at reinforcement depth (Broomfield, 2007 and Sergi et al, 1992) from the environments. Chloride profile tests' outputs detailed in Chapter 5 provide the chloride penetration rate and chloride level at reinforcement depth from corrosion perspective.

3.2.3.1 Depassivating Mechanism of Chloride Ions

The mechanism by which the chloride ions breaks down the passive film is not fully understood (Rosenberg et al, 1989), because the oxide passive film is too thin to be examined and secondly its occurrence inside the OPC concrete. In LCFG concrete passive film could be of oxide film or some form of silicate compound or a combination of both. For depassivation of oxide passive layer in OPC concrete, one theory is that chloride ions become incorporated into the passive film and reduce its resistance. Where the chloride ion gets incorporated, it allows rapid reaction setting up the anodic area for corrosion to continue while remaining steel area remains passive, called pitting or localised corrosion as shown Figure 3.6(b) below.

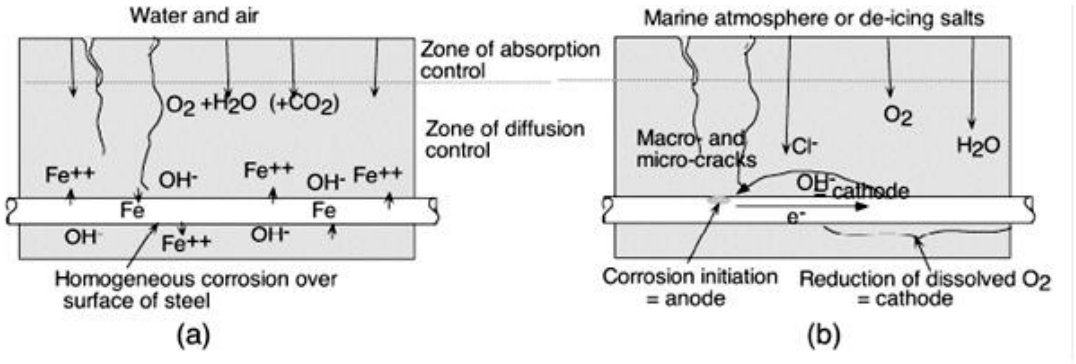

Figure 3-6- (a) Schematic representation of Passive Corrosion and (b) Chloride Induced Active Corrosion (Hanson CM et al 2007)

A second theory is that Cl^- ions compete with the OH^- anions for combining with Fe^{+2} cations and forms the soluble complexes and stop the formation of passive film stimulating the metal dissolution further. The soluble iron complexes diffuse away from the steel and their break down result expansive corrosion products with simultaneous release of Cl^- ions, which are able to migrate back to anode and corrode the steel further. In this process OH^- ions deplete continuously decreasing the pH locally and enhancing the metal dissolution.

So in this process Cl^- ions does not get consumed rather will become available for the attack to occur again and so on (Hansson et al, 2007). Further ingress of Cl^- ions can compound the corrosion process and its rate. These locally active corroding areas behave as anodes while the remaining passive areas become cathodes where reduction of oxygen takes place. This give rise to formation of galvanic cell which may be macro or micro in scale causing corrosion of embedded steel **(**Hansson et al, 2007).

Past research also refers that total chloride content of the pore solution does not alone account for the corrosion rate, it is controlled by other factors; pH, availability of the oxygen, porosity (Hansson et al, 1985) and its electrochemical responses (Azad, 1999). As such pH & carbonation factors and resulting electrical responses of embedded steel in LCFG concrete have been investigated in this research compared to OPC concrete. Literature review of electrochemical techniques detailed in subsequent sections, used in this research revealed the electrochemical properties and the corrosion behaviour of embedded steel in LCFG concrete compared to OPC concrete. These electrochemical properties (concrete resistivity, half cell potential and corrosion current density) emphasise the impact of pH & carbonation from corrosion perspective of embedded steel for respective concretes and hence the durability of reinforced concrete matrix. Test results of these electrochemical techniques are detailed in Chapter 5.

3.3 ELECTROCHEMICAL PROPERTIES

Electrochemical properties of reinforced concrete are of significance due to susceptibility of embedded steel to corrosion. Steel extracted from its primary ore (metal oxides or other free radicals) has a natural tendency to revert to original state under the action of oxygen and water under environmental exposures of varying intensity. This action is called corrosion and the general form of corrosion in atmospheric environments is electrolytic (Eur Ing et al, 1981). For the corrosion to take place, metal must be in contact with electrolyte, oxygen and have anodic reaction (that is an area of steel which has the tendency to go into solution over the other area) and corresponding cathodic reaction to maintain electrical neutrality (Cement and Concrete Aggregate, Australia (CA), 2009). Absence of any one of them can either prevent the corrosion process from happening or control its occurrence.

The susceptibility of reinforced concrete porous structure and its electrolyte composition to corrosion depend on environmental conditions which affects its electrochemical parameters (General Corrosion Corporation, Minneapolis, MN), such as: pH of electrolyte; resistivity of concrete; chloride concentration in electrolyte; dissolved Oxygen or Oxygen concentration of electrolyte; and open circuit potential of coupling metals (Eo). Assessment of these electrochemical properties of reinforced LCFG concrete compared to reinforced OPC concrete is one of the objectives of this research.

Subsequent subsection details briefly the corrosion process and its involved reaction products responsible for the deterioration of concrete in cover zone.

3.3.1 Corrosion of Embedded Steel in Concrete

Metals in environmental exposure conditions such as moisture & corrosive chemicals (acids, salts and gases - O_2, CO_2, H_2S etc.) and high temperature are liable to corrode as result of anodic and cathodic reaction activities. Electrical potential that exists between two metals' surface in an electrolyte of different solution potential allow current to flow in the metallic circuit from the cathode (more electropositive) to anode (more electronegative) as shown in Figure 3.7(a).

The direction of ionic current also known as electrolyte current will be from the anode to cathode and the corrosion will occur at the anode (CA, 2009; Broomfield, 2007) as shown in Figure 3.7(b), but not at the cathode (unless the metal of the cathode is attacked by alkali).

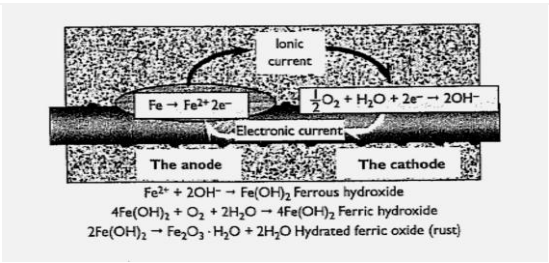

(a)- Broomfield, 2007

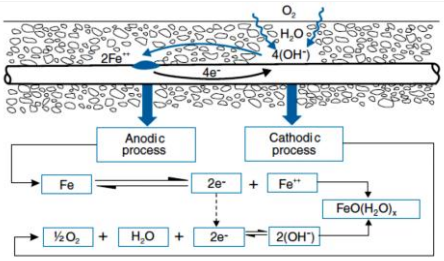

(b) -CA, 2009

Figure 3-7 Corrosion Reactions of Steel in Concrete

The electrons that are released by the anodic reaction (oxidation) travel through the metal to the cathode where they react with water, dissolved oxygen and hydrogen ions to complete cathodic reaction (reduction) maintaining the electrical neutrality. So, for the corrosion of steel embedded in LCFG concrete or conventional concrete to occur, there are four attributive components (anode, cathode, electrolyte and metallic path) which further rely on environmental conditions.

Corrosion, which is an electro-chemical process due to occurrence of both electrical and chemical reactions as shown in Figures 3.7(a) & (b) and once initiated its rate is a complex function of several factors including the availability of oxygen, the overall electrical resistance between anodic & cathodic sites (Mario, C. Uy. Technical Publication, WET, USA). More accurately electrochemical reactions for corrosion are two half cell reactions in high pH solution and in the absence of chloride ions (Hansson et al, 2007):

At the anode: $Fe = Fe^{2++} + 2e^-$

At the cathode: $1/2O_2 + H_2O + 2e^- = 2OH^-$

In cathodic reaction the electron reacts with available oxygen and water at the cathode to form hydroxyl ions (OH^-) and also react with H^+ ion to form hydrogen gas (H_2), which form the barrier preventing the water, O_2, hydrogen and electron from converging and for further reacting. Corrosion rate as a result reduces on account of unavailability of the cathodic site and this phenomenon is called as '*Polarisation*' of the cathode.

But this barrier is subject to '*Depolarisation'* which can result from acidic water solution (due to dissolved CO_2) and its dissociated hydrogen ion can react with hydroxyl ion to form water stripping away the hydroxyl ion barrier and introducing water for cathodic reaction again. Similarly dissolved oxygen can depolarise the cathode by reacting with hydrogen producing water for resuming cathodic reaction and destroying the hydrogen barrier (Mario, C. Uy. Technical Publication, WET, USA).

Thus secondary reactions, the exact form of which depends largely on the availability of oxygen at the anode convert Fe^{2+} ions into oxide compounds. Resulting form of iron oxides and their hydrated forms have specific volume greater than that of steel.

Figure 3.8 below provides the factor by which their volumes vary. The products that ranges between Fe_3O_4 to γ-FeOOH have specific volume between 2.2 and 3.3 times and on becoming more hydrated, they turn into familiar rust which occupy a greater volume than the iron dissolved in their production by a factor between 4 and 6, creating expansive forces in the surrounding concrete. In atmospheric conditions where oxygen is plentiful, the normal reaction will produce hydrated ferric oxide: $2Fe(OH)_3 = Fe_2O_3.(xH_2O)$, Nielsen (1985).

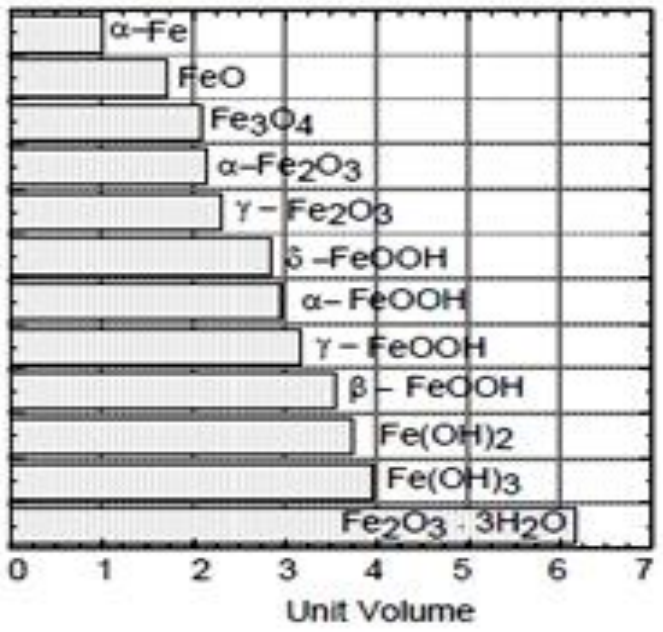

Figure 3-8 Specific Volume of the Corrosion Products (Nielsen, A 1985)

When these forces exceed the tensile capacity of the cover concrete, cracking and/or spalling occurs (Broomfield, 2007). The degree of damage to the concrete depends upon the specific corrosion products and their distribution within the concrete cover as well into the rest of the concrete porous structure affecting its strength (Marcotte & Hansson, 1998 & 2003).

Hence prevention of corrosion of embedded steel can be either through disruption of oxidation and reduction reaction as described above. That is, by preventing depolarisation (which can be either through dissolved oxygen or CO_2 or both or through chloride ions ingress from the environmental surroundings), by increasing pH or through other form of coating barriers reducing the permeability & inhibiting the anodic activities.

Thermodynamically stable boundaries based on pH as a function working electrode potential identify the passive and active corrosion regions of the working electrode, which is a rebar either in OPC concrete or LCFG concrete electrolyte. Pourbaix diagram describes the status of working electrode in porous concrete electrolyte, which subsequent subsection details briefly.

3.3.1.1 Electrochemical Corrosion Equilibriums (Active & Passive)

The Pourbaix diagram in Figure 3.9 (Pourbaix, 1974) thermodynamically predicts the stability of the oxide constituents of the passive film of embedded steel in porous concrete.
Pourbaix diagram (Electrode potential / pH diagram) is a graphical presentation of predominance area diagram presenting dominant aqueous species as a function of pH and E (Hussain & Ishida, 2009). The thermodynamic equilibrium boundaries with different molar concentration of iron ions in the aqueous metal-electrolyte system depict the corrosion equilibriums as shown in Figure 3.9 below.

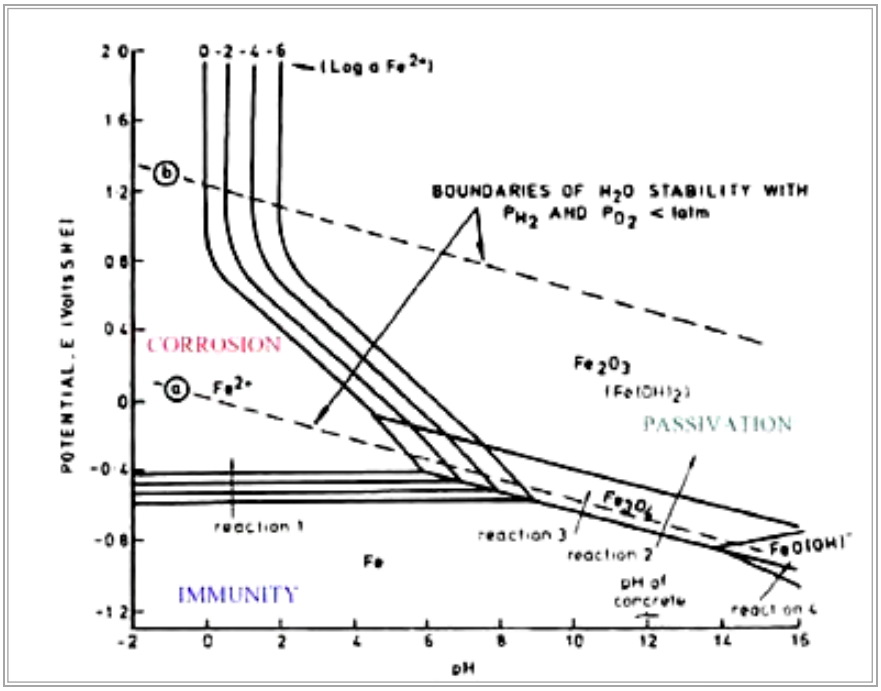

Figure 3-9 The Pourbaix Diagram- Iron/H2O System for Concrete (pH vs. Potential), Pourbaix (1974)

Figure 3.10 below is the simplified version of the Pourbaix diagram showing regions of electrochemical potential and pH , where metallic iron is stable (grey region); where active corrosion occurs (white areas) and where the metal is passivated (blue and light brown areas) - Tullmin (2001). At potentials more positive than -0.6 and pH below 9, passive film is not stable (Pourbaix, 1974) and indicates that iron will corrode under these conditions.

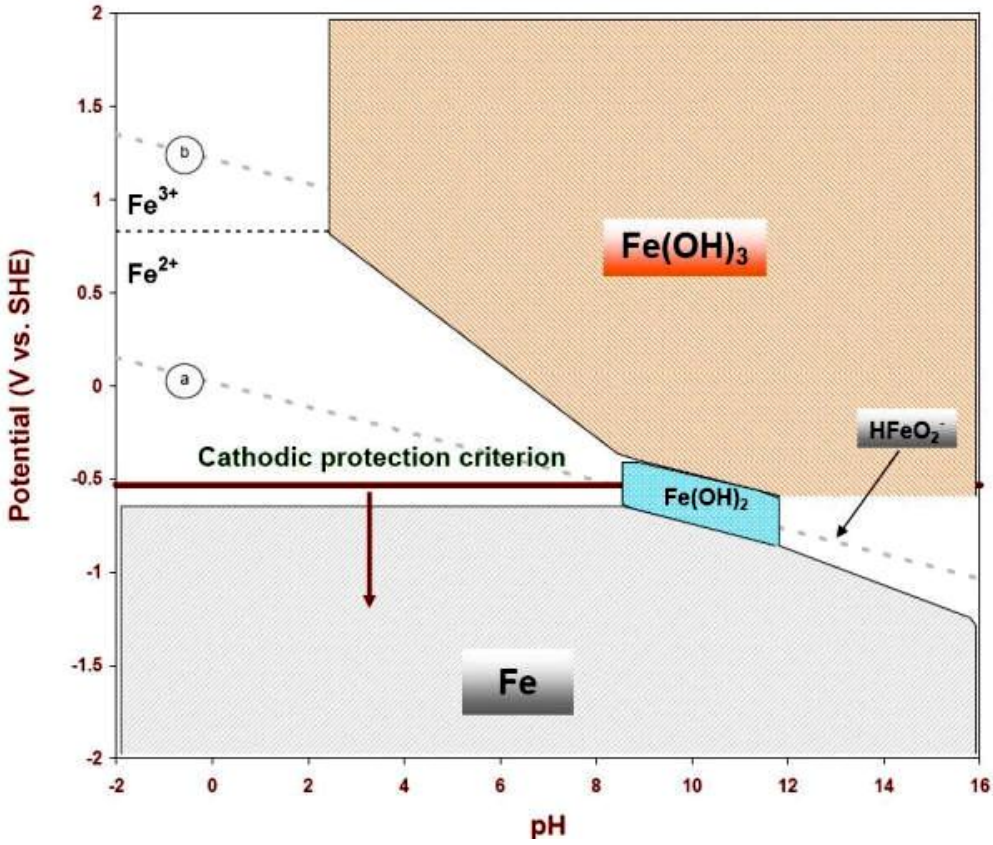

Figure 3-10 Stable, Passive & Active Regions of Steel, Water Stability Boundaries (Tullmin, M. 2001)

If the potential of iron is made sufficiently negative or shifted cathodically below approximately -0.5 V vs. SHE (Standard Hydrogen Electrode) in neutral or acidic environments which correspond to-0.85 V vs. CSE (Copper Sulphate Electrode), as shown in Figure 3.10 the iron will corrode much less. This forms the basis of generally accepted cathodic protection criterion, which is used across industries to protect embedded steel in concrete or steel assets buried in soils.

The line a & b in Figure 3.9 and 3.10 above shows the three regions of H_2O stability. Region between the lines a & b shows the stable water zone where any H_2 present oxidise or reduce to H_2O. Below line 'a' water is unstable and electrolize to release H_2. Above line 'b' water is unstable oxidise to O_2.

These electrochemical responses of rebar from active corrosion perspective have been assessed in this research using electrochemical techniques. These electrochemical techniques include concrete resistivity measurement using Wenner Probe (RESIPOD), HCP vs. standard copper sulphate electrode (CSE) measurements using simple voltmeter, linear polarisation resistance measurement galvanostatically for corrosion current density (using Galvanostatic Pulse Measurement -GPM) and pH measurements.

Subsequent sections briefly detail the principles, criteria and limitations of these electrochemical techniques for assessing corrosion status of embedded steel in porous structure of both OPC and LCFG concrete in this research.

3.4 ELECTROCHEMICAL TESTING TECHNIQUES PRINCIPLES & CRITERIA

3.4.1 Half Cell Potential (HCP)

HCP is a simple device with piece of metal in a solution of its own ions (such as Copper in copper sulphate solution or Silver in silver chloride solution). If the half cell is connected to other metal e.g. iron in its own ions solution- ferrous hydroxide forming single electrical cell. Due to the potential difference between the two 'half cells, voltage will generate. This will happen because of different position of two metals in electrochemical series and due to the different concentration of the solutions they are in.

By using the half cell that is in a constant state, when moved along the concrete surface, it gets changed to a 'full cell' with respect to the steel surface below the half cell. The testing technique assist in portraying the anodic and cathodic portions and provides information on the probability of whether steel reinforcement is in passive state or is actively corroding at those locations, when measured over a given area under investigation (ASTM C 876, 1987).

Figure 3.11 below shows the connection of half-cell potential measurements. By convention the reference electrode is connected to the negative end of the voltmeter and steel reinforcement to the positive giving the negative reading (Gu & Beaudoin, 1998).

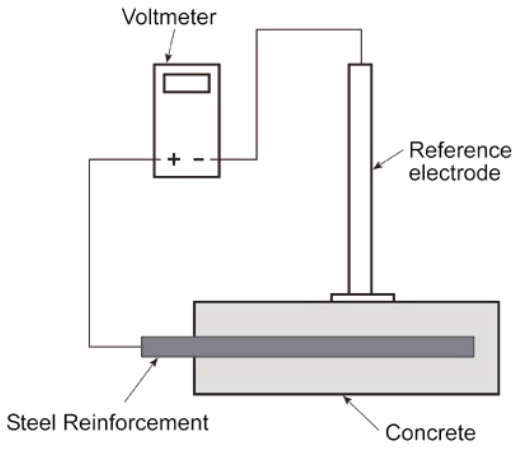

Figure 3-11 Schematic showing basics of the half-cell potential measurement technique (Gu et al. 1998, NRC-CNRC)

The potential measurements are linked by empirical comparisons to the probability of corrosion as per HCP criteria detailed in Table 3.4 below. The measurement of the corrosion potential (Ecorr) with respect to a reference electrode - copper sulphate electrode (CSE) is the simplest measurement in a corrosion system, which can be done simply by using a voltmeter. According to ASTM Standard C876-91 (ASTM 1991), the corrosion potential measured can give an indication of the probability of active corrosion occurrence.

Table 3-4 Half Cell Potential Criteria for the Probability of Corrosion Risk

Half-cell potential reading (Ecorr) vs. $Cu/CuSO_4$	Probability of corrosion
More negative than –0.350	90%
More positive than –0.200	10%
Between –0.200 and –0.350	Uncertain (an increasing probability of corrosion)

Based on the reinforcement condition, the steel in conventional concrete matrix is in passive state if the potential measured is between 0 to -0.200V against standard half-cell of copper in copper sulphate solution. If the passive layer is failing and increasing amount of steel is dissolving the potential moves towards -0.350V. At more negative than -0.350V indicates that the steel is corroding actively.

Therefore HCP is function of the amount iron dissolving or corroding and its extent depends on the depolarising agents present around the steel such as carbonation, presence of sufficient chloride to break down the passive layer. Factors such as oxygen, chloride concentration and concrete electrical resistance, have significant influence on the readings and needs consideration when interpreting half-cell potential data (Gu & Beaudoin, 1998). Following conditions may influence the test results' interpretation.

- Oxygen Concentration: A decrease in oxygen concentration at the surface of the steel reinforcement will cause more negative potential reading which may not necessarily be associated with high probability of steel corrosion (Gu & Beaudoin, 1998). Without O_2, the iron will corrode but will remain stable in solution due to absence compensating cathodic reaction. The HCP measurements may be more negative indicating high corrosion spots under such scenarios while the actual corrosion may be very low. Below the water line in immersed environments where the lack of O_2 often slow the corrosion rate to negligible levels (Hansson et al, 2007), HCP very negative potentials may not true reflection of the situation.

- Chloride Ion Concentration: An increase in chloride ion concentration causes significant steel corrosion. This chloride-induced corrosion is associated with a significant shift of the corrosion potential towards more negative values and an increase in the severity of the steel corrosion. This is a case that the ASTM C876 standard predicts well (Gu & Beaudoin, 1998). Chloride ions are one of the most important causes of localised corrosion of the reinforcing steel, while uniform corrosion of the reinforcement occurs in the presence of carbon dioxide (Hansson et al, 2007).

- Carbonation: Carbonated concrete has anodes and cathodes very close together as such the measured half cell potential may be mixed potential. Also due to the quick drying and wetting tendency of the carbonated concrete by $CaCO_3$ deposits in case of OPC concrete particularly. That is, more positive without wetting and very negative when taken after wetting misrepresenting the true corrosion state of embedded steel in concrete. Also the shift towards negative potential may not very large but such small shift may be associated with a large increase in the rate of corrosion.

However with due reference to the environments, HCP measurements provides a reference to the changes in potential on the surface of the embedded steel bar and can be used to identify regions where corrosion activity is probable.

HCP technique requires wetting during the process of half-cell potential measurement of the materials, that is, the surface of concrete has to be sufficiently wet so that there is a low resistance path between the rebar and the reference electrode in the concrete. The technique does not give any information on the rate of corrosion activity, that is, about the corrosion in progress.

3.4.2 Resistivity

The use of a resistivity measurement together with HCP potential mapping can give an indication of the severity of the problem and its location. A resistivity measurements using Wenner Probe requires the application of low magnitude of AC current (typically 30-60Hz) between the outermost electrodes and volt meter to be connected to inner electrodes to provide the resistance of the concrete in the surface region as shown in Figure 3.12 below (Millard & Sadowski, 2009).

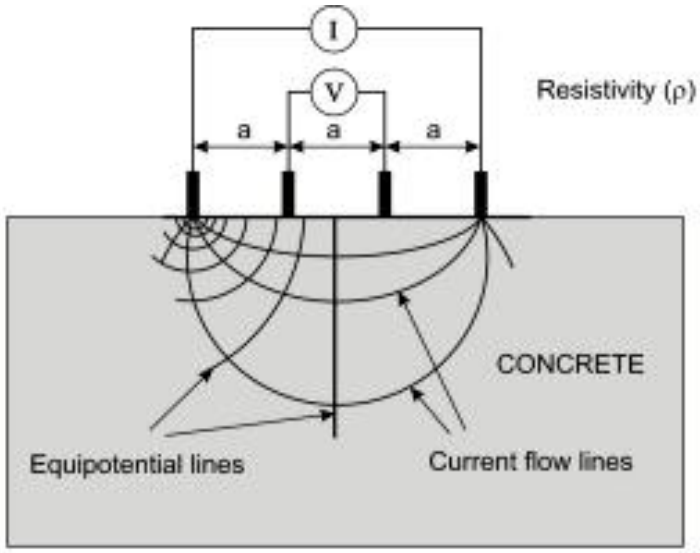

Figure 3-12 Wenner Probe (Millard et al 2009)

Resistivity 'ρ' can be computed as: $\rho = 2\pi aV/I = 2\pi aR$

Concrete resistivity is the ratio between applied voltage and resulting current in the unit cell that is, a specific geometry independent of material properties, which describes the electrical resistance. The dimension of the resistivity is resistance multiplied by length and its unit is ohm meter. The resistivity of the cement based material is the function of porosity, chemical composition of the pore solutions resulting from environmental interactions (Tumidajski et al 1996; Polder et al, 2000; RIELM TC 154-EMC; Simon et al, 2012). Higher water/binder ratio causes lower resistivity (RIELM TC 154-EMC). For interpretation of the results, global reference data from various laboratory studies for the electrical resistivity of the dense aggregate OPC concrete of existing structure (age>10years) under environmental exposures summarised in Table 3.5 (RIELM TC 154-EMC) to assess the quality of concrete and corrosion risk probability on account of chloride ion penetrability.

Table 3-5 Concrete Resistivity & Environmental Exposures

Environments	**Concrete Resistivity in Ohm-m**	
	OPC Concrete	**OPC Concrete with Blast Furnace Slag (>65%) or Fly ash>25% or silica fume (>5%)**
Very Wet, Submerged, Splash zone	50-200	300-1000
Outside Exposed	100-400	500-2000
Outside, Sheltered. Coated, hydrophobised (20^oC/80%RH), not carbonated	200-500	1000-4000
Ditto, carbonated	≥1000	2000-6000 and higher
Indoor(carbonated, 20^oC/50%RH)	≥3000	4000-10000 and higher

Chloride ion penetrability based on surface resistivity is summarised in Table 3.6 (AASHTO Proposed)

Table 3-6 Concrete Penetrability

Chloride ion penetrability (Permeability Class)	Surface Resistivity (kOhm-cm) a =50mm 28 day- Cylinder(100mmx200mm)	Surface Resistivity in (Ohm-m)
High	<12	<120
Moderate	12-21	120-210
Low	21-37	210-370
Very Low	37-254	370-2540
Negligible	>254	>2540

In respect of corrosion risk, resistivity measurements reference is given in the Table 3.7 below as a general rule (RIELM TC 154-EMC), which could be subjected to further study.

Table 3-7 Corrosion Risk

Risk of corrosion of reinforced concrete at 20 ^{o}C	
Surface Resistivity in (Ohm-m)	**Risk of Corrosion**
<100	High
100-500	Moderate
500-1000	Low
>1000	Negligible

Moisture and temperature variation influence the resistivity. The resistivity of concrete increases when it is drying out and carbonates, particularly OPC concrete due to the densification effect of $CaCO_3$ (Adam et al, 2009). Temperature changes affect the resistivity. The change in resistivity can be in the order of 3% to 5% per degree variation in temperature.

Arrhenius equation as below describes the effect of temperature on conductivity.

$$\sigma(Ti) = \sigma(T_0) * \exp(b[T_0^{-1} - Ti^{-1}])$$

Where σ is the conductivity, Ti= the actual temperature, T_0 = the reference temperature and b = empirical factor ranges between 1500-4500 (Bertolini & Polder, 1997).

Also higher RH and temperature cause higher dew point temperature, which is the saturation temperature of the water vapour in the air i.e. that is the temperature at which evaporation and condensation rates are same, as shown in Figure 3.13 below.

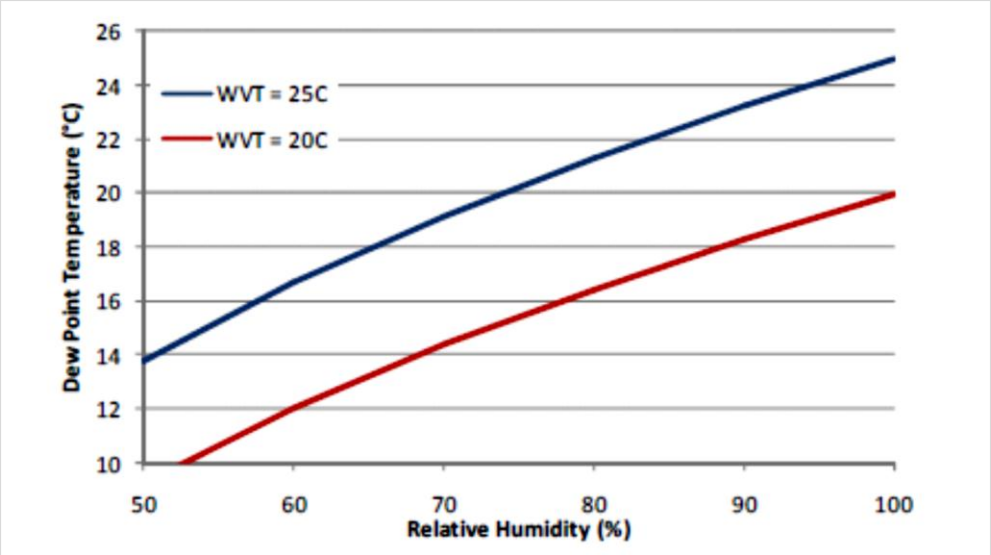

Figure 3-13 Correlations of RH and Dew Point Temperature (BCRC)

The test provide the useful inferences on corrosion risk estimation, relative indication on the permeable parts of the same structure or structure from different mix composition and their exposure level to environments such as severe wet exposure. The test is possible on all exposed part of the concrete structures that are exposed to air and it has limitation for submerged or buried parts (RIELM TC 154-EMC). A low resistivity implies reinforcement corrosion is occurring and rate is likely to be high.

3.4.3 Galvano-static Pulse Measurement Technique

The GalvaPulse™ is a rapid, non-destructive polarization technique for the evaluation of reinforcement corrosion rate as well as half-cell potential. In conventional concrete at high pH, the Fe^{++} forms a complex protective film with oxygen. The interpretation problem is that the potential will drop either because of the loss of passive film due to chloride attack or due to the lack of oxygen. The corrosion process will not be able to proceed without oxygen. GPM distinguish between the active corrosion and lack of oxygen situation, which is not possible with Half Cell Potential test (Klinghoffer et al, 1997).

This linear polarisation resistance (LPR) measurement technique makes possible to calculate corrosion rate within a short time typically 10 seconds. The equipment gives corrosion rate, HCP and as well resistance between the hand- held electrode placed on the concrete surface and the reinforcement. Electrical continuity in the reinforcement is essential (Baessler et al, Federal Institute for Material Research Testing, Berlin/Germany).

Polarisation, which can be static or dynamic depending upon the nature of the application of the potential or current, is the term given to the situation when the voltage or current is changed from the equilibrium potential or current. The equilibrium potential assumed by the metal is open circuit potential (Eoc), that is, in the absence of any electrical connection (GAMRY). Its interchangeable form is the corrosion potential (Ecorr) in electrochemical corrosion testing.

The anodic and cathodic reactions are kept in balance by the potential of the metal and current from each half cell and depend upon the electrochemical potential of the metal. That is, if anodic reaction releases too many electrons into the metal then potential shifts more negative speeds up cathodic reaction and this counteracts the initial perturbation of the system.

The value of either anodic or cathodic current at open circuit potential (Eoc) is corrosion current Icorr and its measurement is not direct, however using electrochemical techniques it can be estimated (GAMRY), which is used to calculate the corrosion rate, (that is how much steel gets dissolved in a year in mm/year). When a short duration of anodic current pulse is induced gavanostatically into the reinforcement by placing the counter electrode together with reference electrode on the concrete surface, the potential of the metal is forced away from Eoc, it is said to be polarising and the response current is measured. From this response current, model is developed to assess the corrosion behaviour of the reinforcement steel using Stern Geary equation. The resulting change in potential, ΔE is measured after a suitable time once the equilibrium is re-established. The polarisation resistance is given by:

$$Rp = \Delta E/\Delta I$$

The corrosion interface comprises a capacitive double layer, Cdl on the surface of the steel bar together with a charge transfer resistive interface, Rct. The rate of corrosion is inversely proportional to Rct. Concrete cover resistance, Rs is geometrically related to the concrete resistivity by the diameter, rebar cover and contact area surface. A simple electrical circuit known as a Randle's circuit can be used to describe the concrete cover and the corrosion interface. (Millard & Sadowski, 2009). Rct is obtained by subtracting the concrete cover resistance (Rs) from the polarisation resistance (Millard & Sadowski, 2009).

$$Rct = Rp - Rs$$

The corrosion current density, Icorr requires a knowledge or assumption of the area of steel being perturbed which to be multiplied with Rct to obtain applicable polarisation resistance to assess Icoor (Millard & Sadowski, 2009). The small anodic current results in change of reinforcement potential which is recorded as function of polarisation time. Reinforcement is polarised in anodic direction compared to its free corrosion potential. Typical transit response is shown in Figure 3.14 below.

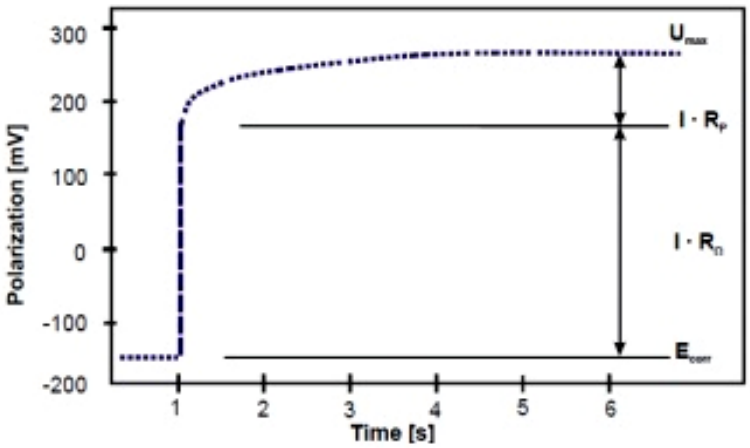

Figure 3-14 Galvanostatic Pulse Response

Under the application of constant current Iapp to the system, the polarised potential of the reinforcement at any given time t is given by the expression as below.

$$Ut = Iapp\ [Rp.\ \{1\text{-}e^{t/Rp.\ Cdl}\} + R\Omega]$$

Where:

Rp = polarisation resistance

Cdl = Double layer capacitance

RΩ = Ohmic resistance

To obtain the value of Rp & Cdl separate from RΩ, the transferred equation into linear form will be as below.

$$In\ (Umax\text{-}Ut) = In\ (Iapp\ Rp) - t/\ Rp.\ Cdl$$

Using linear regression analysis extrapolation of straight line to t = 0 will yield an intercept of (Iapp Rp) with slope $(Rp\ .\ Cdl)^{-1}$

The remaining over potential corresponds to the ohmic drop. After the polarisation resistance is determined by means of this technique, the corrosion current can be calculated by using Stern Geary equation as below.

$$Icoor = B/ Rp$$

Where B is the empirical constant determined to be 25mV for actively corroding and 50 mV for passive steel (Baessler et al; Broomfield, 2007; Arrendinodo-Rea et al, 2011).

It assumes the following assumptions:

- there is a single anodic and cathodic reaction and the corrosion polarisation activation is the single controlling step.
- Corrosion damage is uniform.
- The proportionality constant between corrosion rate and Rp must be known.
- HCP is stable.

This technique has some limitation as well, that is , gives no indication that how long the corrosion has been going on and how the corrosion rate vary with time and ambient conditions such as increasing or decreasing temperature and correspondingly increases or decreases the corrosion rate (Baessler et al).

3.4.4 pH

In conventional concrete at high pH, the Fe^{++} forms a complex protective film with oxygen. The potential will drop either because of the loss of passive film or due to the lack of oxygen.

The pH of a solution is a measure of the molar concentration of hydrogen ions in the solution and as such is a measure of the acidity or basicity of the solution. The letters pH stand for "power of hydrogen" and the numerical value is defined as the negative base 10 logarithm of the molar concentration of hydrogen ions (Hussain & Ishida, 2009).

$$pH = -\log10[H^+]$$

For 1 molar solution of H^+ ions the system defines the zero of the pH scale. Nernst equation, which helps to determine the direction of electrochemical processes with metals in water solutions, is used for constructing Pourbaix diagram (E / pH diagrams) as described above. If an electrode is not under standard conditions the electrode potential may be calculated according to the Nernst equation as below:

$$E = E_0 - (RT/nF)*\ln Cion \qquad \text{…… Equation 3.6}$$

Where:

E_0 - Standard electrode potentials in volt;

R - gas constant R=8.3143 J/(mol*K);

T - temperature, K;

n - number of electrons transferred;

F - Faraday constant F=96500 C/mol (C-coulombs);

Cion - molar activity (concentration) of ions.

At the temperature 298K (25^{o}C) the Nernst equation may be presented as follows:

$$E = E_0 - (0.059/n)*\ln Cion$$

With reference to SHE at 25^{o}C (its E_0 =0), the above Nernst equation for Ecell will be as below

$$E = - (0.059/n)*\ln Cion$$

In most cases the activity of hydrogen ions in solution can be approximated by molar concentration of hydrogen ions and for simplicity above expression in the form decimal logarithm will be as below.

$$E = - 0.059 \log10[H^+]$$

When applied to full cell formed from the cell present inside and outside the concrete Nernst equation takes the form as shown in equation 3.7 below (Hussain & Ishida, 2009).

$$Eo_2 = Eo_2(t\ 25^oC) + (RT/zO_2F)\ In(PO_2/P_{at}) - 0.59pH \quad \text{….. Equation 3.7}$$

Where;

- Eo_2 is the cell potential of O_2 cath. Vs. SHE,
- $Eo_2(t\ 25^oC)$ is the standard cell potential of O_2 at 25^{o}C (=0.40V),
- T is the surrounding temperature in Kelvin scale,
- P_{at} is the atmospheric pressure,
- zO_2 is the number of charge of O_2(=2), and
- pH is power of hydrogen ion concentration (12.3 for non-carbonated model)

Figure 3.15 below provide an indication of corrosion rate with reference to pH of an electrolytic solution surrounding the embedded steel in concrete and free chloride available in the concrete matrix as percentage by mass of binder (Hussain & Ishida, 2009).

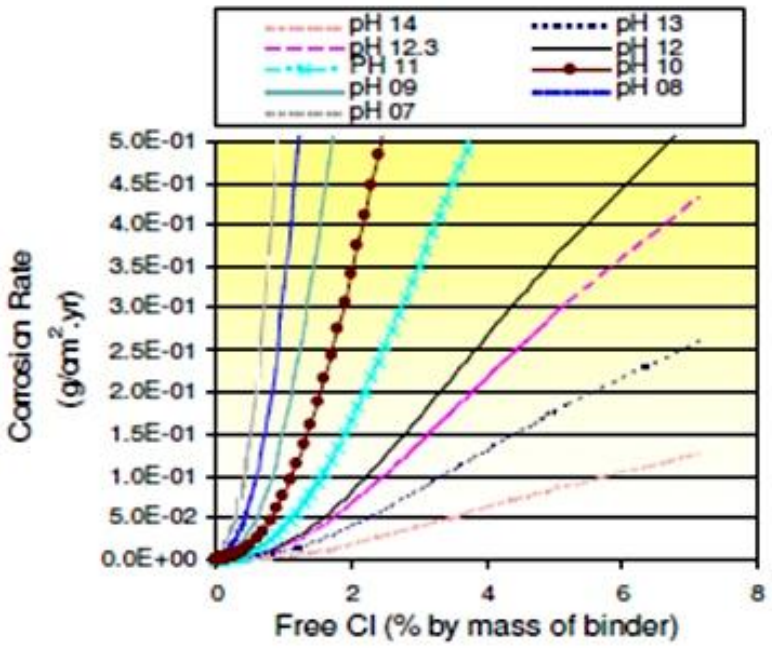

Figure 3-15 Corrosion rate with reference Free Cl (% mass of binder) and pH of the electrolyte

In corrosion potential model, pH of a sample can be measured by obtaining cell potential of that sample in reference to standard hydrogen electrode. In general pH of less than 9 represents the coupled attack of chloride and carbonation and in severe environmental exposures chloride and carbonation can act synergistically.

3.4.5 Carbonation

Carbonation owing to its possibility for corrosion of steel reinforcement under moist conditions is primarily governed by the diffusion of atmospheric CO_2 through the exposed phase and is relatively a slow process for OPC concrete. In water saturated and completely dry scenarios, the level of carbonation is very low for concrete matrix.

However carbonation occurs at intermediate moisture corresponding to relative humidity (RH) 65% -75% and its rate depends on the concentration of CO_2 in the environment. The carbon dioxide from the atmosphere reacts with hydroxides, usually $Ca(OH)_2$ in OPC concrete. The presence of hydroxides in LCFG concrete could be as result of alkaline metal present which could be unreacted Ca and residual NaOH from alkaline solution used in the mix synthesisation of geopolymer initially. In geopolymer binder paste, these are liable to react with atmospheric CO_2 as shown by equation 3.8.

$$M(OH)x + CO_2 = MCO_3 + H_2O \qquad \text{---- Equation 3.8}$$

The reaction is effectively neutralising the pore solution. As detailed above chloride and carbonation attack can act synergistically and could be major durability issue in hot coastal and inland saline areas (Hansson et al, 2007) as the rate of carbonation tend to be more within RH range of 50-70%. As shown in Figure 3.16 below.

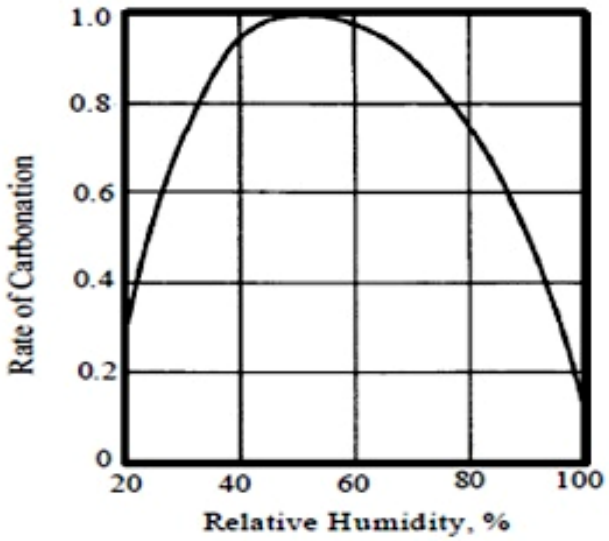

Figure 3-16 Rate of Carbonation relative to RH (Hanson, et al 2007)

The occurrence of soluble carbonates in hydrated form can be possible cause of scaling formations. Such formations are indicator of lower pH and essentially the acidification of the water (Sergi & Panteli, 2011). At pH below 6, the reverse is also true that metal carbonate can dissolve to release CO_2 resulting from the acidic solution (Carroll et al, 1992) as shown in Figure 3.17 below.

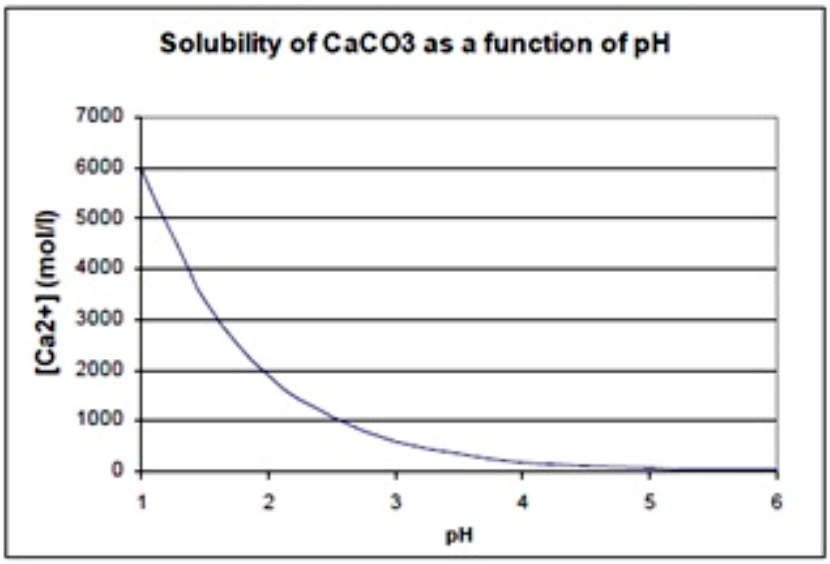

Figure 3-17 Solubility of CaCO3 as a function of pH

Either way carbonation essentially removes the charge on the surface of the pores and eliminates hydroxyl ions. This makes the diffusion path for sodium and chloride ions unrestricted and ensures the equal diffusion rate of sodium cations and chloride anions on the basis of charge neutrality (Sergi & Panteli, 2011). Figure 3.18 below provide the corrosion rate due to carbonation in the absence of chloride and at accelerated concentration of CO_2 (10%) and 0% chloride concentration for OPC concrete (Hussaian & Ishida, 2009).

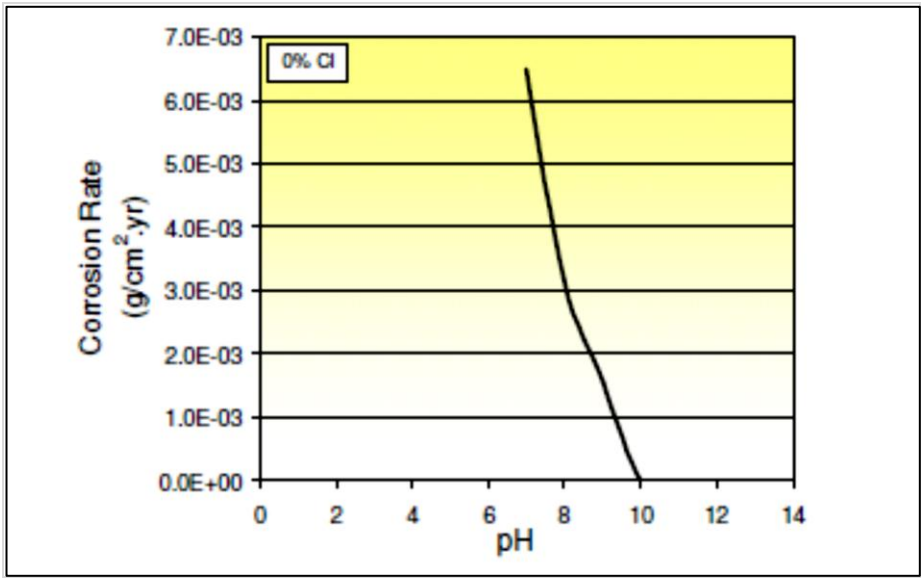

Figure 3-18 Corrosion rate with accelerated CO2 as a function of pH

Sergi et al (2011) study showed that chloride environments accelerate the carbonation under normal atmospheric CO_2 concentration exposure. The normal atmospheric CO_2 concentration is in order of 0.04% (Green et al, 2010). This is on account of humectant effect of NaCl that raises the RH level to 70-75%. Secondly atmospheric CO_2 concentration exposure tends to release considerable bound chloride than high CO_2 concentration environment. Carbonation may impact the OPC concrete the following ways (Sergi et al, 2011) and influenced by the following factors.

- Ionic composition of the pore solution
- Porosity
- Water and carbon dioxide binding capacity
- Diffusion characteristics,
- Proportion of free and bound chlorides in the carbonated hardened cement matrix.
- Rate of carbonation
- Scaling

Similar carbonation impacts may be probable for LCFG concrete to a varied extent, which have been investigated in this research. Test observations and interpretations are detailed in Chapter 5.

3.4.6 Corrosion Rate

In electrochemical corrosion action, electrons released by the iron under anodic reaction get consumed by cathodic reaction on account of dissolved oxygen and constitute a current, which can be measured indirectly. The current represents dissolution of one iron atom for each two electrons in the current, which can be converted to thickness of steel dissolved based on Faraday's Law (Hansson et al, 2007). That is a current density of $1mA/m^2$ or $1\mu A/cm^2$ equates to 1.16 mm/year.

A corrosion current density of $10\mu A/cm^2$ can cause section loss of 116µm/ year and rust growth of 345 µm/ year. These estimates are based on average expansion ratio of 3 (iron oxides have volume increase between 2 to 6) and allowing some of the corrosion products being pushed into the porous structure around the rebar. An expansive growth of 0.01 to 0.1mm can cause cracking (Broomfield, 2007). As per Rodriguez et al (1994) study, section loss of 15-40 µm can attribute to cracking on rebar with cover to diameter ratio between 2 to 4 for OPC concrete. On this basis, probable corrosion of embedded steel in LCFG concrete is detailed in Chapter 5.

3.5 EFFLOROSCENCE AND SCALING RESISTANCE

Even though the common requirements of concrete such as compressive strength & water-cementitious materials ratio are fulfilled, it may not necessarily guarantee the necessary scaling resistance. From durability perspective scaling has significant bearing, that is concrete with high scaling resistance is more durable than the one with not. Possible factors relating to concrete mixture design, construction practices (placing, finishing & curing) and the environmental ones (salt type & its concentration, exposure timing etc.) require comprehensive evaluation (Jana, 2007) to assess the impact of scaling.

Hardened cement paste of concrete near the exposed surface may be subject to damages on account of crystallisation of pores' salts under wetting and drying cycles. While microstructure and pores properties can contribute significantly towards the scaling resistance but it is equally important to assess the nature of ingressing salts and their reaction with concrete matrix reactants resulting soluble compounds.

The hydrated form of these soluble compounds exerts expansive force, which cause scaling of the concrete surface. Soluble salts' exposure to moisture has phases that readily transform between anhydrous (or less hydrous state) and hydrous states during cyclic wetting & drying. This is referred as "salt hydration distress" and is responsible for the scaling (Hime et al, 2001).

Available literature shows that salt hydration distresses may be due to the hydration of thenardite (Na_2SO_4) to mirabilite (Na_2SO_4. $10H_2O$), which can occur in situ or through penetrating solution or both but not like the hydration of free lime taking place at the surface. In these reactions, the total volumes of the reactants (i.e. anhydrous salts plus water) are lower than that of the final resulting solid products. Further hydrated form of these solid products distresses the cementitious layer near the surface causing scaling (Jana, 2007).

Water along with chloride and soluble salts from the environments finds its way to the reaction sites through interconnected capillary pores and micro-cracks and their crystallisation in early phases, results efflorescence. The efflorescence can lead to the accumulation of soluble salts in the pores near the surface, which on hydration can distress concrete matrix near the surface for possible scaling. These hydrated salts can be the transformation of thermonatrite ($Na_2CO_3.H_2O$) to natron ($Na_2CO_3.10H_2O$) which is accompanied by a 261% increase of solid volume, thermonatrite to sodium carbonate hepta-hydrate ($Na_2CO_3.7H_2O$) accompanied by a 179 % increase of solid volume (Hime et al, 2001; Erlin et al, 2003).

Similarly ingress of sulphate salts can react with sodium to form sodium sulphate (Na_2SO_4), which is known as thenardite and during cyclic wetting and drying it turns into mirabilite (Na_2SO_4. $10H_2O$). The thenardite-to-mirabilite conversion is accompanied by 315 precents increase in situ solid volume and is the main reason for concrete surface scaling (Hime et al, 2001 and Erlin et al, 2003).

Other possible soluble salt hydration distress could be due to the presence of magnesium sulphate rich soil, which can contribute hydrated products such as $MgSO_4.H_2O$ salt. Table 3.8 below lists the hydration reaction of various salts, which can cause surface distress (Proceedings of the Twenty-ninth Conference on Cement Microscopy Quebec City, PQ, Canada May 20 -24, 2007 111).

Table 3-8 Reversible Phase Transformation of Various Soluble Salts

Hydration Reaction	Molar Vol (cm^3/mol)		Decrease in Reaction Vol (%)	Increase in Solid volume to cause Salt Hydration Distress
	Solid Reactant	Solid Product		
$CaSO_4 + 2H_2O = CaSO_4.2H_2O$ (Anhydrite) (Gypsum)	45.99	74.21	- 9.5	+ 61.3
$Na_2SO_4 + 10H_2O = Na_2SO_4.10H_2O$ (Thenardite) (Mirabilite)	53	220	- 5.6	+ 315.1
$Na_2CO_3.H_2O + 9H_2O = Na_2CO_3.10H_2O$ (Thermonatrite) (Natron)	55.11	198.7	- 8.5	+ 260.5
$Na_2CO_3.H_2O + 6H_2O = Na_2CO_3.7H_2O$ (Thermonatrite) (7-hydrate)	55.11	153.7	- 5.8	+ 178.9
$MgSO_4.H_2O + 6H_2O = MgSO_4.7H_2O$ (Kieserite) (Epsomite)	56.7	146.71	- 10.9	+ 158.7

Chemically bound or free sodium in the LCFG concrete when gets reacted with the ingressing CO_2 from the environments may cause the scaling due to reversible transformations of these soluble compounds. Zhang et al (2013) investigation of accumulated efflorescence salts using X-ray Diffraction (XRD) on steam cured geopolymer concrete samples at 80^oC and ambient cured ones after 12 hour contact with water under atmospheric condition indicated the formation of 7th hydrate of sodium carbonate ($Na_2CO_3.7H_2O$). The elemental composition of these efflorescence products is shown Figure 3.19. Zhang et al (2013) observed efflorescence activity in both the samples and noted its quicker development on ambient cured samples.

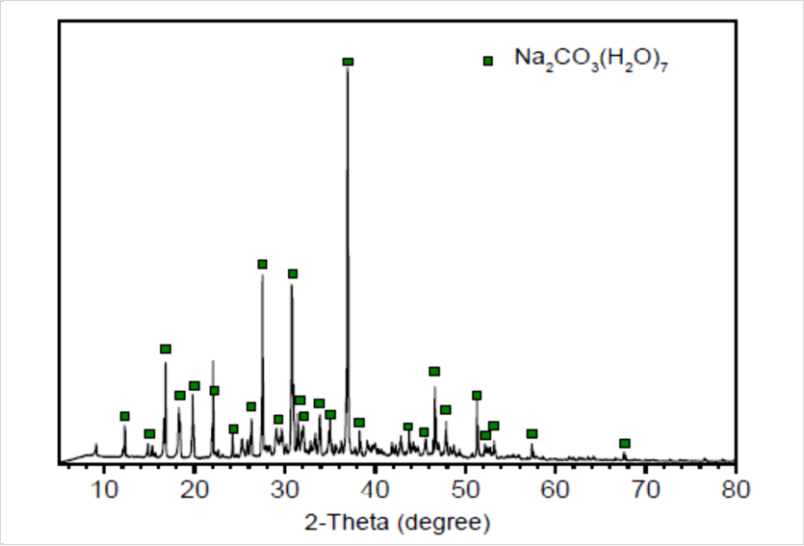

Figure 3-19 XRD Pattern of Efflorescence Salt from Geopolymer Concrete Surface

This 7th hydrate of sodium carbonate ($Na_2CO_3.7H_2O$) can further hydrate to natron as detailed in Table 3.8 above and could result scaling of harden LCFG concrete surface.

Efflorescence is an early indicator of deterioration processes causing scaling. Moisture transport processes carrying soluble salts into porous structure of the concrete, which in concentrated and hydrated form distresses the concrete hardened surface (Hime et al, 2001). The contributing factors to efflorescence and scaling could be as below.

- Water transported species through water absorption under capillary action and water permeation
- Diffusion due to concentration gradient and ionic exchange.
- Reversible transformations of the salts between different hydration states, due to variations in ambient temperature and humidity.
- High chloride contents at the surface region compared to that in the body under severe environmental exposures.
- Ingress of highly soluble salts;
- Exposure to a cyclic wetting and drying environment; and
- The leaching trend of soluble ions such as sodium cations.

Some field and laboratory studies on performances of OPC concrete containing supplementary cementitious materials have conflicting reports in literature, that is, concrete containing fly ash, slag, or silica fume indicated the increased scaling potential as well slightly decreased scaling resistance compared to the Ordinary Portland cement (Marchand, et al, 1994). But there is limited study on an alkaline activated LCFG concrete with 100% low calcium fly ash for its scaling resistance. Qualitative visual assessment in this research provides the extent of scaling and scaling resistance of LCFG concrete compared to OPC concrete as detailed in Chapter 5.

3.6 RELEVANT LITERATURE REVIEW ON LCFG CONCRETE MIX

3.6.1 Influence on Compressive Strength of Na_2O/SiO_2 & H_2O/Na_2O Mix Molar Ratios

Hardjito & Rangan (2005) research indicated that variation of Na_2O/SiO_2 mix molar ratio impacts the compressive strength properties of LCFG concrete, such as, compressive strength decreases with the increase of Na_2O/SiO_2 mix molar ratio while microstructure and pores' structure improve (Skvara et al, 2006) as detailed subsequently. Figure 3.20 shows the compressive strength trend on account of Na_2O/SiO_2 mix molar variation (Hardjito & Rangan, 2005)

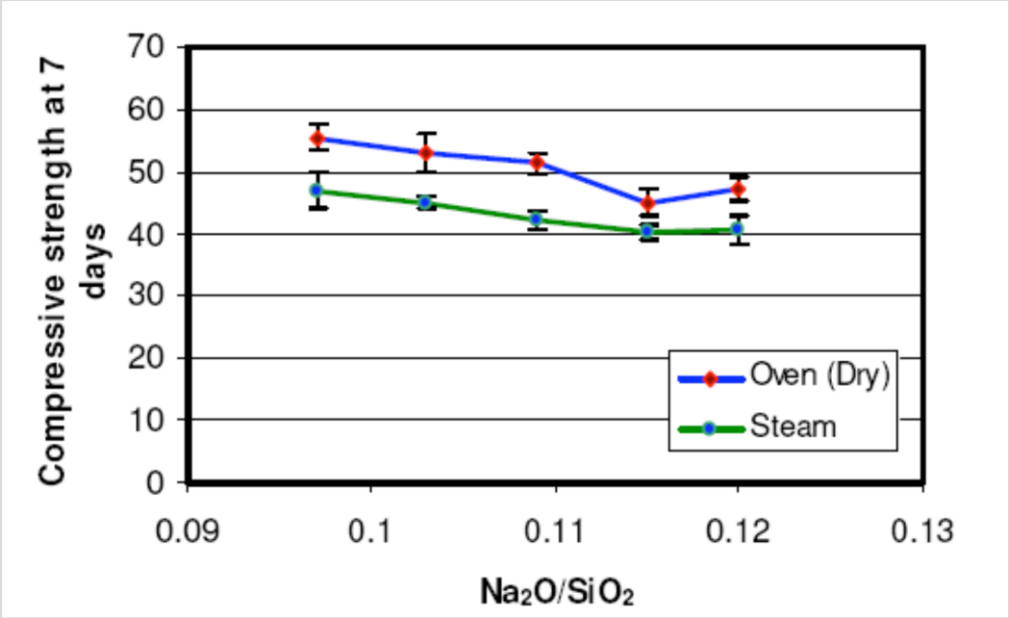

Figure 3-20 Impact on Na_2O/SiO_2 Mix Molar Ratio (Hardjito and Rangan, 2005)

Hardjito & Rangan (2005) study indicated that alkaline with higher molarity NaOH provided higher strength mix with consistent results when Na_2SiO_3/ NaOH ratio of alkaline solution is 2.5. Their research also indicated that H_2O/Na_2O mix molar ratio (which translates to water/ geopolymer solid binder ratio) influence the compressive strength as shown by Figure 3.21 (a) and (b) below.

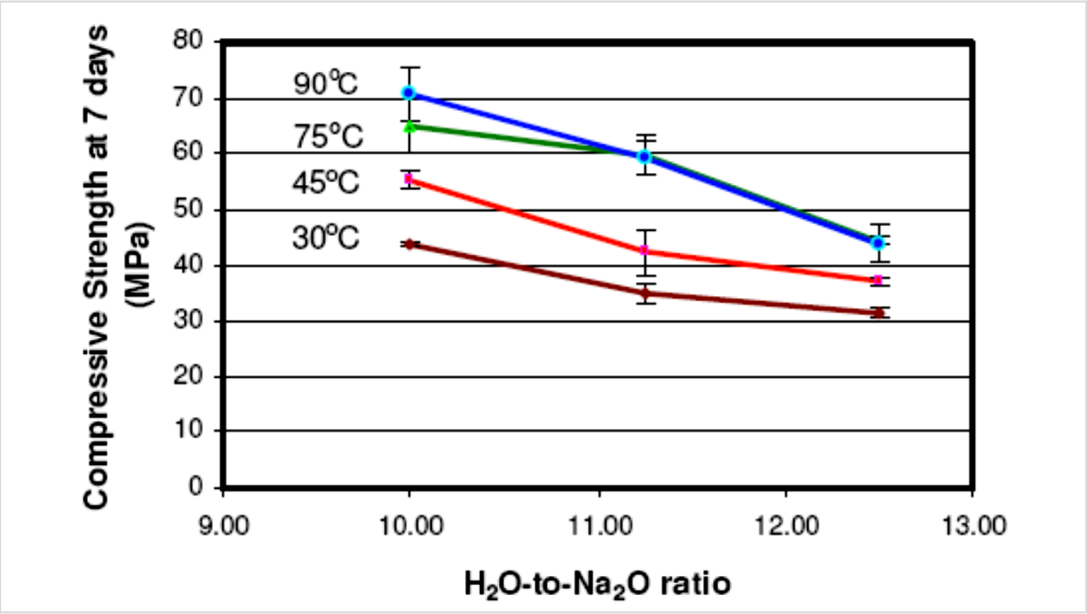

(a)

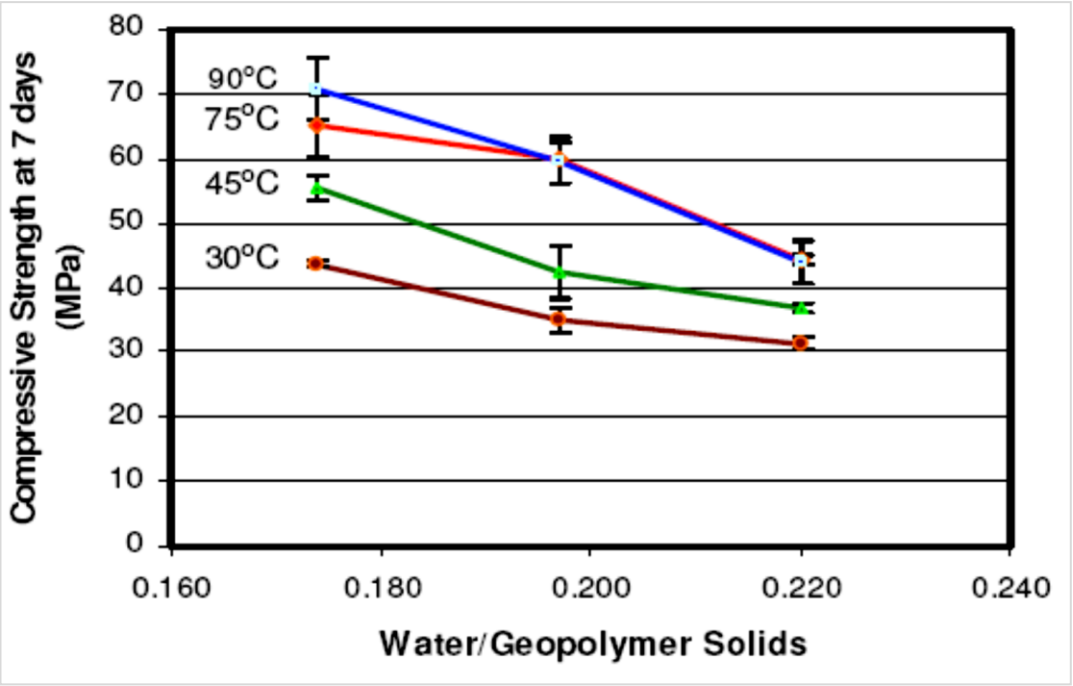

(b)

Figure 3-21 Water/Binder Ratio Influences - Hardjito and Rangan, 2005

Hardjito & Rangan (2005) further indicated that change in water content alone does not affect the compressive strength provided H_2O/Na_2O mix molar ratio is kept constant using different molarity NaOH & extra water.

Hardjito & Rangan (2005) showed that lower water content formulation has relatively higher strength. Sagoe-Crentsil & Brown (2006) study confirmed this trend and indicated that higher water content results more water filled pores in the system with higher porosity.

Followed on research showed some contradictory results. Bakri et al, 2011 observed that 12M NaOH shows more desirable results than higher molarity NaOH as shown below in Figure 3.22 from compressive strength perspective.

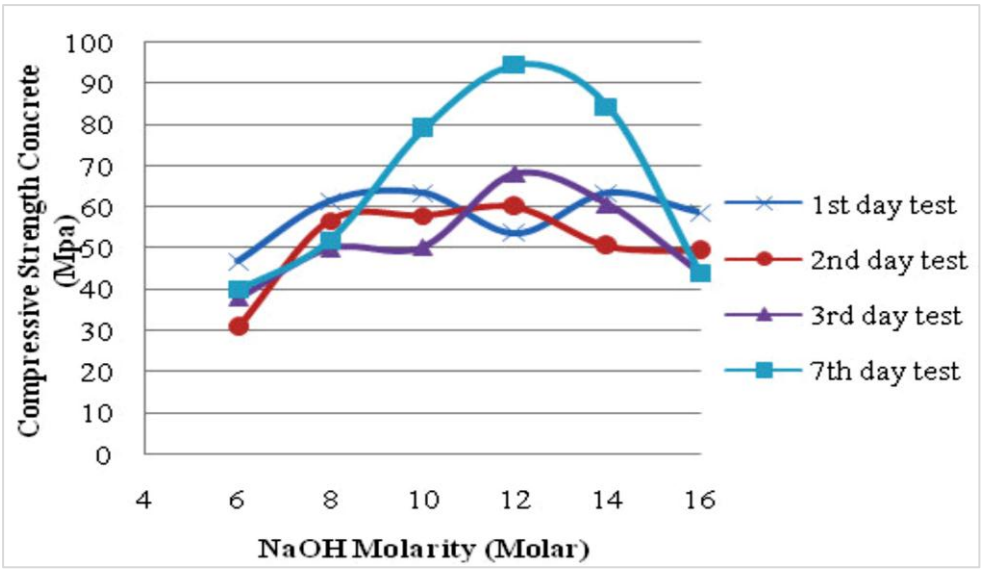

Figure 3-22 Compressive Strength Trend with Different NaOH Molarity (Bakri et al 2011)

Also Palomo et al (1999b) study showed that alkaline solution with 12M NaOH leads to better result than 18M. These contradictory results may need further research. Synthesis of mix molar ratios analysis from Hardjito & Rangan (2005) and mix molar ratios from Bakri's research as detailed in Chapter 6 provided some additional interpretive findings along with possible explanation of these contradictory results. Skvara et al (2006) showed that decrease of combined alkaline oxide percentage in LCFG concrete mix results larger size pore structure than the mix with higher percentage of Na_2O. Following Figures 3.23 (a), (b) & (c) show the impact of alkaline content, water/binder ratio and slag content on pore structure in relation to their sizes and distribution (Skvara et al, 2006).

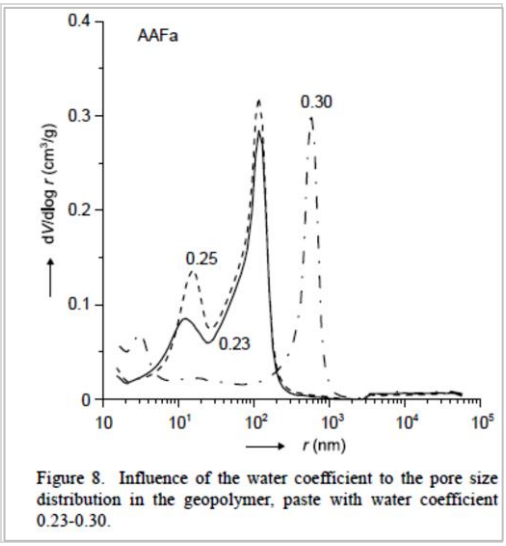

Figure 8. Influence of the water coefficient to the pore size distribution in the geopolymer, paste with water coefficient 0.23-0.30.

(a)

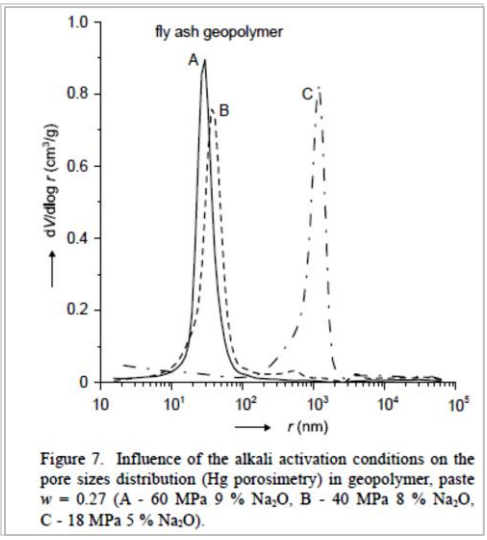

Figure 7. Influence of the alkali activation conditions on the pore sizes distribution (Hg porosimetry) in geopolymer, paste w = 0.27 (A - 60 MPa 9 % Na_2O, B - 40 MPa 8 % Na_2O, C - 18 MPa 5 % Na_2O).

(b)

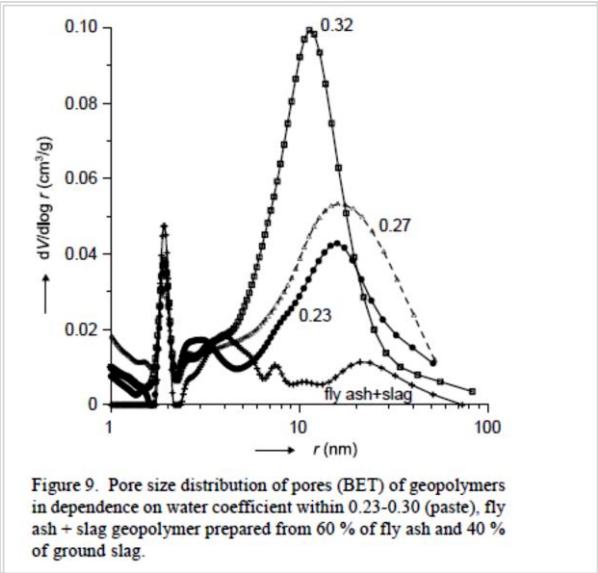

Figure 9. Pore size distribution of pores (BET) of geopolymers in dependence on water coefficient within 0.23-0.30 (paste), fly ash + slag geopolymer prepared from 60 % of fly ash and 40 % of ground slag.

(c)

Figure 3-23 Mix Parameters' Influences on Pore Structure (Skvara et al, 2006)

Skvara et al (2006) study showed that pore structure below 100nm are independent of the preparation conditions of the geopolymer concrete while pore structure with pore sizes above 100nm are affected by water coefficient and composition of alkaline oxide , Figure 3.23 (a).

Hardjito & Rangan's research (2005) has shown the decreasing trend in strength with Na_2O/SiO_2 mix molar ratio exceeding 0.1, while Skvara et al (2006) study showed its impact on the pore structure and pore sizes. That is, higher volume of finer pores results with higher percentage of Na_2O while lesser percentage of Na_2O results higher volume of pores with larger size as shown by Figure 3.23 (b) above.

Skvara et al (2006) study further showed that geopolymer concrete with fly ash & slag has lower porosity and higher strength. This may due to the coexistence of geopolymer & C-S-H phase resulting finer pores volume varying between 2% to 10% with pore radius less than 10nm and strength gain up to 95 MPa when cured at temperature between 60-90 ^oC as shown in Figure 3.23(c). Slag based fly ash geopolymer was with 40% slag and curing temperature was between 60-90^oC for 4 -16 hours in Skvara et al (2006) study.

Sagoe-Crentsil & Brown (2006) study showed the influence of variation of aluminate content of source material on compressive strength of LCFG concrete. The increase in Na_2O/Al_2O_3 mix molar ration from 0.6 to 1 increases the compressive strength by four fold. Sagoe-Crentsil & Brown (2006) study further showed that higher loading of aluminium content assist quicker condensation in the formulation leading to denser network structure and result removal of more hydroxyl groups.

This higher loading of aluminium may limit the development of gel phase constraining other solution species to condense in the growing geopolymer. Whereas low alumina concentration provides the formulation with large proportion of unreacted particles and low crystallinity with strength derived mainly from amorphous gel. An unreacted particle will tend to provide the concrete matrix of more porous nature. Palomo et al (1999) provided the explanation of its porous nature because of crust reaction product partially covering the fly ash microspheres particles as indicated in Figure 3.24 below.

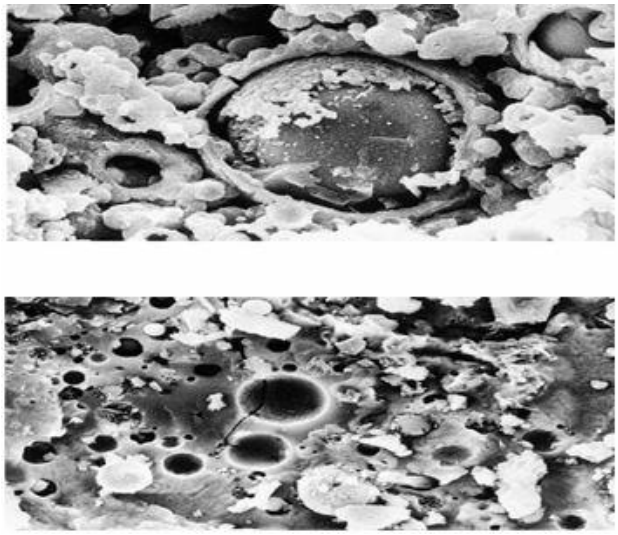

Figure 3-24 Geopolymer Concrete Reaction Products Image Palomo et al. (1999a)

3.6.2 LCFG Concrete Embedded Steel Corrosion & Electrochemical Responses

3.6.2.1 HCP

Olivia, 2011 research observed HCP vs. (Ag/AgCl standard electrode) on OPC and geopolymer concrete lollypop cylinder specimen with 16mm embedded steel bar in simulated seawater environments, that is, water having NaCl content up to 3.5%. Olivia (2011) LCFG mixtures for geopolymer concrete were with mix proportion as summarised in Table 3.9 below

Table 3-9 Optimum mixture proportion of fly ash geopolymer concrete (Olivia, 2011)

Mix	Aggregate content (kg/m3)	Alkaline/fly ash ratio	Ratio of Sodium Silicate/NaOH	Curing condition
T4	1896	0.3	2.5	12h 70^{o}C
T7	1800	0.3	2.5	24h 70^{o}C
T10	1848	0.3	2	24h 75^{o}C

Olivia's observations over duration of 90 days indicated the HCP vs. Ag/AgCl standard electrode ranges between 0-.200V to – 0.400V with its conversion referring to CSE as -0. 310V to -0.510V. Up to duration of one week HCP observation for LCFG concrete was -0.300V, which was within 10% probability of corrosion risk. However after one week HCP value for LCFG concrete exceeded -0.350V, which indicates the probability of corrosion risk up to 90% as per ASTM HCP criteria. These observations are evident from Figure 3.25 below.

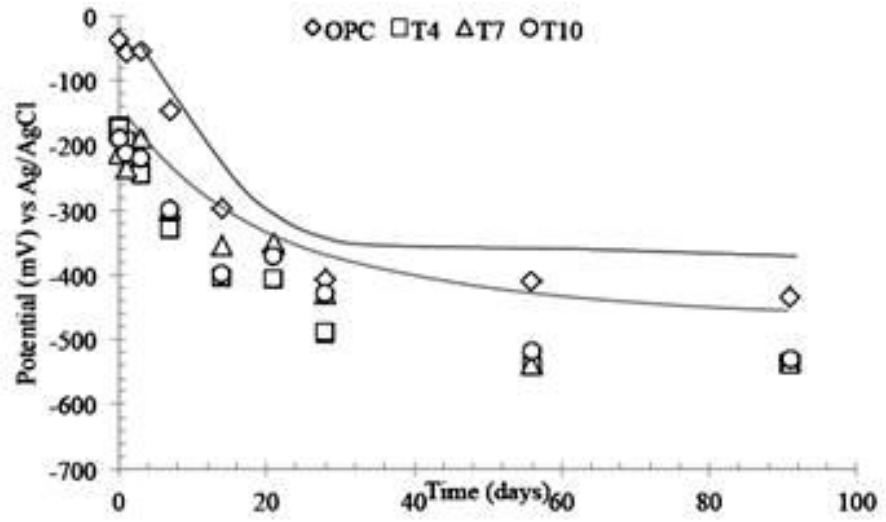

Figure 3-25 Half Cell Potential Observations (Seawater Exposure), Olivia. M PhD Thesis, 2012

Over 90 days duration HCP measurements for LCFG concrete was between -0.500 to -0.550vs Ag/AgCl (-0.610V to -0.660V vs. CSE) while for OPC concrete was between -0.300 to -0.350 vs. Ag/AgCl (-0.410V to -0.460V vs. CSE), as shown in Figure 3.25 above.

It appears from the test method the HCP measurements in Olivia's research study were on specimen immersed in seawater environments. Higher negative trend for both OPC and geopolymer concrete could be either due to the dissolved oxygen or due to the starvation of oxygen, which is undeterminable with this test technique.

Also HCP observations trend inferred by Andrews Phaedonos (2012) for alkali activated slag based goepolymer concrete mix in an outside drier environment, possibly non- aggressive to mild over two years approximately is shown in Figure 3.26 below.

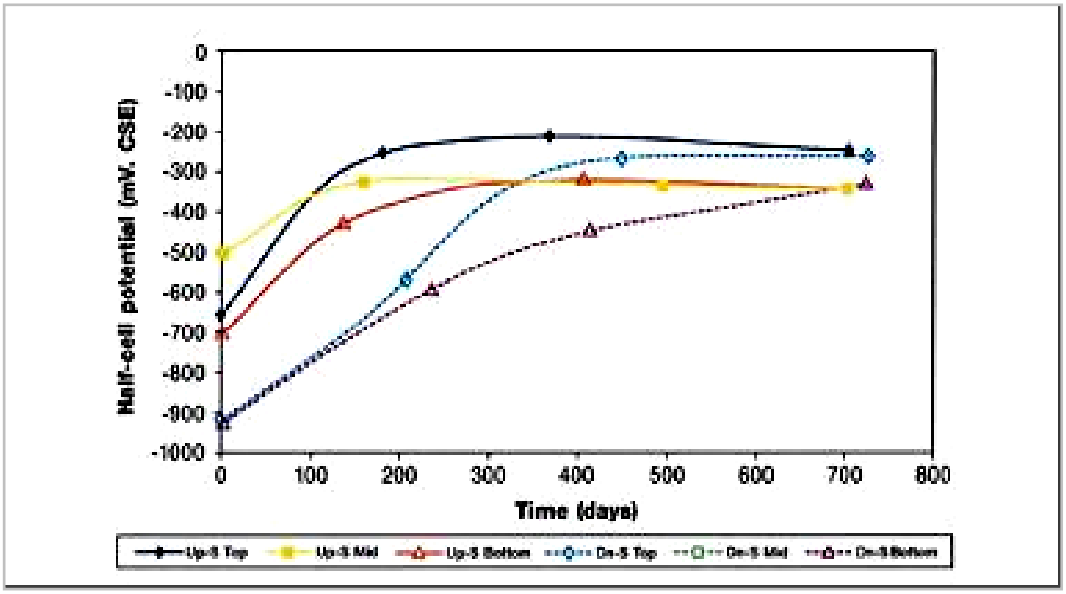

Figure 3-26 Half Cell Potential Slag Mixed Fly Ash Based Geopolymer Concrete

It is evident from Figure 3.26 that initial high corrosion risk probability shifted to low corrosion risk probability over a period of 2 years. This could be from the preventing action of corrosion products, acting as barrier around the steel bar as observed by Olivia (2011) research study.

3.6.2.2 Corrosion of Embedded Steel

For electrochemical properties Olivia (2011) undertook an accelerated corrosion test on 16mm partially bar embedded rebar and induced corrosion by using impressed voltage of 5V and 30V.

Olivia (2011 & 2009) undertook this accelerated test on preconditioned cylinder specimen (3 days in 3.5% NaCl water) before subjecting to the test requiring specimen to be immersed in water with seawater concentration.

Olivia (2011) inferred the LCFG concrete cylinder specimen cracked after 28days while OPC concrete cylinder specimen cracked after 17 days. as shown below in Figure 3.27(e) & (f) compared to OPC concrete. When the samples were not preconditioned LCFG concrete cylinder specimen took 200days to fail while OPC took 25 days. Figure 3.27 (a), (b), (c) & (d) below indicates current correlation over time.

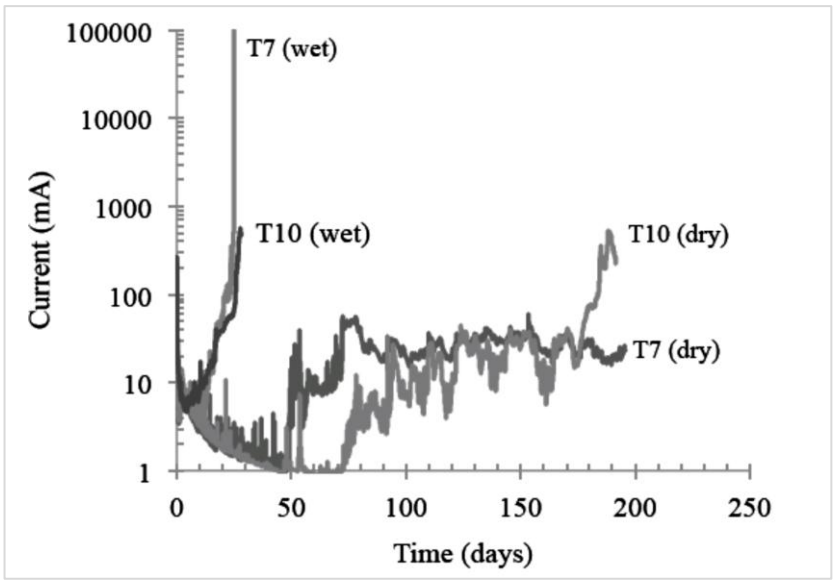

(a) LCFG Concrete

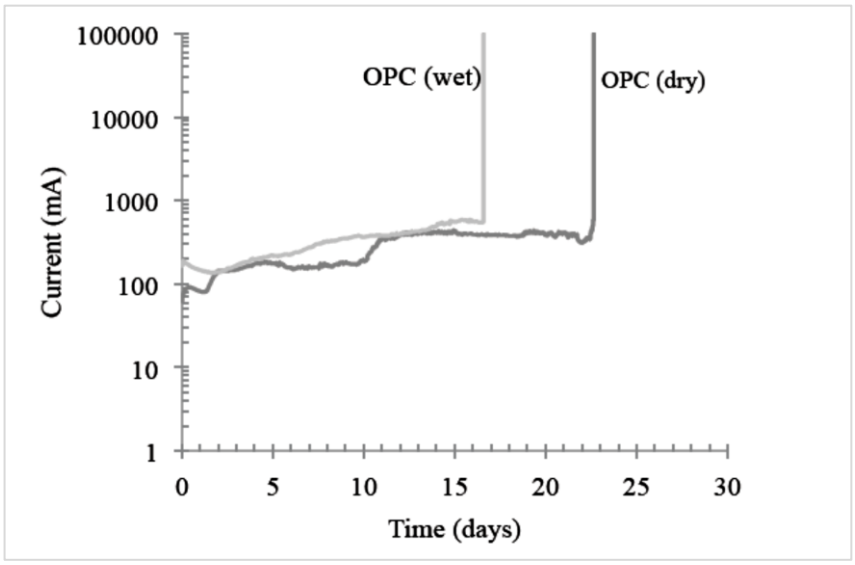

(b) OPC Concrete

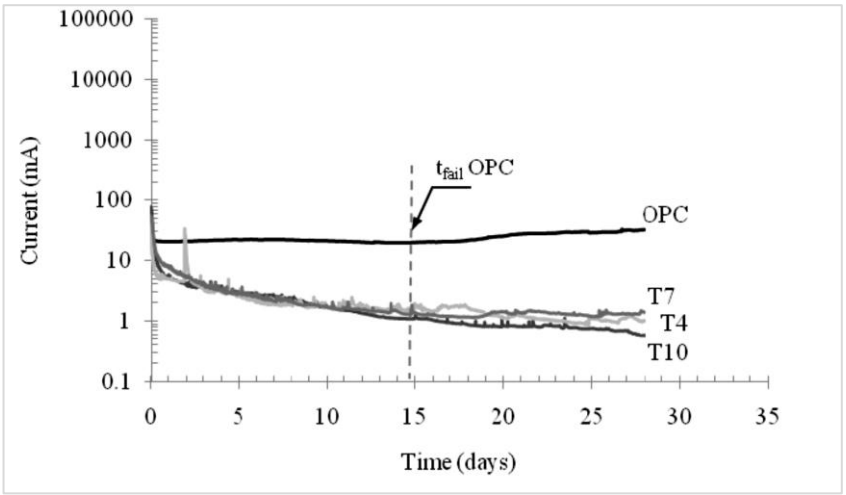

(c) 5v Impressed Voltage

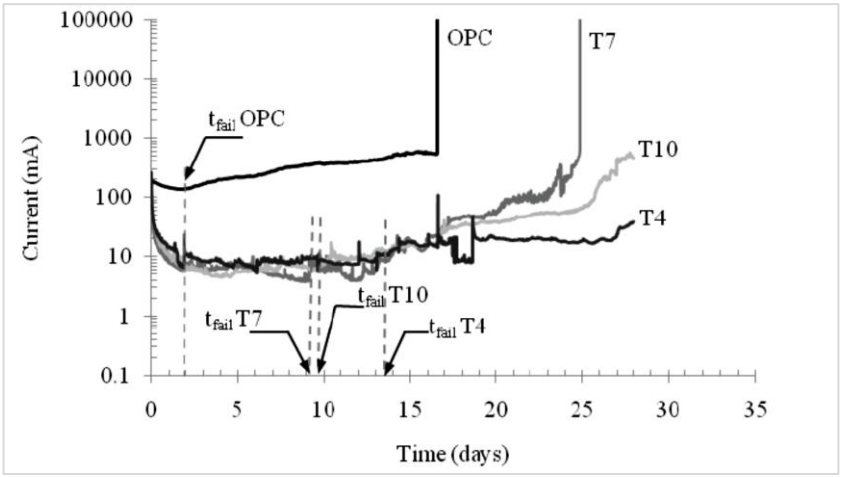

(d) 30 V Immersed Voltage

(e)Failed LCFG Concrete Cylinder

(f) Failed OPC Concrete Cylinder

Figure 3-27 Accelerated Induced Corrosion Test (Lolly Pop), Olivia M 2012

In current- time relationship for LCFG concrete as shown in Figure 3.27 (c) indicated decreasing trend with 5V impressed voltage over time, which however was lower than the one when impressed voltage was 30V as shown in Figure 3.27 (d) above.

CHAPTER 4 TEST PROGRAM AND TESTING METHODS

4 EXPERIMENTAL METHODOLOGY

4.1 INTRODUCTION

This chapter presents samples and specimens preparation as per mixture parameters detailed in Chapter 2 (Section 2.4), laboratory experimental set-up, field experimental set-up, laboratory testing work and test procedure to study the long term durability properties of LCFG concrete in comparison with OPC concrete.

Laboratory experimental set-up model was simulated to severe field environmental conditions as detailed in Section 2.4.3. The severe environmental exposures for both field and the laboratory simulated models represented buried, immersed and exposed scenarios. Severity exposure class of these field and laboratory simulated environments is referred as 'U' as per Australian Standard- 3600.

Following sections provide the detail on mix proportions of LCFG concrete & OPC concrete of equivalent strength, samples and specimen preparation, experimental set-up and test procedure.

4.2 ENVIRONMENTAL EXPOSURE CONDITIONS OF FIELD AND LABORATORY SIMULATED MODEL

Natural inland salt rich lake aggressive conditions model was chosen at Lake King, Western Australia for box culvert samples due to its hostile salinity environments. Appendix A shows the location of this field aggressive model. Box culvert samples were exposed to this severe field environment outside the road reserve in December 2009.

Approximate similar environmental conditions (buried, immersed and exposed) were simulated in the laboratory mimicking the field environmental scenarios of severe nature. A non –aggressive field environmental model was also chosen, which was at Main Roads, Material Engineering Branch yard. Physical and electrochemical behaviour of box culvert samples, laboratory samples and cylinder specimens for both LCFG concrete and OPC concrete in these aggressive and non-aggressive environmental models were investigated in this research.

In the field and laboratory models, exposure scenarios covered the following aggressive and non-aggressive conditions.

Aggressive conditions:

- Elevated chloride levels of brine nature for water in both field and laboratory simulated model.
- Severe levels of chlorides and sulphate for soil in both field and laboratory model.
- Exposed conditions in both field and laboratory models represented atmospheric CO_2, relative humidity(RH) of 50-70%, air borne salts, contaminants migration on account of capillary action, absorption, wicking action & evaporation under cyclic wetting & drying situations and occasional splashing on account of rising or lowering water level in both field and laboratory scenarios.

Non- aggressive conditions:

- External non aggressive conditions covered atmospheric CO_2, relative humidity (50-70%), airborne dust, salt and exposure to rainfall.
- Internal non –aggressive conditions covered atmospheric CO_2, relative humidity and protection from airborne dust, salt & rainfall.

Table 4.1 below summarises the exposure class of these possible scenarios as per AS 3600.

Table 4-1 Environmental Exposure Classes

Sample	Structural Material	Environments	Exposure Classification AS3600(Concrete)
Box Culvert &Laboratory Samples	OPC Concrete & LCFG Concrete	External , atmospheric exposure remote from coast and no saline ground	B1
Laboratory Samples & Specimens	OPC Concrete & LCFG Concrete	Dry and inside atmospheric exposure	A
Laboratory Samples & Specimens	OPC Concrete & LCFG Concrete	Dry and outside atmospheric exposure with regular inundation to severe saline water and aggressive soil for buried part	U
Field Box Culvert Samples	OPC Concrete & LCFG Concrete	Dry and outside atmospheric exposure with regular inundation to severe saline water and aggressive soil for buried part	U

The test results of both field environments and laboratory simulated conditions as summarised below in Table 4.2 showed the similar severity levels possible for studying the impacts of environmental actions on both LCFG concrete and OPC concrete from durability perspectives in this research.

Table 4-2 Concentration of Chloride and Soluble Salts of Field Severe Exposures

Sample Name	Chloride Content (ppm)	Total Soluble Salt Content (ppm)
Laboratory Model Water	152740	401790
Lake King Field Water	150080	468390
Laboratory Model Soil	181060	357200
Lake King Field Soil	157100	374000

As per Australian Standard (AS3600 & 2159) chloride content and total soluble content for both field and laboratory simulated model (water and soil) were classed as very severe. Figure 4.1 below shows the severity trend of water samples and soil samples from field aggressive and laboratory simulated severe environmental models.

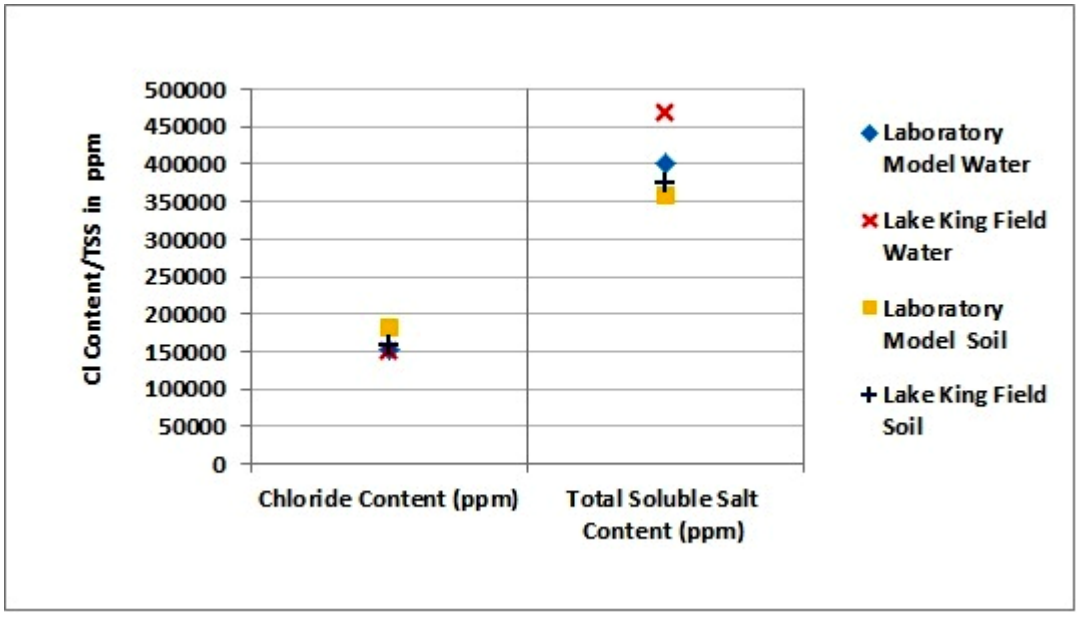

Figure 4-1 Severe Laboratory Simulated Model and Field Environmental Conditions

Experimental test observations under these aggressive field and simulated aggressive & non-aggressive environmental exposure conditions formed the basis of developing an understanding of LCFG concrete durability potential compared to OPC concrete in this research.

4.3 LCFG & OPC CONCRETE MIX CONSTITUENTS AND PREPARATION

Mix preparation for LCFG concrete involved measuring of various constituents in a specified proportion as detailed in Table 4.3 below. Coarse and fine aggregate were 77% of the unit weight of concrete (which has been taken as 2400 kg/m^3).

Remaining mass was split into alkaline liquid and fly ash with ratio as 0.35. An alkaline solution was comprised of sodium silicate of modulus 2 and sodium hydroxide solution in ratio of 2.5. Sodium silicate was sourced from PQ Australia of Grade A53 with its chemical composition as 29.4% of SiO_2, 14.7 % of Na_2O and 55.9% of water.

For G40 LCFG concrete, sodium hydroxide solution used was of 8M concentration containing 26.2% solid content and 68.6% water. For G50 LCFG concrete, sodium hydroxide of 14M with solid content of 40.4% and 58.5% water was used.

Both sodium silicate solution and sodium hydroxide were mixed 24 hours prior to use in dry mixed binder and aggregates. Both coarse and fine aggregates used were in saturated-surface-dry (SSD) condition.

The aggregate grading used for preparing laboratory samples and cylinder specimen comprised of 30% of 14 mm, 38% of 10 mm, and 32% of fine sand. This combined aggregate grading was for the manufacturing of pre-cast OPC small box culverts by ROCLA.

Dry mixing was for three minutes and wet mixing was for four minutes. Table 4.3 below summarises the mix proportions of LCFG concrete (G40) per cubic metre.

Table 4-3 LCFG Concrete Mixture Proportions

Stage	Item	Values	Unit	Remarks
1	Assumed Values for calculation			
	Total unit weight of the concrete	2400	kg/m^3	
	Mass of combined aggregates	77	%	
	Composition of aggregates	35% 14mm 35% 10mm 30% Sand	kg/m^3	
	Alkaline liquid to fly ash ratio	0.35	by mass	
	Ratio of sodium silicate to sodium hydroxide solution	2.5		
	Sodium hydroxide molar (26.2% solid and 68.6% water for 8M)*	8M		98% purity flake
	Sodium silicate modulus (55.9% water , 29.4%, SiO2 & 14.7% NaO2)	2 (SiO_2/Na_2O) = 2		A53
2	Mix Constituents Calculation (aggregate, Fly ash, Sodium Silicate, NaOH and Water			
	Mass of combined aggregates	77% x 2400 = 1848	kg/m^3	
	Mass of 14mm aggregate	0.35x1848=646.8	kg/m^3	
	Mass of 10mm aggregate	0.35x1848=646.8	kg/m^3	
	Mass of fine aggregate	0.30x1848=554.4	kg/m^3	
	Mass of fly ash and alkaline solution	2400-1848 = 552	kg/m^3	
	Mass of fly ash	552/(1+0.35) = 408	kg/m^3	
	Mass of alkaline solution	552-408 = 144	kg/m^3	
	Mass of sodium hydroxide solution	144/(1+2.5) = 41	kg/m^3	
	Mass of sodium silicate	144-41 = 103	kg/m^3	
3	Calculation of total water component its and ratio to solid (water to solid) and aggregate to solids ratio			
	Fly ash solid	408	kg/m^3	
	Water in sodium silicate solution	0.559x103 = 58	kg	
	Solids in sodium silicate solution	103-58 = 45	kg	
	Solid in sodium hydroxide solution	0.262x41= 11	kg	
	Water in sodium hydroxide solution	41-11 = 30	kg	
	Extra water	-	kg	
3.1	Assumed SSD water component			
	0.6% for 14mm	0.006x 646.8= 3.88	kg	
	0.7% for 10mm	0.007x646.8 = 4.53	kg	
	1.3% for sand	0.013x554.4= 7.21	kg	
	Total mass of water	58+30 + 3.88 +4.53 +7.21=103.62	kg	
	Total mass of solids	408+45+11= 464	kg	
	Water to solids ratio	103.62/464 = 0.22		
	Aggregate to solids ratio	1848/ 464 = 3.98		
*For 14M NaOH (40.4% solid & 58.5% water)				

High range water reducing (naphthalene sulphonate- based) super plasticiser was used in the mixtures at the rate 1.5% of fly ash to improve the workability of the fresh LCFG concrete (Hardjito and Rangan, 2005).

For conventional concrete only dry and wet mixing were involved. OPC concrete mix (S40 & S50) constituents are detailed in Appendix B.

Table 4.4 below summarise the mixture components for LCFG concrete and OPC concrete with their average compressive strength and slump test results.

Table 4-4 LCFG Concrete & OPC Concrete Mixture Proportions, Curing Regimes & Specimens' Strength

MIX	G40 Geopolymer		G50 Geopolymer		S40 GP		S40 GP + Xypex		S50 GP	
Sample No	08C 129		08C 130		08C 131		08C 132		08C 133	
Mean Strength (MPa)	54.50		54.00		55.00		56.00		58.50	
Batch 1 Strength (MPa)	58.00		50.50		54.50		55.50		62.50	
Batch 2 Strength (MPa)	51.00		57.00		55.50		58.00		54.50	
Range	7.00		6.50		1.00		2.50		8.00	
Slump	230.00		230.00		75.00		95.00		80.00	
Mix kg	**m3**	**50 L**	**m3**	**50 L**	**m3**	**50 L**	**m3**	**50 L**	**m3**	**50 L**
Cockburn GP					400.00	20.00	400.00	20.00	420.00	21.00
Fly ash	408.90	20.44	408.90	20.44						0.00
14mm	646.80	32.34	646.80	32.34	920.00	46.00	920.00	46.00	1052.00	52.60
10mm	646.80	32.34	646.80	32.34	300.00	15.00	300.00	15.00	247.00	12.35
Sand	554.40	27.72	554.40	27.72	640.00	32.00	640.00	32.00	525.00	26.25
Sodium Silicate	102.22	5.11	102.22	5.11						
NaOH	10.71	0.54	16.52	0.83						
Mixing water for NaOH	30.18	1.51	24.37	1.22						
Target Mixing Water	0.00	0.00	10.00	0.50	170.00	8.50	170.00	8.50	168.00	8.40
Unavailable SSD Water component	15.50	0.78	15.50	0.78	15.50	0.78	15.50	0.78	15.50	0.78
Total H_2O = NaOH (H_2O) + Na_2SiO_3(H_2O) + Extra H_2O	88	4.4	92.4	4.62						
S/P Grace Daracem Kg	6.13	0.31		0.31						
S/P Grace Daracem ml Batch 1									800.00	40.00
S/P Grace Daracem ml Batch 2									120.00	6.00
Xypex							2.00	0.10		
W/R Grace WRDA GWA ml					400.00	20.00	400.00	20.00	400.00	20.00
Target Water to Geopolymer Solids Ratio		0.19		0.19						
Actual Water to Geopolymer Solids Ratio		0.19		0.20						
Maximum Target Water Cement Ratio						0.43		0.43		0.40
Actual Water Cement Ratio						0.43		0.43		0.39
Water Added to bring Agg. to SSD										
Assumed SSD 0.6% - 14mm	3.88	0.19		0.19	5.52	0.28		0.28	6.31	0.32
Assumed SSD 0.7% - 10mm	4.53	0.23		0.23	2.10	0.11		0.11	1.73	0.09
Assumed SSD 1.3%- Sand	7.21	0.36		0.36	8.32	0.42		0.42	6.83	0.34
Total	15.62	0.78		0.78	15.94	0.80		0.80	14.87	0.74

Notes: Extra water was required for G50 mix to make mix workable enough to handle & place in moulds.

- Mixes were performed in two batches due to mixer size restraints all paired batches had the same batch details and samples were cured at 60 ^{o}C for 24 hours, OPC concrete samples were wet cured for 14 days and cylinder specimens for 28 days, S50 GP mix had superplastisiser adjusted to maintain the same slump & water cement ratio.
- Pore Blocking additive (XYPEX) dose rate is 0.5kg/100kg of cement for S40 and GP is general purpose cement

For LCFG concrete box culvert samples mixture proportions were with 8M and 10M NaOH and the detail is provided in Appendix C. For S40 and S50 OPC concrete mix, combined aggregates' grading envelope of ROCLA was used and its detail is provided in Appendix B The specifications of Main Roads Western Australia aggregates' grading envelope has also been included in Appendix B.

Table 4.5 below shows the summary of number of laboratory samples and specimen prepared in this research.

Table 4-5 Summary of Laboratory Samples

Specimen	**G40 (40MPa Geopolymer Concrete)- 08C-129**			**G50 (50MPa Geopolymer Concrete)- 08C-130**			**S40 (40MPa OPC Concrete)- 08C-131**			**Sx40(40MPa OPC Concrete with XYPEX additive)- 08C-132**			**S50 (50MPa OPC Concrete)- 08C-133**		
	Cover in mm			**Cover in mm**			**Cover in mm**			**Cover in mm**			**Cover in mm**		
	25	**35**	**50**	**25**	**35**	**50**	**25**	**35**	**50**	**25**	**35**	**50**	**25**	**35**	**50**
300x300x120mm with protruding steel for electro-chemical testings	1	1	1	1	1	1	1	1	1	1	1	1	1	1	1
300x300x120mm for coring, pH test, chloride profile test and qualitative visual test without protruding steel	1	1	1	1	1	1	1	1	1	1	1	1	1	1	1
Total reinforced samples	6 (Labeled as G40 & Cover Thickness)			6(Labeled as G50 & Cover Thickness)			6(Labeled as S40 & Cover Thickness)			6(Labeled as Sx40 & Cover Thickness)			6(Labeled as S40 & Cover Thickness)		
Cylinders 100x200mm) for compressive strength, VPV and diffusion test.	18 (Labeled as 129G - C1 to C18)			18 (Labeled as 130G- C1 to C18)			18 (Labeled as 131S- C1 to C18)			18 (Labeled as 132S- C1 to C18)			18 (Labeled as 133S- C1 to C18)		
*Box Culvert 1200x1200x 600 mm	G40/50 (50MPa) equivalent box culvert positioned at Lake King exposed to very severe field environments.						S40/50(50MPa) box culvert positioned at Lake King exposed to very severe field environments.								
*Box Culvert 1200x1200x600 mm	G40/50 (50MPa) equivalent box culvert positioned at MEB lab. site exposed to non-aggressive field environments.						S40/50 (50MPa) box culvert positioned at MEB lab. site exposed to non-aggressive field environments.								

LCFG box culvert samples steam curing regime at ROCLA plant site was in two stages at temperature varying between 60-80 ^{o}C. First stage steam curing was for 4 hours, which resulted initial strength gain in the order of 20MPa. This initial strength was adequate to free up the moulds. Second stage steam curing was for 20 hours.

Preparation of reinforced laboratory samples included six samples of size 300 mm x 300 mm x 120mm (approximately) depending upon the cover thickness to the reinforcement for each mix, which were as 25mm, 35mm and 50mm. Reinforced mesh used was of 8mm diameter at 10cm c/c spacing. Special moulds were prepared for reinforced samples (300x300x120mm) using timber and plywood as shown in Figure 4.2 below.

Figure 4-2 Mould for reinforced laboratory samples (300x300x120mm)

One set of three samples has protruding reinforcement bar, facilitating the assessment of electrochemical properties, such as, half-cell potential (HCP), linear polarisation resistance (LPR) measured galvanostatically using galvanostatic pulse measurements (GPM) technique and resistivity measurements during the study period of this research.

One set of samples was without protruding reinforcement for coring purposes and conducting other tests, such as, chloride profile, micro-structural & pore structure, pH, carbonation & visual assessment. Cylinder specimens were for compressive strength, diffusion and volume of permeable void (VPV) testing.

Laboratory samples were cast in two layers and vibrated using pin vibrator. Cylinder specimens were cast in two layers and vibrated using vibrating table. LCFG concrete samples were steam cured for 24 hours at 60^{o}C while OPC concrete samples were wet cured for 14 days using wet hessian. Cylinder specimens were wet cured for 27 days in lime saturated water at 23±2 ^{o}C. Figure 4.3 shows the image of reinforced laboratory samples before subjecting to the severe environmental exposures and samples with protruding steel with cover 25mm, 35mm and 50mm for each type of concrete for electrochemical testing.

25mm Cover to Reinforcement

35mm Cover to Reinforcement

50mm Cover to Reinforcement

(a) Laboratory Samples With Protruding Steel Bar For lectrochemical Testing

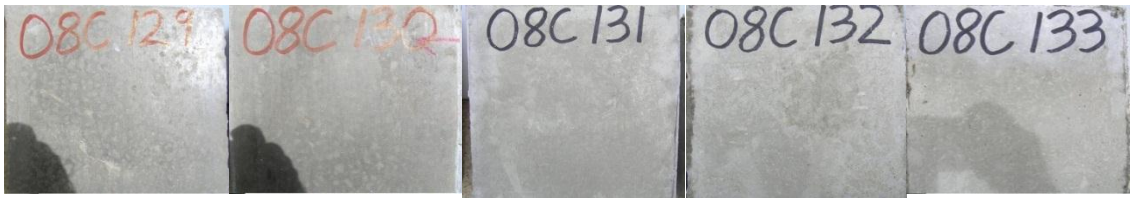

G40 **G50** **S40** **Sx40** **S50**

(a) Laboratory Samples without Protruding Steel for Coring to Test pH, Chloride Profile, Microstructure and Visual Testing

Figure 4-3 Laboratory Samples with Protruding Steel Bar and without Protruding Steel Bar

4.3.1 Laboratory Simulated Severe Environmental Exposure Model

Laboratory samples were exposed to laboratory simulated severe model in March 2009. The actual outlay of the laboratory simulated severe model is shown in Figure 4.4(a) and their schematic sketch is shown in Figure 4.4(b) below. Samples were positioned in a plastic tub containing 100mm submerged soil layer rich in $MgSO_4$ (20gm/100gm of soil) and 100mm water layer rich in NaCl (350g/L) and 100mm exposed part.

Simulated set-up for all samples represented three possible scenarios of environments normally feasible in the field: buried in salt rich soil (100mm); submerged in salty water (100mm) and exposed splash zone (100mm). To represent dry conditions during dry weather, salt rich water was syphoned out from the tubs for reuse during wet season. Concentrations maintained were 10 times stronger than the specified severe aggressive environment in AS 2159-2009 (ten times the sea water concentration).

(a)

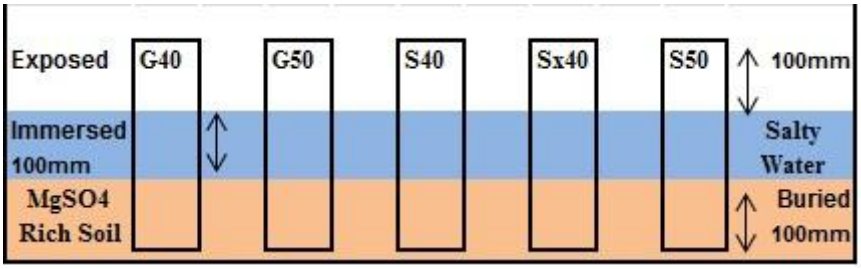

(b)

Figure 4-4 Schematic Sketch of Laboratory Simulated Severe Exposure

The simulated laboratory environments represented the severe field environments of an inland salty lake at Lake King, Western Australia at which one set of box culvert (comprising of LCFG concrete and its equivalent OPC concrete box culvert) was to be set up as detailed in the subsequent sub-section. One set of box culvert samples was to be set up in non- aggressive field environments to assess the impact of environmental exposures' severity as detailed in the subsequent section.

The research study acknowledges the limitations of the laboratory simulated aggressive model on account of variations that may be due to the temperature, relative humidity and absence of drifting wind & flowing water conditions, which may differ from the field aggressive environmental exposures.

4.3.2 Field Severe and Non-Aggressive Environmental Exposure Model

LCFG concrete box culvert samples prepared as a part of previous feasibility research study was installed at Lake King (an inland salty lake) outside the road reserve along with conventional concrete box culvert to study its long term durable properties under field environmental actions over three years. The installation of field model was in December 2009.

Lake King salty lake represents very severe aggressive environments (analogous to exposure conditions stated in AS3735 or Class U in AS3600). One set of box culverts comprised of LCFG concrete and OPC concrete was positioned at the Material Engineering Branch (MEB) laboratory yard exposed to non- aggressive and dry environments except some occasional wetting during wet season but without subjecting to any flow conditions.

Figure 4.5 below shows the set –up of box culverts samples exposed to severe aggressive environments in the field at Lake King, Western Australia.

Figure 4-5 Severe Field Environmental Exposure (Inland Salty Lake at Lake King)

Figure 4.6 shows the set-up box culverts in non – aggressive and dry environments at Material Engineering Branch (MEB) Laboratory yard at Welshpool, Western Australia.

Figure 4-6 Laboratory Simulated Non- Aggressive Field Environmental Exposure

4.4 TESTING METHOD & TEST PROCEDURE

Tests undertaken to determine the LCGF concrete durability properties and its comparison with conventional OPC concrete include:

- Compressive Strength (AS1012.9&12.1)
- Volume of Permeable Voids Test AS 1012.21 previously ASTM (C642-97)
- Chloride and Total Soluble Salts in Soil and Water (MRWA910.1)
- Capillary Suction Test (Non Standard)
- pH Value Test (AS1289, 4.3.1)
- Chloride Profile Test (BS1881:Part 124:1988)
- Chloride Diffusion Coefficient Test (NT Build 443)
- 3-D Tomography Test for Microstructure and Pore Structure
- Carbonation (Using phenolphthalein test & effervescing Interpretation with dilute HCL)
- Visual and Qualitative Test for Concrete Corrosion & Reinforcement Corrosion
- Electrochemical Testing:
    - Half Cell Potential (ASTM C876-91)
    - Concrete Resistivity
    - Galvanostatic Pulse Measurement test basing on linear polarisation resistance (LPR) principle- (Millard et al 2009 and Bromfield, 2007).
    - Passivation effect of silicate and its study using Scanning Electro- Microscopy (SEM) & Energy Dispersive X-rays (EDX) imaging.
- Visual and qualitative test for scaling of concrete and reinforcement corrosion.

Test method and test procedure are briefly described low.

4.4.1 Compressive Strength (AS 1012.9 & 12.1)

Prior to testing in accordance with AS 1012.9-1999, the samples were weighed and measurements of height and average diameter were taken. The cylinders were then applied with a sulphur capping. A compressive load was applied at a rate of 157 kN/min until failure was achieved.

The OPC concrete samples were tested at 28 days. The LCGF concrete samples were tested after 24 hours of steam curing followed by cooling down to room temperature. The mean strength is given in Table 4.4 above. Both LCFG and OPC concrete samples were subjected to simulated severe environments as detailed above and tested at yearly interval to assess the strength regression.

4.4.2 Volume of Permeable Voids (VPV)- AS1012.21 (ASTM C642)

The VPV test method has the ability to demonstrate the durable performance of various concretes. Because of its repeatability and reproducibility compared to other durability tests such as chloride diffusion, permeability and rapid chloride permeability, Vic Roads (Road Authority of Victoria, Australia) has introduced VPV test for structural concrete in their specification from durability perspective.

OPC concrete is sensitive to w/c ratio, water content, cementitious material content, compaction and strength grade (Andrew Phaedonos, 2001 & 2008 and ASTM C642) and for LCFG concrete water/ binder ratio is also critical (Hardjito & Rangan, 2005 and Wallah & Rangan, 2006) as such the test may be able to demonstrate the durable performance of LCFG concrete as well.

Past research studies have shown that concrete has porous structure with pores of sub-nanometre to many micro meters (Neville, 1995). These pores are comprised of capillary pore, gel pores, air voids and micro crack. The interconnected part of this pore system represents the volume of permeable voids (VPV) and is measured by test method A 1012.21.

Concrete with fewer permeable voids on the basis of VPV test means durable concrete with the ability to withstand aggressive environments. The test provides the measurement of the interconnected void space within concrete (i.e. capillary pores, gel pores, air voids and micro cracks).

Void space that can absorb water following normal immersion as a result of capillary suction represents capillary pores & gel pores while subsequent boiling represent pore system that may be due to air voids & micro cracks.

Brief description of the test method is as below. Cylinder specimen of each type of concrete was marked out and cut 50 mm from the top and 50 mm from the bottom leaving two 50 mm x 50 mm specimens from the middle and results were averaged between the two as shown in Figure 4.7 (a) & (b) below from cylinder specimens.

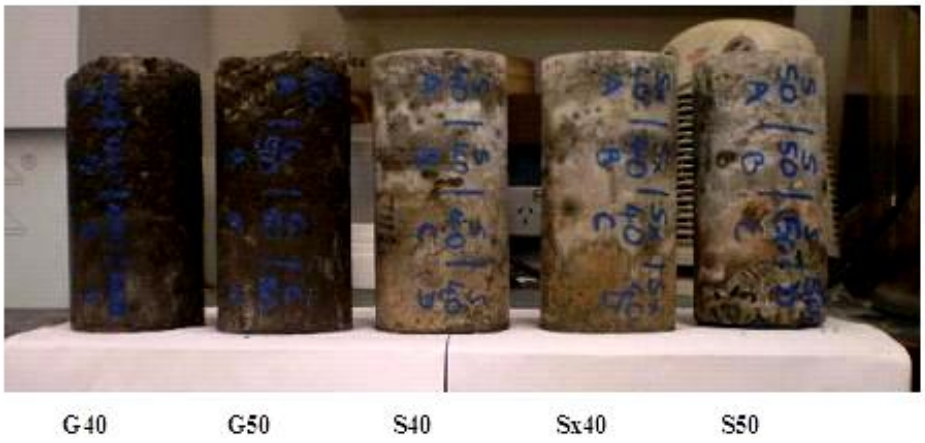

(a)

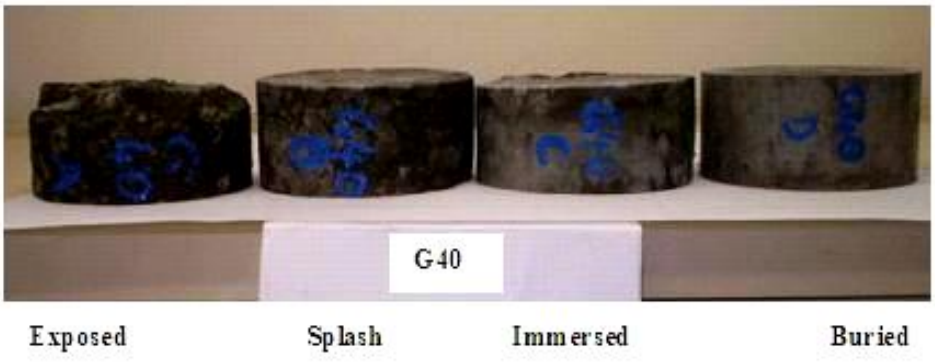

(b)

Figure 4-7 (a) & (b) Cylinder Specimens after Three Year Severe Exposure for VPV

Each specimen was placed in an oven at a temperature of 100-110^{o}C and their weight recorded after 24 hours. The specimens were returned to the oven for another 24 hours to ensure its reweighed recording did not differ more than 0.5%.

The oven-dry specimens were then immersed for 48 hours in water at approximately 21^{o}C. The specimens were surface dried for recording their weight. To ensure the variation less than 0.5% the weight of each specimen was recorded and returned to the water bath for another 24 hours to repeat the observation as indicated by Figure 4.8 (a) and (d) below.

Figure 4-8 VPV Test Process Steps

After obtaining the saturated weight the specimens were immersed in boiling water for 5 hours as shown in Figure 4.8 (c) above. The specimens were then allowed to cool, whilst still immersed, by natural loss of heat for at least 14 hours to achieve a temperature of 20-25^{o}C and their surface-dried weight were recorded. Finally their apparent mass was recorded in water by suspending after immersion and boiling as shown in Figure 4.8 (d) above.

Following calculations determined the density, percentage absorption and percentage volume of voids.

Absorption after immersion, % = [(B-A)/A] x100

Absorption after immersion and boiling, % = [(C-A)/A] x100 *Equation 4.1*

Bulk Density, Dry (t/m^3) = A/(C-D)

Bulk Density, After Immersion (t/m^3) = B/(C-D)

Bulk Density, After Immersion and Boiling (t/m^3) = C/(C-D)

Apparent Density (t/m^3) = A/ (A-D) *Equation 4.2*

Volume of permeable voids, % = [(C-A)/(C-D)] x100 *Equation 4.3*

Where:

A = Mass of oven dried sample (g)

B = Mass of surface-dry sample after immersion (g)

C = Mass of surface-dry sample after immersion and boiling (g)

D = Apparent mass of sample in water after immersion and boiling (g)

ρ = Density of water = $1 g/cm^3$

One VPV test was undertaken at the beginning before subjecting the samples to severe environmental exposures and one after the three years exposure period. Test output data is in Appendix D.

4.4.3 Capillary Suction Test

Cylinder specimen of G40, G50, S40, Sx40 and S50 were taken from the laboratory severe simulated model representing, buried, immersed and exposed environments after three year severe exposure period as shown in Figure 4.9 below.

Figure 4-9 Cylinder Specimen after Three Year Sever Exposure

Initial weight was recorded to determine the evaporable extent of water under driest and hottest temperature environment that could be possible in the field. The drying temperature of 48 ^{c}o. was maintained round the clock for two weeks. Change in mass was recorded at weekly interval. In order to have the uniformity of the cylinder specimen for capillary suction test, top 50mm and bottom 50mm of cylinder specimen of each concrete type was removed to have the uniform middle 100mm section of specimen for each cylinder specimen of LCFG concrete and OPC concrete as shown in Figure 4.10 below.

Figure 4-10 Cylinder Specimen for Capillary Suction Test (Middle 100mm)

The prepared 100mm specimens were further conditioned for 10 days at 48 ^{c}o. to make sure the evaporation of any moisture gained during wet cutting operation. Initial weight was recorded for each specimen before subjecting the specimen in small water tub with a constant water level maintained. Plastic strips were positioned in the water tub to ensure the bottom 5mm of each specimen is always in water over the test duration and not touching the tub as shown in Figure 4.11 below.

Figure 4-11 Capillary Suction Test Apparatus Set-up

Capillary suction observations were recorded at various times over the test period of 502 hours. Capillary water sucked was correlated to square root of the time period along with visual assessment. Test output data is in Appendix D.

4.4.4 3-D Tomography Test for Micro-structural and Pore Structure Properties

To understand the long term durability properties of LCFG concrete in comparison with OPC concrete, the study of microstructure, pore structure and porosity characteristics for both LCFG concrete and OPC concrete was undertaken using micro- tomography technique on cored samples taken from the laboratory samples which have undergone severe exposure for two years approximately.

Figure 4.12 (a) shows these core samples and Figure 4.12 (b) shows the image of the slice sample specimen of just over 2mm thickness for undertaking the microstructure and pores structure study using 3 – D Tomography for each type of concrete (G40, S40 & Sx40).

(a) - 75mm Cores

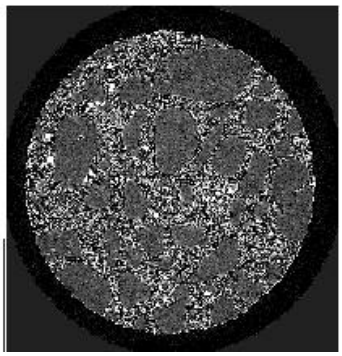

(b)- Slice Specimen Image from 75mm Core for 3-D Tomography Test

Figure 4-12- 75mm Cores for 3-D Tomography Test

Micro-tomographic data was collected at the bending magnet beam line (2-BM) at the Advanced Photon Source, Argonne National Laboratory, Chicago. A Si (111) monochromator provided 27 KeV X-rays; images were collected in transmission mode by a CCD camera behind the sample in the hutch configuration.

Contrast images in X-ray attenuation and reconstructed 3-dimensional images of the distribution of different phases in the sample were obtained. Data was collected through rotating the samples in steps of 0.125° over 180°. The acquisition time for each data set was about 25 minutes, which allowed for nine scans during the experimental run.

Three-dimensional models were reconstructed from 1440 tomographic projections/time step for all data sets using Advanced Photon Source in-house algorithms and facilities. Each reconstructed three-dimensional dataset is discretised into a stack of 1536 horizontal image slices with a vertical spacing of 1.3 microns, each image comprising 2048x2048 pixels in a 32-bit raw format. During 3-D rendering, these image slices are combined in a volumetric dataset consisting of 2048x2048x1536 voxel. The minimum effective pixel size achieved was 1.3 μm, yielding a volume of 2.2 μm^3 per voxel. All the datasets proved of excellent quality, with a minimum of noise and artefacts. Test output data is in Appendix D.

4.4.5 Ingressed Salt Test from Severe Exposure

This test is a non –standard and is an extension to the VPV test conducted after three year severe exposure for assessing the level of salt migration in each concrete specimen. The test involved the determination of total soluble salt content of the water used in the VPV test for immersion and boiling process of VPV cut specimens based on test method MRWA910.1. The volume of water used in VPV process steps was kept approximately constant for all concrete samples and test samples of used water from the VPV test were collected for testing. These samples are as shown in Figure 4.13 below.

Figure 4-13 -Collected Water Samples of Used Water from VPV Test Process

The test outputs were indicative of the water soluble free chloride and total dissolved salts level, LCFG concrete has been able to assimilate from severe environmental exposure compared to OPC concrete.

4.4.6 Chloride Profile Test (BS1881: Part 124:1988)

Past research has shown that total and free chloride profiles could be interpolated to a good approximation by Flick's Law (Sergi et al, 1992). The technique is specified as a general method for the determination of chloride ions by the Danish Standards Association (DS/R 239, 1978), the French Standards Association, AFNOR, (NF T 20-057, 1981) and the International Standards Organisation (ISO 6227-1982 - E).

The American Association of State Highway Testing Officers (AASHTO T260) and the American Society for Testing and Materials (ASTM C114) specify potentiometric titration technique for measuring the chloride content of concrete and concreting materials.

The test was undertaken at SGS laboratory using titration method with silver nitrate as the titrant, a chloride ion selective electrode and an automatic titrator. The digestion procedure is drawn from BS1881: Part 124:1988 which utilises concentrated nitric acid. The chloride penetration depth is measured by staining with silver nitrate.

A silver nitrate solution of (0.1M) was sprayed on the exposed surface which turns white due to the presence of chloride in the specimen and turns black in zone where chloride had not reached by measuring the depth of chloride penetration. From the chloride penetration profiles an estimation of diffusion coefficient can be derived which could be close to the one obtained using mathematical model curves (Flick's Second Law of diffusion theory).

The test was performed on core (75mm diameter) samples taken after first year, second year and third year exposures. First year test was to determine chloride ingress profile up to 25mm cover depth, second year was to up to cover depth 35mm and third year was up to 50mm cover depth in accordance with BS 1881: Part 124:1988" (Method for Analysis of Hardened Concrete Section 10.2), except titration by potentiometric method.

From the acid soluble chloride profile apparent diffusion coefficient (D_a) can be derived which does not take into account the chemical binding of chloride. The diffusion coefficient derived from free chloride concentration measurements is the effective diffusion (D_e) and represents non steady state (Cement Concrete Aggregate Australia (CA), 2009).

4.4.7 Chloride Diffusion Test (NT Build 443)

The Nord test is an accelerated test method for assessment of chloride diffusion into hardened concrete. It requires 28 days old concrete samples which are saturated and totally immersed in sodium chloride solution (simulated water with concentration up to 5 times of the seawater) for at least 35 days. The test assumes diffusion only from one side.

By fitting the experimental chloride profile to Flick's Second Law of diffusion equation, an effective diffusion coefficient can be obtained. Drilled cores from existing structures or cast concrete cylinders (at least 28 days old) are used. The top 10 mm of the cast surface is cut off because it is usually richer in cement paste than the interior.

The specimen is firstly saturated with water. All surfaces excepting the exposure surface are then sealed, and the specimen is immersed in a chloride solution for at least 35 days. The exposed surface is then carefully ground and the chloride content in the concrete is analysed (layer-wise). By fitting the experimental chloride profile to Flick's Second Law equation, an effective diffusion coefficient is obtained.

This test was undertaken at Australian Road Research Board (ARRB) laboratory at Melbourne, Australia. The diffusion coefficient derived from the total or acid soluble chloride profile accounts for both free and bound chloride and is the apparent diffusion coefficient (D_a), which then depends on time (t).

In a non-steady-state diffusion process, the gradient of the free chloride ions in the pore solution is the effective driving force. ASTM C 1556 describes the procedure of standard method for determining the apparent chloride diffusion coefficient of cementitious mixtures by bulk diffusion. The diffusion coefficient derived from free chloride or the water soluble chloride concentration profiles is the effective diffusion coefficient (D_e) and forms the basis of estimating future progress of the chloride penetration (Cement Concrete Aggregate Australia (CA), 2009, 2009).

Test outputs precision estimate of both apparent diffusion coefficient and surface chloride concentration from NT Build 443 test are based on precision data source of an inter-laboratory study of NORDTEST NT Build 443.

4.4.8 pH Value Measurement

The procedure for measuring pH value is as per AS1289, 4.3.1. The test is performed within the temperature range of 15-25 ^{o}C. The test procedure requires preparation of sample passing 2.36mm. To sieved sample of 30g, 75mL of deionised or distilled water is added and is stirred for few minutes followed by stilling for several hours.

Before testing, pH meter is calibrated using standard buffer solution and the prepared sample is stirred well. Readings taken should not differ not more than 0.05pH units. Procedure is repeated checking its calibration until consistent reading within 0.1 units is obtained.

4.4.8.1 Blended LCFG Concrete Mix

Due to low pH results experienced after first, second and third year of severe exposure respectively as detailed in Chapter 5.

A blended LCFG concrete mix was studied with a small proportion of slag to improve the pH level, which generally is expected above 12. This pH level maintains the oxide passivation oxide layer to protect the embedded steel from corrosion over the design life.

Secondly was to develop the LCFG concrete mix for in-situ applications with improved initial strength-gain under ambient curing regimes.

For blended LCFG concrete mix, slag was sourced from Cockburn Cement, Western Australia with chemical composition as summarised in Table 4.6 below.

Table 4-6 Slag Typical Composition (Cockburn Cement Western Australia)

Oxides	SiO_2	Al_2O_3	Fe_2O_3	CaO	MgO	SO_3	K_2O	Na_2O	Fineness	R332	+45µm
Ave Mass %	32.4	13	0.65	41.9	5.5	2.2	0.35	0.15	400	72.3	9.2

The mix proportion with 5% slag and 10% are given in Table 4.7 below. The cylinder specimen tested for compressive strength and pH value before and after the seawater exposure of one year.

Table 4-7 Mixture Proportions of Blended LCFG concrete

Modified Blended LCFG Concrete Mix Proportions with 5% Slag

Modified Mix with Fly Ash and Slag	Fly ash(409kg) - FA95%& 5%Slag	
Mix kg	Mix Quantities per m^3	1Cylinder 2 L
Cockburn GP		
Fly ash(409kg) - FA95%& 5%Slag	408.9	0.818
F/Ash (388.5kg)	388.5	0.777
Slag (20.5kg)	20.5	0.041
14mm	646.8	1.294
10mm	646.8	1.294
Sand	554.4	1.109
Sodium Silicate	102.2	0.204
NaOH(16M)	18.2	0.036
Water for mixing with NaOH	22.8	0.046
Target Mixing Water		
Additional Mixing Water		
Total H_2O = Batching H_2O+NaOh mixing H_2O + H_2O content of Sodium Silicate solution.		
S/P Grace Daracem Kg	6.13	0.012
S/P Grace Daracem ml Batch 1		
S/P Grace Daracem ml Batch 2		
Xypex		
W/R Grace WRDA GWA ml		
Target Water to Geopolymer Solids Ratio		
Actual Water to Geopolymer Solids Ratio		
Maximum Target Water Cement Ratio		
Actual Water Cement Ratio		
Water Added to bring Agg. to SSD		
Assumed SSD 0.6% 14mm	3.88	0.008
Assumed SSD 0.7% 10mm	4.53	0.009
Assumed SSD 1.3% Sand	7.21	0.014
Total	15.62	0.03

Modified Blended LCFG Concrete Mix Proportions with 10% Slag

Modified Mix with Fly Ash and Slag		
Mix kg	Fly ash(409kg) - FA90%& 10%Slag (Batch T3) Mix Quantities per m^3	Specimen Mix Quantity 1Cylinder 2 L
Cockburn GP		
Fly ash(409kg) - FA90%& 10%Slag	408.9	0.818
F/Ash (368kg)	368.0	0.736
Slag (41kg)	41.0	0.082
14mm	646.8	1.294
10mm	646.8	1.294
Sand	554.4	1.109
Sodium Silicate	102.2	0.204
NaOH(16M)	18.2	0.036
Water for mixing with NaOH	22.8	0.046
Target Mixing Water		
Additional Mixing Water		0.03
Total H_2O = Batching H_2O+NaOh mixing H_2O + H_2O content of Sodium Silicate solution.		
S/P Grace Daracem Kg	6.13	0.012
S/P Grace Daracem ml Batch 1		
S/P Grace Daracem ml Batch 2		
Xypex		
W/R Grace WRDA GWA ml		
Target Water to Geopolymer Solids Ratio		
Actual Water to Geopolymer Solids Ratio		
Maximum Target Water Cement Ratio		
Actual Water Cement Ratio		
Water Added to bring Agg to SSD		
Assumed SSD 0.6% 14mm	3.88	0.008
Assumed SSD 0.7% 10mm	4.53	0.009
Assumed SSD 1.3% Sand	7.21	0.014
Total	15.62	0.03

4.4.9 Blended LCFG Concrete Resistance for Seawater Exposure

Concrete specimens of blended LCFG concrete in continuously submerged, tidal zones and splash zones may deteriorate due to seawater exposure. This may result from chemical action, crystallisation & hydration of salts in pores near the surface in the splash zone & exposed zone causing scaling and eventual corrosion of steel reinforcement.

In order to study the effect of seawater on the durability of blended LCFG concrete, cylinder specimens (100x200mm) were used for this test. Cylinder specimens were immersed in water for one year with sodium chloride concentration of 3.5%, which is generally the seawater concentration. The assessed short term parameters from the test were - pH, change in length, change in mass, change in compressive strength and the extent of scaling as shown in Figure 4.14 below.

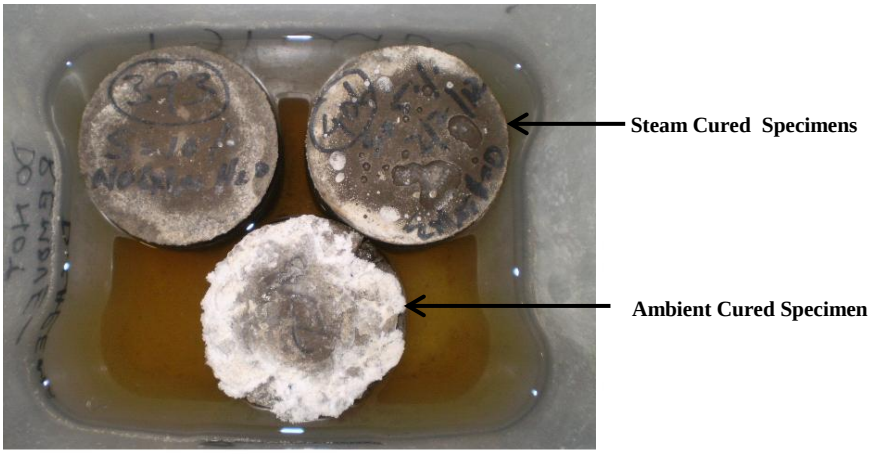

Figure 4-14 Blended LCFG Concrete Cylinder Specimens in Seawater

Test output on pH, compressive strength and scaling are detailed in Chapter 5.

4.4.10 Cored Specimens from Field Box Culvert Samples (Aggressive Environments) for Visual, Chloride Profile Test and pH

Box culvert samples were monitored over the duration of severe exposure for degradation extent visually and for concrete resistivity. Core specimens were obtained after severe exposure period of three years. Field coring of 70mm diameter was from each box culvert samples' leg and top slab. Each coring operation required a pilot cored hole of 20mm size for the attachment of coring machine to box culvert sample vertically and laterally as required. Ancillary units (trailed mounted water pump, generator and adequate traffic management) were essential to undertake the coring along with other safety and health requirements. Various coring extraction test process steps for obtaining core specimens are shown Figure 4.15 below.

Extracted core specimens were visually examined and a quick field test was undertaken on each extracted core specimen for pH assessment using chemical compound indicator phenolphthalein and phenolphthalein red.

Also the exposed and buried part of LCFG concrete box culvert and OPC concrete box culvert were examined qualitatively. Degradation extent of LCFG box culvert compared to OPC concrete box culvert visually over three year severe exposure period were examined from Figure 4.15 (c) and (d). An indicative pH level of both LCFG concrete and OPC concrete after three years of severe exposure were assessed from purple coloration images of core specimens after the application of chemical compound (phenolphthalein) as shown in Figure 4.15 (a) and (b) below.

Figure 4-15 Core Specimens from Field Box Culvert Samples (Aggressive Environments)

Core specimen from each box culvert sample leg (LCFG concrete and OPC concrete) were tested for chloride profile test (Test method - BS1881: Part 124:1988 as detailed under heading 4.4.6) and pH measurements were as per test method detailed under heading 4.4.8.

4.4.11 Carbonation

Test observations of neutralization extent were the mean of assessing the extent of carbonation front for each type of concrete in this research. The test was carried out using chemical compound phenolphthalein (application test) for indicating the carbonation front in the research study (Meyer, 1968). The validity of the carbonation theory, which is based on square root of time principle for OPC concrete, as given by expression below (Hamada, 1968) is assumed to be applicable for LCFG concrete in this research.

$$X \text{ (Carbonation Front)} = K\sqrt{t}$$

Where X is depth of carbonation, t is the exposure time and K is the constant depending upon the quality of concrete, concentration of CO_2, relative humidity (RH) and diffusivity of the concrete.

Extracted cores from the laboratory samples and field box culvert samples were tested for carbonation front with phenolphthalein compound and effervescing inference using dilute HCL for possible carbonation products. Possible inferences outcome and the factors supporting the carbonation in LCFG concrete compared to OPC concrete are detailed in Chapter 5.

4.5 ELECTROCHEMICAL TEST PROGRAM

4.5.1 Half Cell Potential (HCP) Test

According to ASTM Standard C876-91 (ASTM 1991), the corrosion potential measured against the copper sulphate electrode (CSE) gives an indication of the probability of the occurrence of active corrosion. The measurement of the corrosion potential with respect to reference electrode is the simplest measurement in a corrosion system. This can be done simply by using a voltmeter.

Test method has been in use since 1978 for detecting corroding reinforcement in concrete structures. At high pH, the Fe^{++} forms a complex protective film with oxygen. The potential drop is either because of the loss of passive film, which may be due to chlorides ingress causing active corrosion or due to lack of oxygen. Criteria of corrosion probability based on HCP (vs. CSE) are given in Table 3.4 in Chapter 3.

Test measurements can be used to identify regions where corrosion activity is probable. Inferences of corrosion probability of embedded steel in LCFG concrete in this research study are on the basis of criteria specified for OPC concrete (ASTM Standard C876-91). In certain scenarios it requires additional background details to make adequate interpretation as detailed in Chapter 3 (Section 3.4.1).

Synthesisation of HCP test data from this research study and data available in the literature of potential response of reinforcement in LCFG concrete assisted in developing HCP criteria for LCFG concrete and has been detailed in Chapter 5.

4.5.2 Resistivity

Four points Wenner probe resistivity measurement technique (Wenner, 1912), which was originally developed for geophysical evaluations. Based on the principles of soil mechanics, the probing technique is used for measuring the surface resistivity of the concrete. A low magnitude AC current, typically 30-60 Hz, is passed between two outer surface electrodes. A measurement of the potential between two inner current electrodes gives an evaluation of the electrical resistivity of the concrete in the surface region. The current is carried by the ions of pore solution and resistivity is given by:

Resistivity, $\rho = 2\pi aV/I$ in kΩcm. (Millard & Sadowski, 2009)

Where:

- 'a' is distance of electrodes (Industry standard is 50mm spacing and AASHTO standard for "Surface Resistivity Indication of Concrete's Ability to Resist Chloride Ion Penetration" is 38mm)
- V is the voltage between potential electrodes
- I is the magnitude of current

The equipment known as RESIPOD from PCTE was used to measure the resistivity measurements as shown in Figure 4.16 below. The method does not measure the rate of corrosion.

A low resistivity implies that reinforcement corrosion is occurring and the rate is likely to be relatively high. The use of a resistivity measurement together with half-cell potential mapping provides an indication of the location and likely severity of corrosion problems. Chapter 3 (Section 3.4.2) provides the relevant detail on resistivity measurements significance.

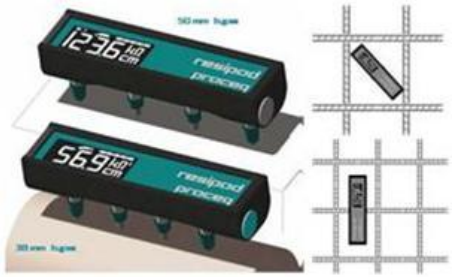

Figure 4-16 RESIPOD (www.pcte.com.au)

4.5.3 Galvanostatic Pulse Measurement (GPM) Test

A Galvanostatic Pulse measurement (GPM) is a linear polarisation resistance (LPR) measurement technique and gives corrosion rate, HCP and as well resistance between the hand - held electrode placed on the concrete surface and the reinforcement (Millard & Sadowski, 2009).

GPM distinguish between the active corrosion and lack of oxygen situation. Both controlled potential (potentiostatic) and controlled current (galvanostatic) polarisation are useful. When polarisation is done galvanostatically, potential is measured and when the polarisation is done potentiostatically, current is measured (Broomfield, 2007)

GPM measures the potential. The equipment requires electrical continuity in the reinforcement and makes corrosion rate assessment possible within a short time typically 10 seconds. The GalvaPulse™ works by inducing a short duration anodic current pulse into the reinforcement galvanostatically from a counter electrode placed on the concrete surface together with a reference electrode.

Small electrical potential in the order of 10-20 mv applied to the corroding reinforcement provides the linear relationship between applied potential and the current. The polarising resistance R_p is ratio of applied potential and resulting current and is inversely proportional to the corrosion rate.

To be able to measure the corrosion rate, the electrode of the GalvaPulse™ has a “Guard Ring” to confine the current to an area equivalent to the central counter electrode, as shown in Figure 4.17.(Baessler, et al- Federal Institute for Material Research & Testing, Berlin/Germany) below.

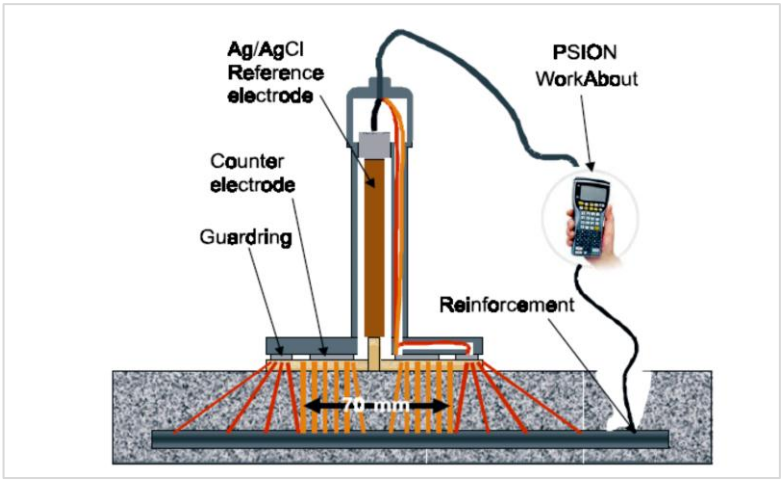

Figure 4-17 GPM Equipment (Baessler R et al, Federal Institute for Materials Research and Testing (BAM), D-12200 Berlin / Germany)

The Guard Ring is indispensable for the system in order to measure the effective polarization resistance and convert this to a corrosion rate. Without the Guard Ring the area of the counter electrode would be much smaller than that of the working electrode (the reinforcement) and the electrical signal would have a tendency to vanish with increasing distance (cover).

The numerical result obtained by fitting corrosion data to model is generally the corrosion current (Icoor) which is used to calculate the corrosion rate, that is, how much steel gets dissolved in a year in mm/year. The principal of LPR is based on small perturbation by applying DC electrical signal ΔI with respect to a reference half cell, to a corroding steel bar using surface counter electrode as shown below in Figure 4.17 (Millard & Sadowski, 2009; and Baessler et al).

The resulting change in potential, ΔE is measured. The change in electrode potential is related to corrosion current (Stern-Geary equation). The change in potential must be kept to less than 20mV or so for the equation to be valid and remain linear (Broomfield, 2007). A plot of change in current vs. change in potential provides the gradient of polarisation resistance to calculate the steel section loss rate. The polarisation resistance is given by the expression:

$$Rp = \Delta E / \Delta I$$

And the corrosion Current density is given by the expression:

$$Icoor = B/Rp$$

Where B is a constant and its value is 26 -52 mV in concrete depending upon the passivity or active state of the embedded steel and Rp is the polarisation resistance in ohms with an allowance for solution resistance drop (Broomfield, 2007) .

The corrosion rate in μm/year is given by the expression (Broomfield, 2007) as X = 11x106B/ Rp.A, where A is the surface area of the steel measured in cm^2. Corrosion current observations as given in the Table 4.8 below are for quick assessment of corrosion risk with GPM (Broomfield, 2007)

Table 4-8 Corrosion Risk based on Corrosion Current with GPM

Measurement of Icoor in $\mu A/cm^2$	Corrosion Rate
<0.1	Passive Condition
0.1-0.5	Low to Moderate Corrosion
0.5-1	Moderate to high
>1	High

4.5.4 Silicate Passivation Effect

Passivation effect of silicate to reinforcement was studied in this research by undertaking non- standard test by electroplating silicate layer on 8mm steel reinforcement for various time periods of 60 min, 45 min, 30 min and 15 min and to test the hypothesis in the literature that silicate has passivation effect. The silicate passivation effect can be compensating to the inconsistency of oxide passive layer formation (Ovchiyan, 2003). The inconsistency of oxide passive layer formation may be expected in hardened LCFG concrete on account of pH depletion in early dissolution & condensation phases followed by short term heat curing regimes.

Silicate film deposition on steel sample was undertaken using potentiostat operating galvanostatically. The technique requires the application of constant current through working electrode of an electrochemical cell and measure the potential of working electrode as a function of time relative to the reference electrode.

For each test duration one steel sample used was cleaned with dilute HCL and one with Ethanol to assess the impact of any existing surface deposits which could be chemically bound, such as, oxide film. Steel samples of 80mm length were used as working electrode. An immersed part of each sample in sodium silicate (Grade A53) solution was 55mm with surface area of 13.8 cm^2 (i.e. 5.5πD , where D is diameter of the steel sample) and exposed part was 25mm. Various test process steps are shown in Figure 4.18 below.

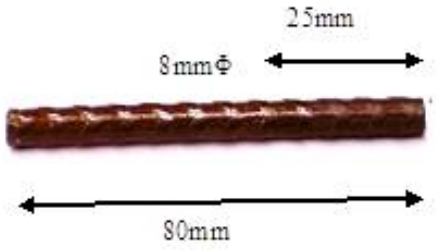

(a) Steel Sample (working Electrode)

(b) Counter Electrode (Titanium mixed metal Oxide)

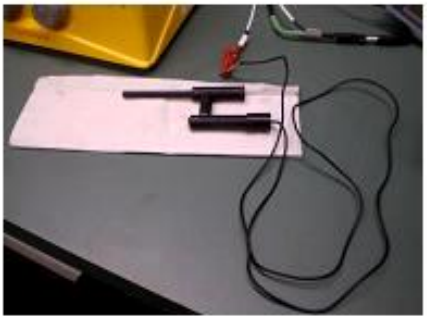

(c) Reference Electrode(Mercury Oxide)

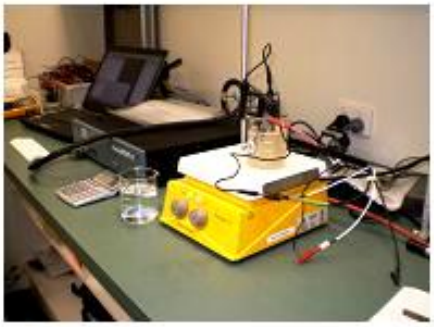

(d) Connection to Potentiostat

Figure 4-18 Silicate Coating Electrochemically

Current density applied was 0.1μA/ cm^2 maintaining a constant current value of 1.4 μA. Qualitative analysis of coated steel samples with silicate film was undertaken by using Scanning Electron Microscopy (SEM) and Electro Diffraction X- rays (EDX) imaging (Cheema, 2011) and is detailed in Chapter 5.

CHAPTER 5 RESULTS AND DISCUSSION

5 EXPERIMENTAL RESULTS

5.1 INTRODUCTION

This Chapter presents the experimental results of testing undertaken for understanding the long term durable properties of reinforced LCFG concrete compared to OPC concrete. The durable properties studied covers pore structure, porosity, diffusivity, resistance to chemical attack, carbonation, pH of pores' electrolyte and electrochemical responses of embedded steel from corrosion perspective inclusive of visual assessment under environmental exposures (aggressive and non- aggressive). Following sections present the experimental results along with possible explanations.

5.2 COMPRESSIVE STRENGTH AND DENSITY RESULTS

LCFG concrete and OPC concrete cylinder specimens' compressive strength and density trend of trial mix is shown in Figure 5.1 (a) and (b) before subjecting to severe laboratory simulated environmental exposure model. Two cylinder specimens of each type of concrete were tested for compressive strength (labelled as: 129GC1 & 2, 130GC1 & 2, 131SC1 & 2, 132SC1 & 2 and 133SC1 & 2). Average compressive strength test results confirmed the strength and density trend of Hardjito & Rangan (2005) & Rangan (2008) research for LCFG concrete.

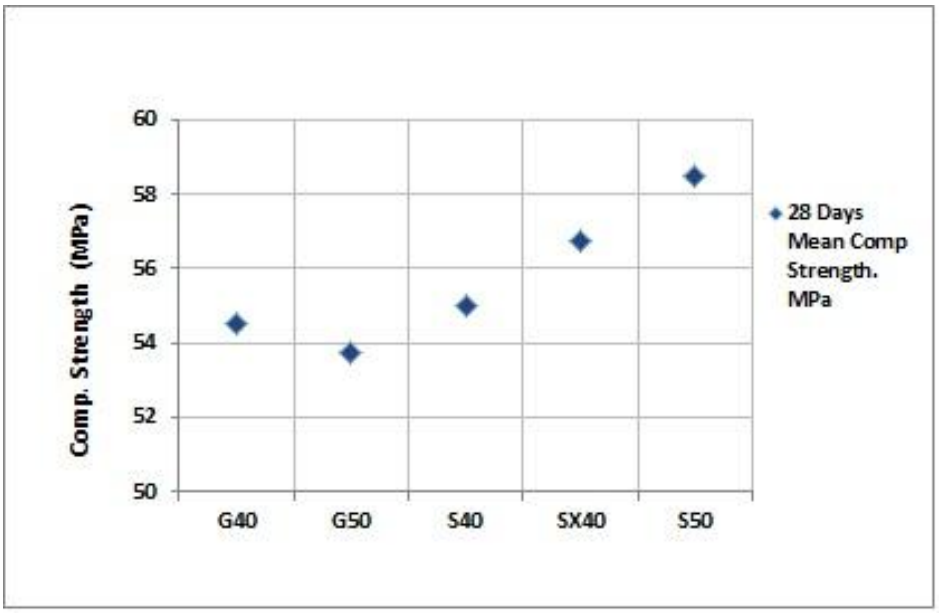

(a)

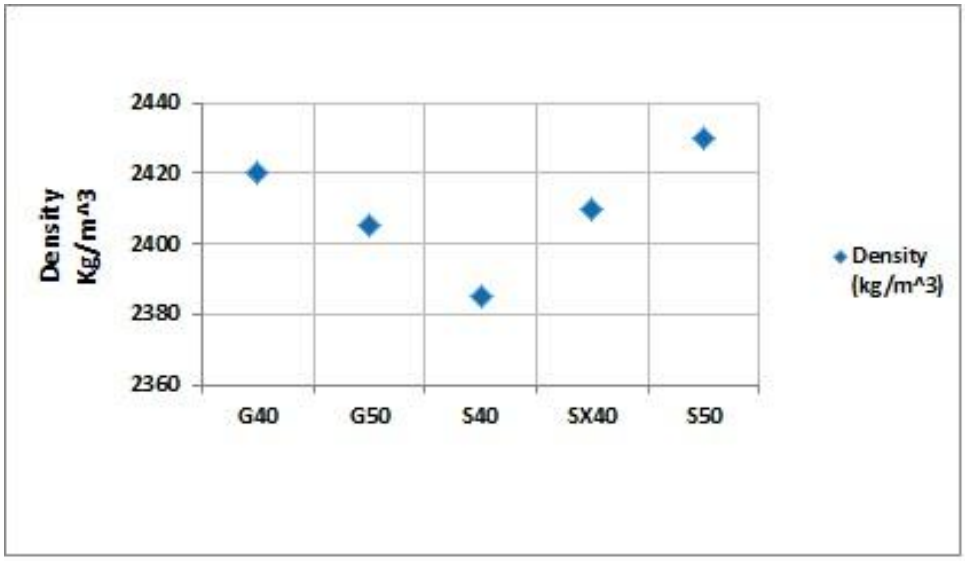

(b)

Figure 5-1 Compressive Strength & Density Trend before Severe Environmental Exposure

These cylinder specimens were subjected to the laboratory simulated severe environmental model along with reinforced laboratory samples of size 300x300 x120mm for each type of concrete for assessing the long term durability properties in combination with environmental exposure.

5.2.1 Compressive Strength after 1 to 3 Years Exposure

Figure 5.2 below shows the yearly mean compressive strength trend over three years of severe exposure. Cylinder specimens labelled as: (129GC5 & 6, 130GC5 & 6, 131SC4 & 5, 132SC5 & 6 and 133SC5 & 6 were tested after one year severe exposure), (129GC7 & 8, 130GC7 & 8, 131SC6 & 7, 132SC7 & 8 and 133SC7 & 8 were tested after two year severe exposure and (129GC9, 10 & 11, 130GC9, 10 & 11, 131SC8 & 9, 132SC9 & 132SC10 and 133SC9 & 10 were tested after three year severe exposure).

The compressive strength test results indicated an increase of 8% for G40 and 7% for G50 in first year of exposure compared to slight falling trend for S40 & S50 (which was 2% and 3% respectively). Sx40 showed gain in strength over the first year of severe exposure by 4%.

However falling trend over the second and third year was observed for LCFG concrete (that is, 6% drop in second year and 33% drop in third year from the initial attained strength for G40, while the respective drop in compressive strength for G50 drop was 10% and 36%).

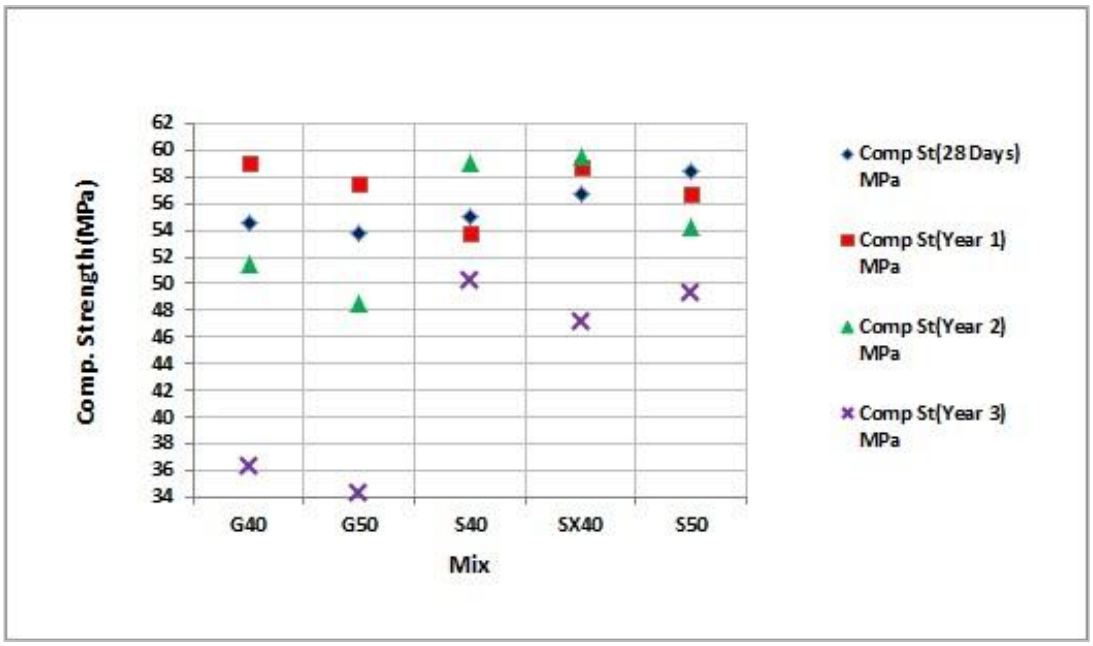

Figure 5-2 Yearly Compressive Strength Trend over Three Years of Severe Exposure

Different compressive strength trend was observed for S40 over the second year and third year. Strength increased by 7% in second year followed by falling trend in third year by 9%.

However decreasing trend in compressive strength was observed for S50 over all the years, that is, 3% in first year, 7% in second year and 16% in third year. For Sx 40, strength increased in first two years by 4-5% followed by falling trend in third by 17%.

Strength regression trend was consistent for both LCFG concrete and OPC after 2 years of severe exposure period, however the strength falling trend for G40 was 3 times more than S40 and 2 times more than Sx40. The strength falling trend for G50 was 2 times more than S50.

5.3 Visual Observations after Exposure – Laboratory Exposure

Figure 5.3 below shows the cracking pattern of G40, G50, S40 & S50 cylinder specimens. LCFG concrete cylinder specimen cracked part was predominantly from the top (degraded exposed part) while for OPC concrete, cracked part was from lower part (buried & degraded part).

Cylinder Specimen	Cracking Pattern after One Year Severe Exposure
G40(129GC5&6)	
G50(130GC5&6)	
S40(131SC4&5)	
S50(133SC5&6)	

Figure 5-3 Cracked Patterns of Cylinder Specimens after First Year severe Exposure

Above compressive strength results in combination with the severe environmental exposure scenarios indicated the different failure behaviour for LCFG concrete and OPC concrete. It was inferred that exposed part of LCFG concrete components under severe environmental exposures (comprising of exposed, immersed and buried scenarios) has more degrading tendency than OPC concrete. As a result LCFG concrete has lower residual strength compared to OPC concrete from long term durability perspective.

5.4 VOLUME OF PERMEABLE VOIDS

5.4.1 Volume of Permeable Voids (VPV) Test Results

The volume of permeable void test was undertaken on cylinder specimens (labelled as: 129GC4, 130GC4, 131SC3, 132SC4 & 133SC5) before their exposure to severe environments. The second VPV test was undertaken cylinder specimens (labelled as: 129GC12, 130GC12, 131SC10, 132SC11, and 133SC11) after three years of severe exposure period. Figure 5.4 below indicates the percentage of density, absorption and voids trend before and after three years severe environmental exposure.

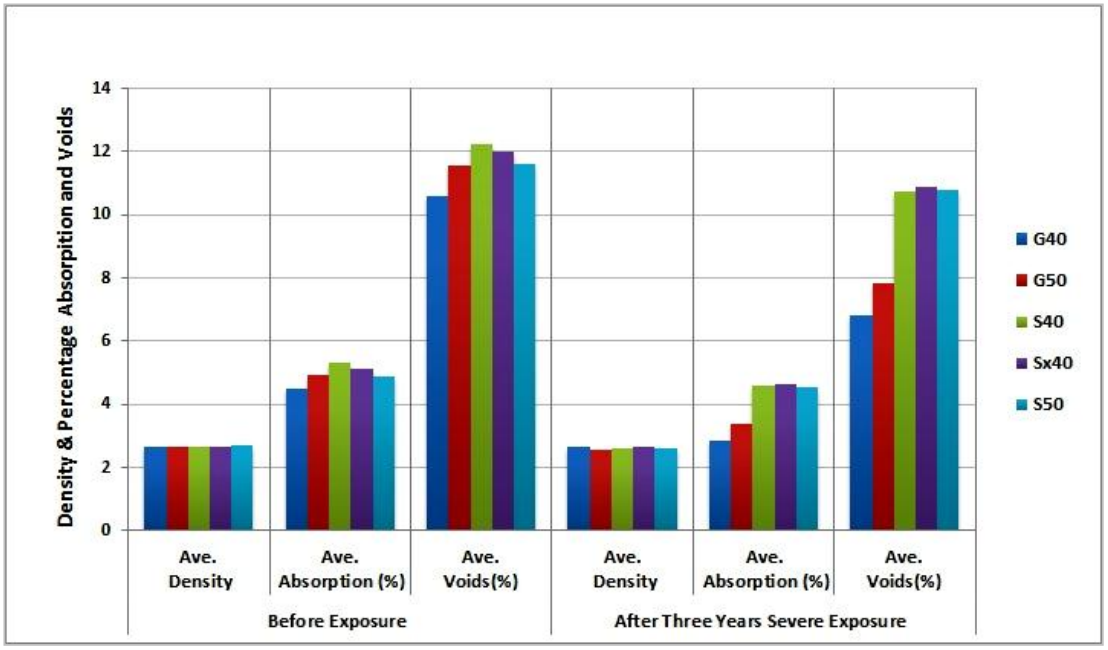

Figure 5-4 Volume of Permeable Voids Trend before and after Three Years Severe Exposure

Figure 5.4 above reveals that percentage absorption & voids dropped after three years severe exposure for LCFG concrete by more than 35% compared to OPC concrete where the respective drop for OPC concrete was in the order of 8%. This higher level of permeable voids drop in LCFG concrete compared to OPC concrete may be either due to the reduction in pore sizes from ingressing salts or through partial blockage of fine pores.

The inference of higher percentage of voids' drop compared to OPC concrete indicates that LCFG concrete may have large number of pores affected by salts' ingress allowing higher level of ingressing chloride and of continuous nature probably. The lower drop in OPC concrete's voids could be due to the presence of discontinuous pore restricting the ingressing salts.

5.4.2 Analysis of Pore Solution Water

Test results on used water (the volume of which was kept approximately identical for each type of concrete) from the VPV test specimens after three years severe exposure indicated higher level of chloride & total soluble salts penetrated into LCFG concrete compared to OPC concrete. These higher level ingressed salts in LCFG concrete compared to OPC concrete as shown in Figure 5.5 below confirm the test observations deduced from the above VPV tests' results.

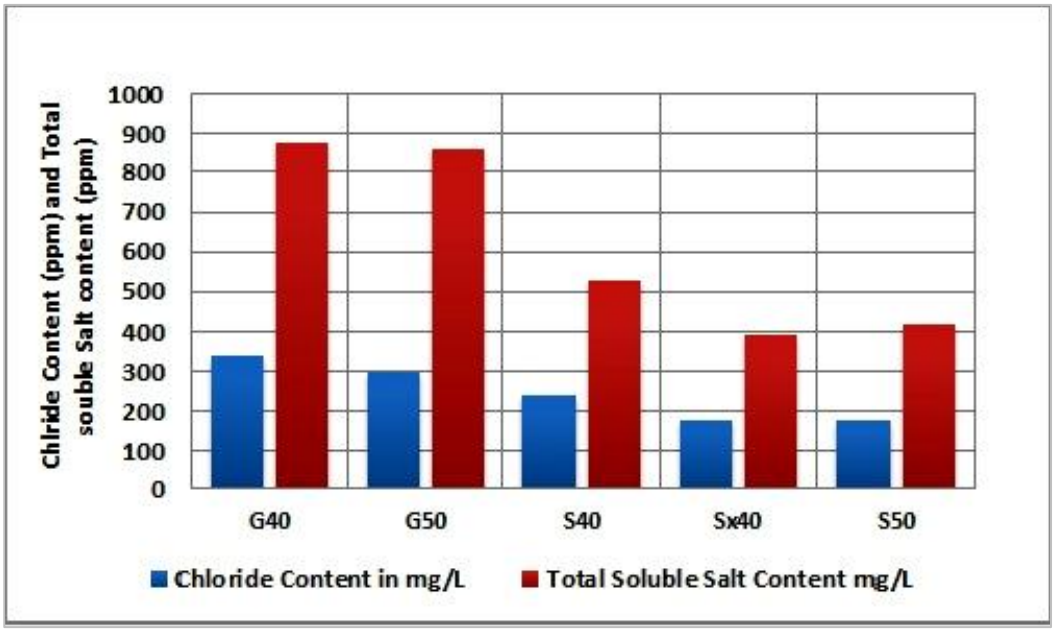

Figure 5-5 Chloride & Salts Content of Used VPV Test Water after Three Years Severe Exposure

5.4.3 Discussion of VPV in Relation to Durability

Table 5.1 below summarises the good quality concrete criteria based on percentage of permeable voids for OPC concrete, which Vic Roads (Road Authority, Victoria, Australia), has adopted for specifying the quality of OPC concrete in their Specifications (Andrew Phaedonos, 2001).

Table 5-1- Volume of Permeable Voids Limits for Good Quality Concrete

Concrete Grade	Percentage Volume of Permeable Voids for OPC Concrete Compacted by Vibration
VR330/32*	14 %
VR400/40	13%
VR450/50	12%
VR470/55	11%

*Cement content 330kg/m3, Comp Strength 32MPa

The VPV test results indicated that percentage volume of permeable voids of LCFG concrete specimen before subjecting to severe exposure is analogous to OPC concrete rather are on better side. But the higher level of ingressed chloride and soluble salts observed after three years severe environmental exposures for LCFG concrete compared to OPC concrete in this research indicates that OPC concrete VPV criteria may not be applicable for LCFG concrete. This indicates that different VPV criteria may be required for LCFG concrete.

This is because of the change in chloride resistance for OPC concrete begins to occur once the VPV tends to exceed the critical value of 12-13% (Sherman et al, 1996). However in case of LCFG concrete, VPV test results showed that change in chloride resistance occurs even at VPV value below 10.5 -11.5%. This critical VPV value for LCFG concrete may be around 8% for the change in chloride resistance to begin and needs further research.

5.5 CAPILLARY SUCTION

5.5.1 Capillary Suction Test Specimen Preconditioning

Capillary suction, absorption, permeation and diffusion are the moisture transport processes, which cause the accumulation of chlorides and other harmful soluble salts from the environments (Azad, 1999; Hong et al, 2006). Capillary pores, gel pores, air voids and micro cracks if interconnected represent the volume of permeable voids in both LCFG concrete and OPC concrete (Andrew- Phaetons, 2001) as detailed in the preceding section.

In OPC concrete, water filled spaces are liable to be filled by hydration products which itself have interconnected interstitial voids known as gel pores (Andrew- Phaetons 2001). Alkali activated fly ash based geopolymer concrete primarily containing silicate and aluminate may have gel pores during the dissolution, gelation and polymerisation process in the beginning. This may be unlike to OPC concrete to the extent in which subsequent C-S-H gel phases may be further contributing to gel pores (Andrew Phaedonos, 2001).

A non-standard test was undertaken on laboratory cylinder specimens, which have undergone three years severe exposure as per test procedure detailed in Chapter 4 (Section 4.4.3). Cylinder specimens (labelled as: 129GC13, 130GC13, 131SC11, 132SC12 & 133SC12) were dried for two weeks at 48 ^{o}C (which represents the driest temperature that could be possible in Australian field environments) prior to undergo the capillary suction test.

5.5.2 Capillary Suction Test Results

Conditioning of the samples specimens at 48 ^{o}C allowed the majority of the free water evaporated from exterior region as shown in Figure 5.6.

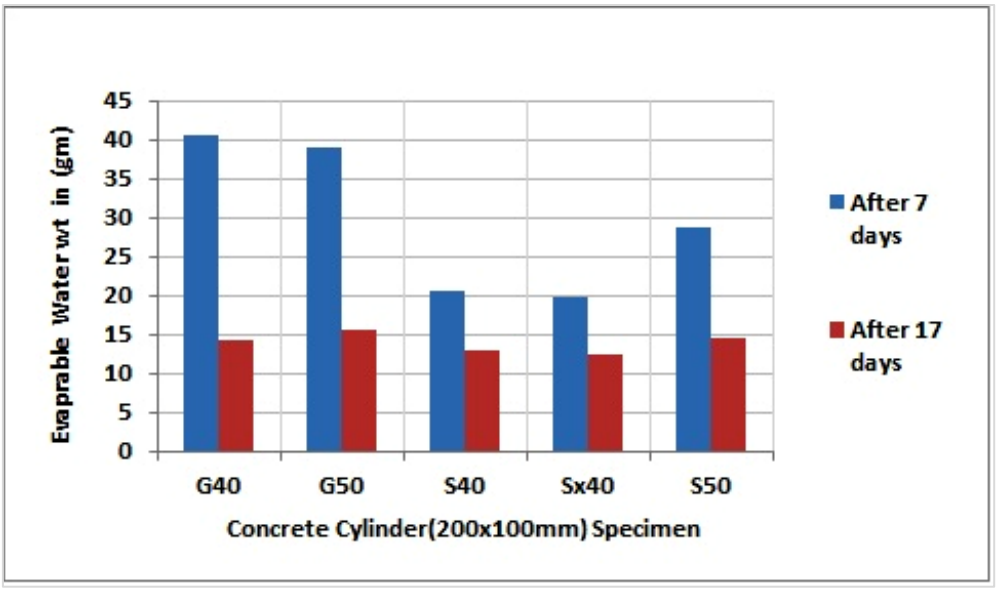

Figure 5-6 Evaporable Free Water

The capillary suction that occurs against gravity measured the quality of pores at different time intervals for absorption. The test was undertaken on specimens of size 100mm x 100mm obtained from each type of concrete cylinder specimen by removing top and bottom 50mm portion. Figure 5.7 (a) & (b) below shows the suction trend of respective concrete samples.

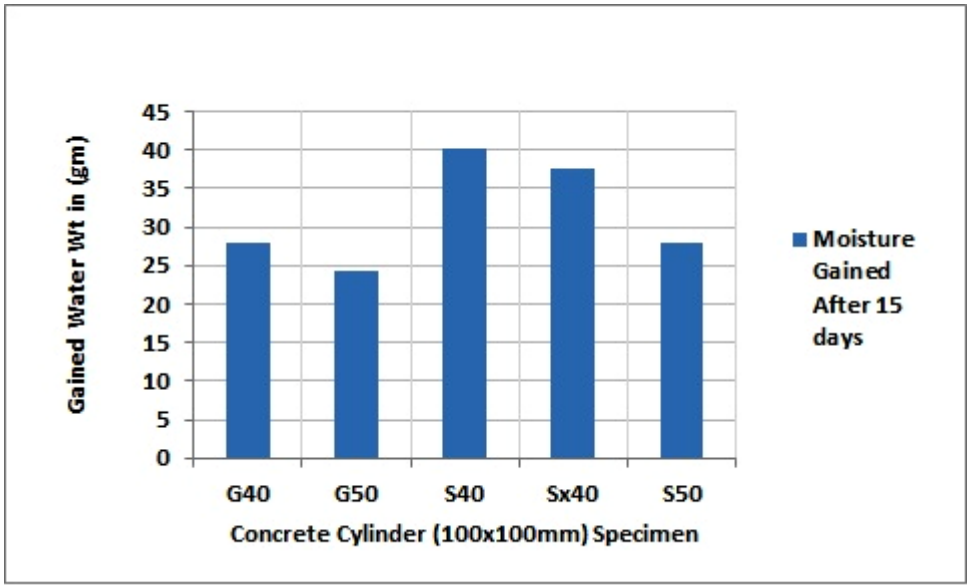

(a)

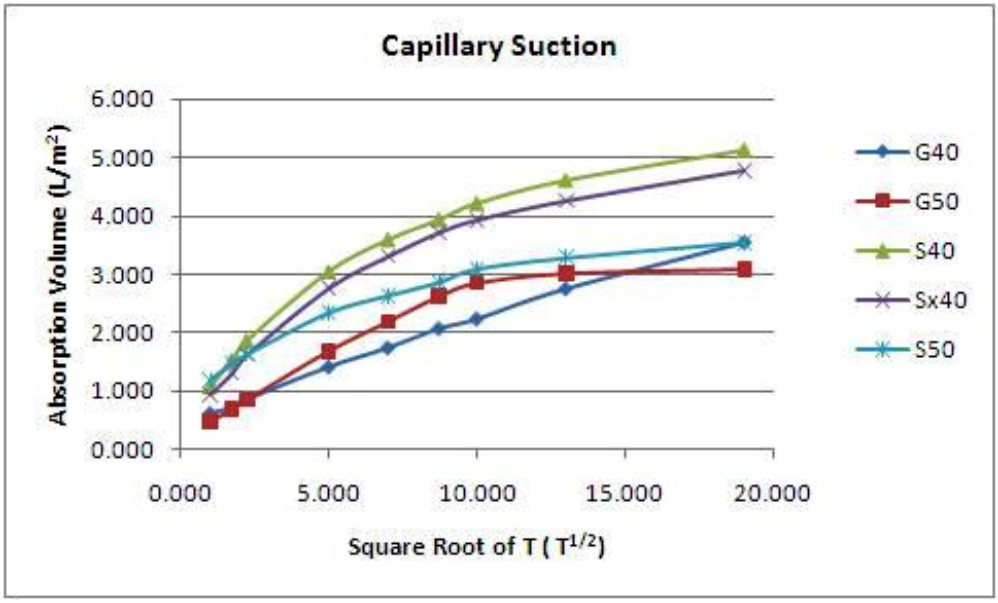

(b)

Figure 5-7 Suction Trend & Water Gained Through Capillary Forces

Liquid that do not reacts chemically in concrete, penetrate into concrete pores according to $t^{1/2}$ law and is expressed by the equation as below (Hong et al, 2006).

$$S = A\sqrt{t}$$

Where:

S is the amount of water absorbed by capillary suction per unit area of contacting surface and 't' is absorption time and 'A' is the coefficient of capillary suction.

5.5.3 Discussion of Capillary Suction in Relation to Durability

It was inferred from Figure 5.7 (b) above that capillary suction coefficient was not constant, it was large in the beginning than at later stages. This indicated that pore structure at the outer region is different than the inner region. This deviation was more pronounced in OPC concrete. Possible explanation could be due to the dissolution of calcium from the pore walls forming $Ca(OH)_2$ or dissolution of ingressed salts from the severe environments by the penetrating water or could be due to more larger voids spaces. Combination of all these possibilities may be the reason for higher absorption.

Secondly low evaporable water was inferred for OPC concrete samples as shown in Figure 5.6 above. This indicates that hydration in OPC concrete could be on- going and may be in excess of one year period. This hydration has the tendency to block pores in OPC concrete, rendering pore system with high degree of tortuosities. However higher evaporable water was inferred for LCFG concrete samples as shown in Figure 5.6 above.

The possible explanation of this higher evaporable water in LCFG concrete could be due to the lack hydration activity. The ratio of part of the pore cross section affected by penetrating water to the entire pore cross section increases with the decreasing pore radii (Hong et al 2006). Its opposite for LCFG concrete could be the possible explanation relative to its larger number of pores and without decreasing tendency of their radii compared to OPC concrete which results from hydration products. As such LCFG concrete pores may more likely to be of continuous nature. Also higher evaporable water from LCFG concrete during drying processes indicated the higher extent of its available free water compared to OPC concrete samples. This evaporable water in LCFG concrete was approximately close to the gained water under capillary suction. This was shown by the evaporable water from cylinder specimens of size (100x200mm) and gained water by cylinder specimens of size (100x100mm), which were of half the size in volume as evident from Figure 5.7 (a).

In OPC concrete, it was inferred that gained volume was 4 times higher than the evaporable one for S40 & Sx40 mix and 2 times higher for S50 mix. This explains the reason for higher absorption in OPC concrete, which could be due to its on- going hydration from the moisture availability of over the experimental period. The second aspect of hydration activity of OPC concrete is to render its pore structure more unsaturated allowing more moisture to be drawn in. This could be more pronounced at the beginning of the experiment. Conversely lower evaporable free water could also be due to its hydration activity, which can be ongoing in moist state as inferred during the conditioning of the specimens at 48 ^{o}C as shown in Figure 5.6 above.

5.5.4 Visual Observation of Moisture Transport Processes during the Experiment

Figure 5.8 below provides the explanation of more continuous moisture pathways in the LCFG concrete than OPC concrete. The bottom section of specimen was kept immersed up to 5mm over the experiment period allowing the progression of moisture under capillary action and absorption from exterior surface to the interior. LCFG concrete specimen top section after 49 hours of exposure to water provided an indication of partial moisture absorption as shown in Figure 5.8(a). After an interval of 76 hours, top section of the LCFG (G40) concrete specimen was inferred completely saturated as shown in Figure 5.8(b) compared to OPC concrete. After 94 hours of exposure it was inferred moisture evaporating from the top section of LCFG (G40 & G50) concrete specimen was faster than the water penetrating under capillary and wicking action, which may be due to fluctuations in Relative Humidity (RH).

Few hours after, the specimens become fully saturated again under the cyclic effect of RH changes as shown in Figure 5.8(c). After 120 hours of exposure, presence of constantly evaporated surface was inferred for G50 specimen indicating the steady state of wicking action. After 360 hours of exposure, traces of salt deposits were noted on G50 specimen top surface. This may be from the crystallising activity of already ingressed salts under wicking action from severe environmental exposure as shown in Figure 5.8(d). Figure 5.8 (e) shows the extent of crystallised salt deposit at the top of G50 after 502 hours. Red marking on the split specimens shows the visible extent of effected section of each specimen by capillary suction.

G40 S40

(a) After 49 Hours In Contact with Water

G40 S40

(b) After 76 Hours In Contact with Water

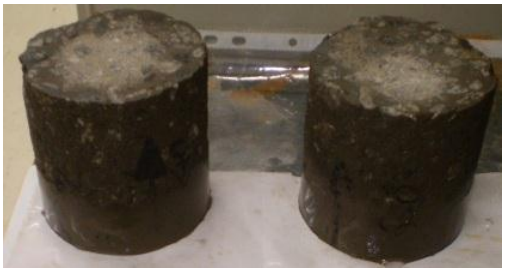

G40 G50

(c)After 94 Hours In Contact with Water

G40 G50

(d) After 120 Hours In Contact with Water

G40 G50

(e) After 502 Hours In Contact with Water

S40 G40

(f) Capillary Suction Visible Effected Section

Figure 5-8 Wicking Action for LCFG Concrete and OPC Concrete

Wetness in LCFG concrete (G40) from capillary suction was visible along the periphery of the specimen. An average thickness of periphery layer was 20mm approximately, while for OPC concrete (S40) wetness inferred was right across the width of specimen and was up to 65mm from the bottom section as shown in 5.8(f).

These capillary suction observations of less absorption volume per square meter in LCFG concrete was due to the involvement of exterior peripheral section of smaller thickness compared to OPC concrete. Secondly the reason for less absorption volume per square meter in LCFG concrete could be due to the partially unsaturated state of its pores near the exterior surface. This is shown by Figure 5.7 (a) & (b).

The penetrating water in LCFG concrete even though was visible through the exterior peripheral section, has shown high capillary rise compared to OPC concrete as evident from 5.8 Figure(a-e). This observation of higher capillary water rise is in line with Mukhin et al (2007) observation for LCFG concrete as detailed in Chapter 3, Section 3.2.1.1. High capillary rise in LCFG concrete is indicative of its finer pore structure with higher pores' connectivity and as well less reactive tendency to penetrating water compared to OPC concrete.

For G50 LCFG concrete visible affected thickness along the periphery was around 10mm. This thinner exterior periphery layer relatively could be the reason for semi dry appearance of its top section. This may result from higher rate of evaporation than the capillary suction. The test outputs also indicated that the LCFG concrete structure components in partially submerged and exposed environments are more prone to ingressing salts through capillary suction and absorption with higher degree of intensity through the exterior region. This also explains the possible cause of surface scaling of LCFG concrete detailed subsequently under scaling resistance in Section 5.7.

Discernible observations for OPC concrete specimens were less capillary rise and higher absorption volume per square meter. The higher absorption in OPC could be due to larger section affected by capillary suction as shown in 5.7 (b), however moisture rise was not right through over the test duration of 502 hours as shown in Figure 5.8(a) &(b). This indicated that OPC concrete has less continuous pores relatively.

However degradation and scaling of buried & immersed part of S50 OPC concrete resulted higher capillary rise, which possibly may be because of sulphate attack.

5.5.4.1 Indicative Pore Structure from Suction Test Results

So moisture transport processes although appear analogous to a greater extent for both LCFG and OPC concrete, however the dominance of individual process depends largely on microstructure characteristics.

Microstructure develops as a result of chemical reaction of mix constituents of source material (low calcium fly ash rich in silica and aluminium activated by alkaline solution in case of LCFG concrete and GP cement with or without SCM activated by water in case of OPC concrete). In OPC concrete water gets consumed chemically during the hydration phases forming C-S-H products, which tend to fill up the capillary pores in the fresh paste of OPC concrete (Andrews Phaedonos, 2001 & Adam et al, 2009). Whereas pore water in LCFG concrete during mix synthesisation tends to communicate to the surface for escaping through the system (Andrews Phaedonos, 2001). This may result in the development of continuous pore systems at micro and nanometric level.

Differing opinion about the pore sizes classification exist in literature. For cementitious materials, Espinosa and Franke (2006) define the pores with hydraulic radii as follows:

- Micro-gel pores <1.0 nm
- Meso-gel pores 1.0-25nm
- Micro-capillary pores/ meso-capillary pores 25-50nm
- Macro capillary pores 50nm-1µm

In more general form these voids in concrete matrix and may be comprised of entrapped air void (between 10-500µm), capillary pore (vary between 2nm-10 µm) and gel pore with diameter 1nm or less (Aldridge et al, 2010).

Capillary suction and absorption coupled with drying and wetting cycles are compounded by water vapour diffusion (Hall & Hoff, 2002). Differing relative humidity in combination with the drifting air borne contaminants associated with drying cycles could be possible durability concerns even in non- aggressive or mild scenarios (Azad, 1999).

To understand the microstructure and porosity characteristics of LCFG concrete compared to OPC concrete, test results of 3-D micro- tomography, chloride profile and diffusion coefficient in the subsequent sections provide further explanation & reasoning of moisture transport processes and chloride ions' migration to the inner region in this research.

5.6 3-D MICRO- TOMOGRAPHY

Mean pore radius and pore size distribution in cementitious material are important micro-structural characteristics and are related to a series of properties of material, such as resistivity to ionic diffusion, flexural strength and fracture toughness. The VPV and capillary suction test results in the preceding sections indicated the possible porosity characteristics of cementitious paste in both LCFG concrete and OPC concrete, which has major control on the ingress of potentially deleterious substances.

The rate of permeation of fluids across the porous cementitious material is related to volume of the pores and their interconnectivity in combination with the environmental exposures. The ingressed species into the cementitious material are water transported one (such as: acids, sulphate ions, chloride ions and permeating gases - carbon dioxide or oxygen depassivating the embedded reinforcing steel). Diffusion through water filled pathways allows migration of ions further into the interior (Kumar &Roy, 1986 & Azad, 1999).

5.6.1 Micro-tomography Test Outputs

The following figures & images of 3 – D Micro-tomography technique output indicates the micro-structural and pore structure characteristics of G40 LCFG concrete compared to S40 OPC concrete. These pores' structure characteristics cover pore numbers, sizes, their shape and distribution.

Figure 5.9 below shows the tomographic images of microstructures and pore structure of LCFG concrete (G40), OPC concrete (S40) and OPC concrete with pore-blocking additive (Sx40) at micro level. Entrapped air at the dissolution phase during cylinder specimens casting process resulted closed ball shaped pores which are shown by black circle in the tomography images. Pore size graphs vs. their isotropy index in Figure 5.9 below quantify the extent of pores, pores sizes and their shape for each concrete matrix. It was inferred from these images that LCFG concrete (G40) binder paste has more circular shaped pores of varying sizes. Many of them might be closed pores due to entrapped air.

In OPC concrete (S40) the distribution of pores represented by black spots are of varying shape, that is, circular to elongated one. In Sx40 pores were predominantly of elongated shape. In both S40 and Sx40 concrete, pores were predominantly at the interface with coarse aggregates. Both S40 and Sx40 have relatively lesser number of pores than G40 but of larger size.

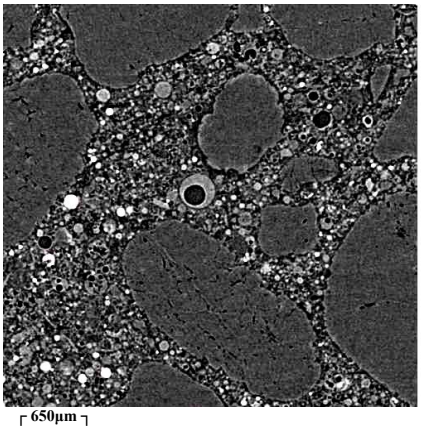

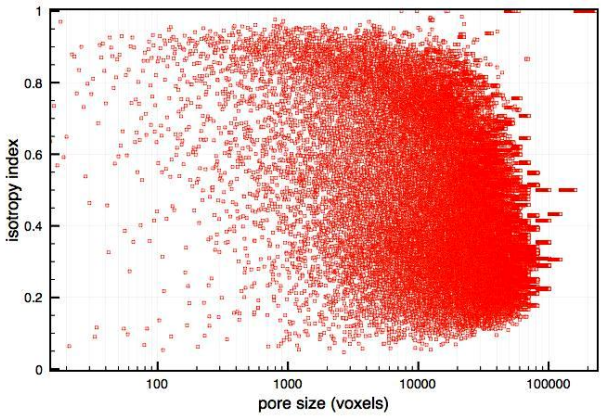

Geopolymer Concrete (G40- 40 MPa)

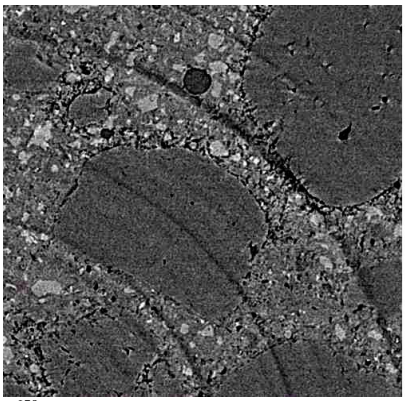

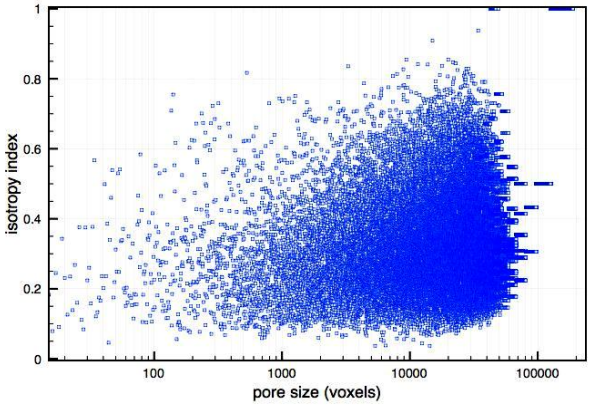

OPC Concrete (S40- 40 MPa)

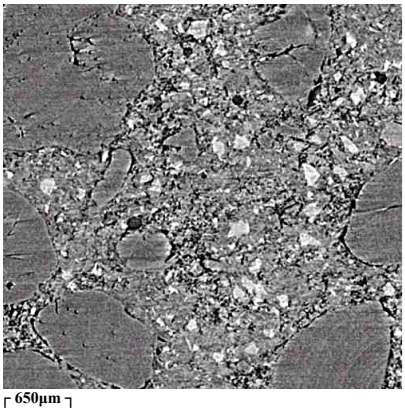

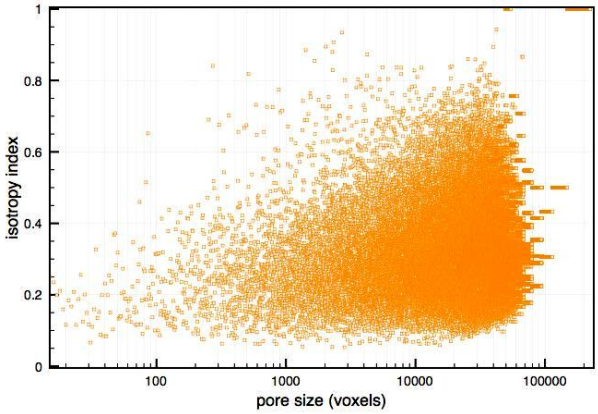

OPC Concrete with Pore Blocking Additive (Sx40- 40MPa)

Figure 5-9 Tomographic Microstructure Images and Pore Structure & Pore Distribution

Figure 5.10 & 5.11 below shows the extent of pores with shape closer to the circle shape in LCFG concrete compared to OPC concrete from distribution perspective visually. Highlighted extent of Figures 5.10 and 5.11 below shows number of pores, their sizes and distribution approximately identical for both LCFG concrete and OPC concrete, while the portion outside the highlighted envelop identifies the relative extent of additional pores numbers and their shape, sizes & distribution for LCFG concrete compared to OPC concrete pores.

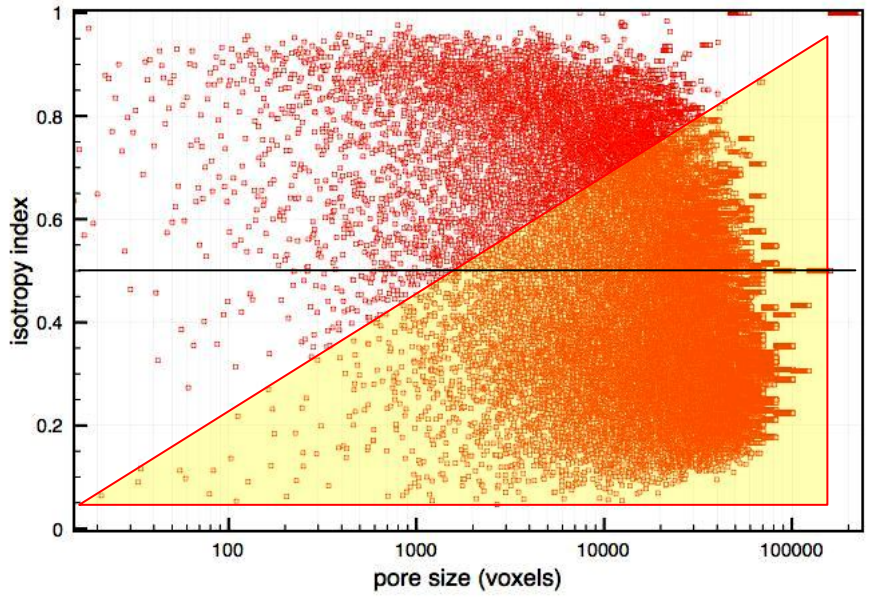

Figure 5-10 LCFG Concrete (G40) Pore Sizes & Number

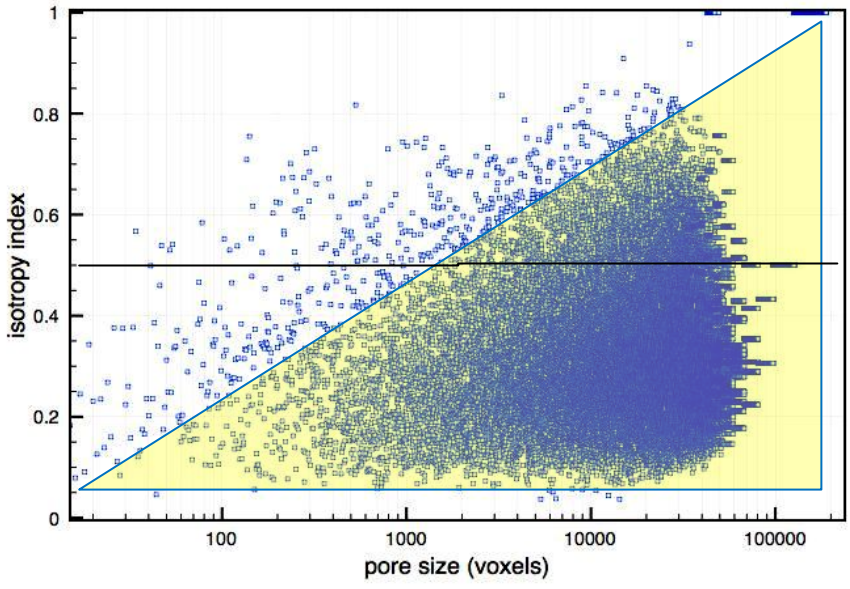

Figure 5-11 OPC Concrete (S40) Pore Sizes & Number

5.6.2 Pore Structure – Shape, Size, Distribution and Number

Visual analysis from these graphs indicated that the pores in LCFG concrete are approximately 40 % more than OPC concrete. Above the middle horizontal line, these pores are aligned towards more circular shape and are finer towards the ordinate as evident from the un-highlighted section of pore distribution graphs for respective concretes in Figure 5.10 and 5.11 above.

This 3-D micro tomography test observation for pore structure of LCFG concrete confirmed the observation of Skvara et al (2006) study, which indicated that the porosity of fly ash based geopolymer concrete is up to 50% high compared to OPC concrete. This test results also confirmed the inferences of Palomo et al (1999) study for porous structure as well.

The pores' distribution graph shows that LCFG concrete (G40) has pore structure with nearly 50% of its total pore clusters having pores with isotropy index between 0.5 to1 and are more aligned to circular shape. The pore structure of OPC concrete has approximately 80% of the pores with isotropy index between 0.1 to 0.5 and is more aligned to elliptical shape.

Also test results in this research indicated that circular shaped pores in LCFG concrete are about 30-40% more and approximately half of them are more finer. This confirms the observation of capillary suction test in the preceding section relative to fineness of pores in LCFG concrete. The above observations of high porosity for LCFG concrete are from mix proportions with a minimum water binder ratio of 0.20, essential from workability point of view compared to OPC concrete.

5.6.2.1 Quantification of Pore Numbers and Their Distribution

In 3-D Micro-tomography test outputs, one voxel represents the cubic size of pore as 2.2μm^3 and 1.3 μm will represent its diameter approximately. Figure 5.12 & 5.13 below shows the quantification of pore distribution and their size for LCFG and OPC concrete of 40MPa. Pore sizes of 20 voxels in G40 are relatively more than S40 and Sx40.

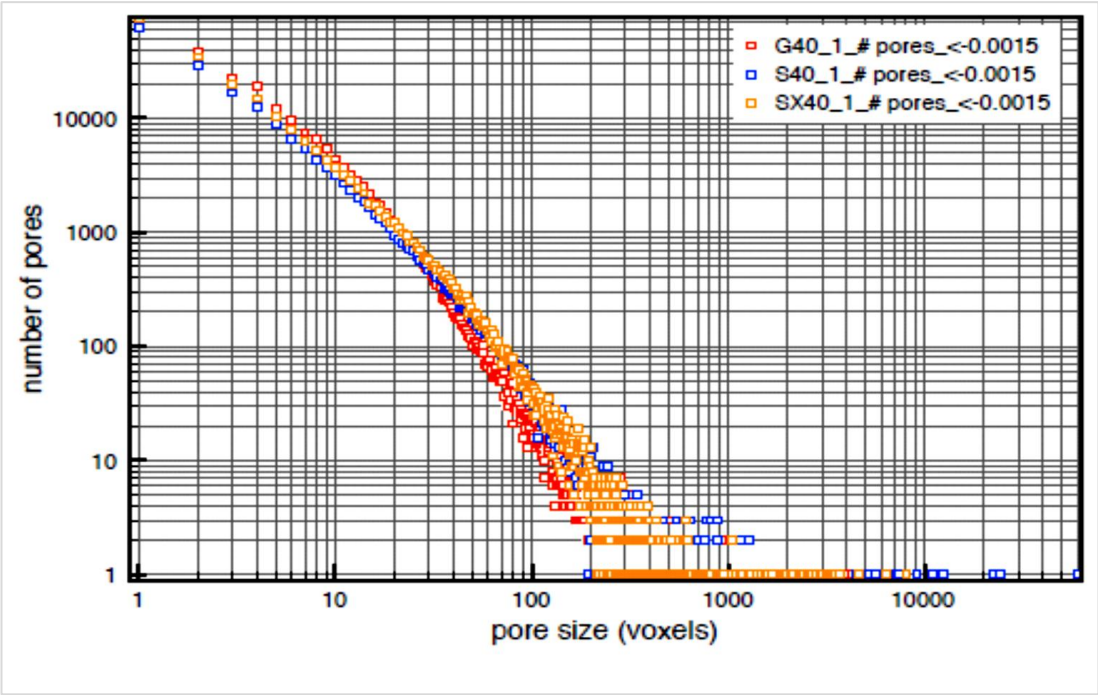

Figure 5-12 Pore Size & Numbers

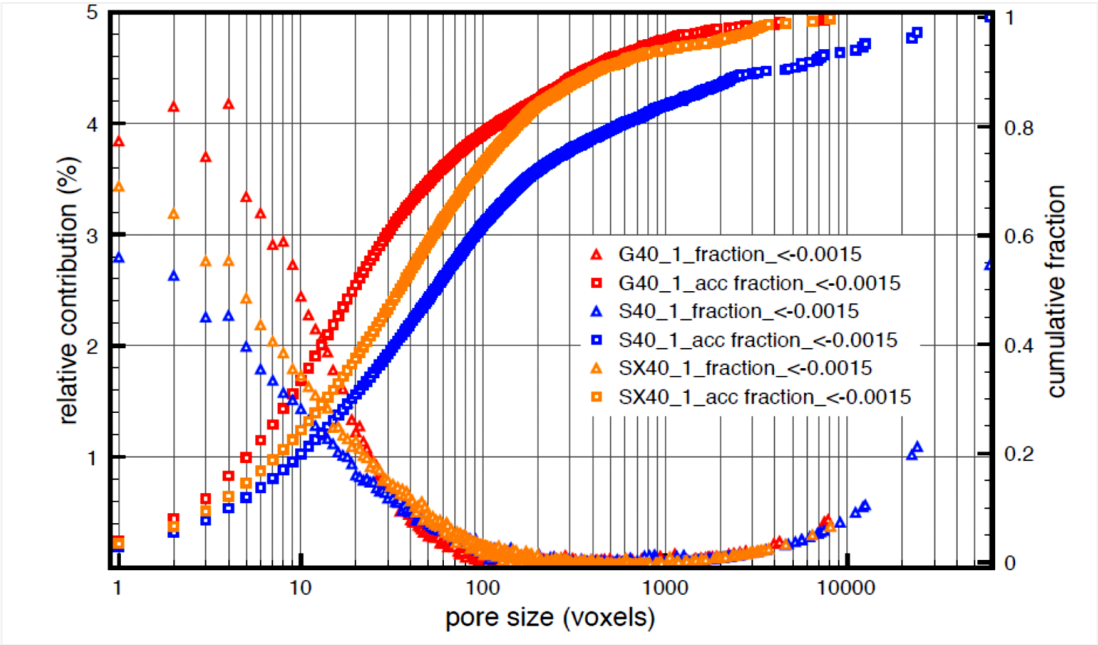

Figure 5-13 Pore Size, Cumulative Fraction and Relative Contribution

Table 5.2 below summarises the pore distribution of 100 voxels size and 50 voxels size from data analysis of Figure 5.13

Table 5-2 Pore Size & Distribution

Pore Size and their Distribution		
Concrete Sample	**% finer than 100 Voxels**	**% finer than 50Voxels**
G40	80	70
S40	60	50
Sx40	70	60

5.6.3 Discussion on microstructure and Pore Structure

The LCFG concrete pore structure with more circular shaped pores as observed in this research ensure more uniform distribution of stress and supports its good mechanical properties such as higher compressive and tensile strength. This inference also confirms the delayed cracking observed by Olivia (2011) as per accelerated induced corrosion test shown in Figure 3.27(e) & (f), which also is an indirect indicative of its higher tensile strength.

Micro-tomography images in Figure 5.9 showed that the transited layer in OPC concrete (S40) around the periphery of aggregates at the interface by dark line has porosity higher than the hardened cement paste, whereas such transited layer in G40 at the interface with aggregate surrounding was not found. The micro structure of interface layer with aggregate in LCFG concrete was different than the interfacing layer in OPC concrete. This was in concurrence with Skvara et al (2006) observations, which revealed the composition of interface layer in OPC concrete is richer in $Ca(OH)_2$ & ettringite content with $Ca(OH)_2$ parts orientated along the aggregate while the composition interface layer in geopolymer concrete was free from such changes. The thickness of this interface layer varied between 20-100 μm revealed by using SEM technique (Diamond, 1986) & Maso, 1986).

The 3-D Micro-tomography test outputs exhibited the pore structure similarities, which Skvara et al (2006) inferred for fly ash based geopolymer concrete of approximately closer composition to LCFG concrete mix being investigated in this research.

Test outputs are appended in Appendix D. Scaling resistance observations, diffusion test and electrochemical test outputs in the subsequent sections signify further the importance these micro-structural and pore structure properties relative to LCFG concrete long term durability in comparison with OPC concrete.

5.7 SCALING RESISTANCE

5.7.1 Scaling Mechanism and its Impairment Visually

Figure 5.14 below shows the efflorescence trend for G40 & G50 samples condition after one year of severe exposure compared to S40, Sx40 & S50. Salts in accumulated form near the surface on hydration resulted the peeling of surficial layer of LCFG concrete samples (G40 & G50) compared to OPC concrete. Peeling of surficial layer exposed the underlying binder paste layers for progressive scaling.

The effervescing action on application of dilute HCL indicated the presence of Na_2CO_3 & Na_2SO_4, while the presence of chloride salts was indicated by application of silver nitrate solution forming white precipitation of silver chloride. Possible explanation of higher level of efflorescence and scaling in LCFG concrete inferred in this research could be because of soluble salts of sodium & magnesium ($NaHCO_3$, Na_2CO_3, Na_2SO_4 , $MgSO_4$, $MgCO_3$ & NACl).

- Sodium carbonate in hydrated form (thermonatrite-$Na_2CO_3.H_2O$) can transform to 7^{th} hydrate and follow on to natron ($Na_2CO_3.10H_2O$), which could result from carbonation inferred in this research. This inference was in line with Zhang et al, 2013 findings for efflorescence products detailed in Section 3.5.

- The simulated soil in this research was rich in $MgSO_4$ (Section 4.3.1), as such presence of sodium sulphate compounds (such as thenardite / mirabilite) in sulphate rich environments were obvious as detailed in Section 3.5. Primary carbonation product in LCFG concrete such as $NaHCO_3$ on reaction with $MgSO_4$ from the environment can result Na_2SO_4, $Mg(OH)_2$ and CO_2 which can carbonate its interior and scaling as well.

- Secondly carbonation product of Mg (that is, $MgCO_3$) on reaction with alkali of the LCFG concrete (alkali- carbonate reaction) can result $Mg(OH)_2$ and Na_2CO_3. $Mg(OH)_2$ can lead to the formation of expansive brucite and likewise is the hydrated form of Na_2CO_3 as detailed above.

So primary carbonation products and secondary alkali- carbonate reaction compounds as detailed above could be the possible cause of higher scaling and higher carbonation in LCFG concrete compared to OPC concrete.

5.7.2 Scaling Results Discussion

It was inferred that peeling or fretting of LCFG concrete was more active in exposed zone than the immersed zone, while buried zone has very insignificant peeling or fretting activity. However peeling activity of surficial layer was not noticeable for OPC concrete samples (S40, Sx40 & S50) over one year duration of severe exposure. This is evident from Figure 5.14 below, which shows the original condition of samples before exposing to severe environments and the condition of the samples after one year exposure.

Samples	Reinforced Laboratory Samples before Exposure	Laboratory Samples after One Year Severe Exposure with Cover: 50mm	35mm	25mm
G40	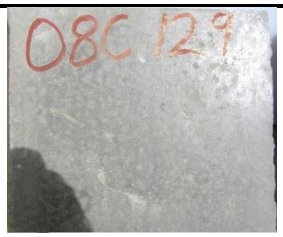			
G50				
S40	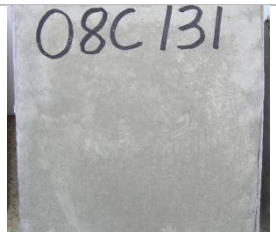			
Sx40	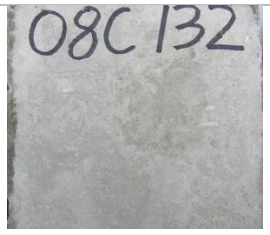			
S50	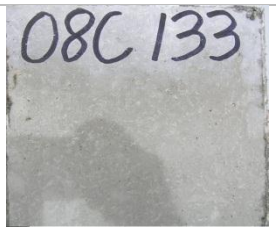			

Figure 5-14 Efflorescence & Scaling Extent after One Year Severe Exposure

However further research to quantify these reaction products is required to determine the dominance of either carbonate or sulphate compound in the chemical attack or their combined action. Figure 5.15(a) below shows efflorescence and peeling activity of LCFG concrete cylinder specimens and laboratory samples after two years severe exposure in comparison with OPC concrete cylinder specimens and laboratory samples. Figure 5.15(b) below showed that peeling activity of LCFG concrete (G40) was more active compared to OPC concrete (S40) after 2 years of severe exposure.

Cylinder Specimens	Efflorescence Activity	Loosening & Peeling of Surficial layer and subsequently underlying layers
129GC7&8 and 130GC7&8		
131SC6&7 and 132SC7&8		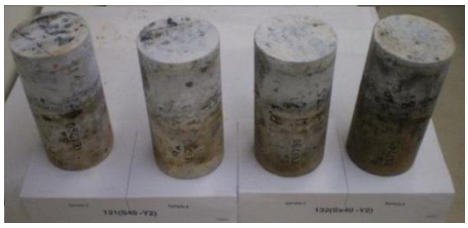

(a)

Surface Condition	Salt Crystallisation & Efflorescence after 2nd year of severe exposure - G40	Crystallisation of Salt & Efflorescence after 2nd year of severe exposure - S40
Efflorescence and Crystallisation		

(b)

Figure 5-15 Efflorescence & Scaling of Cylinder Specimens and Laboratory Samples

5.7.3 Scaling Extent Quantification of Laboratory & Field Box Culvert Samples

The ACI Committee report (116R) on 'Cement and Concrete Terminology' describes concrete scaling as 'local flaking or peeling away of the near-surface portion of hardened concrete or mortar' and rate it as 'light', 'medium', 'severe', and 'very severe' depending on the loss of surface mortar down to depths .Table 5.3 below summarise these extent of scaling severity.

Table 5-3 Scaling Class, ACI Committee- 116R

Extent of Scaling Severity	Scaled Surface Depth (mm)
Light	5
Medium	5-10
Severe	10-20
Very Severe	>20

Table 5.4 below shows the condition of LCFG concrete (G40) and OPC concrete (S40) laboratory samples before and after the severe environmental exposures of 2 years simulated in the laboratory. According to the ACI criteria as detailed in Table 5.3 above, the scaling severity of G40 sample and S40 samples is summarised in Table 5.4 below.

Table 5-4 Efflorescence & Scaling of Laboratory Samples after Two Years Severe Exposure

G40 – Scaling Class	G40 - Sample in Aggressive Exposure after 2 Years)	Exposure Scenarios	S40 - Sample in Aggressive Exposure after 2 Years)	S40 – Scaling Class
Medium		Exposed		
Light		Splashed & Immersed		Invisible Scaling No Scaling
No Scaling		Buried		No Scaling

It was inferred that progressive peeling of underlying layers was intense for LCFG concrete compared to OPC concrete. This peeling activity was more predominant in exposed zone followed by immersed and buried zone for LCFG concrete (G40), while such peeling activity was invisible for S40 sample in exposed, immersed and buried zone.

Table 5.5 below shows the scaling extent of cylinder specimen and laboratory samples after three years exposure. It was inferred that LCFG concrete samples degraded up to 20mm in splashed & exposed zone. Based on scaling criteria summarised in Table 5.3 above, this amounts to a scaling of severe level.

Table 5-5 Scaling Extent of Laboratory Samples after Three Year Severe Exposure

G40 – Scaling Class	G40 - Sample With Lab Simulated Aggressive Exposure -3 Years)	Exposure Scenarios	S40 - Sample With Lab Simulated Aggressive Exposure -3 Years)	S40 – Scaling Class
Severe		Exposed		Invisible Saling
Medium				
Light		Splashed& Immersed		No Scaling
No Scaling		Buried		No Scaling
Severe		Exposed		Invisible Scaling
Medium				
Light		Splashed& Immersed		No Scaling
No Scaling		Buried		No Scaling

Scaling is not only detrimental to mechanical strength of concrete as observed in section 5.2.1 above but also reduces the cover to embedded steel from corrosion perspective significantly. So above observations revealed that severe environmental exposure of prolonged and persistent nature can be of high risk from scaling perspective for LCFG concrete in exposed zone than OPC concrete.

The possible reason for high scaling in LCFG concrete could be due to the presence of sodium and its hydroxides, which may be subject to carbonation. Ongoing hydration of resulting carbonation compounds (detailed in Section 3.4.5 & 3.5) can be responsible for progressive scaling of LCFG concrete.

Table 5.6 below summarises the scaling extent of box culvert samples inferred in aggressive and non-aggressive environments.

Table 5-6 Scaling Extent of Field Box Culvert Samples

G40 – Scaling Class	G40 – Box Culvert Sample in Aggressive Field Environments and Non-aggressive Field Environments (Exposure -2 Years)	Exposure Scenarios	S40 – Box Culvert Sample in Aggressive Field Environments and Non-aggressive Field Environments (Exposure -2 Years)	S40 – Scaling Class
Aggressive Conditions - Internal Wall Face Scaling Extent				
Light		**Exposed**	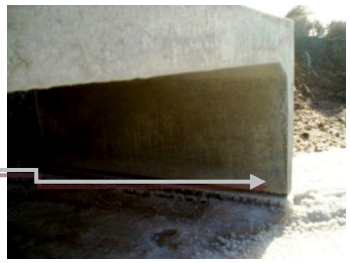	**Invisible Scaling**
Medium		**Exposed & Immersed**		**Invisible Scaling**
Severe				**No Scaling**
No Scaling		**Buried**		
Aggressive Conditions - External Wall Face Scaling Extent				
Invisible Scaling **Light to Medium** **No Scaling**		**Exposed** **Buried**		**Invisible Scaling** **No Scaling**
Non -Aggressive Conditions – Internal & External Wall Face Scaling Extent				
No scaling except localised one near top		**Exposed to atmos-pheric conditions only**		**No Scaling**

High scaling activity observed for LCFG concrete field box culvert sample compared to OPC concrete box culvert under severe environmental exposure was matching with the scaling activity of laboratory samples exposed to simulated severe environments.

This confirmed the identical testing regime approximately followed in this research. However higher level of scaling observed for LCFG concrete under severe environmental exposure indicates its less resistance to scaling compared to OPC concrete.

Progressive scaling caused the reduction in compressive strength & effective cover to rebar despite visual impairment. The decrease in compressive strength for LCFG concrete ranged between 30-40% after the exposure period of three years compared to strength of 15-20% for OPC concrete.

However insignificant sign of scaling was noted for LCFG concrete samples exposed to non-aggressive conditions (exposed to atmospheric conditions only) as summarised in Table 5.6 above. This could be due to the least possibility of moisture ingress in non –aggressive environments transporting deleterious matters into its concrete matrix.

From the field and laboratory simulated severe exposure models, it was also inferred that buried part of LCFG concrete has insignificant scaling compared to the immersed and exposed sections. This was comparable with OPC concrete under severe environmental exposures conditions.

In OPC concrete, calcium induced products such as CSH can interact with atmospheric carbon dioxide to form insoluble $CaCO_{3,}$ which tend to densify the concrete initially and may take long time to loosen the surficial layers. Slow carbonation of OPC concrete may result scaling, which could be apparent after a long time and insignificant observations of its scaling in this research confirms this aspect.

Humectants' nature of chloride salts result increased absorption and is aggravated by scaling or vice versa. Also the degrading intensity of sodium sulphate is higher than the carbonation products as detailed in Section 3.5 and this could result from sulphate rich environments. In LCFG concrete, both seems to be active, degrading its exposed section quicker than OPC concrete. However further research is needed to study their individual and combined effect.

5.8 DIFFUSION COEFFICIENTS AND CHLORIDE PROFILE

5.8.1 Diffusion Coefficient & Chloride Profile Results of LCFG and OPC Concrete

The test results showed that LCFG concrete initial VPV values were comparable with OPC concrete before severe exposure, rather on the lesser side than OPC concrete as detailed in previous section. Table 5.7 below summarizes the diffusion values from NT Build 443 test (an accelerated Diffusion Test) for both LCFG concrete and OPC concrete.

Table 5-7 Diffusion Test Results of Laboratory Samples

Specimen Preparation Conditions	Mix	Effected Depth of Contamination (mm)	Chloride Surface Concentration (Cs)	Diff. Coeff. $x10^{-12}$ (m^2/sec)
Laboratory & controlled steam curing for G40 and G50 and wet curing for OPC concrete. Age 28 days.	G40	19.6	0.36	15
	G50	20	0.37	22.2
	S40	12	0.86	9.5
	S40x	11.3	0.65	9.5
	S50	12.5	0.8	7.9

5.8.2 Discussion – VPV and Diffusion Coefficient

Concrete of lower VPV values generally implies good quality concrete and obviously with lower diffusion coefficient values (Andrews Phaedonos, 2001). However higher diffusion coefficients were observed for LCFG concrete compared to OPC concrete. This was despite the lower VPV values of LCFG concrete.

Table 5.8 summarises the VPV test results undertaken on cylinder specimens before subjecting to the aggressive environments and after three years exposure in this research.

Table 5-8- Volume of Permeable Voids Test Results

Mix:	Before Severe Exposure			After Three Year Severe Exposure		
	Ave. Density (t/m^3)	Ave. Absorption (%)	Ave. Voids (%)	Ave. Density (t/m^3)	Ave. Absorption (%)	Ave. Voids (%)
G40	2.64	4.5	10.6	2,65	2.84	6.83
G50	2.65	4.95	11.55	2.57	3.38	7.81
S40	2.65	5.3	12.25	2.62	4.61	10.75
Sx40	2.67	5.1	12	2.65	4.63	10.90
S50	2.68	4.9	11.6	2.63	4.56	10.78

As chloride ions migration to the interior region is through diffusion and is supported by moist permeable voids.

5.8.3 Diffusion Test Theoretical and Prediction Curves

NT Build 443 test (ASTM C-1556) theoretical curves as shown in Figure 5.16 below provide the approximate estimation of surface chloride concentration for OPC concrete and LCFG concrete.

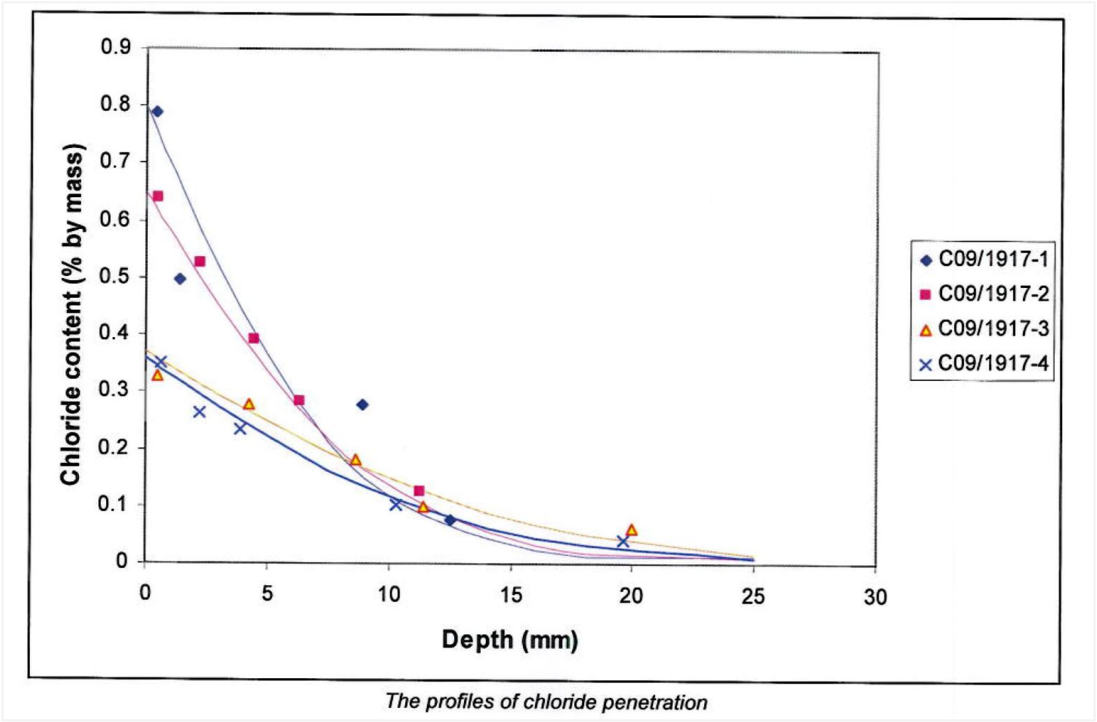

Figure 5-16 Theoretical Diffusion Curves

The approximate estimation of surface concentration (C_s) from these diffusion curves is around 0.65 to 0.8 for OPC concrete (S50-C09/1917-1, Sx40 –C09/1917-2). This surface concentration (C_s) value was close to the suggested ones in the literature as detailed in Table 3.3 in Chapter 3 for severe exposure.

Test parameters reflect the severe exposure, which require very high concentration of chloride almost 5 times the seawater concentration and an exposure of 35 days to determine the chloride content profiles and then the diffusion coefficient. However an indication of estimated value of C_s for LCFG concrete (G50- C09/1917-3, G40 – C09/1917-4) from the theoretical curves was around 0.35. This was significantly lower than suggested literature value for C_s with reference to severe environments.

Based on NT Build 443 test results of diffusion coefficient and chloride threshold value, predicted corrosion initiation curves for LCFG concrete and OPC concrete cylinder specimens are shown in Figure 5.17 below.

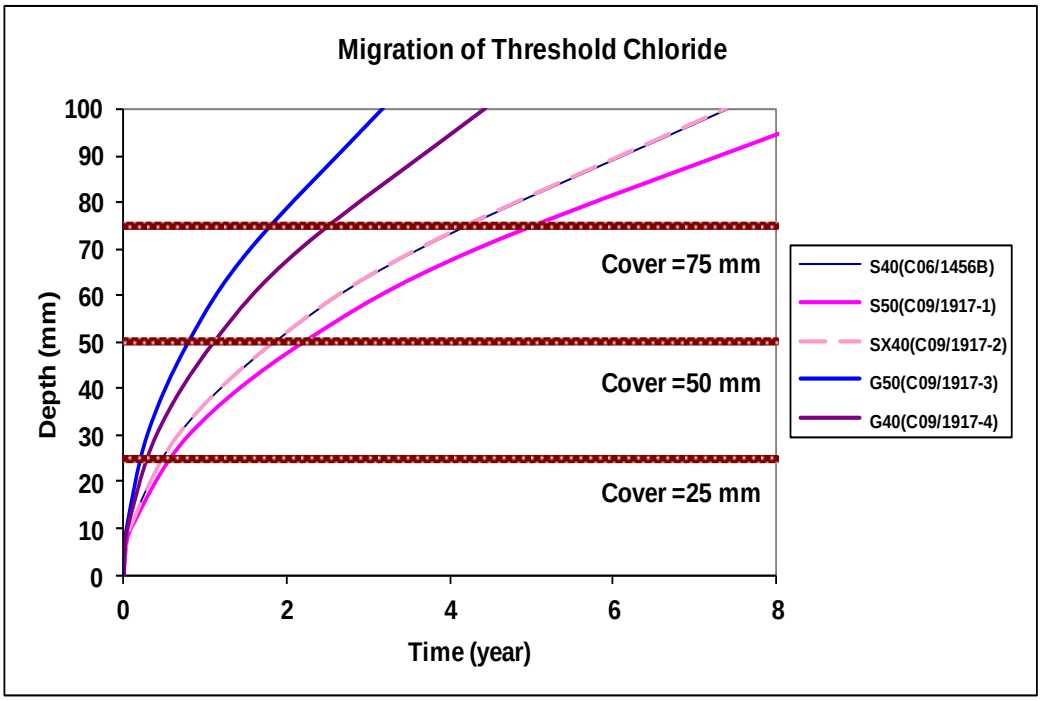

Figure 5-17 Corrosion Initiation Prediction Curves

The analysis from these prediction curves showed that predicted time to initiate corrosion of embedded steel in LCFG concrete was less than a year in LCFG concrete compared to OPC concrete up to 50mm cover depth. In OPC concrete the corrosion initiation time was over two years with 50mm cover. The test results indicated that the corrosion initiation time (T_0) for embedded steel in LCFG concrete was lower than OPC concrete for reinforcement cover up to 50mm. This is based on threshold chloride limit criteria applicable for OPC concrete. With the increased cover thickness up to 75mm, predicted corrosion initiation timing extended up to 1.5 year for LCFG concrete, while for OPC concrete predicted corrosion initiation timing extended up to 5 years. So from empirical test results of this mathematical model, corrosion initiation timing was approximately 3.5 times less in LCFG concrete compared to OPC concrete.

The chloride content from the corrosion initiation predictions were compared with the actual chloride content determined using chloride profile test on core specimens taken from the laboratory samples after one, two and three years of severe exposure periods. Test results are shown in subsequent sub-sections.

5.8.4 Chloride Profile Test from Laboratory Samples and Theoretical Curves

Figure 5.18 (a) & (b) below shows chloride profile result undertook after one year severe exposure on core sample from laboratory sample with cover 25mm and after two year with 35mm cover to the reinforcement.

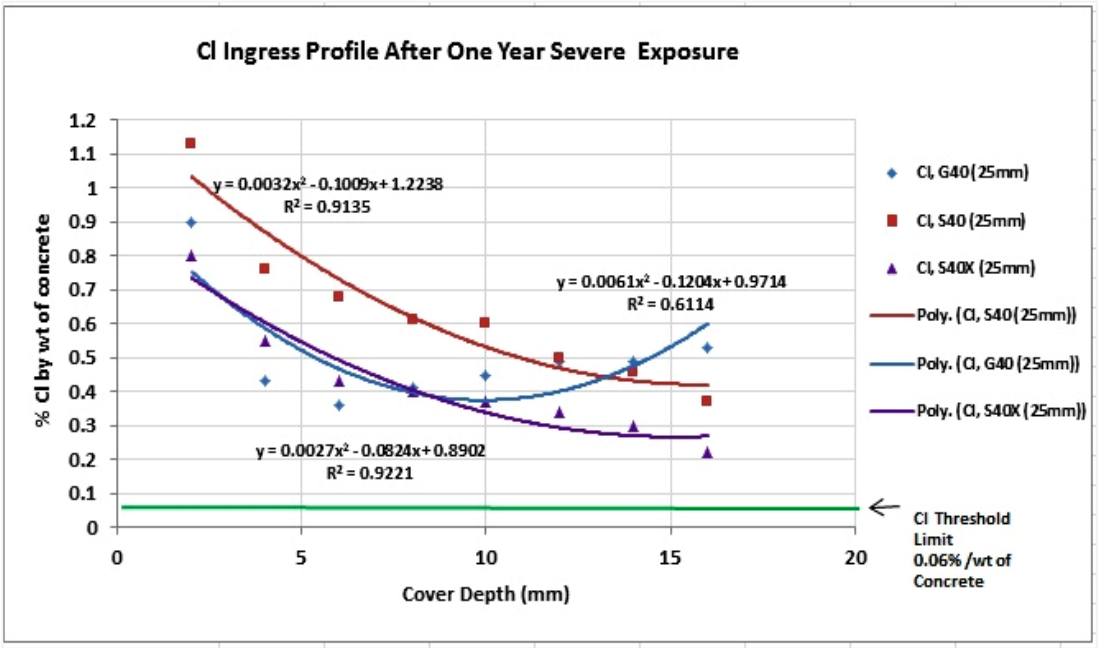

(a)

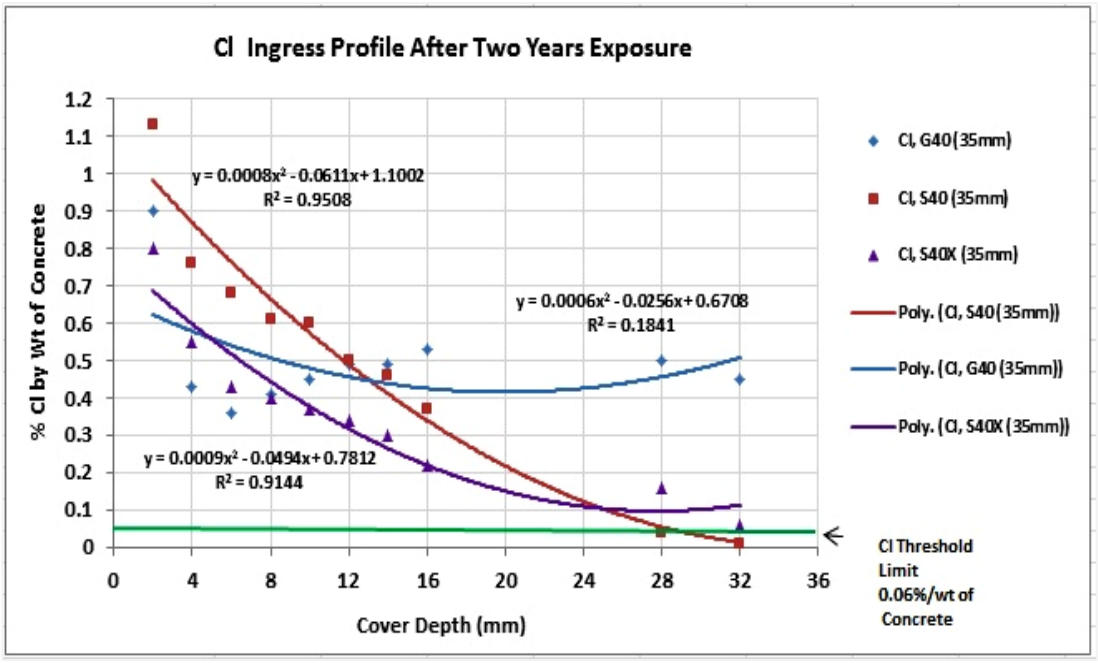

(b)

Figure 5-18 Chloride Content Profiles after one year Exposure

Based on the actual content, the coefficient of co-relation for both S40 and Sx40 samples was 0.91 & 0.92 for the first year of severe exposure and 0.95 & 0.91 for the second year of severe exposure respectively. Whereas coefficient of co-relation for LCFG concrete was 0.61 for the first year and 0.18 was for the second year under severe exposure.

These co-relation coefficients were on the basis of curve fitting based on quadratic equation as shown in Figure 5.18 above.

Diffusion curves' fitting from the mathematical model based on Fick's Second Law with surface concentration C_s as 0.65, 0.9 and 1.2 are shown in Figure 5.19 below.

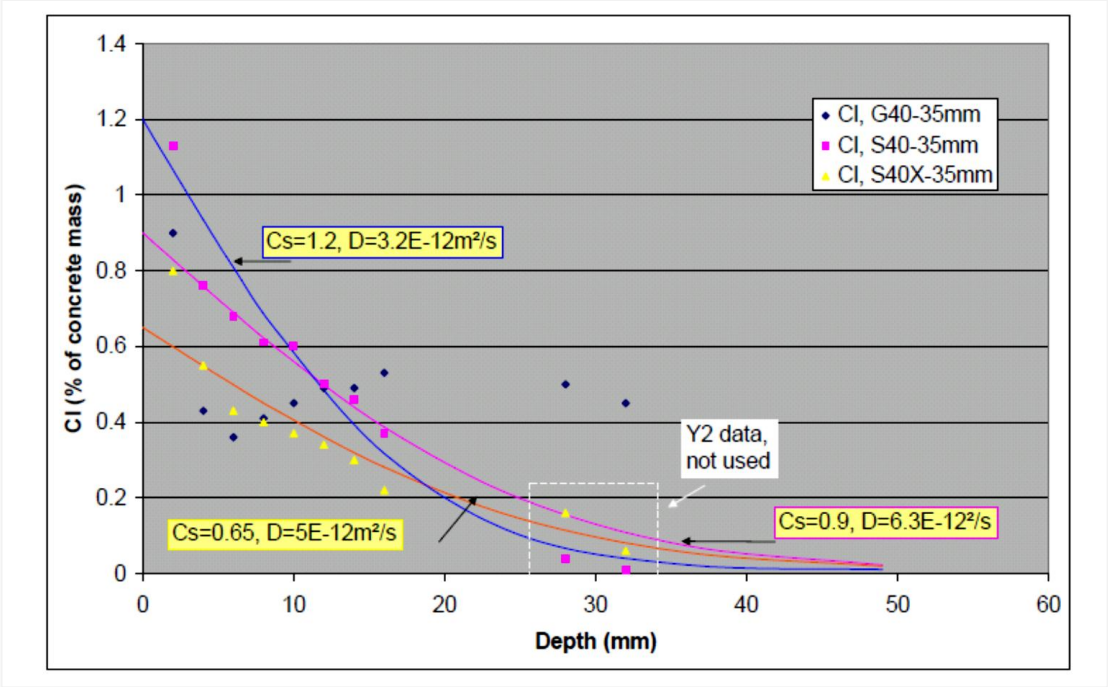

Figure 5-19 Diffusion Model Curves

The curve fittings for one year and two years severe exposure conditions predicted well for OPC concrete (S40 &Sx40). However the curve fittings under-predicted the chloride content for LCFG concrete over two years of severe exposure. As such the diffusion model underestimated the level of chloride content ingressed into LCFG concrete (G40) matrix against surface concentration (C_s) of either1.2 or 0.9 or 0.65.

The predicted values from the mathematical model were 250 - 400% lower than the actual values of ingressed chloride content in LCFG concrete exposed to severe environments. Alternatively actual chloride content in LCFG concrete observed was 2.5 to 4 times higher than the predicted values of chloride content from the mathematical model.

Table 5.9 below summarises the actual and predicted chloride content results for S40, Sx40 and G40 at 35mm cover depth. The actual results showed the degree of confidence with the mathematical model predicted results.

Table 5-9 Predicted Vs. Actual Chloride Content from Chloride Profile Test

Mix	Diffusion Model Parameters and Output from Chloride Concentration Profile		Predicted Chloride Content from the Diffusion model for Year 2		Actual chloride content from the Chloride Profile Test for Year 2	Ratio to the predicted chloride content
	Surface Concentration	Diffusion Coefficient $x10^{-12}$ m^2/sec	Cover Depth (mm)	Cl Concentration (% of Conc. Mass)		
S40	1.2	3.17	28	0.20	0.04	0.2
			32	0.14	0.01	0.07
	0.9	6.34	28	0.15	0.04	0.27
			32	0.11	0.01	0.10
Sx40	0.9	6.34	28	0.30	0.16	0.53
			32	0.24	0.06	0.25
	0.65	5.07	28	0.18	0.16	0.89
			32	0.14	0.06	0.43
G40	1.2	3.17	28	0.20	0.50	2.5
			32	0.14	0.45	3.2
	0.9	6.34	28	0.15	0.50	3.3
			32	0.11	0.45	4.1
	0.65	5.07	28	0.18	0.50	2.8
			32	0.14	0.45	3.2

Higher level of ingressed chloride content in LCFG concrete than the predicted ones from NT Build 443 test will cause the corrosion of embedded steel quicker and at a higher rate.

After 3rd year of exposure chloride content profiles were determined up to 50mm cover depth as shown in Figure 5.20 below.

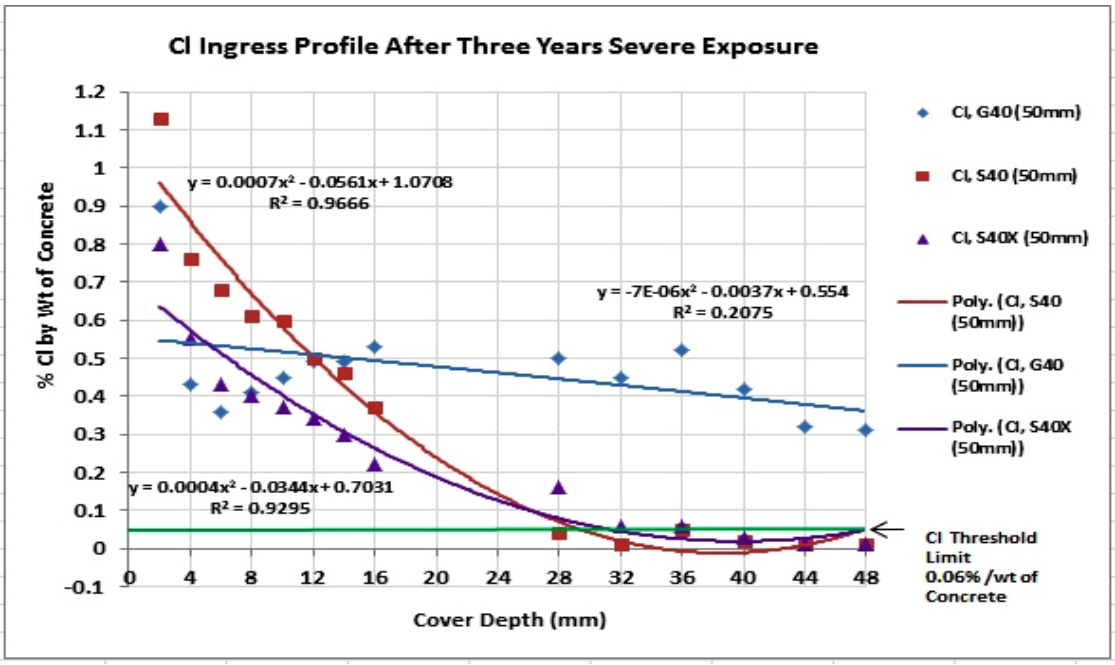

Figure 5-20 Chloride Content Profiles after two years Exposure

In OPC concrete, chloride content falls below the threshold limit after 32mm cover depth, for OPC concrete and remained so up to 50mm cover depth. However chloride content in LCFG concrete was 6-7 times higher than the threshold limit at 32 mm cover depth and was 4-5 times higher the threshold limit at 50mm cover depth.

Figure 5.21 below shows the model curves' fitting for all type of concretes with one, two and three year's exposure.

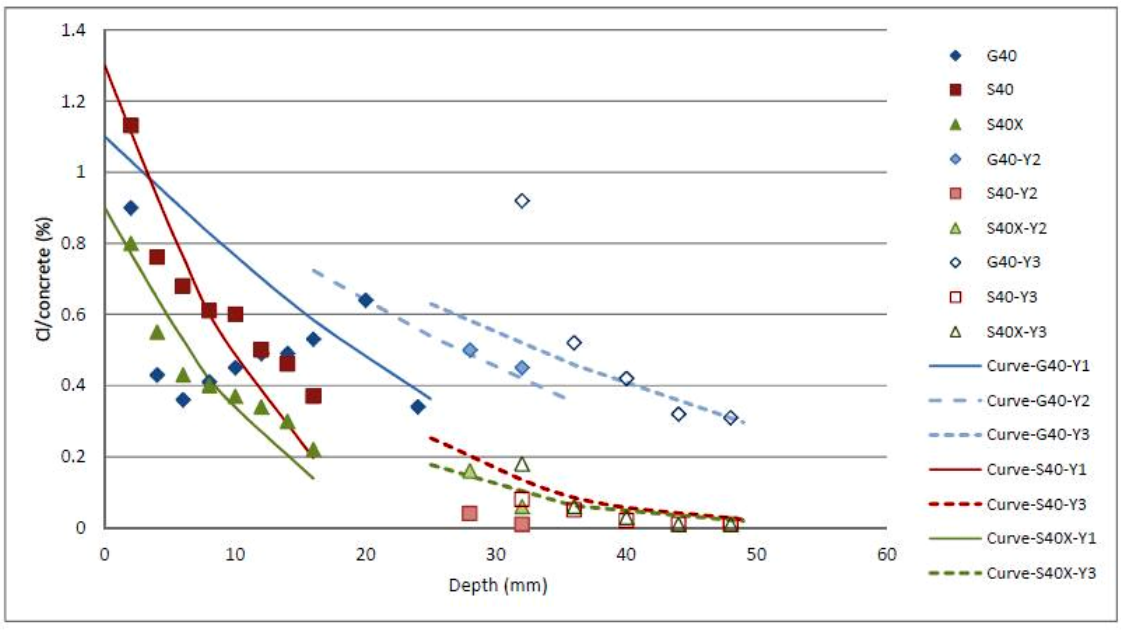

Figure 5-21 Theoretical Diffusion Curves

The data plotted in Figure 5.21 above are as: Y1 is after one year exposure, Y2 is after two year and Y3 is after three year exposure. The parameters used for the curves and the predicted diffusion coefficient values are summarised in Table 5.10 below.

Table 5-10 Diffusion Curves' Fitting Parameters

	G40	S40	S40X
Cs	1.1	1.3	0.9
D (mm²/year)	320	60	60
OR: D (m²/s)	10.1×10^{-12}	1.9×10^{-12}	1.9×10^{-12}
C_0	0.01	0.01	0.01

Although theoretical curves as shown in Figure 5.21 above shows the decreasing chloride content trend with cover depth and time for LCFG concrete, but the indication of chloride content ingressed remained higher than OPC concrete. With lower surface concentration value (Cs = 0.9), diffusion curve fitting for G40 showed diffusion coefficient value as D = 475mm²/year (or 15×10^{-12} m²/s), which was 8 times higher.

Chloride profile test undertaken on core specimens after three year severe field exposure extracted from box culvert samples' leg of respective concrete (approximately from identical location) are shown is Figure 5.22 below.

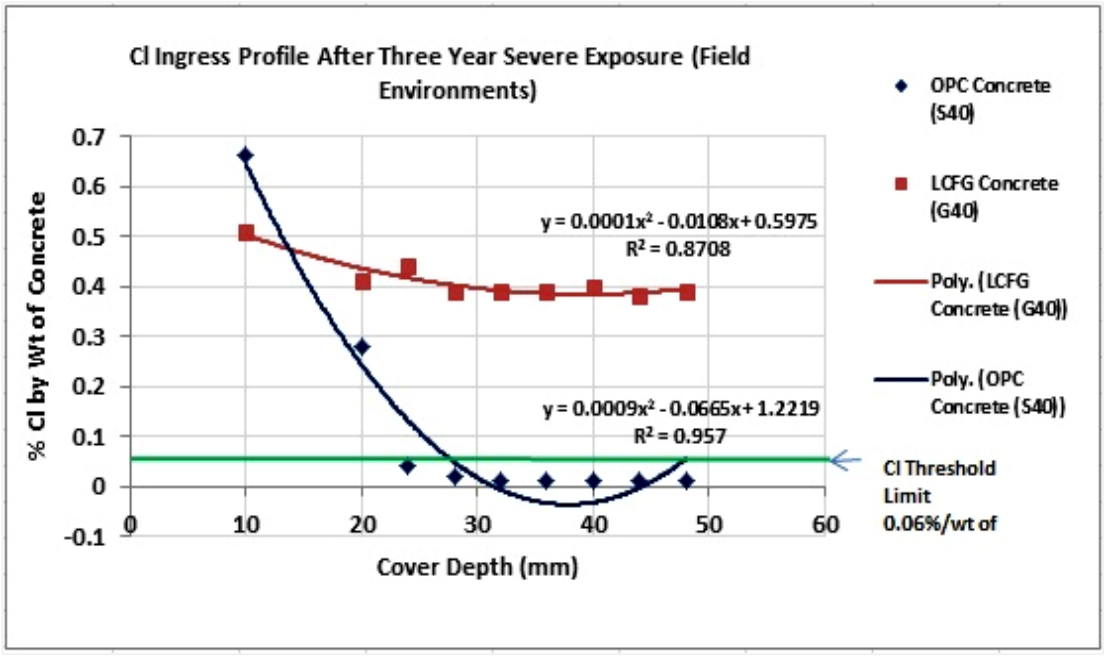

Figure 5-22 Chloride Content Profiles of Field Box Culverts after three Years Exposure

5.8.5 Chloride Profile Test from Field Box Culvert and Theoretical Curves

The chloride profile of S40 indicates the apparent diffusion coefficient as D_a = 6.34 x10^{-13} m^2/s (or 20 mm^2/year) for surface chloride content (C_S) as 1.2%.

Figure 5.23 below shows the chloride content profile and mathematical model curve for OPC concrete box culvert sample.

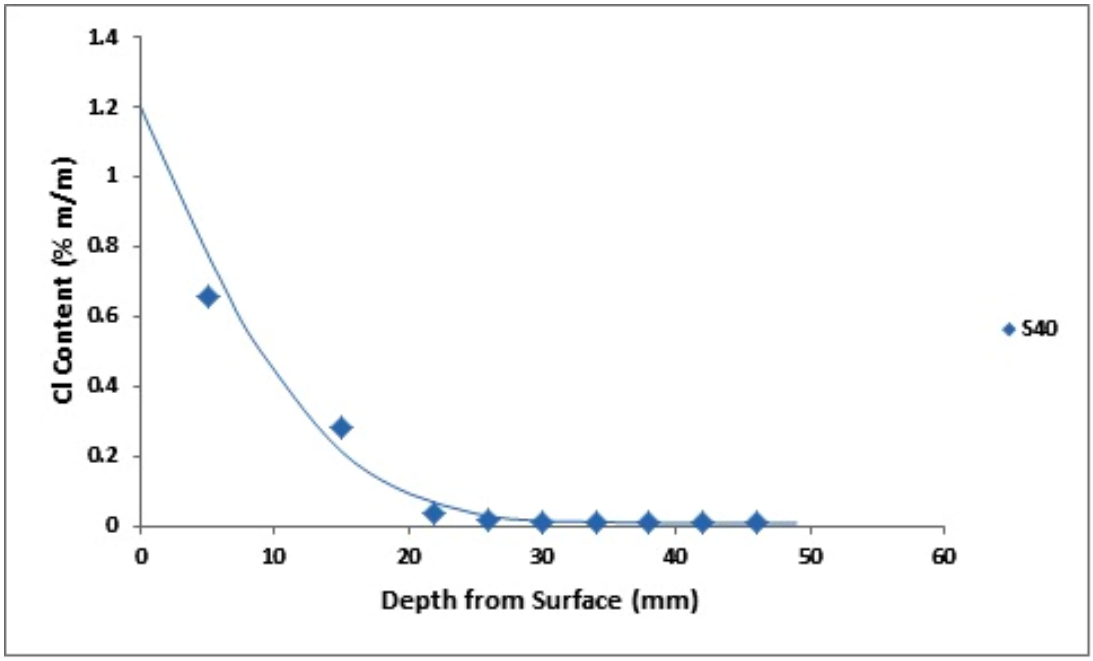

Figure 5-23 Diffusion Curve from the Model for Field Box Culvert Sample (OPC Concrete)

Whereas chloride content profile of LCFG concrete (G40) specimen does not fit the diffusion curve. The explanation for this inference can be related to the exposure conditions and the quality of the respective concretes, which are represented by above VPV parameters. Field severe model in this research has chloride rich water, containing chloride as 150080 ppm and an average temperature around 24°C as shown in Figure 4.1 in Chapter 4. VPV test results of absorption level after three years severe exposure of summarised as below in Table 5.11 reflects the quality of respective concrete.

The chloride content in LCFG concrete pores was approximately close to what can be derived from the environmental exposure concentration level. This can be calculated by multiplying the absorption to Cl^- concentration in the environment.

Table 5-11 VPV Test Results

Concrete Type	Before Exposure		After Exposure	
	Absorption (%)	VPV (%)	Absorption (%)	VPV (%)
S40 (OPC 400kg/m^3)	5.3	12.25	4.6	10.7
G40 (LCFG Concrete)	4.5 – 4.9	11.6	2.84 – 3.38	7.8

Chloride profile test revealed that the chloride concentration in LCFG concrete pores is approximately close to Cl^- concentration in the environment as shown in Figure 5.24 below.

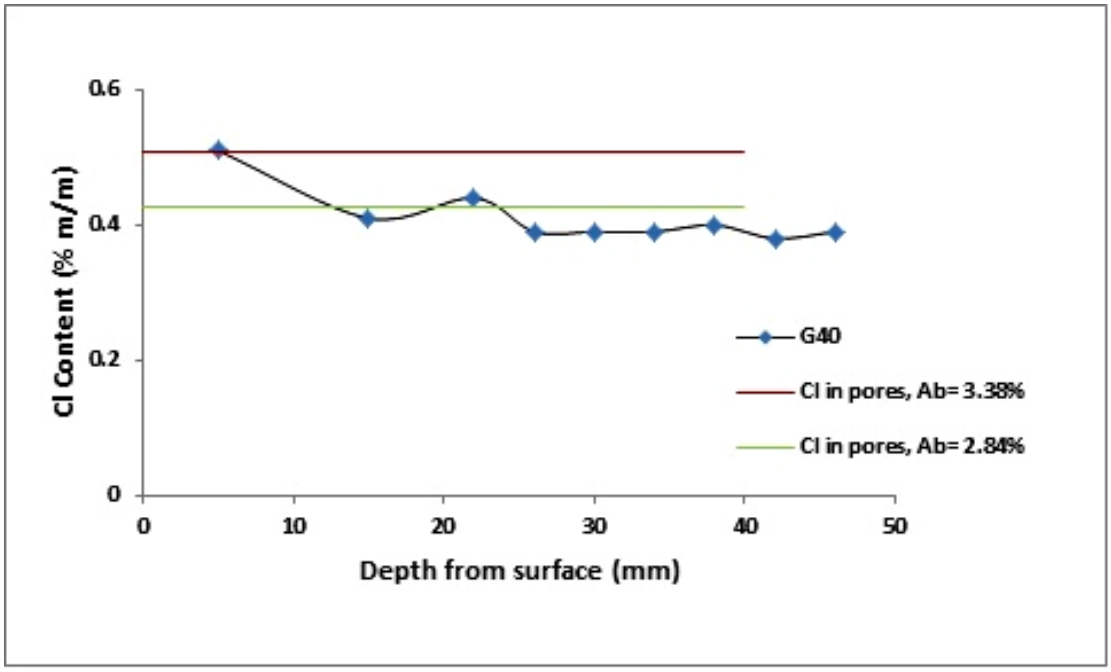

Figure 5-24 LCFG Box Culvert Chloride Profile

The upper line in red colour represented the chloride concentration in LCFG concrete pores which equates to 0.0338 x 0.15008 = 0.5073%. This chloride concentration in LCFG concrete pores is the approximate representation of surface chloride concentration as evident from the chloride profile test.

So above test results showed that low chloride binding and consequent higher diffusion rate is probable for LCFG concrete compared to OPC concrete under severe environmental exposure. This can be inferred from estimated value of chloride surface concentration (C_s), which is 0.5% for LCFG concrete box culvert and 1.2% for OPC concrete box culvert for severe field exposure scenarios. Low surface concentration is indicative of low resistance to chloride penetration as detailed in the subsequent sections.

5.8.6 LCFG Concrete Diffusion Coefficient & Indicative Correlations Based on Limited Data

For LCFG concrete enough diffusion data is not available yet to confirm analogous trend which are perceivable in case of OPC concrete as detailed in Chapter 3 and shown in Figure 3.3 (a) & (b). However following can be inferred based on diffusion tests undertaken in this research. Table 5.12 below summarises these test results.

Table 5-12 Diffusion Coefficient Values

Sample	Cl^- at Surface, C_s(%)	Diffusion Coefficient x 10^{-12} (m^2/s)	Ratio to Controlled OPC Concrete
G40	0.36	15.8	1
S40	0.86	9.5	0.60
Sx40	0.65	9.5	0.60
G50	0.37	22.2	1
S50	0.80	7.9	0.35

The LCFG concrete of 50MPa contains additional water in the mix synthesisation raising its water to geopolymer solid ratio. This additional water resulted 65% higher diffusion coefficient than controlled OPC concrete of same grade. The LCFG concrete of 40MPa was without additional water in the mix synthesisation and the resulting diffusion coefficient was 40% higher than controlled OPC concrete of same grade.

Diffusion test results of G40 provided that 25% lower diffusion coefficient resulted with no added water compared to G50 specimen, which has additional water. This indicates that higher strength grade LCFG concrete may happen to be not as durable as lower grade LCFG concrete from long term perspective, if water/geopolymer solid ratio is allowed to increase even slightly.

Very high diffusion coefficient resulted when an accelerated diffusion test was undertaken on cylinder specimens representing box culvert samples prepared in previous feasibility study. These diffusion coefficient values are summarised in Table 5.13 below.

Table 5-13 Diffusion Coefficient of LCFG Concrete Used for preparing Box Culvert Samples

Sample	Cl^- at Surface, C_s (%)	Diffusion Coefficient x 10^{-12} (m^2/s)
G40	0.44	350
G40	0.45	165
G40	0.52	170

The diffusion coefficient ranged between 165- 350 x 10^{-12} (m^2/s) with surface chloride concentration (Cs) estimate between 0.44-0.0.45%. This higher diffusion value could attribute to many factors, such as, normal operative environments with lesser degree of control in respect of mix synthesisation, curing temperature and curing time in previous feasibility study for manufacturing LCFG concrete pre-cast box culvert (Siddique, 2007 and Cheema et al, 2009).

5.8.6.1 Chloride Binding and Penetration Resistance

As detailed in the preceding section that an indication of lower surface concentration for LCFG concrete implies its low resistance to chloride penetration and its higher diffusion coefficient value is an indication of its low chloride binding ability.

The explanation of this low chloride binding in LCFG concrete is evident from lower Cs value estimated by the NT Build 443 test in the beginning (Figure 5.16) before subjecting the respective concrete samples and specimen to severe exposure. From NT Build 443 test results, chloride surface concentration was around 0.35% for LCFG concrete compared to OPC concrete for which surface concentration of Cl^- ions was 0.86 %. For high risk area surface concentration minimum extent is around 0.8% (Green et al, 2010). This low chloride surface concentration for LCFG concrete is indicative of its low resistance to chloride penetration.

Following interpretations from these test results also give an indication of free chloride content that could be available in LCFG concrete, which relies on the severity level of exposure environments.

Cs (OPC concrete) – Cs (LCFG concrete) = 0.86 – 0.37 = 0.49 (LCFG concrete free chloride content)

From field samples similar trend was observed.
Cs (OPC concrete) – Cs (LCFG concrete) = 1.2 -0.5 = 0.7 (LCFG concrete free chloride content)

This high level of free chloride content in LCFG concrete is responsible for high apparent diffusion coefficient (D_a). This was apparent from the test results, which showed higher diffusion coefficient values for LCFG concrete between 15.8- 22.2x 10^{-12} (m^2/s) compared to OPC concrete diffusion coefficient, which ranges between 8-9.5 x 10^{-12} (m^2/s).

Concrete with reinforcement cover of up 50mm needs $2.5x10^{-13}m^2/s$ diffusion coefficient for 50 year design life. This is with other parameters as : chloride threshold limit(Ct) of 0.5% by weight of binder, surface chloride concentration (Cs) as 0.6% and initial chloride concentration (Co) as 0.005%- 0.01% (Refer diffusion coefficient calculations in Appendix -D). However based on the chloride profile test results output, diffusion coefficient derived for LCFG concrete is $8.2x10^{-11}m^2/s$. At this diffusion coefficient value, threshold chloride concentration can build- up in a month up to 35mm cover depth, which is approximately 5- 6 times quicker than the predicted values by NT Build 443 test.

So whereas higher diffusion coefficient of LCFG concrete are indicative of its low chloride binding abilities compared to OPC concrete, test results are also indicative of early corrosion initiation and higher corrosion rate risk to the embedded steel in LCFG concrete.

5.8.7 Sensitivity Level

Inference of high diffusion coefficient values also indicates that LCFG concrete porous structure may be more sensitive to the water/binder ratio compared to the sensitivity of OPC concrete on account higher w/c ratio. Small increase in water/geopolymer solid ratio can cause the development of larger size interconnected and continuous pore system in LCFG concrete. As such higher level of sensitivity on account of water/binder ratio and curing parameters may impact the durability of LCFG concrete.

Following Figures (5.25 a - e) show the correlation trend of w/b ratio corresponding to strength and diffusion coefficients values for both LCFG concrete and OPC concrete.

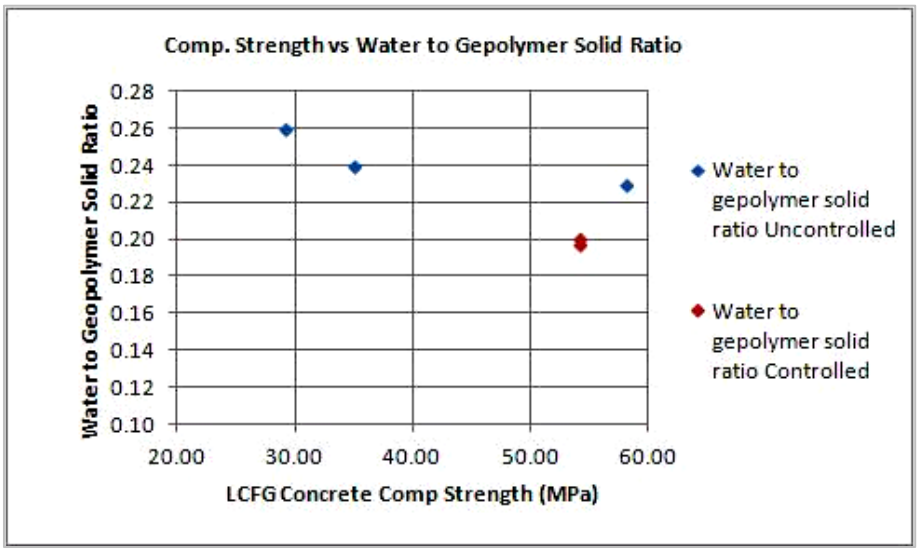

(a)

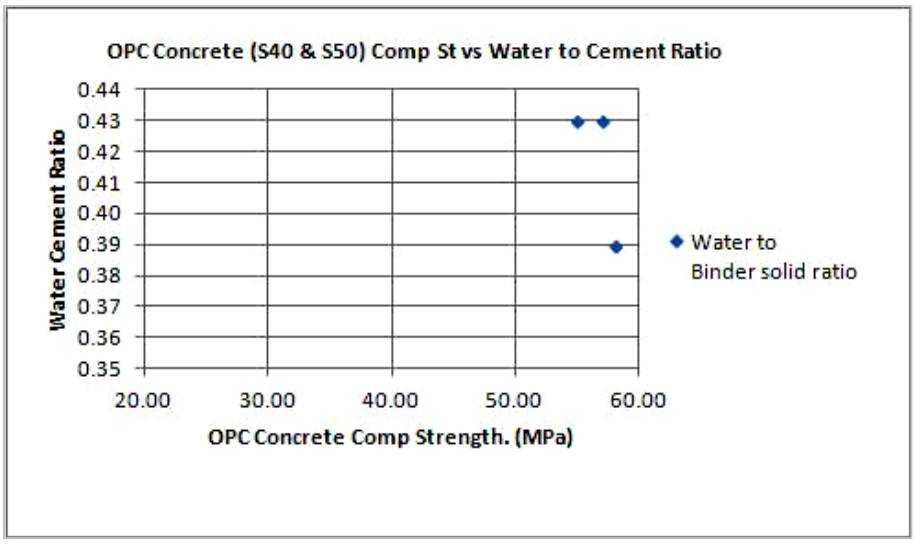
OPC Concrete (S40 & S50) Comp St vs Water to Cement Ratio
Water Cement Ratio
0.44
0.43
0.42
0.41
0.40
0.39
0.38
0.37
0.36
0.35
20.00
30.00
40.00
50.00
60.00
OPC Concrete Comp Strength. (MPa)
Water to Binder solid ratio

(b)

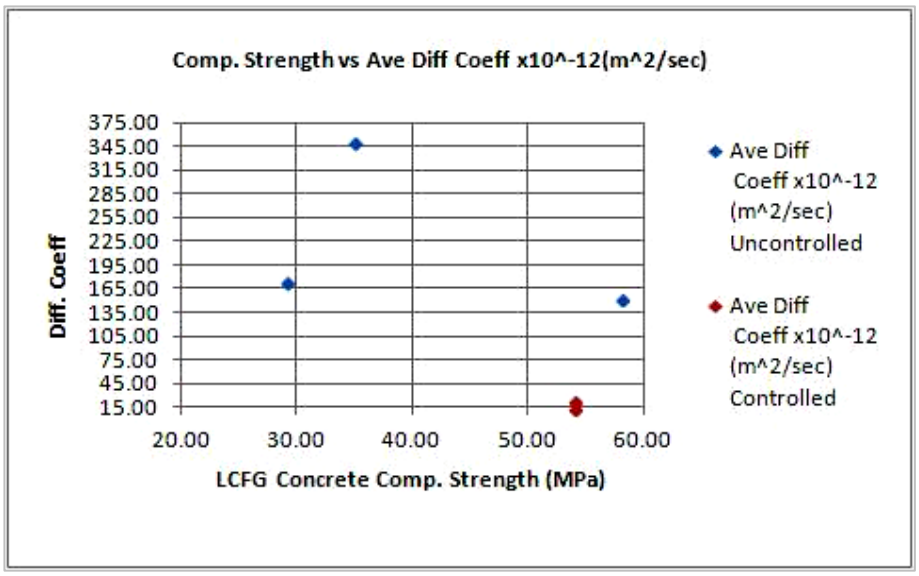
Comp. Strength vs Ave Diff Coeff x10^-12(m^2/sec)
Diff. Coeff
375.00
345.00
315.00
285.00
255.00
225.00
195.00
165.00
135.00
105.00
75.00
45.00
15.00
20.00
30.00
40.00
50.00
60.00
LCFG Concrete Comp. Strength (MPa)
Ave Diff Coeff x10^-12 (m^2/sec) Uncontrolled
Ave Diff Coeff x10^-12 (m^2/sec) Controlled

(c)

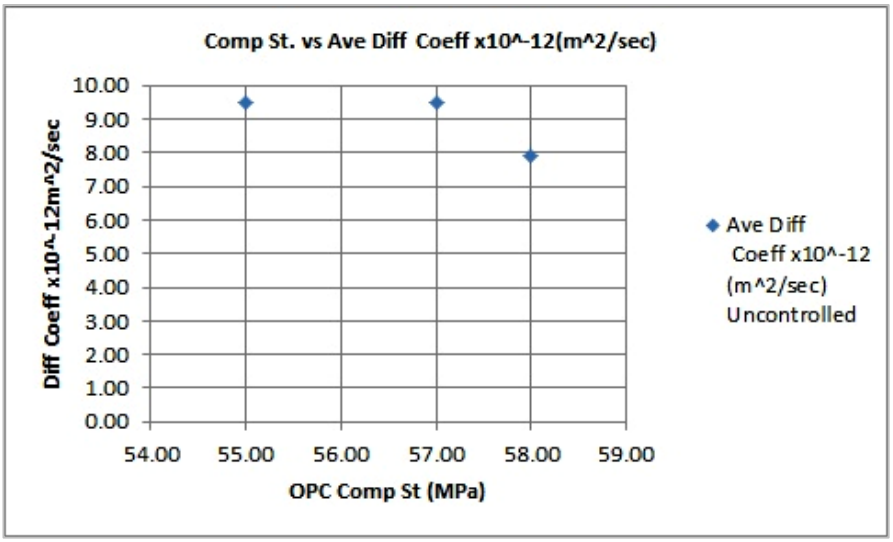
Comp St. vs Ave Diff Coeff x10^-12(m^2/sec)
Diff Coeff x10^-12m^2/sec
10.00
9.00
8.00
7.00
6.00
5.00
4.00
3.00
2.00
1.00
0.00
54.00
55.00
56.00
57.00
58.00
59.00
OPC Comp St (MPa)
Ave Diff Coeff x10^-12 (m^2/sec) Uncontrolled

(d)

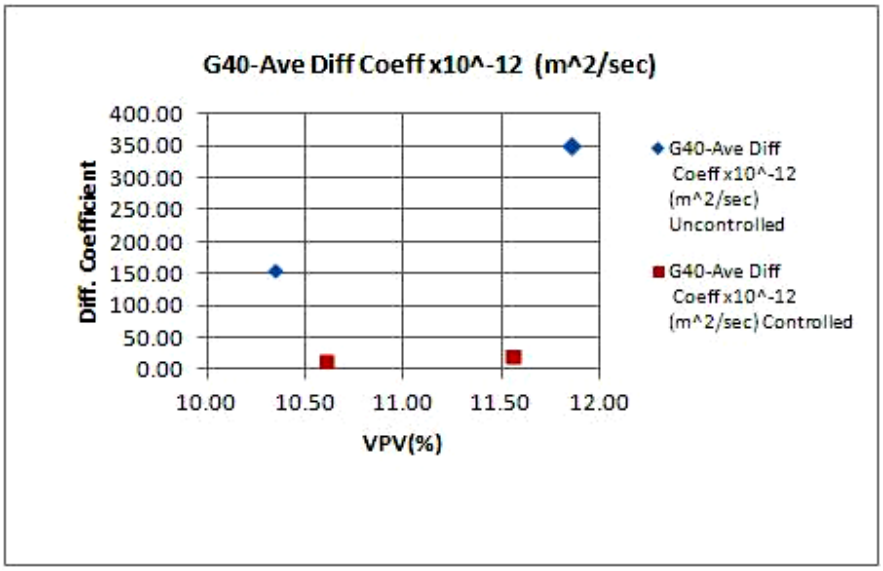

(e)

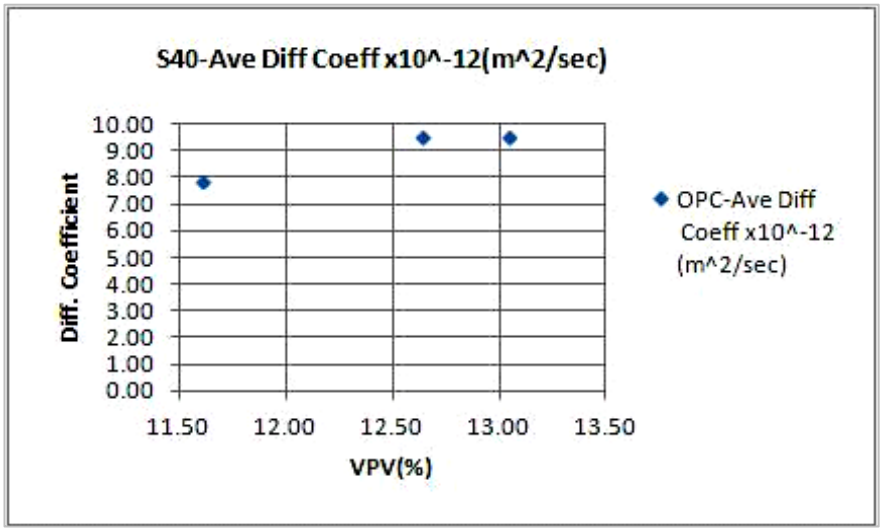

(f)

Figure 5-25 Compressive Strength, water/Binder Ratio, Diff. Coefficient & VPV Correlations Trend

In above correlations OPC concrete compressive strength follows the water/binder ratio variation with significant lesser degree of sensitivity (strength variation range is between 55-58 MPa). That is higher water/binder ratio results lower compressive strength. Similar trend was observed for LCFG concrete with a higher degree of sensitivity (Strength variation range was between 30- 58 MPa as shown in Figure 5.25-(a). This observation also confirms the trend of lower strength with higher water/binder ratio, Hardjito & Rangan (2005) have observed in their research study.

Figure 5.25-(c) shows higher diffusion coefficient value under uncontrolled conditions compared to controlled condition. Variation extent of diffusion coefficient values was between 165-350x10^{-12} m^2/s with uncontrolled conditions compared to controlled one which has variation between 15.8 - 22.2 x10^{-12} m^2/s. For LCFG concrete this was without regard to the instance where compressive strength result could be higher under uncontrolled condition as shown in Figure 5.25 –(c). This vide variation of key durability indicator (diffusion coefficient) indicates the higher level of sensitivity of LCFG concrete compared to OPC concrete. This higher level of sensitivity of LCFG concrete means that the higher level of quality control measures during mixing, casting and curing stages for LCFG concrete compared to OPC concrete are required.

OPC concrete and LCFG concrete diffusion coefficient followed the VPV values trend but LCFG concrete diffusion value was significantly higher than diffusion coefficient values of OPC concrete, which further gets influenced by uncontrolled conditions as shown in Figure 5.25 (e) & (f). These correlations trend indicates the sensitive nature of the LCFG concrete and confirms the observations of Duxson et al (2007) in respect of sensitivity to small changes in the parameters for geopolymer concrete.

5.9 CARBONATION

Carbonation assessment on cores taken from both LCFG and OPC concrete samples and as well from field box culvert samples when sprayed with chemical compound (phenolphthalein) on their immediate extraction indicated no pink coloration. For OPC concrete $Ca(OH)_2$ behind the carbonation front is completely reacted and pH could be as low as 8 however ahead of the front, pH were 12 or more. This trend however was absent in LCFG concrete. This indicates that the LCFG concrete specimens were carbonated.

Information available in the literature refers that carbonation in OPC concrete is very slow process, which could be up to 5mm over 30-40 years as a complete carbonated zone and 10-15mm as an incomplete carbonated zone (Hong et al, 2006).

However further research for the similarity of such carbonation scenarios in LCFG concrete is required on long term basis under normal atmospheric CO_2 concentration, which is in order of 0.04% (Greene et al, 2010).

The effervescing action on spray of dilute HCL on efflorescence products as detailed in Section 5.7.1 indicated the presence of carbonation activity. This carbonation activity at primary and secondary reaction level in LCFG concrete as detailed in Section 5.7.1 may cause the carbonation of its interior as evident from these extracted cores tested for their carbonation front.

This carbonation observation was in line with the findings of Zhang et al, 2013; Bernal, et al, 2012 and Adam et al, 2009. Zhang et al (2013) research showed the efflorescence products on LCG concrete contain sodium carbonates' formation, which resulted on ambient cured specimens after a short duration of 3 hours atmospheric exposure compared to the heat cured one. Bernal et al (2012) research showed that alkali activated binders under normal and accelerated CO_2 concentration result the development of sodium carbonate & sodium bicarbonate. Adam et al (2009) showed that slag activated binder has almost 8 times higher carbonation front than OPC concrete.

The possible carbonation processes which may occur in LCFG concrete, may be from potential un-reacted source material Ca and residual NaOH from alkaline solution used in the mix synthesisation of geopolymer binder paste initially. The other possibility is from atmospheric CO_2 reacting with free water in LCFG concrete forming carbonic acid (with ionisation constant, $K1 = 4.3x10^{-7}$), which can dissociate into CO_3^{--} and HCO_3^{-} ions. These dissociate ions can form insoluble carbonate on reacting with cations present in the pore solution such as Ca, Mg and Mn, which may affect the LCFG concrete matrix similar to OPC concrete from its densification aspect.

Availability of other type of cations, such as, Na and K may form soluble sodium and potassium carbonate. These soluble carbonates may maintain the pH level present in the LCFG concrete matrix initially but with eventual acidification (Sergi & Panteli, 2011). Based on the high level of scaling observed for LCFG concrete compared to OPC concrete in this research (Section 5.7) indicates the presence of $NaHCO_3$, Na_2CO_3, $MgSO_4$, $MgCO_3$, which may be active for carbonation in LCFG concrete and need further research.

Secondly carbonation reaction releases water which may be of significance for OPC concrete from further hydration point of view, however from LCFG concrete perspective water produced from the reaction can exasperate the deteriorating processes resulting from chloride, low pH and scaling.

The corrosion rate due to carbonation in the absence of chloride (at accelerated concentration of CO_2 -10%) as a function of pH is evident from Figure 3.18 (Hussaian & Ishida, 2009) in Chapter 3.

In immersed and completely dry scenarios, low level of carbonation was observed for LCFG concrete. This observation was in line with Hansson et al (2007), which indicated that CO_2 concentration in the environment affects the carbonation rate. This occurs at higher rate at intermediate moisture corresponding to relative humidity (RH) 65% -75% as shown in Figure 3.16.

Carbonation synergistically action with chloride at low pH around 9 can exasperate the deterioration process by releasing the bound chloride in case of OPC concrete, while in LCFG concrete synergistically action may be possible with unbound chloride and need further research.

5.10 pH (Alkalinity)

pH as a function of potential is an indicator of thermodynamic stability of aqua species in term of electrochemical responses from corrosion and corrosion rate perspective of rebar (Hussaian & Ishida, 2009). As such concrete pH is of significant importance from passivation perspective of reinforcement.

The cores extracted from both LCFG and OPC concrete samples with 25mm cover after one year severe exposure, two years after from samples with 35mm cover and three years after from samples with 50 mm cover when sprayed with chemical compound (phenolphthalein), turned the OPC concrete specimens from colourless to purple except the LCFG concrete ones.

This is shown in Figure 5.26 below. The intensity of purple coloration gives the extent of possible pH environment of rebar surroundings from visual aspect. Obvious purple coloration is an indication of pH greater than 10 and less than 13. While core specimens with insignificant or no change in colour from the colourless indicate pH value around 10 or less.

Figure 5.26 below indicated that pH of G40 is around 10 or less compared to OPC concrete.

Exposure period in years	Core Specimens from Laboratory Samples G40	S40	Sx40
1 Year (Sample with 25mm cover)			
2 Year (Sample with 35mm cover)	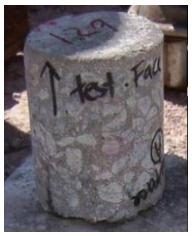		
3 Year (Sample with 50mm cover)		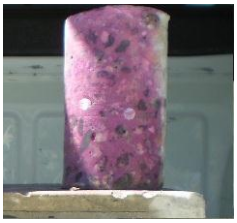	

Figure 5-26 pH indication from phenolphthalein compound indicator

This visual test indication of both LCFG concrete and OPC concrete was confirmed by actual pH test carried out as per AS 1289.4.3.1. The pH test results are summarised in Table 5.14 below.

Table 5-14 pH

Sample Mix	pH from Laboratory Samples at Interval of 1, 2 and 3 Years of Severe Exposure			pH from Field Box Culvert Samples after 3 Years Severe Exposure
	pH -25mm cover at Ave. Depth of 22mm (1 Year Exposure)-	pH- 35mm cover at Ave. Depth of 22mm (2 Year Exposure)-	pH -50mm cover at Ave. Depth of 46mm (3 Year Exposure)-	
G40	10.2	9.3	10.3	8.9
S40	12.3	12.3	12.1	11.6
S40X	12.4	12.3	12.1	-

Figure 5.27 below shows the pH trend of LCFG concrete, which is around 10 or less compared to OPC concrete tested as per AS 1289.4.3.1 which is around 12.

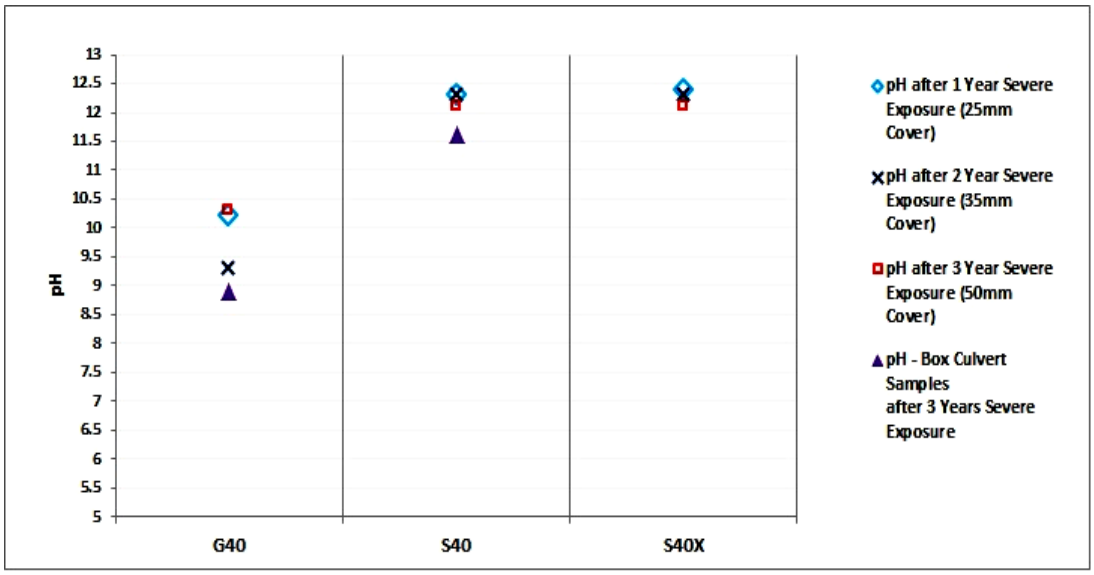

Figure 5-27 pH Trend for Laboratory and Field Box Culvert Samples

High pH environments (around 12.5 - 13) in OPC concrete forms the basis of oxide passive film formation and its stability. This oxide passive film on the surface of the steel reinforcement acts as a protection barrier from active corrosion and does not form immediately. However this oxide passive film starts forming soon as the pH level reaches 12 or above. This pH level develops in OPC concrete from more and more hydration of Ordinary Portland Cement (OPC) in the beginning and tend to stay at steady level of 12 or above over long time unless is impacted negatively by external factors.

5.10.1 pH Results Discussion Relative to Chloride Content from Profile Chloride

High pH of 12 or above is considered imperative for the development oxide passive film over a week or so initially (Hansson et al, 2007), and then to maintain the passive film over a long period for the integrity of embedded steel in OPC concrete. But low pH environments as shown by the test results indicate that the passivation status of reinforcement in LCFG concrete is of lower level (that is, corrosion risk may be high) compared OPC concrete from long term durability perspective.

Figure 5.28 below shows that pH around 10 and available free chloride around 0.5 % by mass of binder (which approximately equates to 0.05% by mass of concrete) observed for LCFG concrete in this research will cause the corrosion rate of embedded steel in excess of $0.02 gm/cm^2$ per year.

While pH around 12 and free chloride content of 0.4% by mass of binder approximately will result the corrosion rate as 0.01 gm/cm^2 per year for embedded steel in OPC concrete as evident from Figure 5.28 below (Hussaian & Ishida, 2009). This analysis indicates that the corrosion rate gets doubled by drop of pH level by 2 and with the increase of chloride content by 0.1% mass of binder.

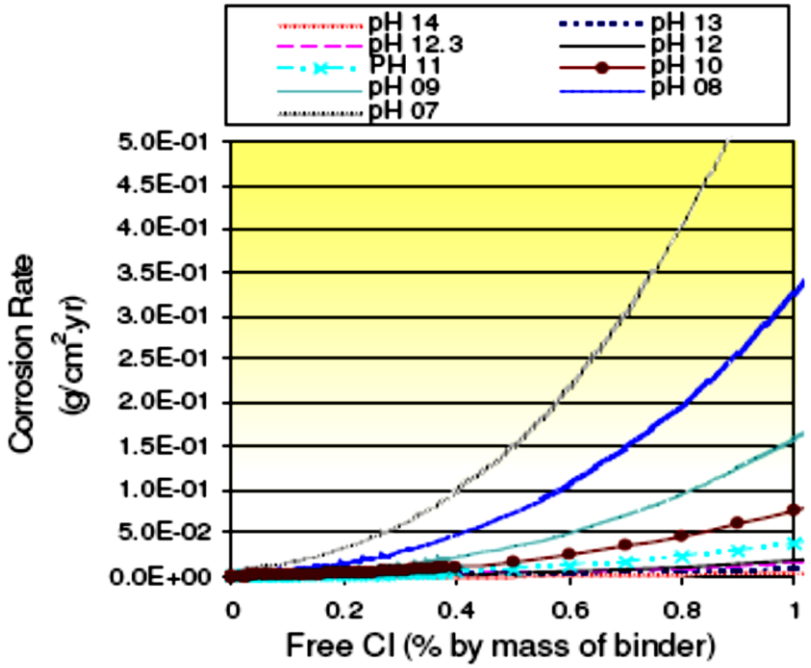

Figure 5-28 Corrosion Relative to pH values

At 35 mm cover depth chloride content from chloride profile test for OPC concrete is around at 0.04% (by mass of concrete), but for LCFG concrete at 35 mm cover depth chloride content is 0.5% by mass of concrete (which equates to 5% by mass of binder). This is 10 times higher on the scale for free chloride assessment on the basis of above analysis.

Corrosion rate in LCFG concrete (by simple approximation) will be around 0.2gm / cm^2 per year for chloride content 0.5% by mass of concrete from Figure 5.28 above. When the corrosion rate is compared based on actual chloride content as per chloride profile test then the corrosion rate for LCFG concrete will be 20 times higher compared to OPC concrete.

The chloride content dropped with the increased cover thickness in LCFG concrete but the drop was not significant. It was from 0.5 % to 0.3% by mass of concrete. This equates to 40% drop. Obviously drop in corrosion rate will occur, if assumed by the same percentage, corrosion rate will be still 12 times higher than OPC concrete approximately.

This higher corrosion risk and corrosion rate to embedded steel with reference to low pH of electrolytic solution surrounding the rebar and free chloride available in the concrete matrix as percentage by mass of binder is probable in LCFG concrete compared to OPC concrete.

The formation of passive film in LCFG concrete and its stability over the service life is not fully understood yet. One reason for low pH in LCFG concrete could be from the consumption of the alkaline solution during the chemical reaction that take place in polymerisation process involving:

- Dissolution of aluminosilicate species
- Polycondensation of the aluminium and silicon species
- Multiple gel formation phases of aluminosilicate species
- Connectivity of gel network through continued rearrangement and reorganisation resulting hardened polymerised product called geopolymer with two-up- three dimensional amorphous structures (Skvara et al, 2006).

pH value of the electrolyte in porous concrete characterises the electrochemical behaviour of the embedded steel. Electrochemical techniques (concrete resistivity, half- cell potential, linear polarisation resistance technique for corrosion current assessment galvano- statically) evaluate these electrochemical behaviours for both LCFG concrete and OPC concrete.

Subsequent sections detail the testing outputs of electrochemical techniques and quantify the active corrosion and corrosion risk for LCFG concrete & OPC concrete from long term durability perspective under severe exposure.

5.11 ELECTROCHEMICAL TEST OUTPUTS FROM CORROSION PERSPECTIVE

The susceptibility of corrosion to reinforcement in concrete is due to the composition of electrolyte in concrete pores' structure. LCFG concrete mix shows different chemical reaction and consequently its ability to maintain the protection to the steel will be different in comparison with OPC concrete.

So passivating mechanism for embedded steel in LCFG concrete could be either an oxide film or some other form of silica compound film or combination of both. Environmental conditions influence the electrolyte composition.

Chloride induced corrosion is the predominant one causing active corrosion of embedded steel in concrete. Metals having exposure to environmental conditions such as moisture, corrosive chemicals – acids, salts and gases (O_2, CO_2, H_2S etc.) and high temperature are liable to be corroded as a result of anodic and cathodic reaction activities as detailed in Chapter 3 (Section 3.3.1). Corrosion process once initiated; its rate is a complex function of several factors, such as:

- pH of electrolyte
- Open circuit potential of coupling metals (Eo) - difference in natural potential in galvanic (bimetallic) couples, metallurgical variations in the state of the metal at different points on the surface, local differences in the environment (such as variations in the supply of oxygen at the surface, chloride ingress and carbonation causing the passage of electrical currents on micro or macro scale resulting corrosion at anodic locations - oxygen depleted areas become the anode & oxygen rich areas become the cathode).
- Resistivity of concrete
- Chloride concentration of the electrolyte
- Dissolved Oxygen or Oxygen concentration of electrolyte

Following sub-sections provide the test outputs of electrochemical testing techniques used to evaluate the protection level of embedded steel in LCFG concrete and its comparison with OPC concrete.

5.11.1 Resistivity

Resistivity measurements test is possible on all exposed part of the concrete structures that are exposed to air although it has limitation for submerged or buried parts (RIELM TC 154-EMC, 2000). A low resistivity implies that reinforcement corrosion is occurring and the corrosion rate is likely to be high.

Resistivity tests were undertaken on laboratory samples and field samples (box culverts sample) exposed to environmental exposures as summarised in Table 4.1. Resistivity of not exceeding 10 kilo-ohm cm is not the controlling parameter of corrosion rate, however is indicative of high corrosion risk (Arredondo et al, 2011).

Figure 5.29(a) shows the non-aggressive set-up and Figure 5.29 (b) below shows the severe field exposure set –up. RESIPOD resistivity test outputs are provided in Appendix -E.

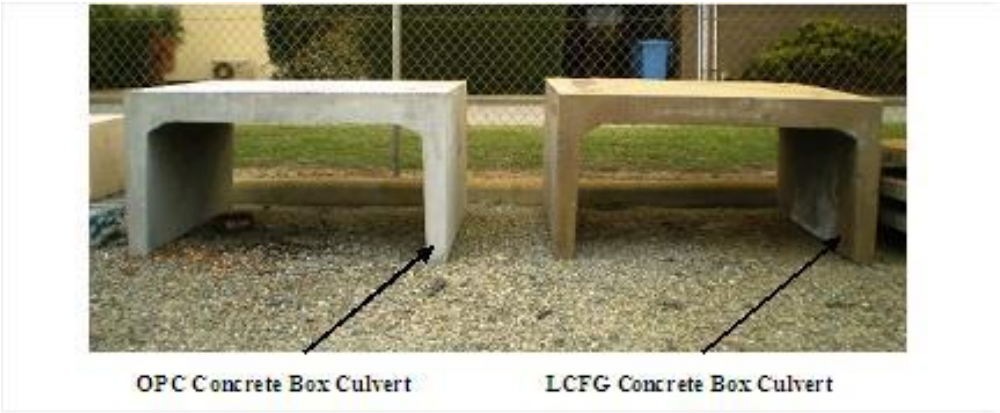

(a)

(b)

Figure 5-29 Field Box Culvert Samples Exposed to Non-aggressive and Aggressive Environments

The resistivity test results showed low resistance of 59 Ohm m for LCFG box culvert sample exposed to non- aggressive to mild atmospheric conditions compared to OPC box culvert sample which showed resistivity of 388 Ohm m.

Similar trend was inferred for laboratory specimens which were in outside & dry environments and has undergone regular inundation to severe saline water and soil cycles over two years. These samples showed resistivity of 72 Ohm m for G40, 382 Ohm m for S40 and 208 Ohm m for Sx40.

But the laboratory samples in wet form with regular inundation of severe saline water and soil showed very low resistivity of 3 Ohm-m for G40 and 75 Ohm-m for S40 and 21 Ohm-m for Sx40 OPC

Table 5.15 below summarise these resistivity measurements and probable corrosion risk based on the criteria detailed in Chapter 3.

Table 5-15 Corrosion Risk from Resistivity Observations

Environments	Ave Surface Resistivity (Ohm m)								
	G40	**Cl ion pene-trability prob-ability**	**Corr-osion Risk**	**S40**	**Cl ion pene-trability prob-ability**	**Corr-osion Risk**	**Sx40**	**Cl ion pene-trability prob-ability**	**Corr-osion Risk**
Laboratory non – aggressive and simulated aggressive environments									
B1(mild to non-aggressive) –Lab Box Culvert Samples	59	High	High	388	Low	Mode-rate	-	-	-
A (Dry & Inside) Lab Sample Specimens	2648	Neg-ligible	Neg-ligible						
B1(Dry and Exposed) Lab conditions	72	High	High	382	Very Low	Mode-rate	208	Mode-rate	Mode-rate
U (Exposed to severe lab conditions)	3	High	High	75	High	High	21	High	High
Field Aggressive Environments									
U (Very Severe to severe) – Field Box Culvert Samples	18	High	High	-	-		199	Mode-rate	Mode-rate

Electrical resistivity of the concrete is liable to be influenced by porosity, RH and the resistivity of pore solution (i.e. pore water containing dissolved salts). Test results revealed improved resistivity in less moist environments.

Very high resistivity of 2648 Ohm- m for LCFG concrete cylinder specimen was inferred, which were in sheltered and dry environments. Field box culvert samples resistivity (from critical location on side-leg) was 18 for LCFG concrete and 199 for OPC concrete.

Figure 5.30 below provides the resistivity trend of laboratory samples and field samples in relation to their environmental exposure and their severity level.

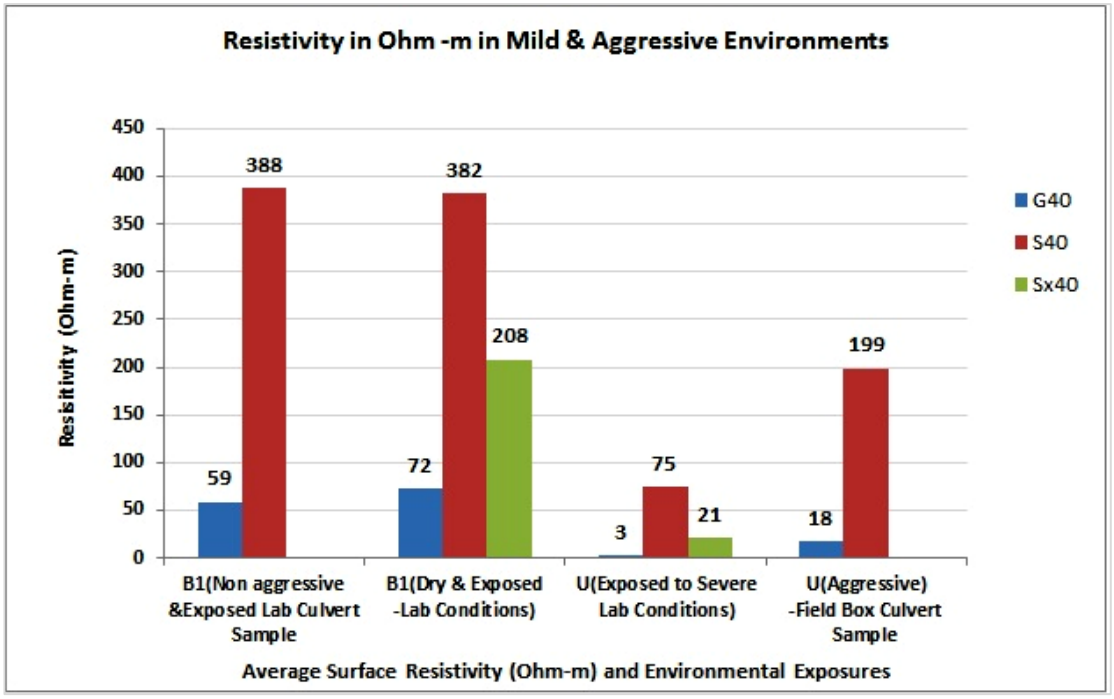

Figure 5-30 Surfaces Resistivity & Environmental Exposure Class

5.11.1.1 Resistivity Result Discussion

Low resistivity of LCFG concrete indicated higher probability of chloride penetrability under normal prevailing RH conditions and severe exposure of saline water and salt rich soil.

The reason for lower resistivity of LCFG concrete could be due to the depletion of OH^- ions from pore water solution on account of polymerisation or carbonation action which increases the conductivity of pore water (Simon et al, 2012).

Opposite is probable in OPC concrete as carbonation densify the OPC concrete, which result high resistivity (RIELM TC 154-EMC, 2000).

Secondly increasing amount of chloride ingress into the pore liquid under severe exposure may result it more homogeneous conductor, which could be the potential reason of low resistivity of LCFG concrete compared to OPC concrete.

Resistivity test results trend of laboratory samples with severe exposure and cover to reinforcement as 25mm, 35mm and 50mm are summarised as below in Table 5.16.

Table 5-16 Resistivity Measurements

Sample No	Resistivity and Reinforcement Cover					
	Cover	k Ohm cm	Cover	k Ohm cm	Cover	k Ohm cm
G40	25mm	3	35mm	3	50mm	2
G50		2		2		2
S40		94		75		59
Sx40		59		21		27
S50		50		58		78

The resistivity results indicate that probability of corrosion risk to embedded steel over long time in LCFG concrete is higher than OPC concrete. The above resistivity test results are based on an average daily relative humidity (RH) 60-70 during morning hours and 50-60 afternoon (Australian Meteorology Department based 30 years data) as per figure in Appendix –A, which shows the samples' location as well.

- Relative Humidity and Temperature Influence on Resistivity

Lower RH results pore solution more concentrated, which results high pore wall surface area to liquid ratio. This high pore wall surface area to liquid ratio leads to higher degree of interaction between the ions and solid and hence the increased conductivity, which means lower resistivity (conductivity being reciprocal of resistivity - RIELM TC 154-EMC, 2000).

Finer and continuous pore structure of LCFG concrete could be the possible reason of its lower resistivity. This may be because of higher level of interaction between ions and solid explained above at low RH combined with aggressive environments in particular. This may need further research.

Secondly resistivity increases with the decrease in temperature. Within the temperature range of 0 - 40^{o}C, resistivity doubles with the decrease of 20^{o}C. Because of humidity dependence of the temperature exponent in binder paste of concrete as detailed in Section 3.4.2, higher temperature & RH make the conditions more favourable for deterioration mechanism affecting both type of concrete. However low resistivity observations for LCFG concrete under severe exposure in this research indicated its embedded steel more vulnerable to corrosion compared to OPC concrete.

The use of a resistivity measurement together with Half Cell Potential (HCP) measurements provides an indication of the severity of the problem and its location. Subsequent subsection provides the HCP test results.

5.11.2 Half Cell Potential Measurements

The measurement of the corrosion potential (Ecorr) with respect to a reference electrode - copper sulphate electrode (CSE) using a simple voltmeter is shown in Figure 5.32 below. By convention the reference electrode is connected to the negative end of the voltmeter and steel reinforcement to the positive giving the negative reading (Gu & Beaudoin, 1998). Figure 5.31 shows the reference and working electrode connection to voltmeter.

Figure 5-31 Half Cell Equipment

According to ASTM Standard C876-91 (ASTM 1991), the corrosion potential measured against the CSE gives probability of the occurrence of active corrosion. Criteria of corrosion risk probability according to ASTM standard C876-91 and its limitations are detailed in Chapter 3 (Section 3.4.1).

5.11.2.1 HCP Test Outputs before Severe Exposure

HCP test were undertaken on laboratory samples with protruding reinforcing bar for electrical connection during the testing. Initial HCP test observations were at 7 days interval at locations 50mm, 100mm, 150mm and 200mm from the top of laboratory samples for a month before subjecting them to simulated severe environmental laboratory model.

Figure 5.32 (a), (b) & (c) below show HCP vs. CSE before subjecting the samples to severe environment of Class –U as per AS 3600.

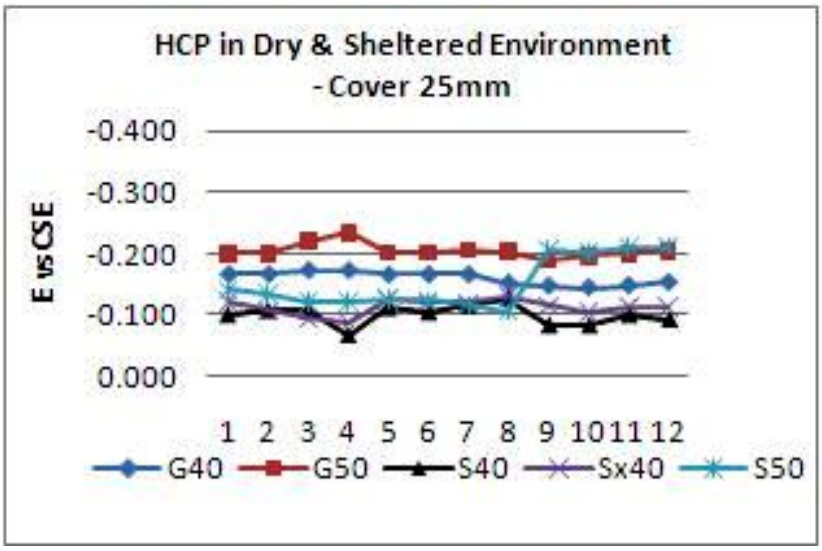

(a)

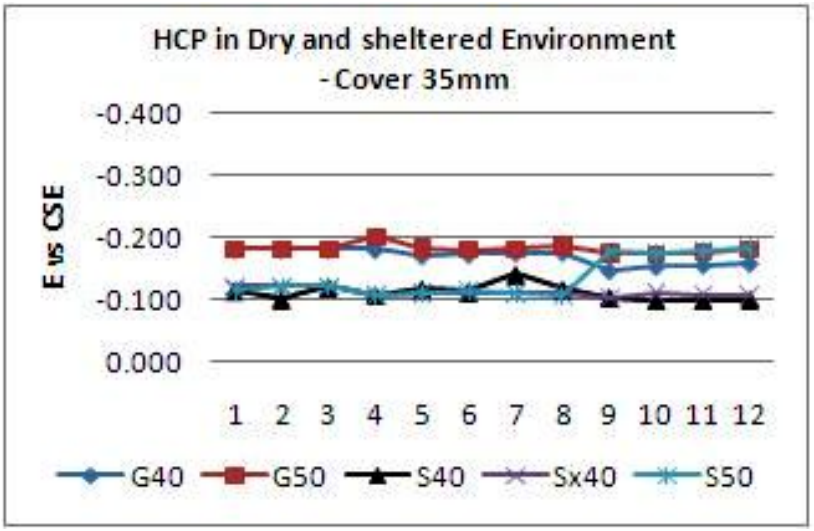

(b)

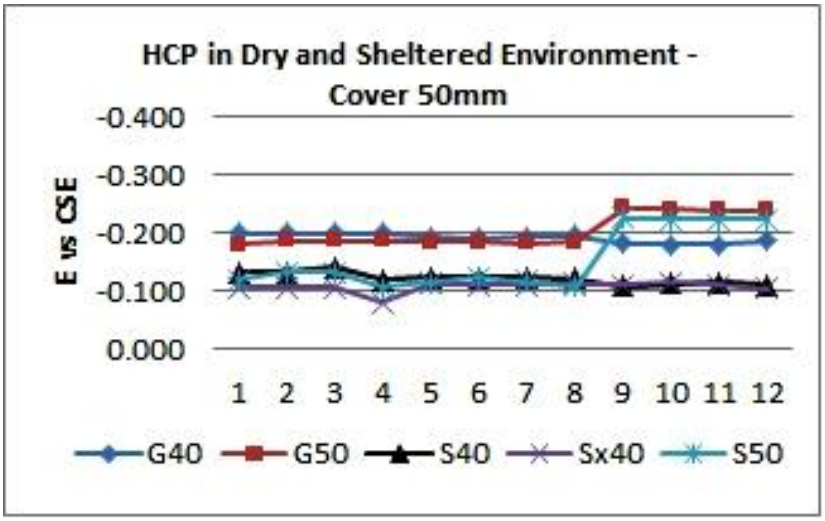

(c)

Figure 5-32 Half Cell Potential

So initial HCP test results provided the embedded steel potential corresponding to environments of exposure Class A to B1. It was inferred that the initial potential of the reinforcement in LCFG concrete was approximately two folds higher than OPC concrete but the potential values were not exceeding the HCP criteria value indicating higher probability of corrosion risk as detailed in Section 3.4.1, Table 3.4.

5.11.2.2 HCP Test Outputs during Severe Exposure

After subjecting the samples to severe environments, first few HCP observations were undertaken at 7days interval for one month followed by fortnightly interval for 3 months, monthly interval for 3 months and finally at quarterly interval during three years duration in this research. Salty water was syphoned out during dry season and was restored back during wet seasons to match the cyclic field environments of wet to semi-wet soil and dry soil environment approximately.

In LCFG concrete negative potential increased from 0.200V to -0.700v over first few observations at 7 days interval after exposure to the severe environments in one month. This was 3-3.5 times higher than initial observations undertaken during dry environments. The change in potential of embedded reinforcement in OPC concrete was from -0.100V to -0.200V, which was 1.5 – 2 times higher than the initial observations under dry environments. These HCP observations of both LCFG concrete and OPC concrete are shown in Figure 5.33 (a), (b) & (c) below.

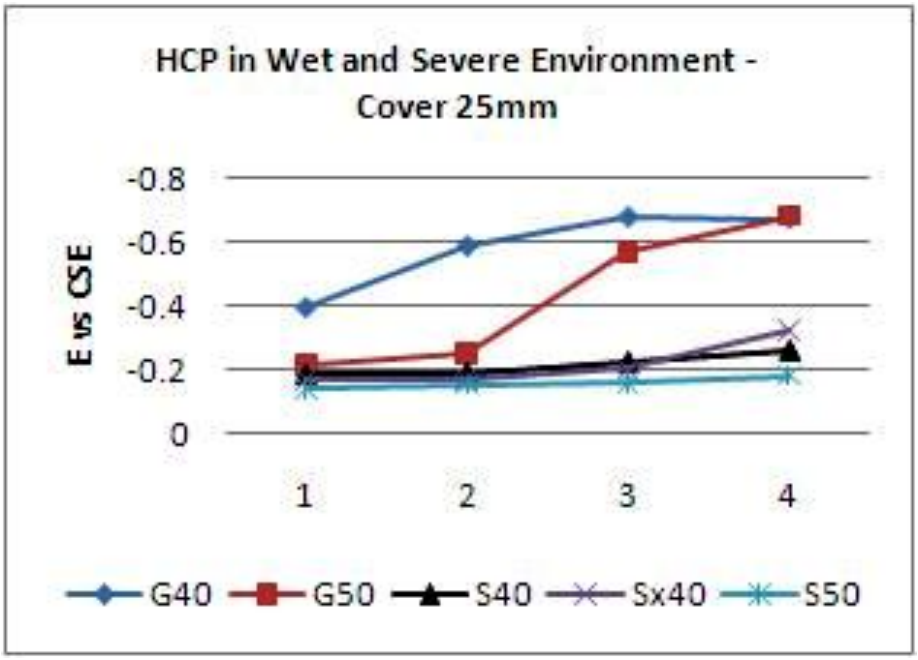

(a)

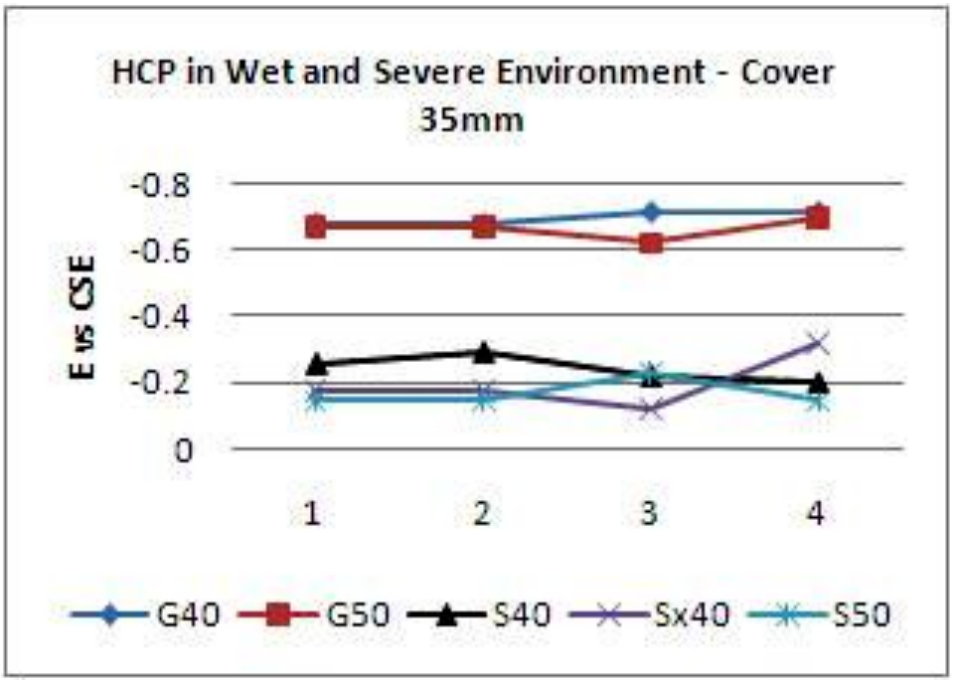

(b)

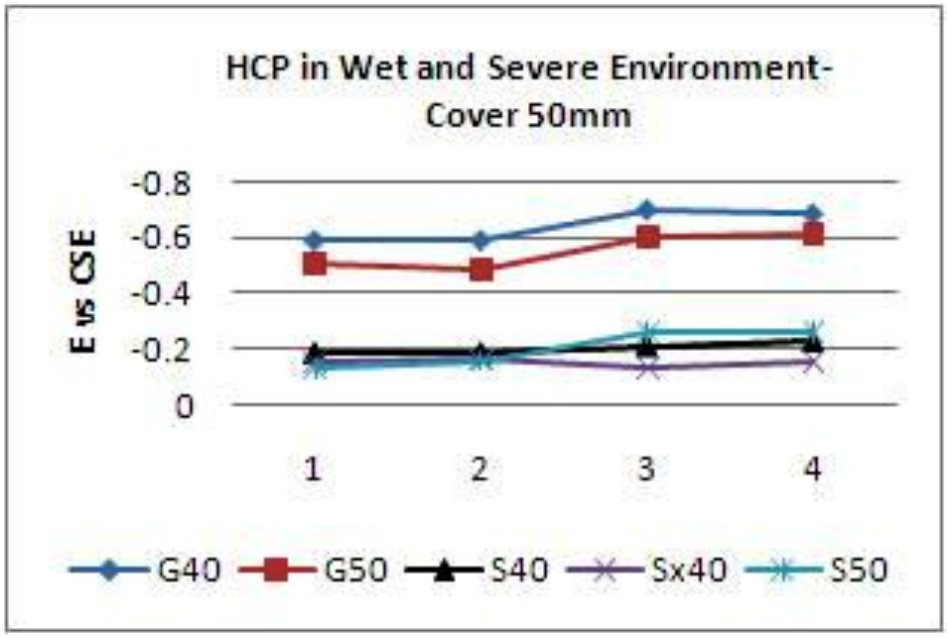

(c)

Figure 5-33 Half Cell Potential of Specimens Exposed to Severe Environments

HCP observed over a long period for LCFG concrete reinforcement under environmental exposures subject to seasonal changes (wet, partially wet and dry) ranged from -0.400V to -0.700V (vs. CSE), while for OPC it was from -0.100 to -0.300V vs. CSE as shown in Figure 5.34 below. Figure 5.34 below shows the average HCP (vs. CSE) measurements trend over two years.

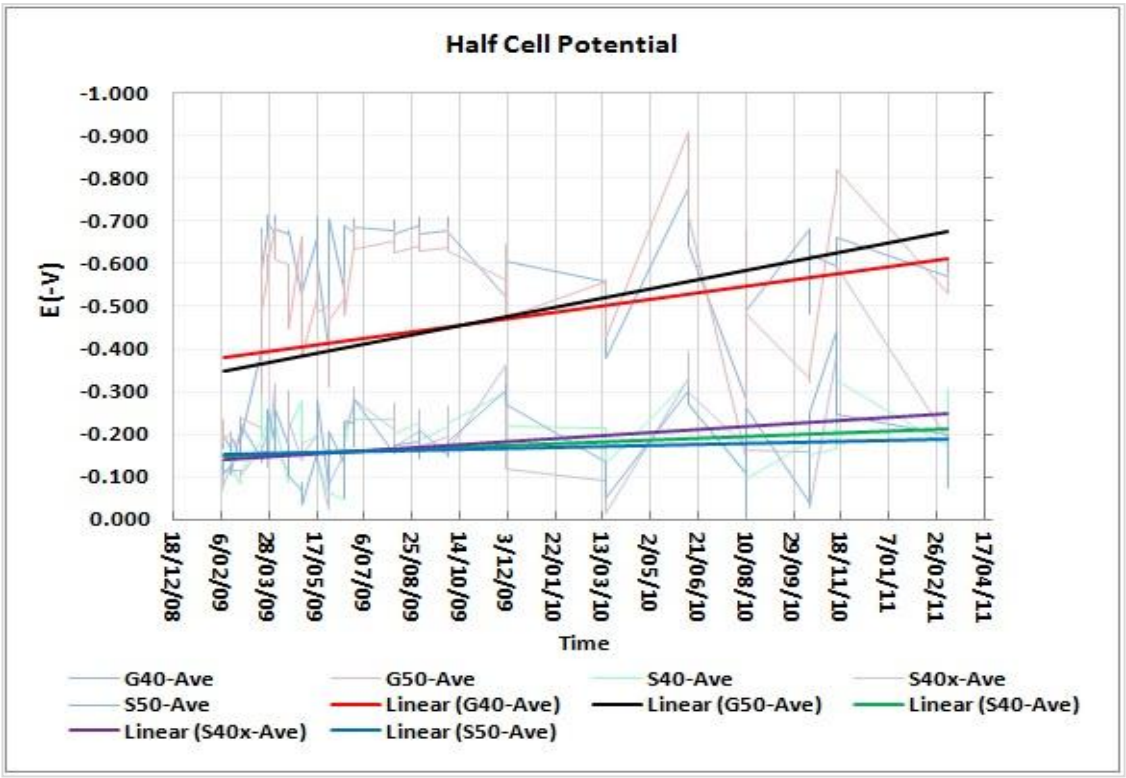

Figure 5-34 HCP Measurement Trend over Two Years Severe Exposure

HCP measurement trend over three years with respect to reinforcement cover thickness of 25mm, 35mm and 50mm under severe environmental exposure are shown in Figure 5.35 (a to c).

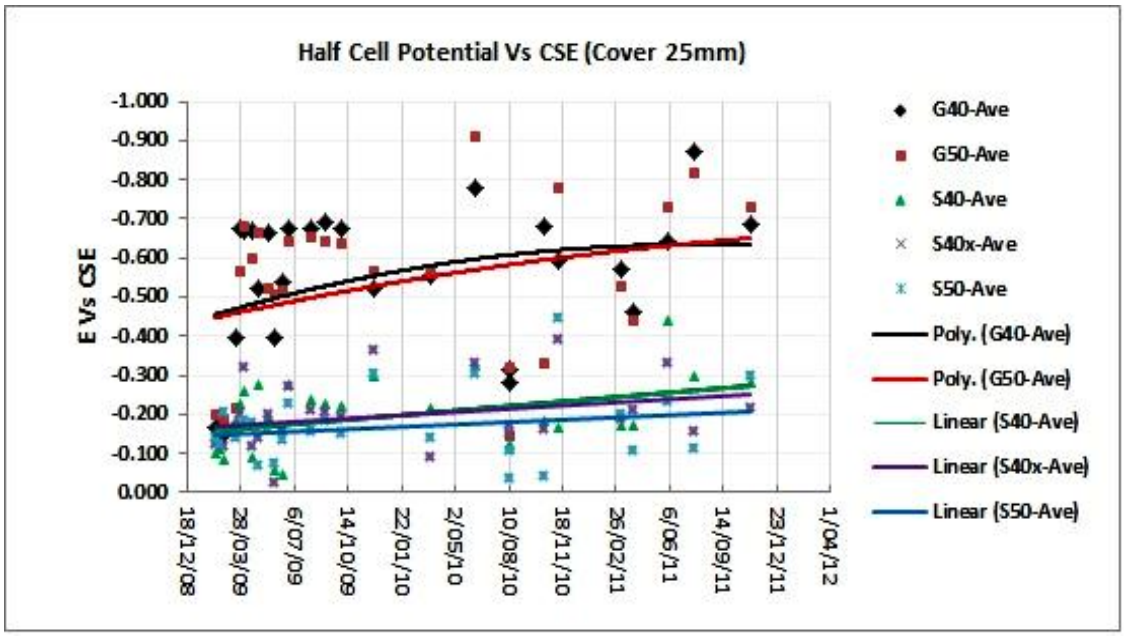

(a)

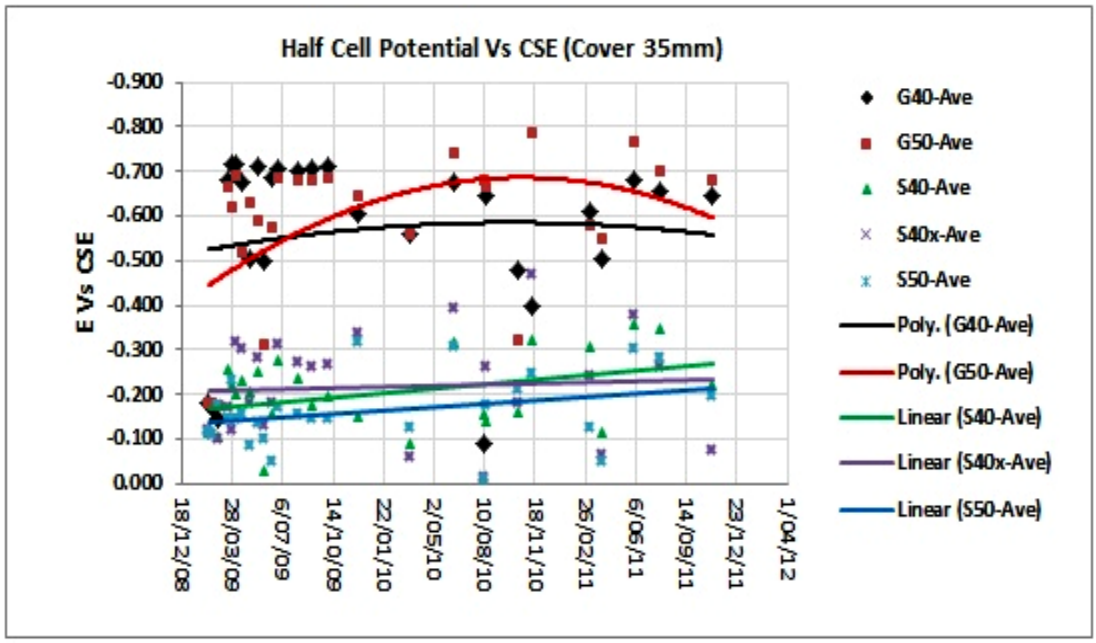

(b)

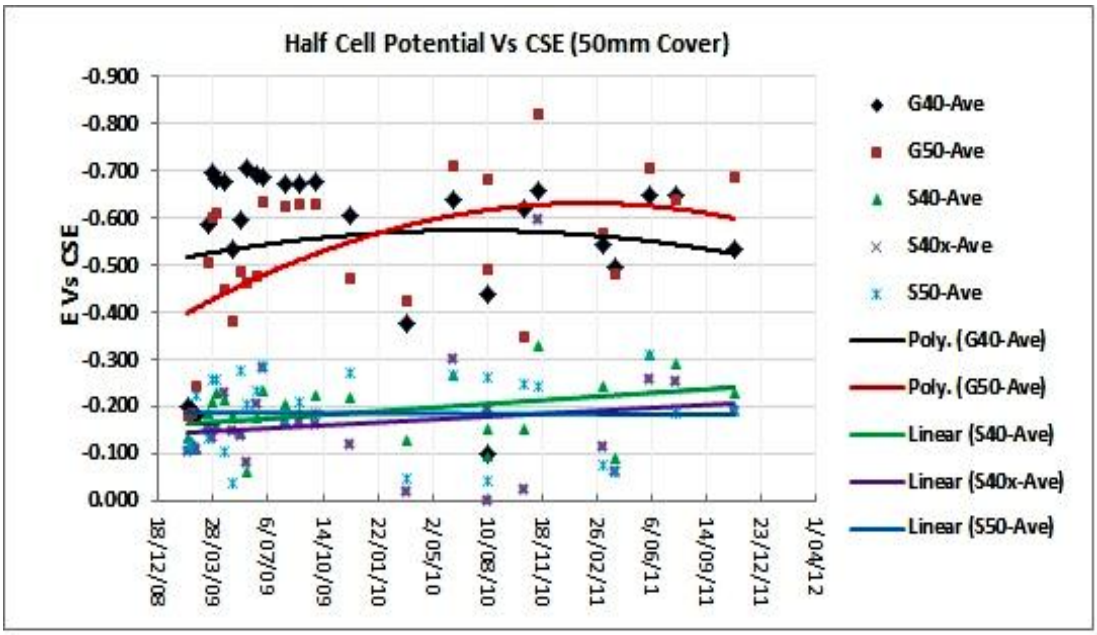

(c)

Figure 5-35 Half Cell Potential for Reinforcement with Different Cover & Severe Exposure

5.11.2.3 HCP Test Results Discussion

Under severe environmental exposure, it was inferred that increased cover to reinforcement in LCFG concrete showed negligible improvement as far its protection level was concerned. However protection level improvement was noticeable in OPC concrete under long term severe environmental exposure. This is evident from Figure 5.35 (a to c) above.

HCP criteria specified above in Table 3.4 (Chapter 3) indicates the corrosion status of embedded steel in OPC concrete (ASTM Standard C876-91) and on this basis, higher range of negative half- cell potential of -0.600 to-0.700V vs. CSE soon after the exposure to severe environments for LCFG concrete inferred higher corrosion risk to reinforcement compared to OPC concrete. The half- cell potential measurements of reinforcement in OPC concrete ranged between -0.100 to -0.300V vs. CSE inferred very low risk of corrosion (Cheema, 2011).

Also HCP vs. CSE observations taken on dry and sheltered cylinder specimen after a period of 21 months by exposing the totally embedded 8mm steel represented non- aggressive environment (Class A as per AS3600).

No sign of rust was noticed on the steel bar having a nominal cover of 25mm. The average value of 25 HCP observations taken were as shown in Figure 5.36 below along with average HCP observation value on G40 and S40 samples, which were initially exposed to severe environment for two years and then subjected to dry and sheltered environmental spill of one year. An average HCP observation of - 0.434V and - 0.135V were noted respectively for LCFG concrete in dry and sheltered environments.

Although a sign of an increased corrosion activity was present initially under severe environments for both type of concrete but change of environmental conditions to dry & sheltered for spill of one year approximately reduced the high risk corrosion probability (of 90%) to low corrosion risk probability. This was shown by low negative HCP readings of -0.135V for G40, while for S40 it was -0.025V indicating very low corrosion risk comparatively.

The change in environments from severe to non- aggressive improved the probability of corrosion risk better for both LCFG concrete and OPC concrete. This is in line with the previous research findings that corrosion formed on the steel bar surface prevent further active corrosion by acting as barrier around the steel bar (Olivia, 2011).

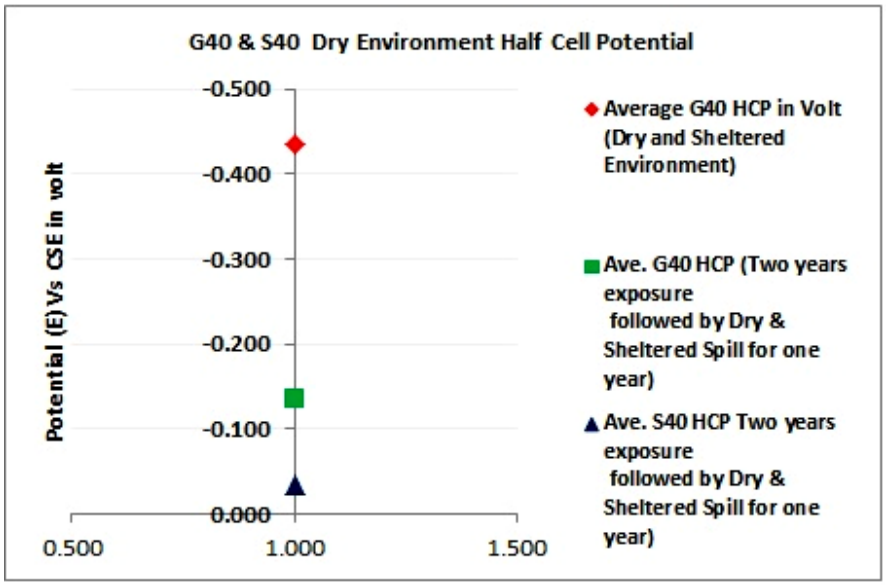

Figure 5-36 Half Cell Potential in Non –aggressive Environments

High initial HCP for LCFG concrete under severe environments in this research confirmed the trend as shown in Figure 3.26 (Chapter 3) for alkali activated slag based geopolymer concrete mix. Andrews Phaedonos (2012) observations were in field environments possibly non- aggressive to mild one showing the stabilisation of HCP over a period of 2 years to -0.400V. This could be from the corrosion product formed on steel bar surface under environmental actions initially.

5.11.2.4 HCP Criteria for LCFG Concrete

Based on the available information in the literature on HCP observations for LCFG concrete (which may have slight variation in mix composition and curing condition such as Olivia's study involved higher curing temperature up to 70 ^{o}C, while Andrews Phaedonos study was for slag based geopolymer) and from the HCP observations in this research as detailed above (Fig 5.33, 5.34, 5.35, 5.37 and 3.25 & 3.26), potential HCP criteria developed for LCFG concrete is summarised in Table 5.17 below.

Table 5-17 HCP Criteria for LCFG Concrete

Half-cell potential reading (Ecorr) vs. $Cu/CuSO_4$	Probability of corrosion
More negative than –0.400V	90%
Between –0.200 – 0.400V	10%
More positive than –0.200	Uncertain (decreased probability of corrosion due to corrosion products formation)

An explanation supporting the HCP criteria for LCFG concrete is as below.

HCP value of -0.200V on laboratory samples (300x300x120mm) was in dry and sheltered environments in the beginning and on cylinder specimen was around -0.400V. The variation in HCP for dry and sheltered environments may be from the large surface area of laboratory samples available for moisture evaporation even in dry and sheltered environment under the prevailing relative humidity around 50% compared to cylinder specimen surface area.

HCP soon after the exposure to wet and severe environment raised the HCP to more negative than -0.400V when observed at an interval of 7days in the beginning and gradually increased to-0.600 to -0.700V CSE. This may be on account of the severity of the simulated environmental model.

Further GPM measuring technique provided the HCP reading vs. AgCl standard electrode and its conversion with respect to CSE varied between -0.600V to -0.850V (as detailed in the sub-subsection). Measurements of HCP with GPM technique were at quarterly intervals with seasonal wetting and drying environments. This high HCP was in concurrence with Andrews Phaedonos (2012) HCP measurements, which was undertaken on the geopolymer concrete retaining wall panels and stabilised to -0.300 to -0.400V over 2 years as shown above in Figure 3.26.

HCP in Olivia (2011) research was on samples submerged in seawater, which showed initial HCP vs. CSE as - 0.200V, and increasing to – 0.400V within first couple of weeks and thereafter increased to a steady value of to -0.660V over 90 days. Due to submerged nature of samples in Olivia study, higher HCP could be due to dissolved oxygen or lack of oxygen. However initial HCP variation between -0.200 to -0.400V was in concurrence with the findings of this research study supporting the HCP criteria for LCFG concrete as summarised in the Table 5.17 above. This criterion may be subject to refinement with future research on electrochemical properties of LCFG concrete with mix composition, which may be different from the optimum mix of this research. The HCP test observations' data is appended in Appendix E.

5.11.3 Galvanostatic Pulse Measurements (GPM) for Corrosion Rate Assessment

The Galvano-Pulse Measurement (GPM) is a rapid, non-destructive polarization technique based on linear polarisation resistance (LPR) principle for the evaluation of reinforcement corrosion rate as well as its half-cell potential for estimating the probable corrosion risk of embedded steel in concrete.

GPM distinguish between the active corrosion and lack of oxygen situation, which is not possible with Half Cell Potential (HCP) test using simple voltmeter. The equipment gives corrosion rate, HCP and as well resistance between the hand- held electrode placed on the concrete surface and the reinforcement. Electrical continuity in the reinforcement is essential for this technique and is briefly detailed in Chapter 3 (Section 3.4.3).

5.11.3.1 HCP Test Output Observations with GPM

The GPM confirmed the half- cell potential measurements trend observed for LCFG concrete and OPC concrete using simple volt meter versus standard Copper Sulphate Electrode (CSE) as detailed above.

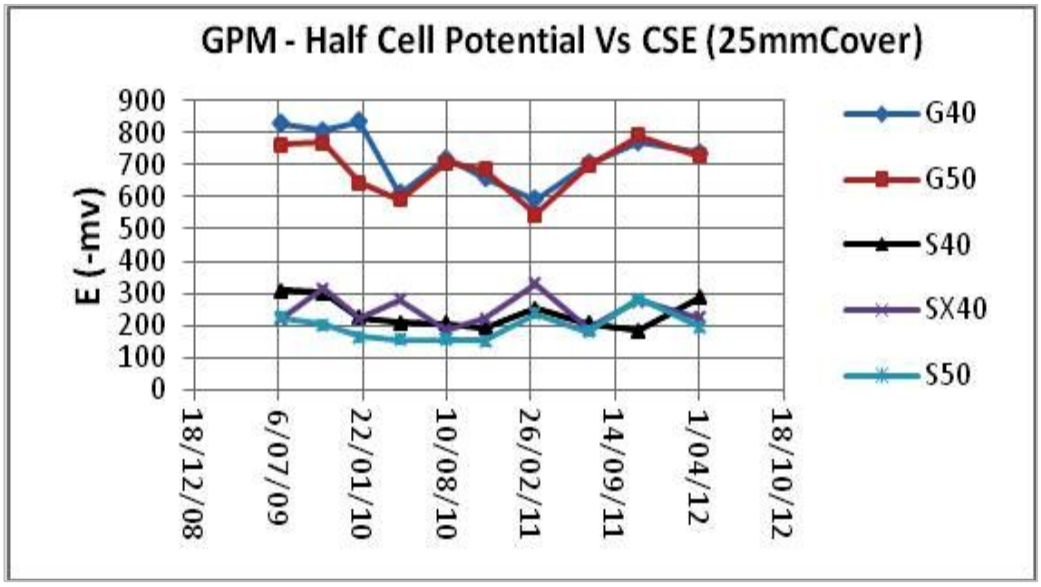

(a)

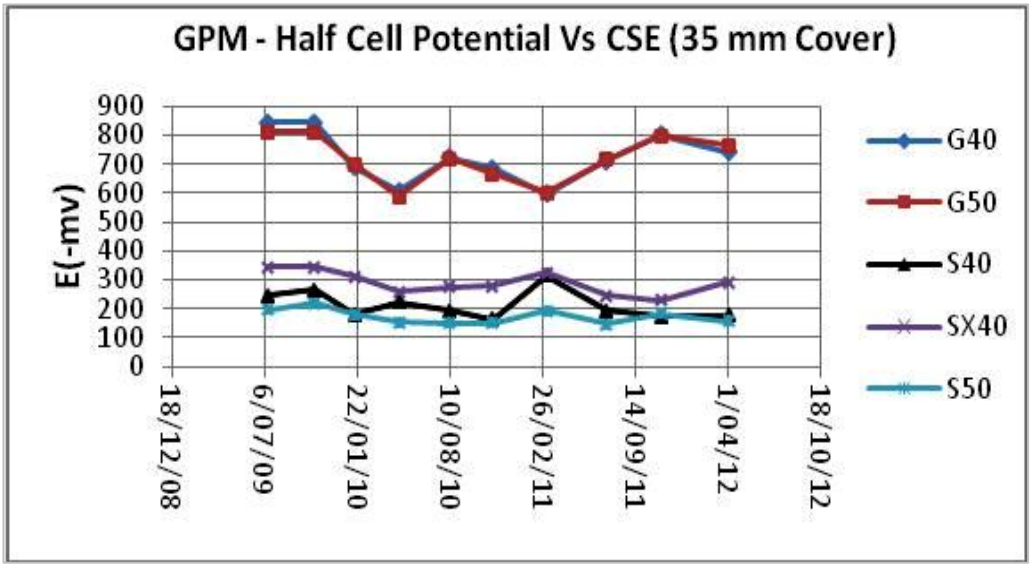

(b)

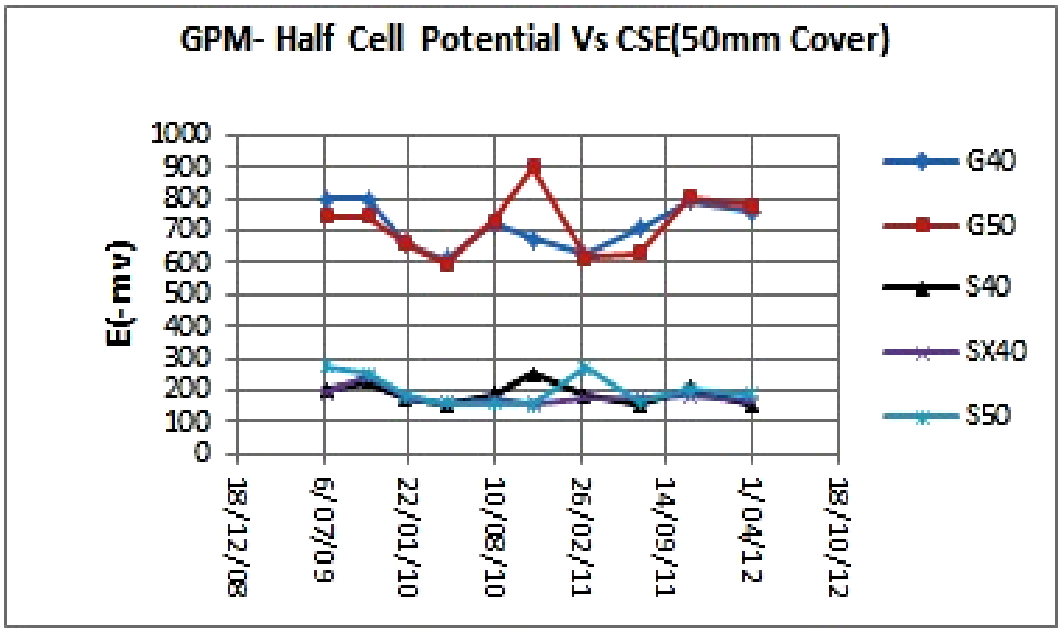

(c)

Figure 5-37 Half Cell Potential with GPM Technique

The HCP with GPM standard electrode was vs. AgCl. Converted HCP with respect to standard CSE for LCFG concrete and OPC concrete embedded steel with cover thickness of 25mm, 35mm and 50mm over a period of three years severe exposure are as shown in Figure 5.37 (a),(b) & (c) above .

Variations in half cell potential was quite distinct in case of LCFG concrete with seasonal variation of dry and wet conditions compared to OPC concrete, however higher HCP observations in LCFG concrete were indicative of higher corrosion risk to its embedded steel compared to OPC concrete. Test data is in Appendix E.

5.11.3.2 GPM Pulse Chart Observations for Corrosion Current Density & Corrosion Rate

The pulse chart from GPM for LCFG concrete provided inclusive information as far as corrosion current density was concerned for determining the corrosion rate.

Following GPM pulse charts indicated the corrosion density and ohmic resistance of OPC concrete and LCFG concrete. Figure 5.38 (a) below shows the pulse chart of OPC concrete under wet environments after six month exposure period and Figure 5.38(b) for LCFG concrete.

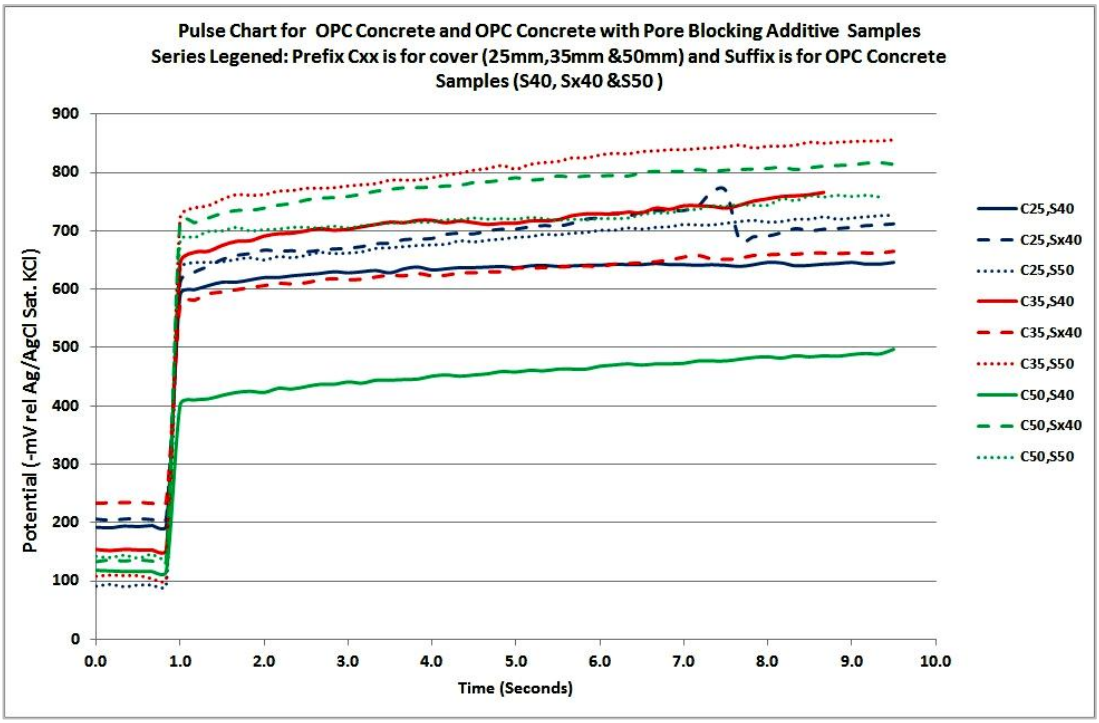

(a)

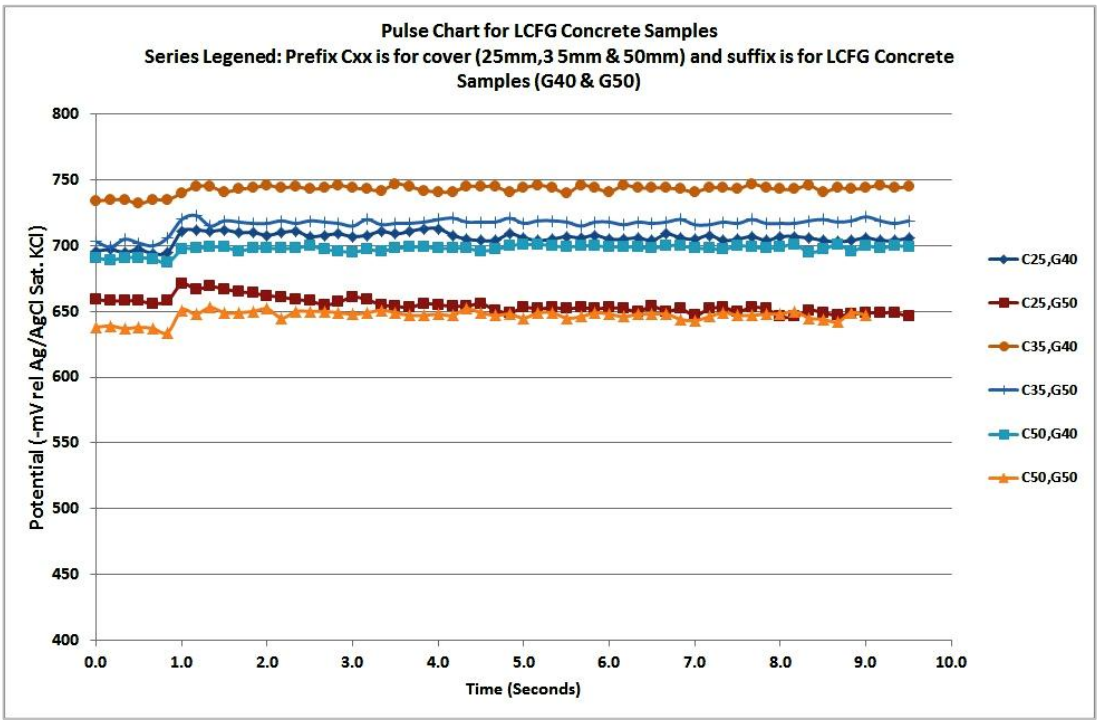

(b)

Figure 5-38 GPM Pulse Chart after Six Month Exposure

Figure 5.38 above shows that over the first six month of exposure in case of OPC concrete, ohmic resistance was high as represented by the near vertical segment of the chart and was quite distinct for various cover thickness being investigated in the research.

Ohmic resistance was highest for Sx40 and S50 followed by S40. The interface resistance shown by the gradient of upper inclined line of the chart is indicative of the corrosion rate in OPC concrete and is detailed subsequently with respect to corrosion current density measurements.

While for LCFG concrete ohmic resistance was low, which also has been confirmed by Wenner Probing in resistivity testing (Resipod). The gradient of chart line after the ohmic resistance (which was represented by very small segment of near vertical line) was very flat and undefined. As such pulse chart for LCFG concrete provided no inference on an indicative corrosion rate for embedded steel in LCFG concrete.

GPM pulse charts after a dry and wet spill over an exposure period of over one year for OPC concrete and LCFG concrete are shown in Figure 5.39 (a) & (b).

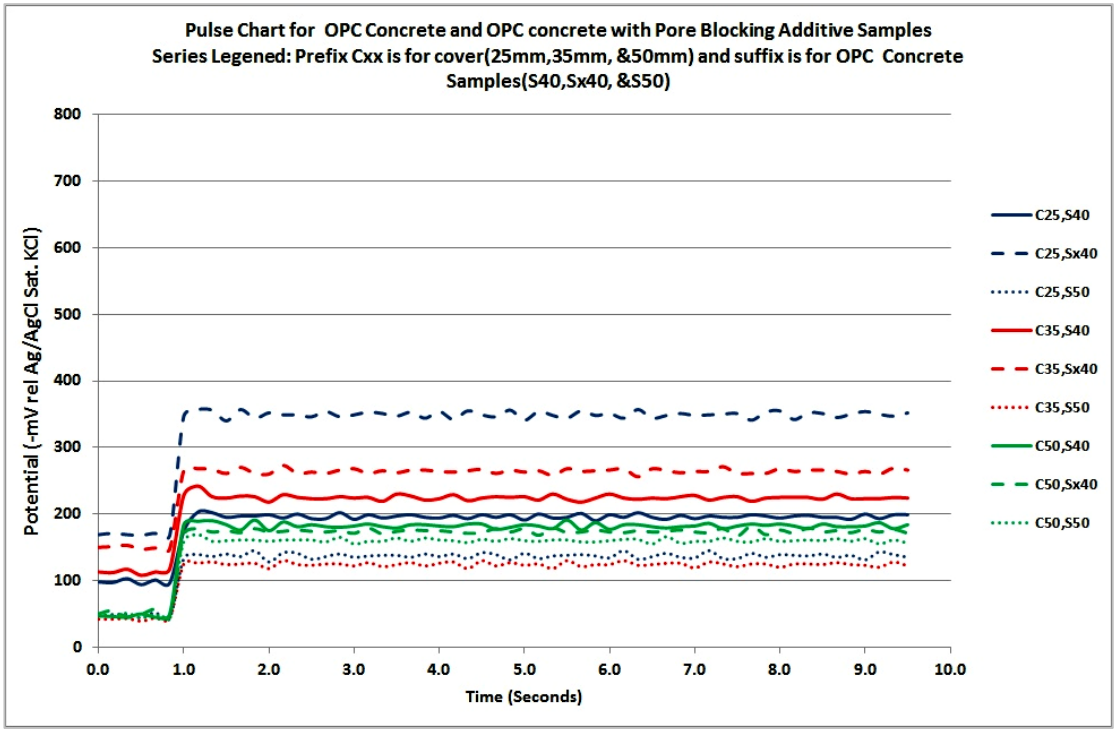

(a)

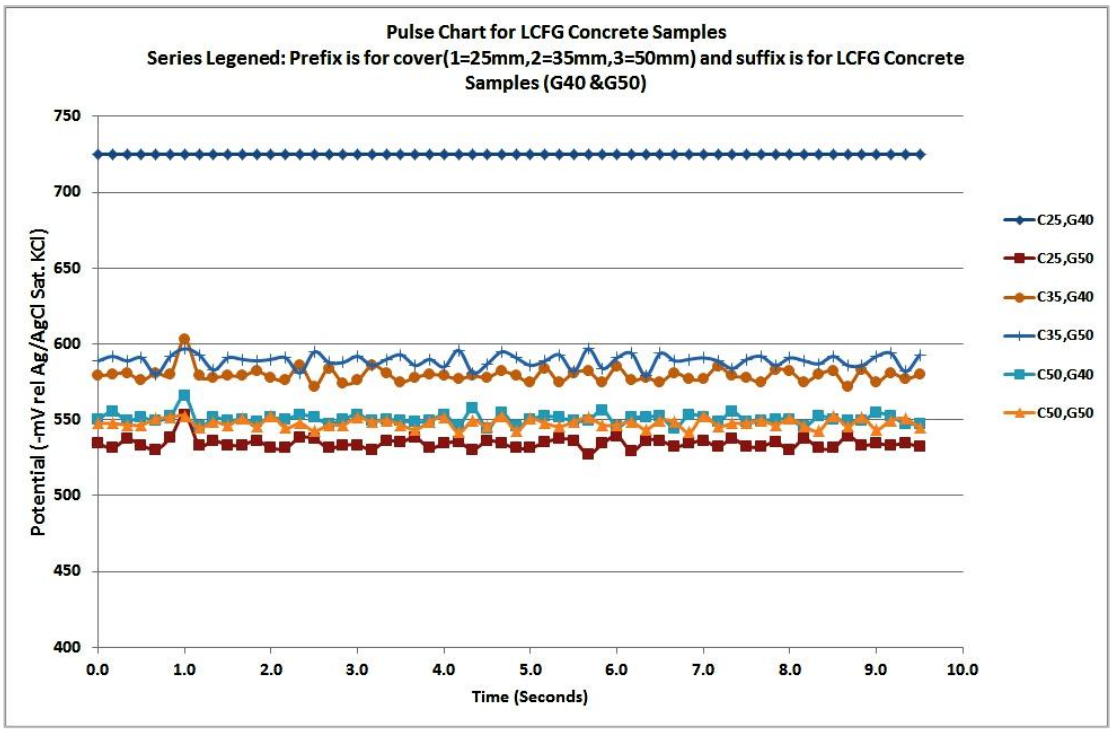

(b)

Figure 5-39 GPM Pulse Chart after One year Exposure

After an exposure period of one year, decrease in slope of the line representing resistance at the interface of embedded steel in OPC concrete indicated lower corrosion current density and lower corrosion rate. This may be due to passivating effect of iron oxide layer formed over a period of 6-12 month exposure periods.

However for corrosion rate in LCFG concrete, no interpretation could be drawn from these GPM pulse charts due to undefined nature of the pulse chart with this GPM technique. The potential response of embedded steel in LCFG concrete under drying season showed similar trend with exception of G40 with 25mm cover.

Figure 5.40 (a) & (b) shows the potential response of embedded steel in LCFG and OPC concrete in dry season.

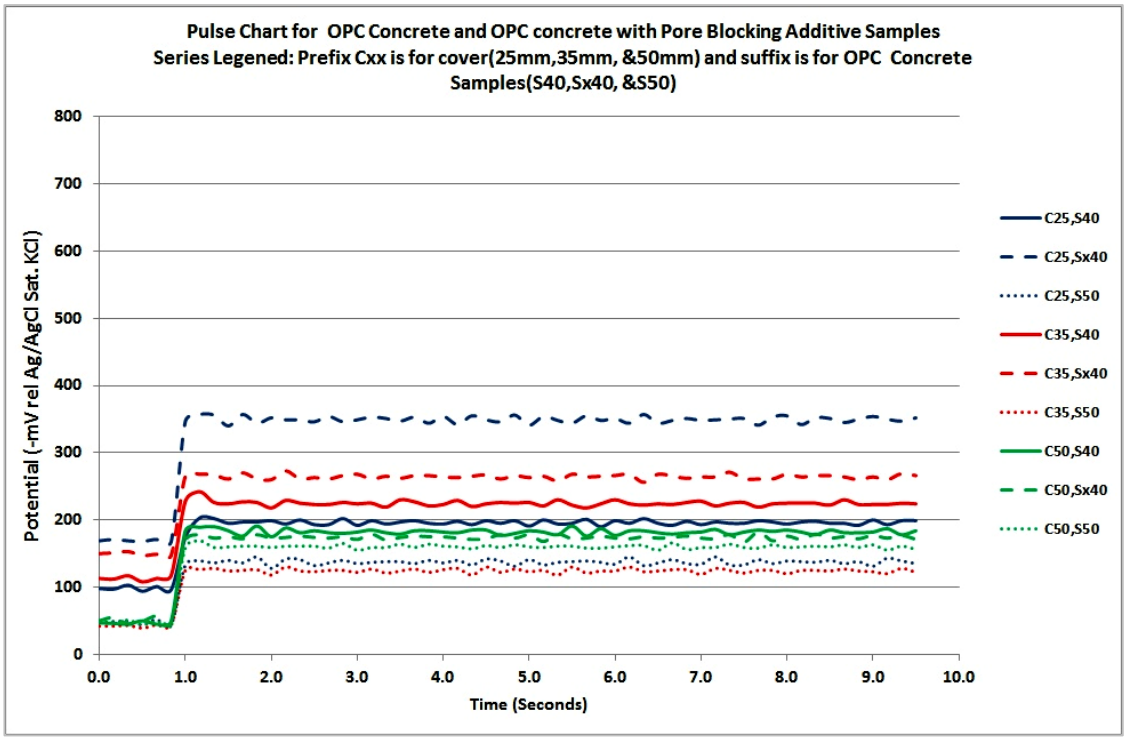

(a)

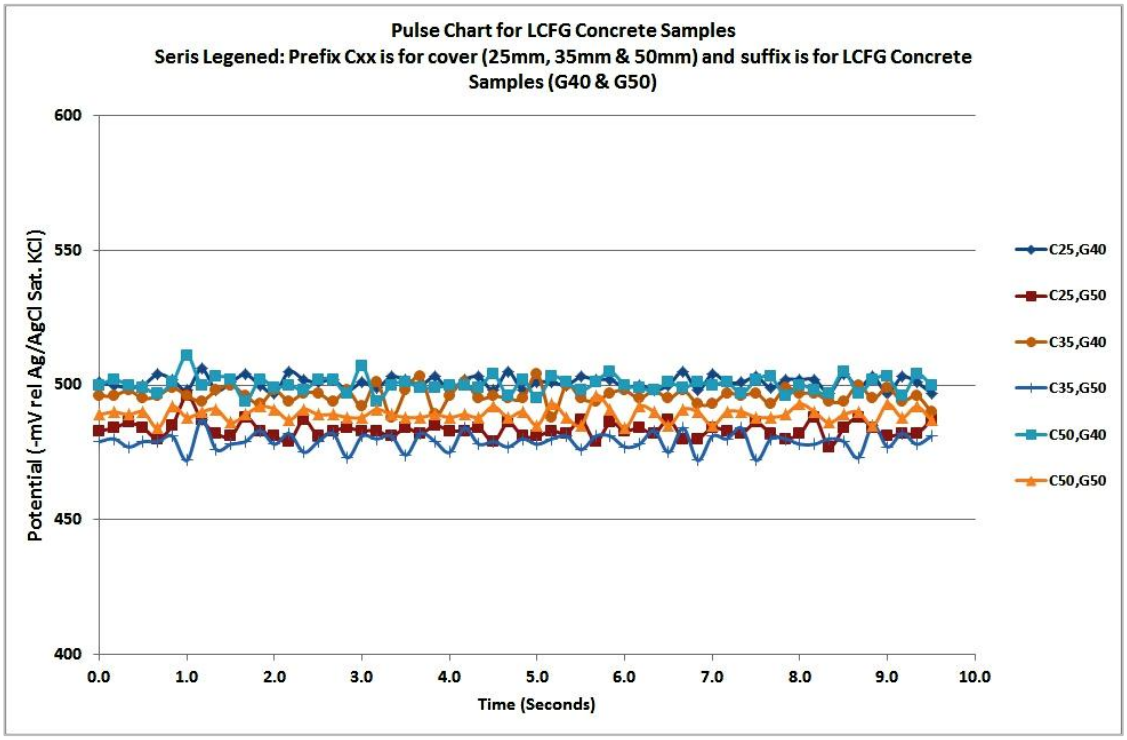

(b)

Figure 5-40 GPM Pulse in Dry Conditions

5.11.3.3 GPM Test Results Discussion

Above observations indicate that GPM testing technique for assessing the corrosion rate in LCFG concrete seems not appropriate. However HCP observations vs. Ag/AgCl with this technique and its conversion to HCP vs. CSE confirmed the HCP observations trend obtained with simple voltmeter for both OPC and LCFG concrete.

So above observations revealed that GPM, which is relatively a newer electrochemical testing technique for determining the corrosion rate of embedded steel in OPC concrete may not be suitable for determining corrosion rate of embedded steel in LCFG concrete. This needs further research. However indications of higher negative HCP with GPM technique do infer that imbedded steel in LCFG has higher probability of corrosion risk than the steel in OPC concrete. Corrosion current density obtained for OPC concrete samples indicating the corrosion rate is apparent from the following Figures 5.41 (a), (b) and (c).

5.11.3.4 Corrosion Current Density for Probable Corrosion Rate

From GPM testing technique, corrosion current density trend for OPC concrete is shown in Figure 5.41 (a), (b) and (c) for 25mm, 35mm & 50mm reinforcement cover scenarios. The GPM technique provided no corrosion current density measurements for LCFG concrete. Reason for not providing any indication of corrosion current density to estimate the corrosion rate in LCFG concrete by GPM technique is given in subsequent Section 6.4.

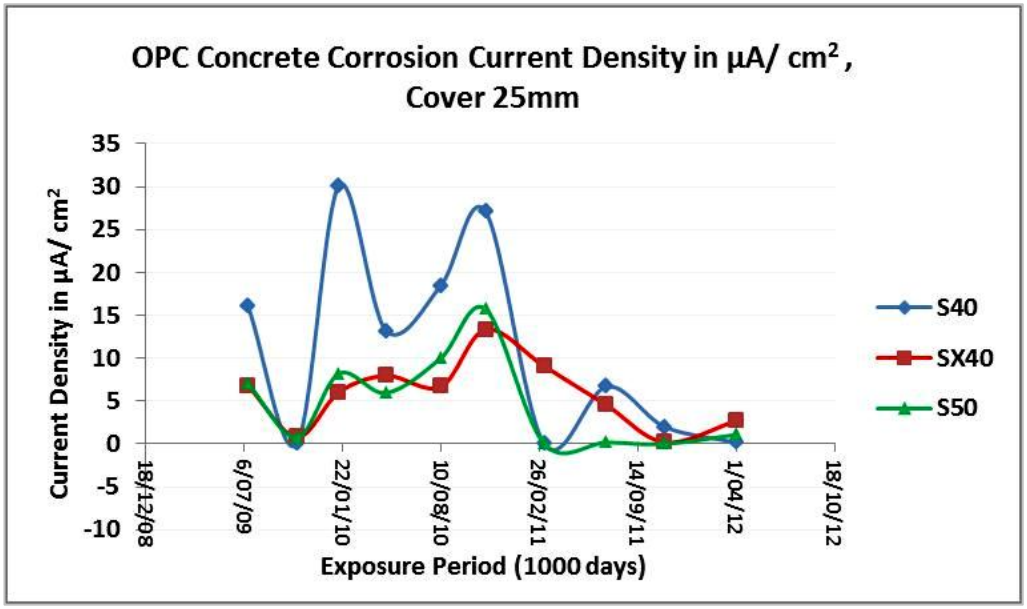

(a)

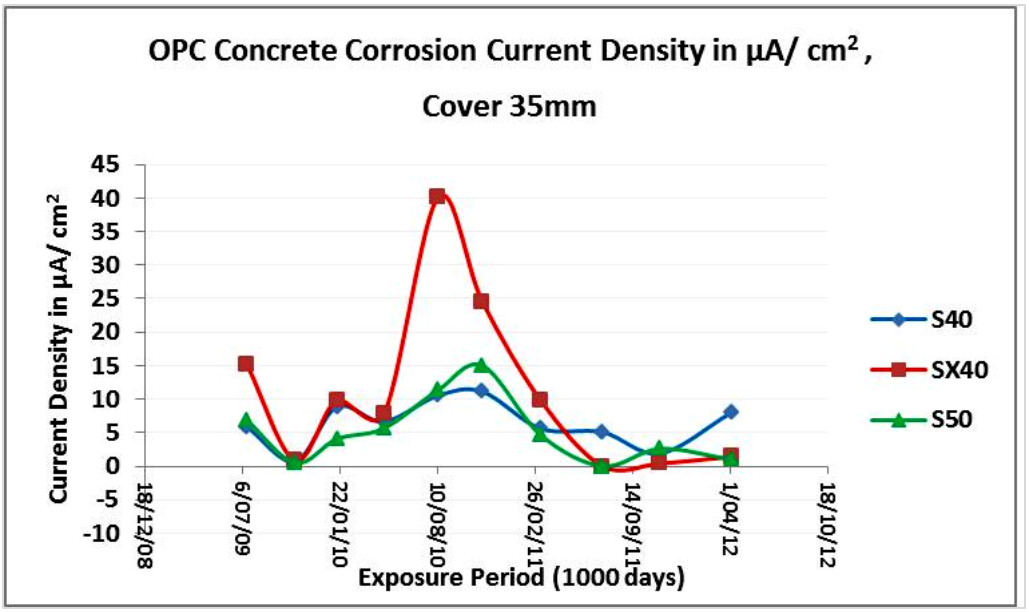

(b)

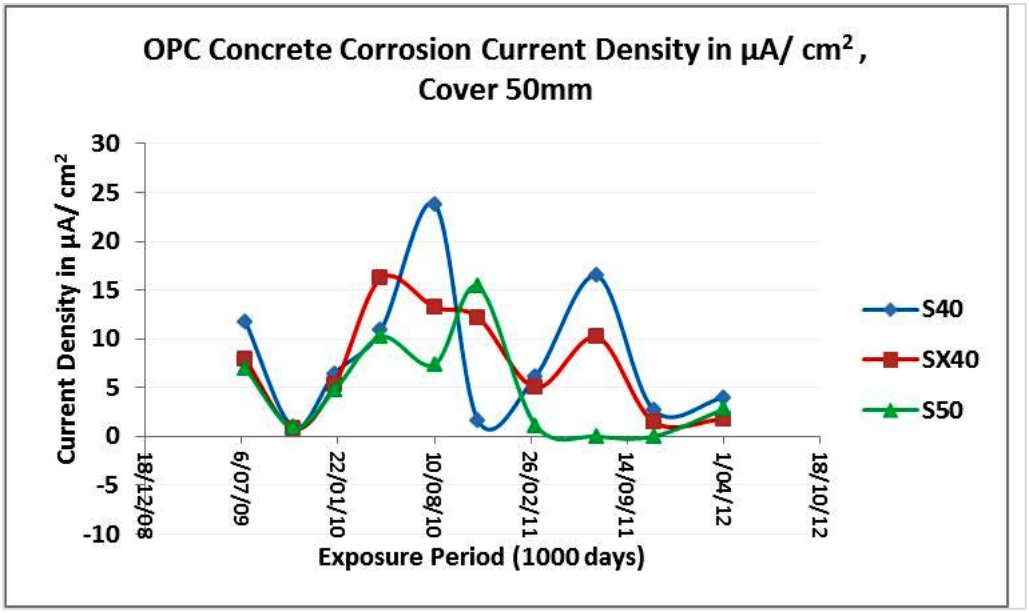

(c)

Figure 5-41 Corrosion Current Density

From Figure 5.41 (a), (b) & (c) average corrosion density over the study period for S40 laboratory sample with 25mm cover is 10µA/cm^2, 35mm cover is 5µA/cm^2 and 50mm cover is 10µA/cm^2, while for S50 corrosion current density for all cover depths is 5µA/cm^2 approximately. Table 5.18 below summarise the corrosion current density range for the assessment of corrosion risk.

Table 5-18 Corrosion Current Density

Corrosion Current Density	Corrosion Risk
0.5 µA/cm^2	Negligible
0.5 -5µA/cm^2	Slow
5 - 15 µA/cm^2	Moderate
>15 µA/cm^2	High

The above observations indicate that increased cover thickness and high strength concrete lowers the corrosion risk in OPC concrete, while the technique was unable to provide any trend for LCFG concrete. Over three years of cyclic dry and wet exposure, the corrosion risk trend decreased in the second year of exposure for S40 & S50 which might be due to the initial oxides' formation suppressing the corrosion activities during early stages. However trend was rising in third year of exposure.

Based on Faradays' law, corrosion density of 10µA/cm^2 can cause section loss of 115µm/ year and rust growth of 345 µm/ year while corrosion density of 5µA/cm^2 will reduce these deterioration levels to half. These estimates are based on average expansion ratio of 3 and allowing some of the corrosion products being pushed into the porous structure around the rebar (Broomfield, 2007). The corrosion risk for embedded steel in OPC concrete was inferred as moderate.

Subsequent test results in Section 5.11.4 provide the indicative passivating effect of silicate and visual assessment of active corrosion in LCFG concrete (section 5.11.5) where the rebar silicate coating may be imperfect.

5.11.4 Potentiostate Test Observations for Silicate Passivation Effect

Pre-passivation technique was used in this research to assess the silicate passivation effect to embedded steel in LCFG concrete and to confirm the findings of (Ovchiyan, 2003) and (Lehraman, 1964). Electrochemical silicate coating over a short duration of up to 60 minutes on 8mm steel bar using potentiostate was undertaken. In this pre-passivation test, applied current density was 0.1µA/cm^2 on an immersed area of 13.8cm^2.

Before undertaking electrochemical coating one steel bar sample was cleaned with dilute HCL and other with Ethanol. The effectiveness of silicate coating was studied using Scanning Electron Microscope (SEM) and Energy Dispersive X-ray (EDX) analysis. Figures 5.42 & 5.43 below show the SEM images of silicate coating.

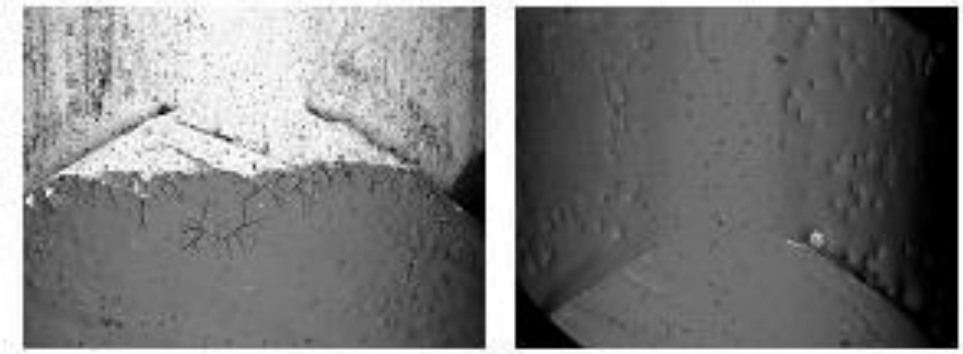

(a)

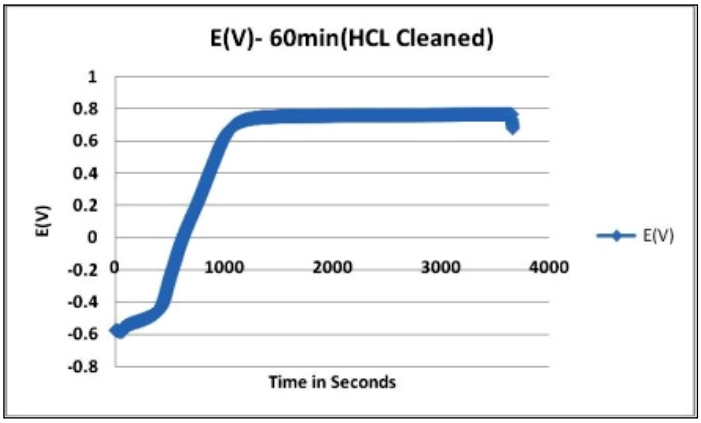

(b)

Figure 5-42 SEM Images of – 60 minute Electrochemical Coating of Sodium Silicate (on 8mm reinforcement bar – Dilute HCL Cleaned)

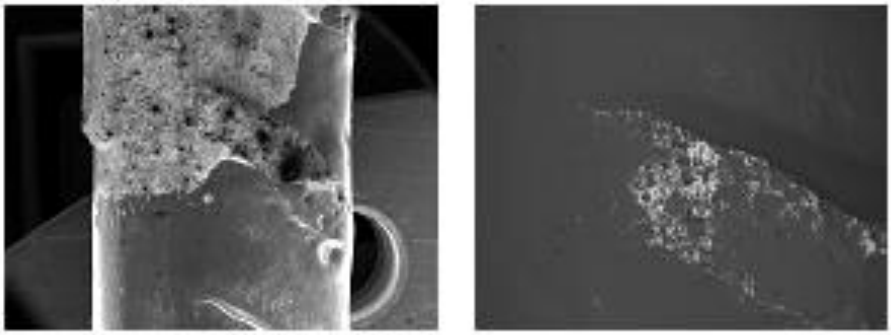

(a)

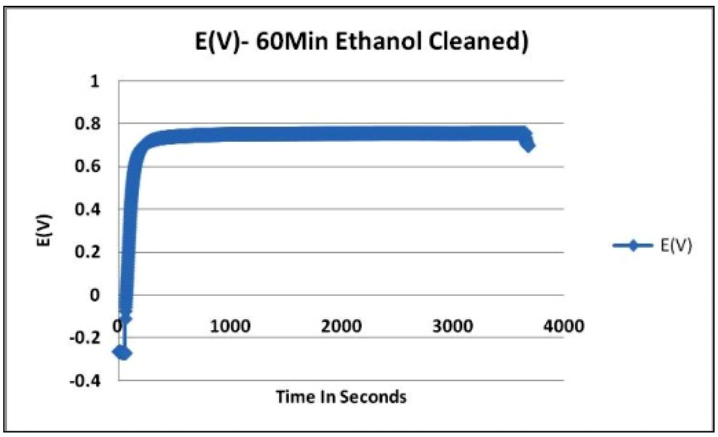

(b)

Figure 5-43 SEM Images of – 60 minute Electrochemical coating of sodium silicate (on 8mm reinforcement bar- Ethanol Cleaned)

Figure 5.44 below shows SEM and EDX images of uncoated steel reinforcement and Figure 5.45 shows the images after sodium silicate coating, protecting steel elements from direct exposures.

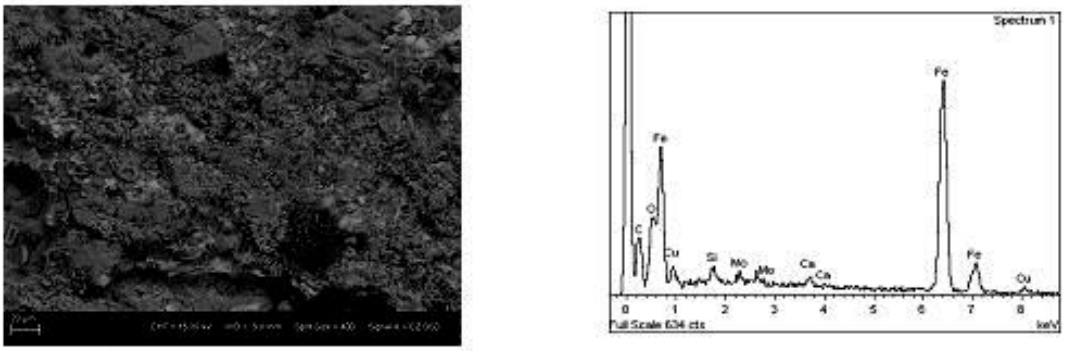

(a) (b)

Figure 5-44 SEM & EDX Images of Uncoated Steel Reinforcement

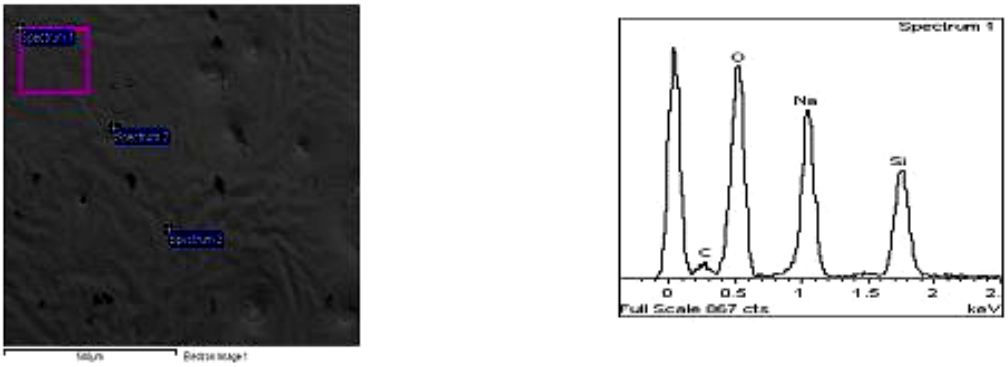

(a) (b)

Figure 5-45 SEM & EDX Images of Coated Steel Reinforcement

5.11.4.1 Silicate Passivation Assessment and Discussion

The negatively charged siliceous species (anions) can react with metallic cations (+ve ions) to form the protective film. The deposition of the silicate film depends on the presence of small amount of corrosion products on metal surfaces for having silicate inhibiting action (Lehraman, 1964) & (Ovchiyan, 2003). Presence of small amount of corrosion could be as result of following reactions.

The oxidation of metals occurs at anodic areas:

$$\text{Metal} = \text{metal}^{n+} + ne^-$$

Ferrous metal in the presence of moisture reduce to:

$$Fe + 2H_2O = Fe(OH)_2 + 2H^+ + 2e^-$$

In the presence of oxygen, the ferrous ions will oxidise to ferric.

$$2Fe^{++}\ 1/2O_2 + 2H^+ = 2Fe^{+++} + H_2O$$

In Figure 5.42 electrochemical coating of silicate on cleaned reinforcement bar with dilute HCL, showed the formation of oxide layer first followed by silicate coating, whereas Figure 5.43 showed the formation of immediate silicate coating on the existing oxide layer. This finding was in accordance with the Ovchiyan's findings (2003), that inhibiting silicate coating happens when the surface layers on the metal possess a protective properties to a lesser or greater extent as result of oxide passive film formation.

Figure 5.44 (b) above shows the reinforcement with imperfect passive oxide film and its elemental composition prior to the silicate coating (Cheema, 2011). The morphology of amorphous sodium silicate coating, which can contribute towards the passivated state of steel surface, is shown by EDX images above in Figure 5.45 (b).

Silicate passivation effect was assessed using half-cell potential (HCP) measurements, which were taken on embedded steel in geopolymer concrete electrochemically silicate coated for 45 minutes. Figure 5.46 below showed that silicate pre-passivated embedded steel in geopolymer concrete has low negative potential before subjecting the samples to severe environment as shown by the first few HCP observations.

This lower negative HCP of– 0.100- 0.150V approximately against the -0.200-0.400V observed at the start of the experimental work for LCFG concrete as shown in Figure 5.33 (a) above confirms that silicate coating has corrosion inhibiting potential.

However subsequent HCP measurements showed higher negative potential when LCFG concrete cylinder specimens were subjected to the simulated severe environments. Porous silicate coating of steel bar specimen over a short duration of 45 minutes could be the possible reason of this observation of higher negative HCP under severe exposure. These measurements initially showed some fluctuations but stabilising trend to lower negative potential was observed in both the samples.

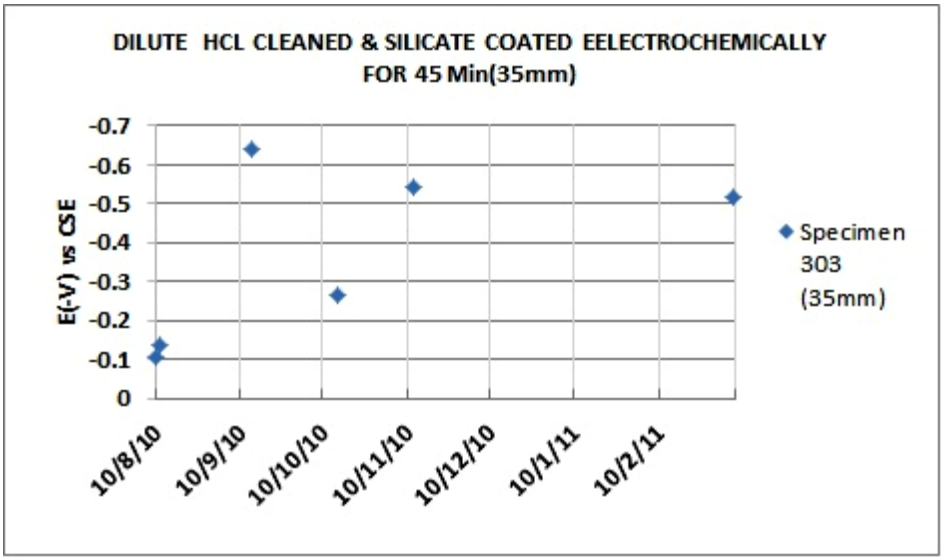

(a)

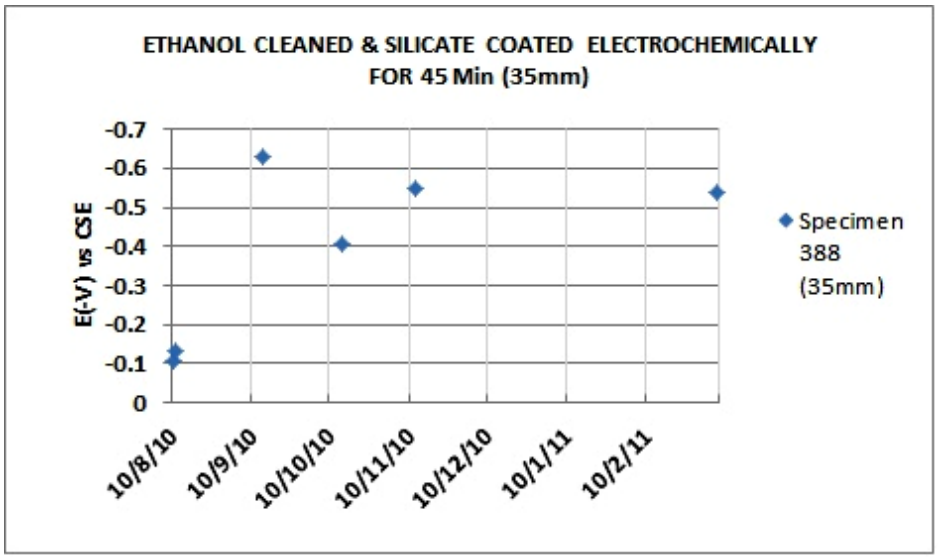

(b)

Figure 5-46 HCP Measurements of Silicate Pre-Passivated Steel IN LCFG Concrete

Further coating test by simply immersing steel bar in sodium silicate solution and then curing the steel sample at 110 ^{o}C for two hours showed very high resistance to current measured using volt meter at various locations. These resistance measurements at various locations were in the order of 24 M- ohm. These high resistance measurements indicate that silicate is of passivating nature and its passivation effect is of adding nature to the passive oxide film in non –aggressive to mild environmental exposure, however its robustness in severe exposures may need further research (Cheema, 2011).

In OPC concrete formation of passive oxide film is expected over a week or so and under continually increasing pH environments on account of $Ca(OH)_2$ formation followed by hydration of cement. However passive oxide film in LCFG reinforced concrete is expected to form during the concreting and any rest period allowed followed by silicate layer before curing at elevated temperature.

In LCFG concrete initial high pH environment for the complete formation of passive oxide film over a short period needs further research. Test observations in this research indicated that high temperature curing in excess of 90 ^{o}C may be beneficial from the added passivation effect of silicate provided the underlying oxide film formation to the adequate level is possible. This silicate passivation leads to a higher degree of stability to thin ferric oxide passivation film by healing its imperfect regions.

5.11.5 Qualitative Assessment of Revealed Corrosion Activities

Qualitative observations such as, the extent of corrosion activities, rust mark, approximate section loss estimate resulting from corrosion, visible pores, moisture mark and cracks etc. for both LCFG and OPC concrete samples were taken after breaking apart the core specimens and reinforced laboratory samples.

Figure 5.47 below shows the extent of corrosion activities on embedded steel. The core specimen taken from laboratory samples with 25mm cover was broken apart after one year exposure for both LCFG and OPC concrete. The core specimens were from exposed part of the laboratory samples representing the splash zone of severe environments.

Active corrosion was inferred on nearly 40-50% of rebar surface area in LCFG concrete compared to insignificant corrosion activity on rebar surface in OPC concrete. Higher level of corrosion activities were noted on steel bars in LCFG concrete with 35mm cover compared to OPC concrete after two years severe exposure (Figure 5.47).

G40 Cover 25mm Year 1 **S40 Cover 25mm Year 1** **Sx40 Cover 25mm Year 1**

G40 Cover 35mm Year 2 **S40 Cover 35mm Year 2** **Sx40 Cover 35mm Year 2**

Figure 5-47 Embedded Steel Corrosion from Core Samples (25mm & 35mm Cover)

Figure 5.48 below shows the corrosion status of reinforcements in laboratory samples with 35mm cover when broken apart after two years exposure.

The prominent and distinct rust marks on fragmented concrete parts from the laboratory sample at steel bar locations in LCFG concrete confirms the higher level of corrosion particularly where the steel was supported by the cover chairs compared to OPC concrete. This might be due to the trapped moisture over the plastic cover chairs compared to other locations.

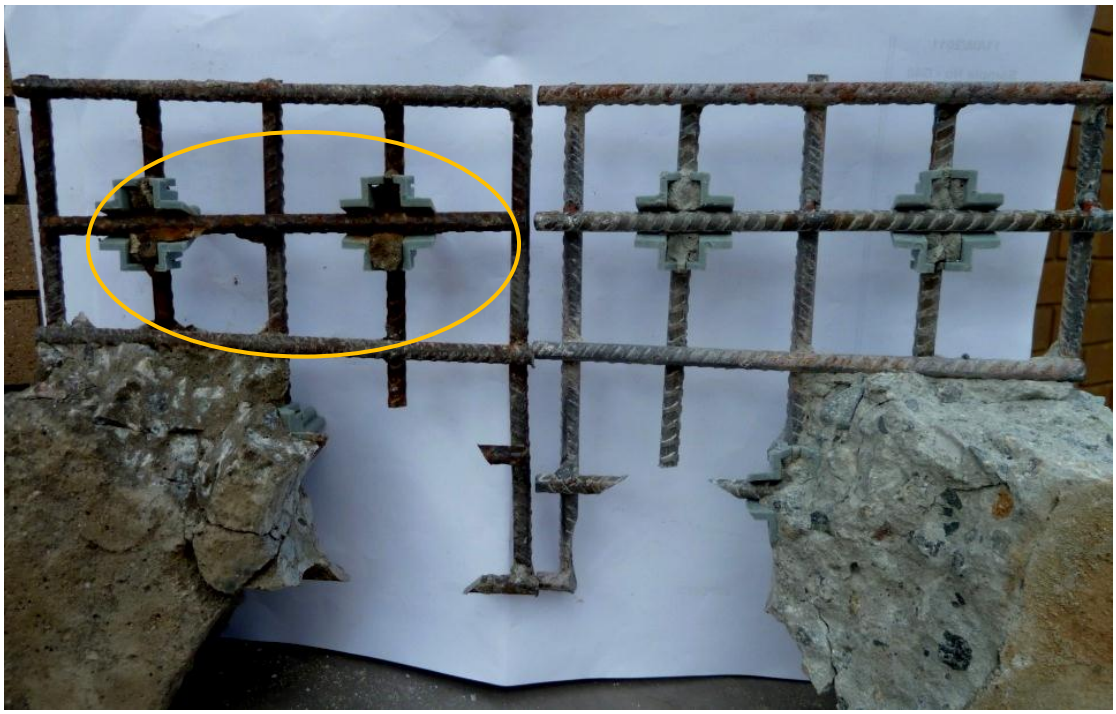

G40 **S40**

Rust Mark G40 **Rust Mark S40**

Figure 5-48 Embedded Steel Condition and Rust Marks on Concrete at Steel bar Locations

Figure 5.49 below shows the status of LCFG concrete in exposed severe zone and buried severe zone and for pre-passivated steel bars used in cylinder specimens after 30 months severe exposure.

One cylinder specimen of LCFG concrete with pre-passivated steel was with embedment of silicate- coated steel bar for 45 minutes with protruding section for facilitating HCP measurements while the other cylinder specimen was with silicate- coated steel for 30 minutes, completely embedded in the specimen.

Pre-passivated Embeded Steel Sample, HCL Cleaned Sample (303), Age -30 months & Exposure - Severe	Pre-passivated Embeded Steel Sample, Ethanol Cleaned Sample (388), Age -30 months & Exposure - Severe
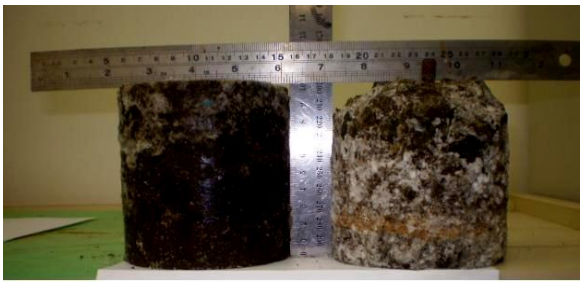	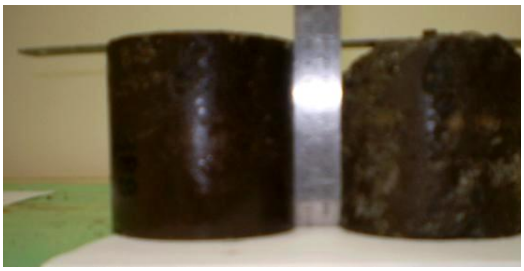
Burried Partially Exposed	**Burried Partially Exposed**
	
Blck Rust Scaling & Stain	**Black Rust Scaling & Stain**
	
With exposure black rust turned brown.	

Figure 5-49 Corrosion of Silicate Pre-passivated Embedded Steel

On breaking apart these specimens black stained steel bars and black stained LCFG concrete were inferred. This black rust activity might be due to the conditions with no oxygen in buried part. This black rust mark turned brown on oxidation after a while in the exposed environments. This observation confirmed the black rust activity Olivia (2011) inferred in her research with an accelerated corrosion lollypop test.

It was also inferred that exposed cylinder specimen degraded significantly while the buried and immersed specimen stayed intact without any noticeable surface degrading. This was in line with previous observations in the preceding section for efflorescence & scaling. Table 5.19 summarises the visual observations of corrosion status of rebar in LCFG concrete.

Table 5-19 Visual Assessment of Corrosion Activity

Observations	LCFG CONCRETE
	Galvanic Corrosion (After 1 year exposure for 25mm cover specimen and after 2 year exposure for cover 35mm specimen
Corrosion activity (Brown Rust)	More brown rust activity on embedded steel in G40 compared to S40 and Sx40 for samples exposed to severe exposure with wetting and drying cycle.
Corrosion activity (Black Rust)	**Pre-passivated steel specimen corrosion after 30 months exposure**
	More black rust activity on pre-passivated embedded steel in G40 for samples completely immersed and buried for 30 months severe exposure.

From the visual assessment it was inferred that active corrosion of embedded steel in LCFG concrete under severe environmental exposure is more pronounced than OPC concrete over the study duration of three years. This active corrosion of embedded steel in LCFG concrete indicates the higher probable corrosion rate. This is in line with the different test results (higher diffusion, low pH and higher HCP) in the preceding sections in comparison with OPC concrete.

Low pH environments in LCFG concrete observed in this research prompted the blended LCFG mix concrete, which was investigated in this research in order to improve the pH and to target initial high compressive strength under ambient curing. Sub-section 4.4.8.1 in Chapter details the blended LCFG concrete mix. Following section provides the test results and test observation of blended LCFG concrete investigated in this research.

5.12 BLENDED LCFG CONCRETE AMBIENT & STEAM CURED MIX

5.12.1 Mix Proportions, Oxides Molar Ratios of Blended LCFG Concrete & Results

For in -situ applications, a concrete of non- structural concrete class (N) of strength below or up to 40MPa is generally the requirement. However for in-situ applications (like rigid concrete road furniture), ambient curing is more practical for achieving the desired initial strength.

Because of low initial strength gain of LCFG concrete when cured ambiently, a modified mix with small proportion of slag (blended LCFG concrete) was investigated for short term durable properties (such as initial & residual strength, pH and scaling). Test results showed that, blended LCFG concrete mix achieved average initial strength of 50 MPa under ambient curing conditions compared to LCFG concrete mix with 100% low calcium fly ash. Compressive strength results are detailed in Table 5.21 subsequently.

This high initial strength gain may be because of resulting increased calcium content (that is, addition of 5% slag raised the calcium content of fly ash from 1.5% to 3.5% while 10% slag raised the calcium content to 6%) and increased oxides components. In term of oxide components, addition of 5% to 10 % slag raised the fly ash SiO_2 composition to 55-57% and Al_2O_3 composition to 28-30%. Consequently higher mix molar ratios will result. Modified mix with 5% slag to fly ash binder and 16M NaOH solution to alkaline raised SiO_2/Al_2O_3 mix molar ratio from 3.89 to 3.93 and corresponding increase of Na_2O/SiO_2 mix molar ratio was 0.122 from 0.120. Table 5.20 below summarises these oxides mix molar ratios of blended LCFG concrete mix and Table 5.21 below summarise the mix proportion of blended LCFG concrete with 5% slag.

Table 5-20 Mix Molar Ratio of Blended LCFG Concrete

Blended LCFG Concrete Mix	**Mix Molar Ratios**		
	Na_2O/SiO_2	**SiO_2/Al_2O_3**	**H_2O/Na_2O**
5% Slag + 95% FA	0.122	3.93	9.13
10% Slag + 90% FA	0.124	3.96	10.91

Table 5-21 Ambient Cured Blended LCFG concrete Mix

Materials	**Mass (kg/m^3)**	**Mass (kg/m^3)**	**Remarks**
	G40/50	**G40/50**	
Cockburn Cement (GP)	-	-	
Coarse Aggregates 14 mm	647	647	
Coarse Aggregates 10 mm	647	647	
Fine Sand	554	554	
ASTM Class Fly Ash 95 %	388.5	388.5	
Slag (5 %)	20.5	20.5	
Sodium Silicate Solution (SiO_2/Na_2O =2)	102	102	
Sodium Hydroxide Solution (NaOH)	41	41	16 M
Super plasticiser (SP)	6	6	
Target Water	0	0	
Extra water in aggregates	0	15.60	
Water/Cement Ratio	0.17	0.17	
Curing Temperature	Steam (60 ^oC)	Ambient	
Curing Time	24 hours	Demoulding after 5 days	14 wet curing
3 Days Mean Comp. Strength (MPa)	55.5		
7 Days Mean Comp. Strength (MPa)		66.5	
28 Days Mean Comp. Strength (MPa)		80.5	

Test results of mix with 5% slag showed compressive strength in the order of 66MPa after 7 days (cured under ambient conditions for 5 days by covering the specimens with polyethylene sheet in order to reduce quick loss of moisture before de-moulding) and 80 MPa after wet curing for 21 days. However steam curing at 60 ^{o}C for 24 hours showed relatively less strength, which was in order of 55MPa.

5.12.1.1 Blended LCFG Concrete pH and Strength Results after One Year Seawater Exposure

Blended LCFG concrete mix maintained relatively higher pH for specimens exposed to seawater for one year. Figure 5.50 (a) & (b) shows the pH trend and compressive strength of blended LCFG concrete after one year seawater exposure.

(a)

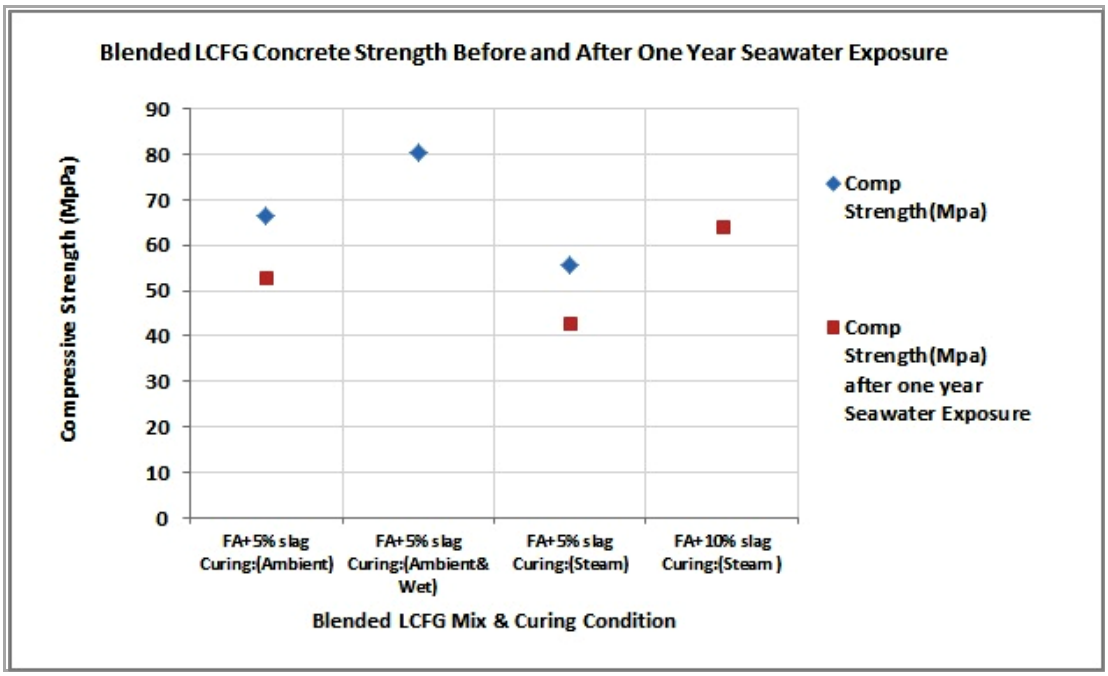

(b)

Figure 5-50 pH before and after one Year Seawater Exposure

Test results are summarised in Table 5.22 below along with residual strength.

Table 5-22 Blended LCFG Concrete pH and Compressive Strength and Impact Seawater Exposure

Blended LCFG Concrete Mix Curing Conditions	pH		Compressive Strength MPa	
	5% Slag + 95% Fly Ash (FA)	10% Slag + 90% Fly Ash (FA)	5% Slag + 95% Fly Ash (FA)	10% Slag + 90% Fly Ash (FA)
Steam- 24 hours at 60°C	11.1		55.5	
Ambient (Summer)	11.3		66.5	
After One Year Seawater Exposure				
Steam – 24 hours at 60°C	10.7	10.9	43	64
Ambient (Summer)	10.6		53	

Test results showed that pH of blended LCFG concrete was 11.3 and after one year of seawater exposure it dropped to 10.6. This pH drop was 5% approximately and strength drop was by 20% (Cheema & Lloyd, 2014). However blended LCFG concrete with 10% slag maintained relatively higher strength and higher pH. The pH of LCFG concrete regressed from 10.3 to 9 over three year of severe exposure in this research.

Also blended LCFG concrete showed less efflorescence, as such will be less liable to scaling compared to LCFG concrete. Test observation of high compressive strength under ambient conditions and better pH indicates that blended LCFG concrete have the potential to be more durable than LCFG concrete.

5.12.1.2 Blended LCFG Concrete Results Discussion

Seven days initial compressive strength gain of slag based LCFG concrete was three times higher than the ambient cured LCFG concrete containing 100% low calcium fly ash activated by 8M alkaline solution (Rangan, 2008 - GC4). It was inferred that slag based LCFG concrete cured at elevated temperature of 60^{o}C for 24 hours resulted slightly lower strength of 55.5MPa. This could be due to the formation of CSH products interfering with polymerisation process.

Higher SiO_2/Al_2O_3 mix molar ratios could attribute to higher strength gain and higher Na_2O/SiO_2 mix molar ratio as well may result finer pore structure in line with Skvara et al, 2006 study. No early setting with 5% and 10% slag was inferred during mixing of blended LCFG concrete mix and the mix behaved similar to LCFG concrete mix.

However blended LCFG concrete mix with 20% slag content showed early setting during wet mixing as shown in Figure 5.51 below. Possible reason of early setting could be due to high molarity NaOH solution of 16M in alkaline solution resulting lower water/geopolymer solid ratio, combined modulus of alkaline solution to nearly 1 as shown in Figure 6.2 subsequently and high calcium content interfering with the polymerisation (Gourley, 2003). This was despite the use of additional water, which essentially lowers the NaOH molarity.

Figure 5-51 Unworkable Blended Mix with 20% Slag

However further research may be needed to investigate the other contributing factors for its early setting as reference in the literature shows the use of slag content could be up to 40% (Skvara et al, 2006). Possible reason of this high slag doses might be due to high aluminate content of their source material used (which was up to 35%), lower molarity NaOH and higher water/binder ratio (which was up to 0.23) in Skvara et al (2006) study.

Higher strength gain under ambient conditions is however an indirect indication of its durability (Cheema, 2012 & Cheema & Lloyd, 2013). This may be due to the formation of CSH products in an alkali activated blended LCFG concrete mix, which have the potential to render discontinuous pore structure with increased tortuosities. This inference was in line with Yang et al 2012 study, which showed fly ash- slag blend activated by sodium silicate has sodium – calcium-aluminate hydrates (N-C-A-S-H) with more compact microstructure compared to the LCFG concrete.

The past research has shown that 100% fly ash based LCFG concrete cured under ambient conditions has shrinkage higher than the steam cured one. This higher shrinkage occurs over the first two weeks and is approximately 13 times higher than the steam cured LCFG concrete, Rangan (2008) and Wallah & Rangan (2006). Mukhin et al (2007) research study has shown that addition of small proportion of low shrinkage cement (SL) in alkali activated fly ash geopolymer concrete caused 50% reduction in shrinkage for mix cured under ambient conditions. This is notional that small proportion of slag in blended LCFG concrete due to its slow hydration of slag over an extended period is liable to obtain desirable properties relative to drying shrinkage and need further research.

Past research also showed that LCFG concrete achieved initial strength in the order of 20 MPa when allowed to cure ambiently and increased gradually over time (approximately 40 MPa in 4 weeks and 50MPa in 12 weeks – Rangan (2008). As such LCFG concrete in – situ application may be feasible where high early strength and commissioning of the project prior to 4 weeks may not be the main requirement, whereas blended LCFG concrete may be preferred concrete construction material on this account.

5.12.2 Chloride Threshold for LCFG Concrete & Blended LCFG Concrete

Based on the intrinsic low pH value of LCFG concrete & blended LCFG concrete (that is, between 10 to 11) with possible higher corrosion rate, the chloride threshold criteria developed for LCFG concrete is detailed in Table 5.23 below. This chloride threshold criteria is based on the slope of corrosion rate curve shown in Figure 5.28, which is assumed as linear up to 10 pH value.

Table 5-23 Chloride Threshold (Cth) Criteria for LCFG Concrete for the Initiation of Corrosion

pH	Corrosion Rate Curve Slope	Control	Chloride Threshold (Cth) for plain steel in LCFG concrete with pH 10- 11	Chloride Threshold (Cth)for stainless steel in LCFG concrete with pH 10-11
10	0.0129	4.45	0.014% by wt of concrete	0.112% by wt of concrete
11	0.0071	2.45	0.025% by wt of concrete	0.204% by wt of concrete
12	0.0029	1	0.06% by wt of concrete (Cth for OPC concrete at pH 12 or above)	0.5% by wt of concrete (Cth for OPC concrete at pH 12 or above)

Low level of chloride threshold tolerances for the initiation of active corrosion of embedded steel in LCFG concrete, which is 4 times lesser at pH 10 and 2.5 times lesser at pH 11 compared to OPC concrete. Threshold criteria in Table 5.23 above for LCFG concrete will be more responsive from its durability aspect relative to the severity level of environmental exposure scenarios.

Thus from the indicative pH level of blended LCFG concrete and LCFG concrete, blended LCFG concrete could be the potential construction material for in-situ applications from durability aspect and subsequent section details its potential sustainable applications.

5.12.3 Positive Impacts of Blended LCFG Concrete and its Sustainable Applications

Blended LCFG concrete with small proportion of slag in this research study confirmed most of Skvara et al (2006) research findings such as, higher strength, lower porosity, and negative impact of higher water / binder ratio on pore structure and about the fineness of its pores.

Short term durable properties of blended LCFG concrete in this research revealed that it could be a potential construction for in –situ rigid road furniture and rail projects applications as shown Figure 5.52 below. These may include dual use path, crash barrier, curtain & noise walls, underpasses, traffic island in- fill and paved access street/road and kerbing.

Previous feasibility research undertaken in co-operation with local pre-cast industry (ROCLA) for manufacturing LCFG concrete box culverts of size 200x1200x600mm has shown that LCFG concrete is a feasible construction material like OPC concrete for pre-cast concrete structure components (Cheema et al, 2009). As such LCFG concrete could be a potential construction material for pre-cast components for non- aggressive to mild environmental exposure scenarios.

Figure 5.52 below shows the potential applications where blended LCFG concrete could replace OPC concrete.

Crash Barrier & Rail Sleeper

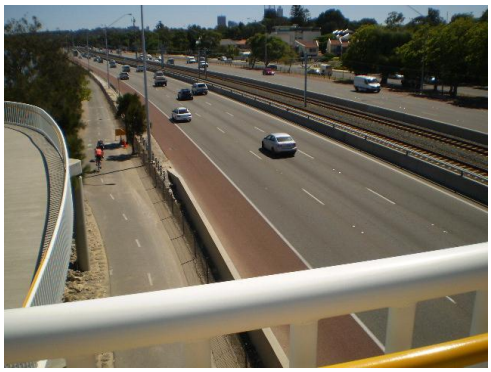

Curtin Wall

Traffic Island Infill

Under Pass

Figure 5-52 Blended LCFG Concrete Potential Applications in Non-aggressive Environments

Thus LCFG concrete pre-cast applications and blended LCFG concrete in-situ applications can be of significant advantage. This is because of their alleviating potential to reduce negative foot print of fly ash disposal and its potential downstream health issues, which could be from concentration build –up of its heavy and radioactive metals' traces over time. Secondly such applications will be useful for ongoing improvement of its long term durability properties. Illustration demonstrating its CO_2 saving & sustainable potential is appended in Appendix E.

5.13 Consistency & Quality of LCFG Concrete Mix Relative to OPC Concrete

Unlike cement binder in OPC concrete as detailed in the preceding chapters, the LCFG concrete binder's (low calcium fly ash) components and the composition of commercially available sodium silicate & NaOH solution for its alkaline solution have significant bearing on the eventual development of its microstructure and pore structure from long term durability perspectives..

Therefore main components influencing LCFG concrete are: low calcium fly ash composition, alkaline solution & its combined modulus, quality of fine and coarse aggregates & their saturated surface dry (SSD) conditions, controlled mix preparing conditions and curing conditions (accelerated or ambient).

Chapter 6 details the influence of these parameters, which are particularly important for maintaining the consistency and quality of the LCFG concrete in view of sensitive nature of its mix components and their preparing and curing aspects compared to OPC concrete. Potential fundamental outcomes on the basis of synthesis analysis & limitations of these components will assist further research for achieving consistency and quality of LCFG concrete mix from long term durability perspective.

CHAPTER 6 SOURCE MATERIAL AND ALKALINE COMPOSITION SYNTHESIS ANALYSIS, ANALOGY AND RESULTS DISCUSSION

6 SOURCE MATERIAL COMPOSITION SYNTHESIS ANALYSIS

6.1 Source Material Composition Variability

As alkaline activated low calcium fly ash (ASTM Class F) replaces Ordinary Portland Cement (OPC) totally in LCFG concrete, its material composition variation can influence the final LCFG concrete product.

Figure 6.1 below shows the variation extent of main components of low calcium fly ash used in the past research studies over the period of around 7 years. Batches 1 to 3 are from Hardjito & Rangan (2005) and Batch 4 & 5 are from Olivia (2011) research.

All batches were from Collie Power Station, Western Australia with the variation of their chemical composition as shown in Figure 6.1.

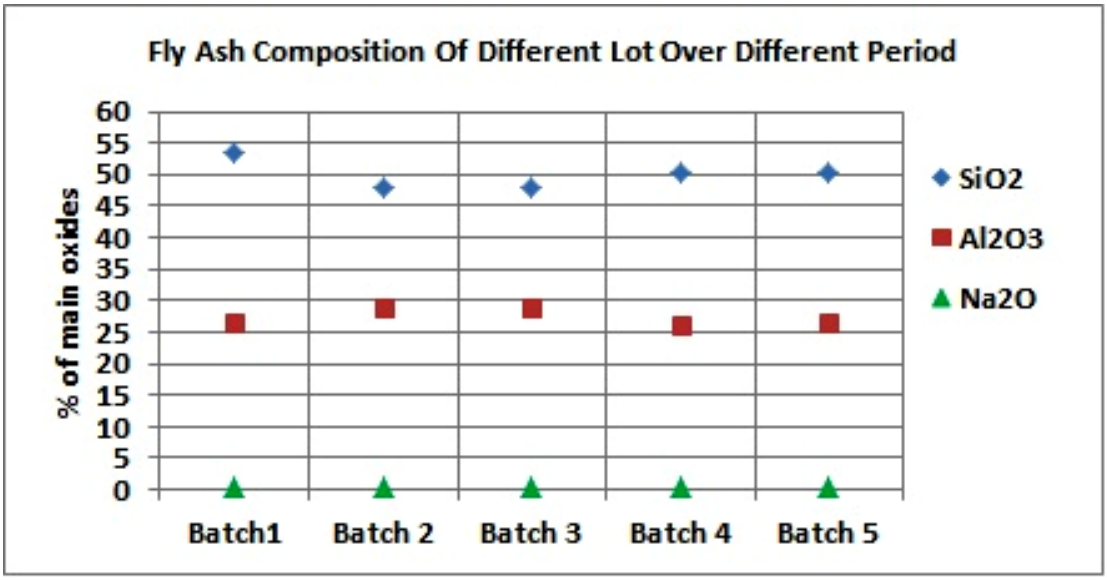

Figure 6-1 Collie Power Station Low Calcium Fly Ash Main Constituents' Variation Extent of Different Lots since 2005.

Fly ash source material composition referred in Batch 1 was used for analysis purpose in previous research (Hardjito & Rangan, 2005) and also forms the basis of analysis in this research. Some level of tolerances can be expected with the variation extent of source material main components as shown in Figure 6.1 above.

6.2 Influence of NAOH Solution Molarity and Sodium Silicate Solution Modulus

Table 6.1 below summarise these tolerances for the source material from Collie Power Station and the concomitant tolerances of oxides' mix molar ratios. These variations of fly ash by-product are inevitable to some extent because of its production from naturally available coal.

Table 6-1 Mix Molar Variations' Tolerances

Main Compo-nents	**Variation Ranges**	**Main Compo-nents' Tolerances**	**Oxides Molar Ratio Variation Ranges for NaOH of 8M to 16M**					
			SiO_2/ Al_2O_3	***Tole-rances**	**Na_2O/ SiO_2**	**+Tole-rances**	**H_2O/ Na_2O**	**+Tole-rances**
SiO_2	48-53.5	± 9%	3.24-3.89	± 17%	0.098-0.120	± 18%	9.11-12.06	± 24%
Al_2O_3	26.5-29	± 9%						
Na_2O	0.31-0.45	± 30%						

* SiO_2/Al_2O_3 mix molar ratio tolerance is dependent on fly ash components' variation, alkaline/fly ash ratio (which is 0.35 in this research study) and sodium silicate modulus (which is 2, with chemical composition consisting of SiO_2= 29.4%, Na_2O =14.7% and H_2O = 55.9% of Grade A53 (Hardjito and Rangan, 2005 and Rangan, 2008). Variation of aluminate content in source material has predominant impact on SiO_2/Al_2O_3 mix molar ratio.

+ Na_2O/SiO_2 & H_2O/Na_2O mix molar ratios' tolerances are dependent on fly ash components' variation, alkaline/fly ash ratio, sodium silicate solution modulus and NaOH solution molarity and their ratio (which is 2.5 in this research study).

Above analysis results indicate that SiO_2/Al_2O_3 mix molar ratio can vary with small variations of fly ash main components and its range is between 3.24-3.89 for source material from Collie Power Station. This variation has bearing on Na_2O/SiO_2 mix molar ratio. The variation of Na_2O/SiO_2 mix molar ratio impacts the durable properties of LCFG concrete, such as, compressive strength decreases with the increase of Na_2O/SiO_2 mix molar ratio (Hardjito &Rangan, 2005) while microstructure and pores' structure improve (Skvara et al, 2006) as detailed in Chapter 3 Section 3.6.1.

Davidovits' (1982) optimised the minimum value of SiO_2/Al_2O_3 mix molar ratio as 3.5 and Sagoe et al (2006) further confirmed this minimum requirement. But Na_2O/SiO_2 mix molar ratio increases with the decrease of SiO_2/Al_2O_3 mix molar ratio and vice versa.

Figure 3.20 shows the compressive strength trend on account of Na_2O/SiO_2 mix molar variation (Hardjito and Rangan, 2005). Davidovits (1982) provided Na_2O/SiO_2 mix molar range as $0.2< Na_2O/SiO_2 <0.28$ for calcined kaolin source material and Barbosa et al (2000) optimised it as 0.25.

Hardjito & Rangan (2005) research showed the optimum range of Na_2O/SiO_2 mix molar ratio as 0.098-0.115 and of SiO_2/Al_2O_3 ratio as 3.89 for low calcium fly ash source material from Collie Power Station. Hardjito & Rangan (2005) research used Batch 1 source material composition for optimum mix molar ratios, which reflected SiO_2/Al_2O_3 mix molar ratio of constant value of 3.89 for their study purpose.

However SiO_2/Al_2O_3 mix molar ratio may subject to vary with possible tolerance limits as summarised above in Table 6.1. The minimum limit indicated by Davidovits and Sagoe-Crentsil & Brown (2006) for SiO_2/Al_2O_3 mix molar ratio may not be applicable for source material from Collie Power Plant, which ranges between 3.24-3.89 on lot basis.

Further, the influence of NaOH molarity on Na_2SiO_3 solution of modulus 2 (commercially available of A53 grade) results the combined alkaline solution modulus between 1.07- 1.32 as shown in Figure 6.2 below. Figure 6.2 shows the decreasing trend of alkaline solution modulus value with the increased molarity of NaOH solution.

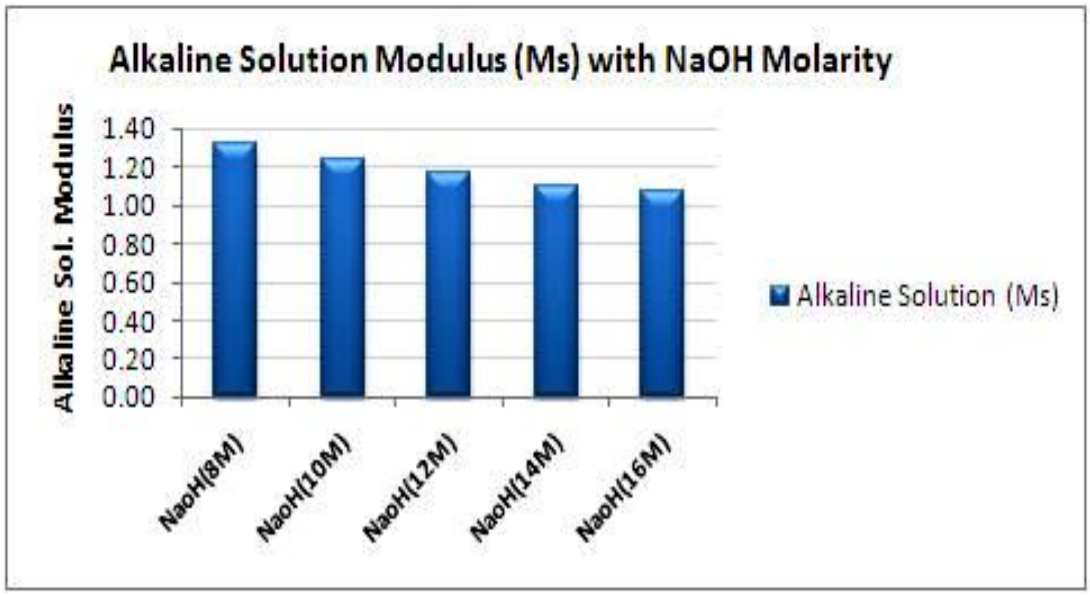

Figure 6-2 Alkaline Solution Modulus with Different NoOH Molarity

The modulus value of alkaline solution decreases to almost 1 with 16M NaOH solution as shown in Figure 6.2 above. As such the use of NaOH of higher molarity than 16M with sodium silicate solution of modulus value 2 will tend to lower the combined alkaline solution modulus below 1. For desirable properties, Skvara et al (2006) research showed that the alkaline solution combined modulus should range between 1-1.6.

Use of 14M NaOH with sodium silicate solution of modulus 2 will result H_2O/Na_2O mix molar ratio below 10 as summarised in Table 6.2 below. This equates to water/ geopolymer solid binder ratio less than 0.18.

At this water/geopolymer binder ratio (i.e. less than 0.18), mix is unworkable unless additional water is added into the mix (Hardjito and Rangan 2005). Additional water in the mix effectively amounts to decreasing the molarity of NaOH solution in the alkaline solution.

The decreasing trend of alkaline combined modulus with increasing molarity of NaOH solution indicates that NaOH solution of higher molarity from 14M to 16M or more than 16M may not be appropriate for a sodium silicate solution of modulus 2. Alternatively combined modulus of alkaline solution below 1.2 will result unworkable LCFG concrete mix.

However Hardjito & Rangan (2005) research reveals that lower H_2O/Na_2O mix molar ratio provide higher strength, which translates to water/ geopolymer solid binder ratio as shown by Figure 3.21 (a) and (b) in Chapter 3 and result from higher molarity NAOH solution.

Figure 6.3 below shows the influence of source material main components variation and NaOH solution of different molarity on Na_2O/SiO_2 mix molar ratio. It was inferred that 12M NaOH tend to average out the tolerances' limit that may result from the source material main components variation even from the same source.

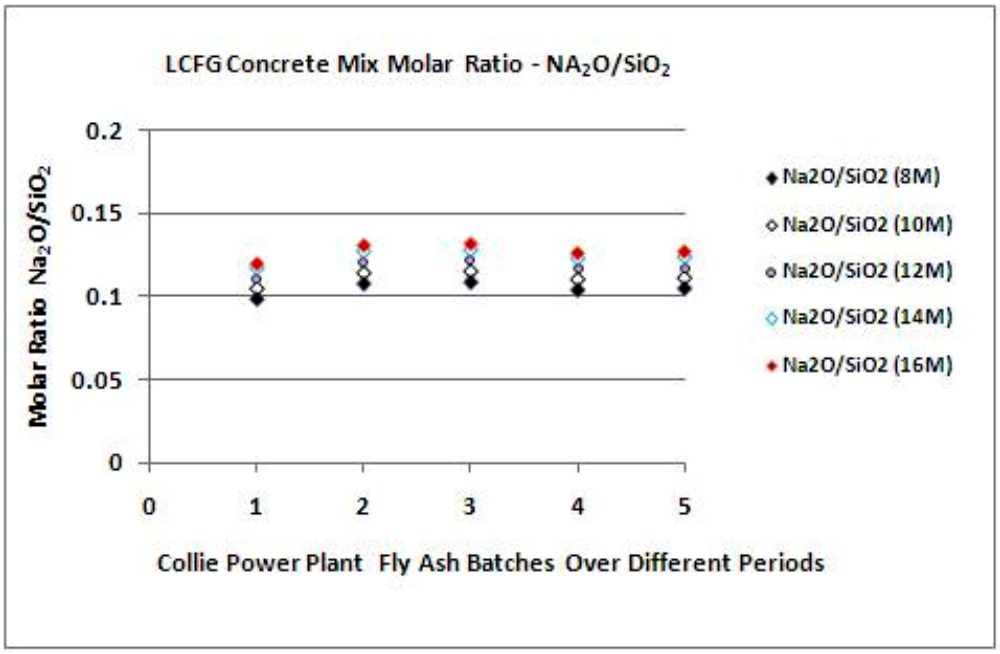

Figure 6-3 Low Calcium Fly Ash Composition Variations' Impact on Alkaline Oxide Molar Ratio

Table 6.2 below summarises the influence on combined alkaline solution modulus and consequent Na_2O/SiO_2 and H_2O/Na_2O mix molar ratios, when a sodium silicate solution of modulus 2 and higher than 2 is mixed with NaOH solution of molarity ranging between 8M-16M for LCFG concrete mix with alkaline /fly ash ratio as 0.35.

Table 6-2 Na_2SiO_3 Modulus Impacts on Na_2O/ SiO_2 & H_2O/Na_2O Mix Molar Ratios

	Na_2SiO_3 Modulus (Sio_2/Na_2O)=3.2-3.3 (SiO_2 =30.1%, NaO_2= 9.4% & H_2O=60.5%)		**H_2O/Na_2O**	**Na_2SiO_3 Modulus (Sio_2/Na_2O)=2 (SiO_2 =29.7%, NaO_2= 14.7% & H_2O=55.9%)**		**H_2O/Na_2O**
NaOH	**Na_2O/SiO_2 (Bakri)**	**Ms (Bakri)**		**Na_2O/SiO_2 (A53)**	**Ms (A53)**	
8M	0.077	1.756	14.58	0.098	1.320	12.036
10M	0.083	1.619	13.20	0.104	1.239	11.08
12M	0.089	1.501	12	0.111	1.167	10.23
14M	0.095	1.399	10.95	0.117	1.103	9.47
16M	0.098	1.353	10.48	0.120	1.074	9.11

Figure 6.4 (a) & (b) below shows the influence trend of NaOH molarity on Na_2SiO_3 with higher modulus value of 3.2 -3.3 (as per Bakri et al, 2011) compared to the one being used in this research study of modulus 2 (A53 Grade) on alkaline combined modulus and Figure 6.4 (b) shows the impact on Na_2O/SiO_2 mix molar ratio for mix with alkaline/fly ash ratio as 0.35.

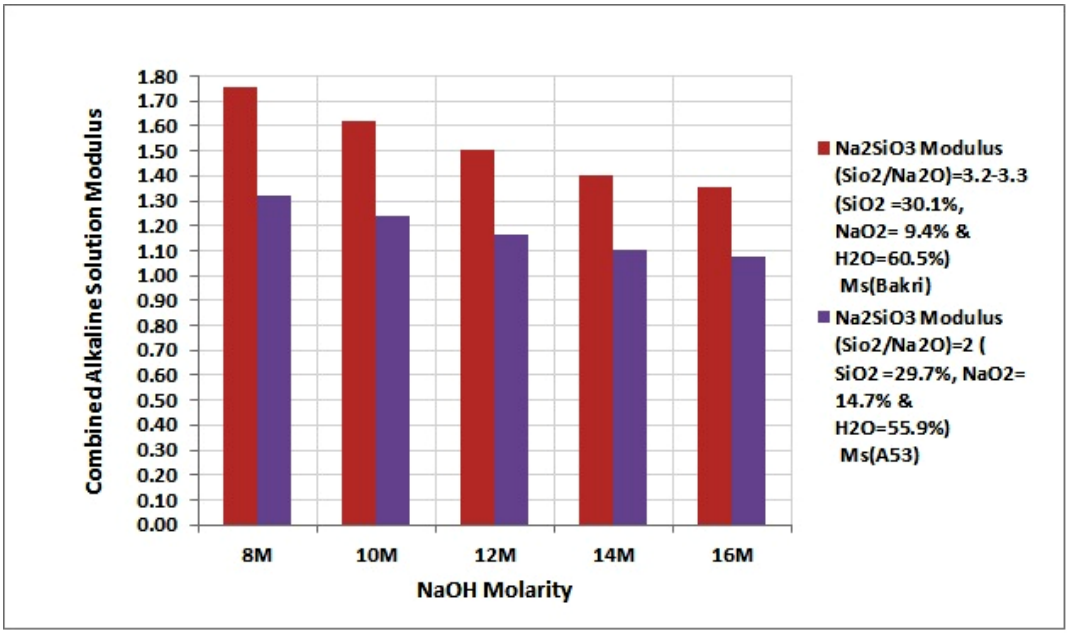

(a)

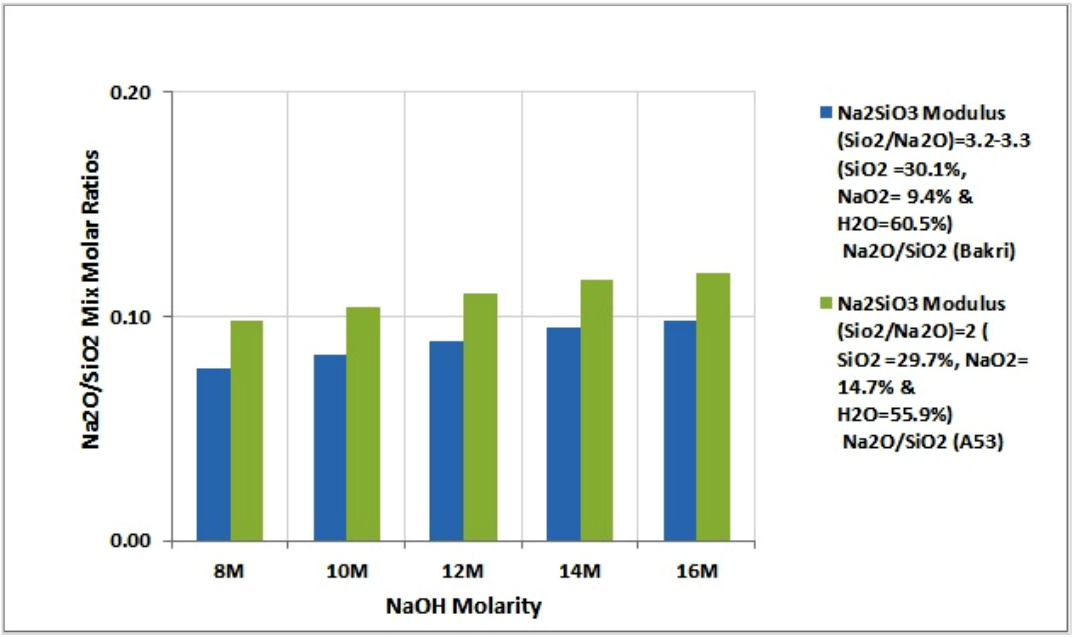

(b)

Figure 6-4 NaOH Molarity Influence on Na2SiO3 Modulus and Na2O/SiO2 Mix Molar Ratio

Figure 6.4 (b) above shows the decreased Na_2O/SiO_2 mix molar ratio with sodium silicate solution of higher modulus than 2. This supports the higher compressive strength trend as shown in Figure 3.20 above (Hardjito & Rangan 2005). Figure 6.5 below shows the influence on H_2O/Na_2O mix molar ratio of alkaline/ fly ash ratio, NAOH solution molarity and sodium silicate solution modulus.

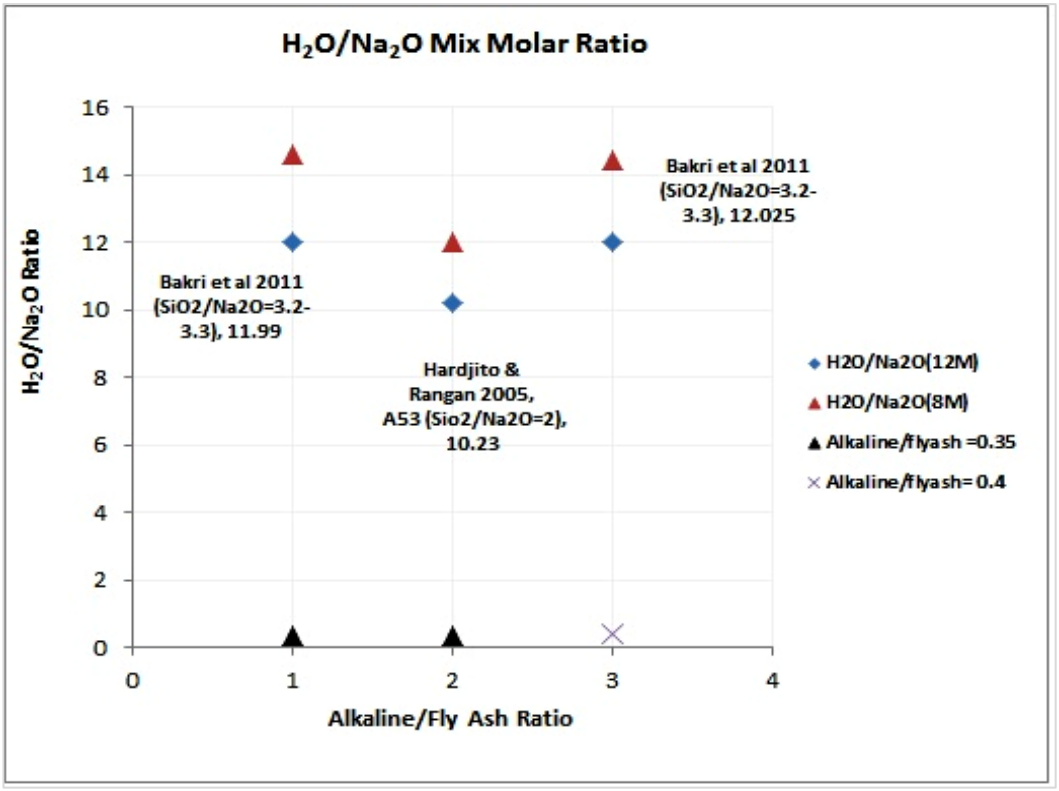

Figure 6-5 Alkaline/Fly ash Ratio & Na2SiO3 Modulus Impact on H2O/Na2O Mix Molar Ratios

Higher molarity NaOH solution can assist in dissolving more silica and alumina, which can result higher strength (Chindaprasirt, 2009). Table 6.3 summarises the influence of high modulus sodium silicate solution on Na_2O/SiO_2, H_2O/Na_2O mix molar ratios and combined alkaline solution modulus.

Table 6-3 Na2SiO3 Modulus Impacts on Na2O/ SiO2 & H2O/Na2O Mix Molar Ratios

NaOH	Na_2SiO_3 Modulus (SiO_2/Na_2O)=3.2-3.3 (SiO_2 =30.1%, NaO_2= 9.4% & H_2O=60.5%)		H_2O/Na_2O
	Na_2O/SiO_2 (Bakri)	Ms(Bakri)	
8M	0.083	1.861	14.62
10M	0.089	1.724	13.23
12M	0.095	1.606	12.03
14M	0.101	1.503	10.98
16M	0.104	1.456	10.5

Above analysis reveals that that workable mix may be probable with 16M NaOH with sodium silicate of modulus 3.2.

If modulus of Na_2SiO_3 is kept constant, water/binder ratio decreases with higher molar NaOH solution as summarised in Table 6.2 and 6.3. This is notional for getting higher compressive strength results as per trend shown in Figure 3.21 (a) & (b). However some contradictory compressive strength trend was observed by other researchers in the past. For example Bakri et al (2011) showed higher compressive strength results in the order of 90 MPa with 12M NAOH solution compared to higher molarity NAOH solution than 12M.

An alkaline solution of combined modulus 1.6 (using 12M NaOH) for mix with alkaline / fly ash ratio as 0.4 and aggregate proportion as 80% resulted H_2O/Na_2O mix molar ratio of 13.8 and corresponding higher compressive strength as shown in Figure 3.22. This H_2O/Na_2O mix molar ratio of 13.8 in accordance with Hardjito & Rangan, 2005 research translate to water/geopolymer solid ratio in excess of 0.24. This water/binder ratio as per correlation in Figure 3.21(b) should correspond to lower compressive strength.

The explanation for this different trend of higher compressive strength could be as a result of 2% increase in SiO_2/Al_2O_3 mix molar ratio and corresponding 15% decrease in Na_2O/SiO_2 mix molar ratio. Secondly resulting higher water/binder ratio may not be diluting the polymerisation reaction.

So slight increase in SiO_2/Al_2O_3 mix molar may compromise the higher water/binder ratio, however higher water/binder ratios will results more porous microstructure. These contradictory inferences may need further research.

As indicated above that higher water binder ratio results more porous structure analogous to OPC concrete as shown by test results in preceding sections and may be compromising from long term durability perspective. NaOH solution of lower molarity than 8M will provide higher water binder ratio and result LCFG concrete of high porosity as observed in this research. This finding is in line with Skvara et al (2006) findings, which showed that decrease of combined alkaline oxide percentage in the mix results larger size pore structure than the mix with higher percentage of Na_2O.

6.2.1 Influence of Aluminate Content

Low aluminate content leads to a geopolymer microstructure with large proportion of unreacted particles (Sagoe- Crentsil & Brown, 2006). This is notional that microstructure and pore structure development will be with high porosity.

Whereas high aluminate content tends to consume hydroxyl groups quicker and results early condensation, which limits the development geopolymer gel phase and constraint the growing polymer. It was further showed that Na_2O / Al_2O_3 mix molar ratio between 0.6-1 provides higher strength mix (Steveson & Sagoe- Crentsil, 2005b; Sagoe- Crentsil & Brown, 2006).

As seen from the nature of chemical reaction in LCFG concrete resulting polysialate in which four-coordinated aluminate $(AlO_4)^{-5}$ has charge balancing requirement due its negative valence of more than 4. If this charge balancing is with Ca^{+2} in the mix synthesisation, it results higher strength polymer than the one with Na^+ which has lower resistance to leaching tendency (Skvara et al, 2006). This could be the one reason of having blended LCFG concrete with higher compressive. This is because of higher aluminate content and higher calcium ions from slag addition for charge balancing activity.

In Skvara et al (2006) research, fly ash source material was with 35% aluminate content, which resulted SiO_2/Al_2O_3 mix molar ratio up to 3 and could be the probable reason for accommodating higher doses of slag up to 40%. Therefore inferences from the analysis of previous studies suggest that minimum SiO_2/Al_2O_3 mix molar ratio can be up to 3 instead of 3.5.

Thus the factors, which have the controlling ability from long term durability aspects for LCFG mix include combined modulus of alkaline solution, Na_2O/SiO_2 & H_2O/Na_2O mix molar ratios and aluminate content of the source material. H_2O/Na_2O mix molar ratio is critical, that is, its low values may result unworkable mix with incomplete polymerisation reaction activity while higher value will result larger pores' size structure with higher porosity and may be also of diluting nature to the reaction.

So minor chemical composition variations as detailed above and their influence on the final LCFG concrete product from durability aspect is of sensitive nature. This indicates the need of strict requirements, such as: source material composition variability, sodium silicate solution modulus, NaOH molarity, combined alkaline solution modulus, aggregate proportion, alkaline solution/ fly ratio, curing regimes and the environmental exposure severity are essential to ensure the durable performance of LCFG concrete.

6.2.2 Molar Oxides Ratios of the Research Mix

Low calcium fly ash source material with composition of main components based on Batch 1 as SiO_2 (53.4%), Al_2O_3 (26.49%) and Na_2O (0.37 %) from previous of Hardjito and Rangan (2005) and Rangan (2008) formed the base of findings in this research. Hardjito and Rangan (2005) research used this Batch 1 composition from analysis and findings purposes irrespective to the varied composition of other batches used in their research.

So based on Batch 1 composition in this research, alkaline solution combined modulus was 1.24 using NaOH (8M) for G40 and 1.10 for G50 with 14M NaOH solution. G50 mix was with 10L extra water/m^3. Following ranges of Na_2O/SiO_2, SiO_2/Al_2O_3 and H_2O/Na_2O mix molar ratios were obtained for the mix in this research study on the basis of source composition as referred in Batch 1.

- Na_2O/SiO_2 = 0.098 -0.117
- H_2O/Na_2O = 10.6-12.04
- Water/binder = 0.19 (for mix with 8M NaOH) & 0.2 (for mix with 14M NaOH)
- SiO_2/Al_2O_3 = 3.89

Na_2O/ Al_2O_3 mix molar ratio was 0.38 for 8M alkaline solution and 0.45 for 14M alkaline solution in this research.

Test results in preceding sections revealed that LCFG concrete mix within above mix molar ratios parameters provided LCFG concrete matrix with porous structure from long term durability perspective. Lower percentage of Na_2O content in this research study mix may be the cause of higher porous structure.

Rather the extent of alkaline oxide in LCFG concrete mix has competing interest, that is, higher percentage content of Na_2O provides micro-structure with better durability but compromises with the compressive strength to some extent. This may need further research to balance these competing properties.

6.3 LCFG CONCRETE POROSITY DEDUCED FROM OPC CONCRETE ANALOGY

Some deduced porosity trend from OPC concrete analogy support the porous nature of LCFG concrete. In conventional OPC concrete, water gets consumed on account hydration process as detailed above. At water- binder (w/b) ratio of 0.38 in OPC concrete, all the mixed water gets consumed (TN024, BCRC). Usual water binder ratio ranges between 0.4-0.43 for OPC concrete. Figure 6.6 shows the water/binder variation extent and its impact on the development of capillary pores in OPC concrete.

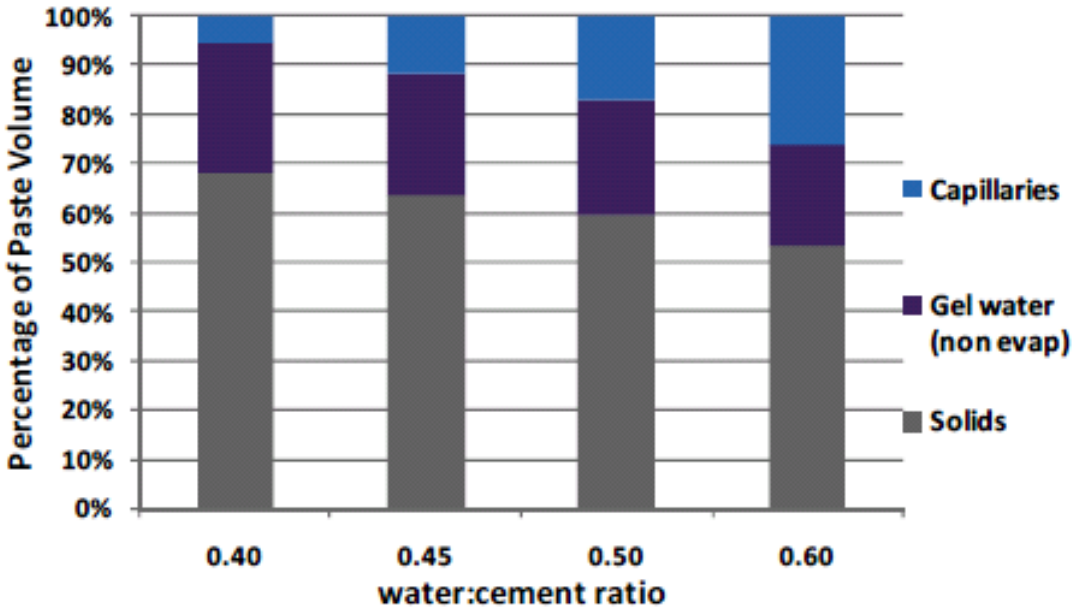

Figure 6-6 Water/Binder Ratios Impact on Capillary Pores (TN024, BCRC)

Variation of plus 0.02 in water/binder ratio from the minimum value can raise the capillary pore volume by 5% (which translate to 2kg/m^2 free water). Similarly 0.07 plus variation in binder/water raise the capillary pore volume by 15% and variation of 0.22 plus increases the capillary pore volume up to 25% which translate to 10 kg/m^2 free water. Every increment of 5% amounts to releasable water of 2kg/m^2 from the surface (TN024, BCRC). Also w/b ratio of 0.4 in OPC concrete results capillary pores, which tend to become discontinuous in 3 days. Water binder ratio of 0.6 pore will extend pore blocking tendency to 6 months and w/b ratio of more than 0.6 will render the pores of continuous nature in OPC concrete (TN024, BCRC).

Discernible features of chemical reaction that take place for each type of concrete is detailed in Table 2.2 above, that the reactant water in both type of concrete has two components – evaporable water and non- evaporable water. Non-evaporable water represents the greater proportion in OPC concrete due to calcium bearing hydration phases while in LCFG concrete greater proportion of water is free and evaporable one due to the nature of chemical reaction, which releases water as a by- product in the mix synthesisation.

In LCFG concrete water/ binder ratio below 0.19 results mix with low workability while water/binder ratio higher than 0.20 reduces the compressive strength (subject to further research) and results larger size pore structure.

From the analysis of resulting capillary pores in OPC concrete with the increasing w/b ratio as shown in Figure 6.6 above, water/binder ratio of 0.19-0.21 in LCFG concrete will equate to a water/ binder ratio of 0.6 applicable to OPC concrete. This water-binder ratio of 0.6 can contribute the development of capillary pore system up to 25% in OPC concrete as detailed above and so can be possible for LCFG concrete.

This OPC concrete analogy provides good explanation of LCFG concrete porous structure that is possible from its H_2O/Na_2O mix molar ratio. This has been kept between 0.19-0.20 from its workability point of view in this research.

Test results in preceding sections confirm the pore structure in LCFG concrete of continuous nature, despite its analogous permeability trend to OPC concrete shown in the previous research study (Cheema et al, 2009). Other complimentary reasons of LCFG concrete continuous porous structure is the nature of its chemical reaction supporting very meagre or nil formation of CHS products. Thus the pore system in LCFG concrete is likely to be with more free water in the interior region.

This interior water is less prone to evaporation unless very high temperature environment (above 105 ^{o}C) is possible. However the evaporable water in the exterior region may be more liable to evaporate under ambient temperature environment.

As such the resulting porous structure of LCFG concrete compared to OPC concrete supports moisture transport processes (capillary suction, absorption, permeation & diffusion). These processes cause the accumulation of chlorides and other harmful soluble salts from the environments (Azad, 1999 & Hong et al, 2006). Crystallisation of these accumulated salts at concrete surface on account of evaporation (supported by wicking action in combination with sorptivity & water vapour diffusion processes- Buenfeld et al, 1997; RIELM 1995; Hall and Hoff, 2002) could be the potential causes of efflorescence and subsequent scaling observed in this research.

Secondly ingress of hydroscopic salt has ability to absorb sufficient amounts of water from moist air and this may be potential reason of low resistivity for LCFG concrete and higher negative HCP compared to OPC concrete. Consequently increased level of moisture can lead to active corrosion of embedded steel with follow on deterioration of LCFG concrete through cracking and spalling within the cover zone in severe environments quicker than OPC concrete. As such LCFG concrete is more vulnerable to these degrading factors than OPC concrete as observed under severe exposures in this research.

So higher degree of sensitivity of LCFG concrete due to the variation of source material chemical composition and water - binder (w/b) ratio as detailed in the preceding section will be the challenge from its long term durability perspective in severe exposures.

6.3.1 Chloride Ions Migration Behaviour to Interior Region of LCFG Concrete

Above test results indicated in this research that LCFG concrete responses under severe environmental exposures are different than OPC concrete. Such as constant submergence of the OPC concrete may represents the ideal conditions for the improvement of intrinsic diffusion properties due to constant availability of water necessary for the hydration, refining its pore structure compared to wetting and drying cycles zone where self- sealing reactions are less likely to develop (Hong et al, 2006).

However such similar hydration scenario for LCFG concrete may not be present, which can cause improvement of its pore structure and intrinsic diffusion properties. Rather discernible feature for LCFG concrete was progressive fretting of its hardened paste surface as seen under Section 5.7. This could be from the combination of low scaling resistance to salt hydration distress and absence of self- sealing hydration reaction compared to OPC concrete.

The fretting of hardened paste surface of OPC concrete relatively was insignificant over the research period of three years. However OPC concrete with high cement content (S50) has high tri-calcium aluminate (C3A) content, which is more prone to react with sulphate rich soil to form expansive sulphate compounds causing fretting of its buried part as shown in Figure 6.7 below compared to LCFG concrete (G40 & G50).

Figure 6-7 Exposed & Buried Part of LCFG & OPC Cylinder Specimen.

LCFG concrete surface fretting make it more vulnerable to capillary action, wicking action & absorption carrying the invading chloride ions.

This leads to the development of constant content of induced chloride eventually, which supports the migration of chloride ions further to the inner region by diffusion through water-filled pathways (Hong et al, 2006; Azad, 1999). Diffusion due to its encompassing ability to diffuse free molecule or ions of other deteriorating agents such as dissolved gases (oxygen or carbon dioxide) transported by convection with permeating fluid into the concrete (Cement Concrete Aggregate Australia (CA), 2009; Hong et al, 2006 and Roy, 1986) will be the key indicator for LCFG concrete long term durability.

Evaporation, absorption and convection (when fluid transports them) exasperate this mechanism further (Nillson et al, 1996), which rely on the severity of the environmental exposures. When the chloride content exceeds the threshold, it causes the active corrosion of the reinforcement and their thicknesses depend upon the exposure conditions, location and quality of concrete (Hong et al, 2006).

As observed in this research LCFG concrete is susceptible to higher diffusion than OPC concrete, as such its application will be for selective environmental scenarios, predominantly non- aggressive.

6.4 INABILITY OF GPM TECHNIQUE FOR CORROSION RATE ASSESSMENT

GPM technique requires very small perturbation voltage application, that is, less than 20mV in order to maintain the linear relationship between the applied voltage and the current, which assist in estimating the corrosion current density and hence the corrosion rate.

For electrochemical properties in this research, samples' mix proportions were very close to the one, Olivia (2011) has investigated with the exceptions of testing techniques and the environmental exposures in this research.

Olivia (2011) has undertaken an accelerated corrosion test on 16mm partially embedded rebar and by using impressed voltage of 5V and 30V to induce corrosion. At such high voltage resulting current cannot be termed as corrosion current as per linear polarisation resistance (LPR) principles, however the test outputs of Olivia's research study provided some basis of reasoning as to why GPM was not appropriate for LCFG concrete inferred in this research. This might be because of very small perturbation voltage application requirement with GPM technique, that is, less than 20mV to maintain the linear relationship between the applied voltage and the current.

In current- time relationship for LCFG concrete as shown in Figure 3.27(c) indicated the decreasing current trend with 5V impressed voltage over time. This was lower than the one when impressed voltage was 30V as shown in Figure 3.27 (d) in Chapter 3 above.

The reasoning for low current with time may be due to the higher impedance of the capacitive double layer, Cdl on the surface of the steel at the corrosion interface as detailed above (Section 3.4.3). GPM technique which requires very small perturbation in the order of 10-20mV may be unable to perform due to the higher impedance of the capacitive double layer (Cdl) at the corrosion interface between the rebar surface and silicate layer as an Interface Transition Zone (ITZ). This could be the possible reason for GPM technique not been able to measure the corrosion current and hence no corrosion rate of embedded steel in LCFG concrete and needs further research.

The other observation noted in this research supporting this reasoning is from cored specimen of field box culvert sample which showed the existence of alkaline environment ring around rebar and concrete interface as shown in Figure 6.8 below.

Figure 6-8 Field Box Culvert Samples' Core Specimens Alkaline Environmental around Rebar

This indication of alkaline environment around rebar may be possible where the interface between the surface of the steel and silicate coating from the LCFG concrete mix may be intact during casting and hardening process in the beginning. These scenarios may offer high resistive environments to the corrosion current flow. This is also evident from decreasing trend of current over time observed by Olivia (2011) in an accelerated induced corrosion test.

CHAPTER 7 CONCLUSIONS

7 INTRODUCTION

The conclusions of this research regarding the long term durability properties of low calcium fly ash based geopolymer concrete produced using optimised mix proportion from previous research (Hardjito & Rangan, 2005) under environmental actions (non-aggressive to severe exposure with possible scenarios - buried, immersed and exposed) are as below.

7.1 DURABILITY OUTCOME

The matrix of identified properties for low calcium fly ash (LCFG) concrete from long term durability perspectives compared to OPC concrete under severe environmental exposures in this research as summarised in Table 7.1 reveals its durability status.

Table 7-1 Identified Properties from Long Term Durability Perspective

Durability Properties	Free water availability	Sensitivity to water/binder ratios, controlled & un-controlled mix preparing conditions, curing regimes	Finer continuous pore structure & larger pores numbers	Moisture transport processes capillary, absorption & permeation	Scaling Resistance	Diff. Coeff. Values	Residual Comp. Strength (MPa)	pH	Electrochemical Responses : Resistivity, Half Cell Potential (HCP)
LCFG Conc.	More	More	More	More	Low	High	Low	Low	Low & high negative HCP
OPC Conc.	Less	Less	Less	Less	High	Low	High	High	High and low negative

Based on the rating of above properties and their negative impacts on durability, it is concluded that LCFG concrete potential applications are more feasible in non-aggressive to mild environments, which predominantly should be dry.

7.2 Volume of Permeable Voids (VPV)

- Volume of permeable voids (VPV) test results before subjecting the samples to severe environments showed that volume of permeable voids of LCFG concrete are analogous to OPC concrete. Rather percentage of average absorption and percentage of average voids volume for LCFG concrete was lower than OPC concrete. VPV criteria detailed in Table 5.2 for OPC concrete appears applicable for LCFG concrete, however VPV test results after three years severe exposure showed that VPV criteria of OPC concrete is not appropriate for LCFG concrete. The empirical finding of this research indicates that critical VPV value for LCFG concrete may be around 8% compared to the critical VPV value of OPC concrete, which is 12-13% beyond which change in chloride resistance will occur and need further research.

- VPV test after three severe exposures revealed lesser percentage of average absorption in LCFG concrete, which could be indicative of the availability of free moisture already present in the system compared to OPC concrete. In OPC concrete higher absorption could be due to its ongoing hydration activity.

- Also VPV test results after severe environmental exposure of three years showed that drop in percentage average voids for LCFG concrete was 32-36% while the percentage average voids drop for OPC concrete was 7-12%. This higher drop of percentage voids in LCFG concrete is an indication of its ability to accommodate higher level of ingressed salts from the environments. Secondly the presence of higher level of free salts in LCFG concrete is indicative of its low binding ability for chloride & soluble salt compared to OPC concrete.

7.3 Capillary Suction

- Capillary suction test results revealed higher capillary rise in LCFG concrete compared to OPC concrete. The affected section was the exterior peripheral section of 20mm approximately for G40 and 10mm for G50, when assessed visually on splitting the specimen diametrically after the test duration of 502 hours. The affected section of OPC specimen was right through the section width but to a lesser height, which might be due to its large and closed size voids. High capillary rise in LCFG concrete was indicative of its finer and continuous pore structure compared to OPC concrete.

- Capillary suction test revealed that LCFG concrete has lower absorption over time relative to OPC concrete. This might be due to the partially saturated or saturated state of pore walls in LCFG concrete paste from the availability of its free water resulting from chemical reaction compared to OPC concrete.

- Capillary action in LCFG concrete was predominantly through outer dry section and was relatively through thinner section for G50 specimen compared to G40 specimen, which supported the steady state of wicking action quicker in G50 than G40 specimen. This could be the potential reason of higher level of efflorescence noticed on LCFG concrete samples and specimens with subsequent scaling in this research as discussed in Section 5.5.4.

7.4 3-D Tomography Outputs

- Test results of 3- D micro-tomography revealed that pores' number in LCFG concrete are 40% higher approximately compared to OPC concrete. This higher porosity test results of LCFG concrete concurred with Skvara et al (2006) research findings, which details that porosity of fly ash based geopolymer concrete at nano level could be up to 50% higher.

- Three- D micro-tomography results also revealed that LCFG concrete has more circular shaped pores with isotropy index 0.5-1, which constitute 40% more pores than OPC concrete approximately. OPC concrete pores are of elliptical shapes with isotropy index 0.1-0.5 and are 80% approximately. More circular shaped pores in LCFG concrete are indicative of its better mechanical properties than OPC concrete strength-wise when least affected by environmental actions.

- The other significant output of 3-D micro-tomography test indicated that LCFG concrete has finer pores compared to OPC concrete. Finer pores are indicative of more favourable conditions for moisture transfer processes (capillary, absorption, permeation and diffusion) in LCFG concrete compared to OPC concrete supporting moist pathways for diffusion of chloride ions to the interior region.

7.5 Visual Qualitative & Quantitative Observations

- Research results revealed that exposed zone of LCFG concrete has low scaling resistance than OPC concrete under severe environmental exposure. Quantitatively, scaling extent for LCFG concrete in exposed zone after three years of severe exposure was between 5- 15mm, while scaling for OPC concrete was invisible.

Effectively, high level of scaling reduces the effective cover to the reinforcement and causes the reduction in compressive strength. Predominantly soluble salts (sodium carbonate, sulphate and chloride as discussed in Section 5.7.1) are the dominant ones causing hydration distress in LCFG concrete. However for their individual dominance effect, further research is required.

- LCFG concrete in buried zone under sulphate rich soil exposure remained intact compared to OPC concrete. OPC concrete with cement content $\geq 420 kg/m^3$, usually required for high strength OPC concrete (S50) showed fretting of its buried part, which could be due to high content of tri-calcium aluminates forming expansive hydrated sulphate salt products distressing the buried part. The possibility of formation of such sulphate salts and their hydrated products in LCFG concrete may be absent or very low.

7.6 Diffusion & Chloride Profile Test Outputs

- NT Build 443 Diffusion coefficient test results on cylinder specimens before subjecting the samples to the severe environmental exposure revealed higher diffusion coefficient values (15- 22 x 10^{-12} m^2/sec) for LCFG concrete against (8-9.5x 10^{-12} m^2/sec) for OPC concrete. Higher diffusion coefficient values for LCFG concrete will predict early corrosion initiation of embedded steel in LCFG concrete compared to OPC concrete.

- Chloride profile test results undertaken at yearly interval (that is, after one year severe exposure for samples with 25mm cover to the reinforcement, two year severe exposure for sample with 35mm cover and 3 years severe exposure for sample with 50 mm cover) for both LCFG concrete and OPC concrete in this research confirmed the higher level of ingressed chloride in LCFG concrete compared to OPC concrete. The migrated level of chloride in LCFG concrete exceeded chloride threshold limit by many folds as discussed in Section 5.8.4. Both diffusion & chloride profile test results indicated that corrosion initiation of embedded steel in LCFG concrete is quicker than OPC concrete.

- Mathematical model curves' fitting based on the chloride profile test data indicated that model predicts well for OPC concrete, whereas it under-predicts for LCFG concrete. Although the diffusion coefficient has decreasing trend with time but the curve fittings from the mathematical model based on Fick's Second Law of diffusion were not near-true representation of chloride-ingressed content in LCFG concrete exposed to very severe environment exposure.

7.6.1 Chloride Binding and Resistance to Chloride Penetration

- It was inferred from diffusion coefficient curves that chloride surface concentration (Cs) level for LCFG concrete was lower than the surface concentration level of OPC concrete. Surface concentration for OPC concrete was close to the one suggested in the literature for severe exposure as detailed in Section 3.2.2.1, Table 3.3.This indicated that resistance to the chloride ingress in LCFG concrete is less compared to OPC concrete. This is also an indicator of less chloride binding ability of LCFG concrete compared to OPC concrete.

- Chloride profile test for LCFG concrete showed ingressed chloride content 3-4 times higher than the predicted one by the model. Similar observations were inferred from box culvert samples after three years of severe exposure. Test results on field core specimens revealed that ingressed chloride content in LCFG concrete pores equated to the chloride content that could be possible in the environment as discussed in Section 5.8.5. This indicated that lower corrosion initiation timing and higher corrosion rate for embedded steel in LCFG concrete may be probable compared to OPC concrete.

7.7 Carbonation

- It was inferred that the application of chemical compound (phenolphthalein) did not provide the indication of possible carbonation front in LCFG concrete when applied on immediate extracted core specimen from laboratory samples undertaken on yearly basis relative to OPC concrete. This could be due to high carbonation tendency of LCFG concrete compared to OPC concrete. Possible reasoning of this high carbonation in LCFG concrete is from the formation of primary and secondary carbonation products under severe environmental exposures as detailed in Section 5.7.1. However further research is needed to identify and quantify all possible carbonate products that may be possible in LCFG concrete on account of carbonation from atmospheric CO_2 and their secondary effect.

7.8 pH Outputs

- pH test results over the severe exposure period of three years showed the pH value of LCFG concrete between 9.3-10.3 for laboratory samples and around 9 for field box culvert sample. This low pH environment in combination with higher level of ingressed chloride from the severe environments for LCFG concrete is indicative of high corrosion risk to its embedded steel compared to OPC concrete as discussed in Section 5.10.1.

- Low pH environment of LCFG concrete around 10 compared to OPC concrete means chloride threshold limit for the initiation of corrosion in LCFG concrete may be different than OPC concrete. Chloride threshold criteria developed for LCFG concrete is detailed in Table 5.23 and its basis in Section 5.12.2.

7.8.1 Passivation

- Formation of passive oxide film in OPC concrete requires about 7 days to form under high alkaline conditions, whereas heat curing scenarios of shorter duration up to 24 hours in case of LCFG concrete and depleting alkaline conditions during its hardening process need further research as to the formation of adequate level oxide passive film on embedded steel surface. Silicate passivation findings of this research showed that - in order to drive the benefit of silicate passivation effect, it requires the formation of oxide film beneath first. Test outputs of this research was in concurrence with (Ovchiyan, 2003) findings.

7.9 Electrochemical Responses

- Electrochemical testing techniques' outputs used in this research indicated that LCFG concrete has lower resistivity, higher negative half- cell potential (HCP) vs. standard copper sulphate electrode (CSE) and higher HCP vs. silver chloride standard electrode measured with Galvanostatic Pulse Measurement (GPM). These electrochemical techniques test outputs revealed that active corrosion of embedded steel in LCFG concrete is quicker than OPC concrete in severe exposure and supported the investigated properties such as high porosity transmitting moisture to the interior, low pH and high carbonation as detailed above.

- Based on the HCP vs. CSE measurements over this research duration and limited HCP vs. CSE observations available in the literature from other researches on fly ash based geopolymer concrete of approximately similar mix proportions and curing regimes revealed that different HCP criteria for LCFG concrete may be probable compared to OPC concrete. Possible HCP criteria for LCFG concrete is detailed in Table 5.17 and its basis in Section 5.11.2.4.

7.9.1 Galvanostatic Pulse Measurement (Electrochemical Technique)

- Electrochemical tests revealed that GPM technique, which is relatively a new technique to measure the corrosion rate of embedded steel in OPC concrete on the basis of Linear Polarisation Resistance theory (Stern Grey equation) is not appropriate for measuring corrosion rate of embedded steel in LCFG concrete.

Possible reason for the inability of GPM technique for LCFG concrete may be due to the high impedance of corrosion interface transition zone (ITZ) between surface of the rebar and complete sodium silicate layer, which is supposed to be formed during the casting and curing stages of LCFG concrete. This needs further research.

7.10 Compressive Strength and its Degradation under Severe Exposure

- LCFG concrete mix in this research with mix proportions parameters as detailed in Table 4.4 achieved mean compressive strength 54 to 55 MPa with steam curing regime of 24 hours at 60 ^{o}C. This confirmed the compressive strength trend, Hardjito and Rangan (2005) have observed in their research study. Results indicated that repeatable mix with low calcium fly ash binder material from a particular source are feasible, provided mix proportions parameters and curing regimes are followed. However the strength degradation under severe exposure was in the order of 35% for both G40 &G50 while the strength reduction for S40 was 9% and 16% for S50 as discussed in Section 5.2.1.

7.11 Source Material & Alkaline Solution Composition Synthesis Analysis

- Mix formulation in this was using alkaline solution comprising of A53 Grade Sodium Silicate solution of modulus 2 and NaOH solution of molarity 8M for G40 laboratory samples & specimens and 14M for G50 samples & specimens. NAOH solution of 14M molarity resulted H_2O/Na_2O mix molar ratios less than 10 and have workability issue unless additional water is used. This observation was in line with Hardjito and Rangan (2005) study which also indicated the need of additional water from workability requirement. The addition of extra water will either lower the molarity of NAOH or impact modulus of commercial available Sodium Silicate solution or both used in the mix formulation from their specification point of view.

- Formulation synthesis analysis further revealed that combined modulus of alkaline solution has bearing on the workability of the mix. That is, a use of NaOH solution of molarity 16M will result combined modulus of alkaline solution close to 1 when mixed with Sodium Silicate solution of modulus 2. This will result unworkable mix with water/geopolymer solid binder ratio of less than 0.18 provided source material chemical composition more or less stay unchanged. This shows that commercially available sodium silicate solution of higher modulus than 2 will need to be used if NaOH solution of 14M or higher is to be applied for alkaline solution formation. NaOH solution of low molarity than 12M will result LCFG concrete with high porosity, undesirable from durability perspective under severe exposure.

- Also synthesis analysis of mix formulation indicated that variation of source material composition even from one source (for instance in this research was from Collie Power Station, Western Australia) influences the eventual microstructure formation for LCFG concrete. Analysis of fly ash main components data used over the past 7 years in previous research studies indicated the possible range of SiO_2/Al_2O_3 mix molar ratio could range between 3.2 - 3.9, while suggested minimum value in the literature is 3.5 (Davidovits, 1982). Minimum SiO_2/Al_2O_3 mix molar from fly ash source material with high aluminate content can be down to 3, as such suggested literature value of SiO_2/Al_2O_3 mix molar can be between 3 - 4.5 instead of 3.5 - 4.5.

7.12 Blended LCFG Concrete

- Due to heat sensitive curing requirements of LCFG concrete, blended LCFG concrete mix with 5% and 10% slag showed higher compressive strength results under ambient curing conditions over a short period of 5 days. The blended LCFG concrete higher compressive strength properties for steam and ambient curing regimes was in concurrence with Skvara et al (2006) findings for slag mixed fly ash based geopolymer.

- Blended LCFG concrete cylinder specimens from these both mixes showed improved residual compressive strength after a one year exposure to seawater with no noticeable change in mass.

- Blended LCFG concrete maintained the better pH value (between 10.5 to 11) after one year exposure to seawater compared to LCFG concrete samples under severe exposure.

- Mix with 20% slag content showed early setting even with additional water. Possible reasoning for this early setting is detailed in Section 5.12.1.2.

- Blended LCFG concrete potential on the basis of its short term durable properties to withstand the aggressive exposure scenarios is better than LCFG concrete and need further research for its long term durable properties.

CHAPTER 8 FUTURE RESEARCH AVENUES

8 RECOMMENDATIONS AND CONCLUDING REMARK

Because of sustainable potential of blended LCFG concrete and LCFG concrete, significant environmental benefit will be seen even with low risk applications. Such low risk applications will be instrumental for the ongoing improvement of this environmentally friendly material. Following research opportunities will enhance the level of confidence for their adoption by the construction industries.

8.1 FUTURE RESEARCH OPPORTUNITIES

Following future research opportunities can be of consideration.

- Further research needs to be conducted to confirm the strength loss trend over long term and as well the deterioration mechanisms involved in this research.
- Establish elemental composition tolerances of available low calcium fly ash source material, which could be from different sources once the commercial viability of LCFG concrete increased for possible various applications.
- Combined modulus of commercially available sodium silicate solution of different modulus & NaOH of different molarity from practicality, quality assurance and long term durability perspectives responsive to elemental composition of the source material.
- Chloride penetration & carbonation responsible for corrosion status of steel bar in geopolymer concrete would need further work to confirm findings of this research.
- Long term impacts of LCFG concrete low pH and its possible future improvements with slag proportion may need refinement for long term durable properties under environmental actions of blended LCFG concrete.
- Primary and secondary carbonation products' identification and their impacts on long term durability of LCFG concrete.
- Quantification of chemical compounds, responsible for high level of scaling of LCFG concrete in exposed zone and from environmental scenarios' selection perspective.
- Identification of any other reasons, why Linear Polarisation Resistance measurement technique (GPM) is not appropriate for corrosion rate measurements of embedded steel in LCFG concrete.
- Research study on the limitations of mathematical model based on Flick's Second Law of diffusion for LCFG concrete exposed to severe environments.
- Investigate its potential for flexible and rigid road pavements.

REFERENCES

ACI Committee 116R-00, "Cement and Concrete Terminology," *Manual of Concrete Practice*, Part1; American Concrete Institute, P.O. Box 9094, Farmington Hills, MI, 2003.

ACI Committee 222, 222R-96, 1996. Corrosion of Metal in Concrete.

ADAA Statistics Page [Internet]. Wollongong: Ash Development Association of Australia; 2009 [updated 2009 October 15; cited 2010 May 20]. Available from:http://www.adaa.asn.au/statistics.htm

Adam, AA, Molyneaux, TK, Patnaikuni, I & Law, DW 2009, 'Chloride penetration and carbonation in blended OPC-GGBS, alkali-activated slag, and fly ash-based geopolymer concrete', Concrete Institute of Australia conference, 24th, 2009, Sydney, New South Wales, Australia, Concrete Institute of Australia, Sydney, NSW, paper 3c-3.

Aldred, J.M., 2008. ' Water Transport due to Wick Action through Concrete', PhD Thesis, Curtin University of Technology, Western Australia.

Aldridge, L.P., Fernado, K., Costa, M. and Ray, A 2008. "Comparison of Durability Measures of Concrete as Function of Cure Times", CIA Vol 36 Issue 4.

Alonso S, Palomo A. Alkaline activation of metakaolin and calcium hydroxide mixtures: influence of temperature, activator concentration and solids ratio. Materials Letters. 2001; 47(1-2):55-62.

Andrew- Phaedonos.F, 2001. "Volume of Permeable Voids (VPV)- Ensuring the Durability performance of Structural Concrete, CIA June –August 2001.

Andrew- Phaedonos.F., Shyan, A. and Xu, A. 2007. " Extending the Service Life of Concrete Bridges- Corrosion Monitoring of Lynch's Bridge over Maribyrnong River" CIA–Vol 37 Issue 2.

Andrew- Phaedonos.F., 2008. " Test Methods for Assessing Durability", CIA June –Vol 34 Issue 4.

Andrew- Phaedonos.F., 2012. Reducing the Carbon footprint- The Vic Roads Experience, CIA Vol 38 Issue 1

Arup, H., (1983), " The Mechanism of Penetration of Steel by Concrete", Corrosion of Reinforcement in Concrete, Ellis Horwood Ltd, pp, 151-157.

Arredondo-Rea, S.P., Correl- Higuera, R, Nerri-Flores, M.A., Gomez-Soberon, J.M., Almeraya-Calderon, F., Castorena-Gonzalez, J.H., Almaral-Sanchez, J.L.2011. " Electrochemical Corrosion and Electrical Resistivity of Reinforced Recycled Aggregate Concrete" Int J. Electrochemical Sci., 6(2011) 475-483.

ASTM, *C876-91: Standard Test Method for Half-cell Potentials of Uncoated Reinforcing Steel in Concrete*, 1999, pages 446 to 451.

ASTM Standards: C642 Standards test method for density, absorption and voids in hardened concrete.
ASTM Standards: C 1556 Test method for apparent chloride diffusion of cementitious mixture.

ASTM Standards: C 114 Test method for chloride profile of cementitious mixture.

ASTM Standards: C1202 Test method for the electrical indication of concrete's ability to resist chloride ion penetration.

Asrar, N., Malik, A.U., Ahmed, S., 1998 "Technical Report No. TR 3804/EVP95013.

Anesley, D., Porteous, M.and Zhang, D., 2003, ' Coal Ash: A review of Legislation and Regulations within Australia.

Australian Standards, 2009, Concrete Structures, AS3600-2009, Standards Australia, Australia

Australian Standards, 2001, Concrete structures for retaining liquids, AS3735-2001, Standards Australia, Australia

Australian Standards, 2009, Piling- Design & installation -AS2159-2009, Standards Australia, Australia

Australian Standards, 2009, Bridge- Design–AS5100, Standards Australia, Australia

Australian Standards, 2001, Concrete structures for retaining liquids, AS3735-2001, Standards Australia, Australia

Australian Standards, 1999, Determination of water absorption and apparent volume of permeable voids in hardened concrete, AS1012.21, Standards Australia, Australia

AS 1289, 4.3.1 "Method of testing soils for engineering purpose. Method 4.3.1: Soils chemical tests – determination of pH value of soil – Electrometric method".

Australian Standards, 1974, Pre-cast reinforced concrete box culverts, AS 1597.1-1974, Standards Australia, Australia

Azad, Abul K.1999, "Chloride Diffusion in Concrete and its Impact on Corrosion of Reinforcement". King Fahd University of Petroleum and Minerals, Dhahran, Saudi Arabia.

Baessler, R., Burket, A., Frolund, T., Klighoffer, O. " Usage of Portable Equipment for Determination of Corrosion Stage of Concrete Structures", Federal institute for Materials Research and Testing (BAM), D-12200 Berlin/Germany, Force Institute, DK-2605 Brondby/Denmark.

Bakharev, T. 2005. Resistance of geopolymer material to acid attack. *Cement & Concrete Research* 35(4): 658-670.

Bakri, A.M. Mustafa Al, Kamarudin, H., Bnhussain, M., Khairul Nizar, I., Rafiza, A. R. and Zarina, Y. 2011**, "**The Processing, Characterization, and Properties of Fly Ash Based Geopolymer Concrete", Rev.Adv.Mater. Sci. 30 (2012) 90-97.

Barbosa, V. F. F., K. J. D. MacKenzie, C. Thaumaturgo. (2000). "Synthesis and Characterisation of Materials Based on Inorganic Polymers of Alumina and Silica: Sodium Polysialate Polymers." International Journal of Inorganic Materials 2(4): 309-317.

Bell, A.T. (1999), "NMR applied to zeolite synthesis", Colloids and Surfaces, 158, 221-234.

Bergna, H.E., Roberts, W.O., 2006 " Colloidal Silica", Taylor and Francis Group.

Bernal, SA, Mejia de Gutierrez, R, Pedraza, AL, Provis, JL, Rodriguez, ED & Delvasto, S 2011, 'Effect of binder content on the performance of alkali-activated slag concretes', *Cement and Concrete Research*, vol.41, no.1, pp.1-8.

Bernal, SA, Provis, JL, Brice, DG, Kilcullen, A, Duxson, P & van Deventer, JSJ 2012, 'Accelerated carbonation testing of alkai-activated binders significantly underestimates service life: the role of pore solution chemistry', *Cement and Concrete Research*, vol.42, pp.1317-26.

Bertolini, L. and Polder, R.B.1997. "Concrete Resistivity and Corrosion Rate as a Function of temperature and Humidity of the Environment" TNO Report 97-BT-R0574, pp 85.

Broomfield, John P. 2007. "2nd Edition Corrosion of Steel in Concrete", Taylor and Francis Group.

Browne, R.D. 1982, "Design Prediction of the Life for Reinforced Concrete in Marine and other Chloride Environment", Durability of Bldg. Materials (Amsterdam), No 1, pp 113-125

Browne, R.D. and Geoghegan, M.P.1985, " Mechanism of Corrosion of Steel in Concrete in Relation to Design, Inspection and Repair of Offshore and Coastal structures", Performance of Concrete in Marine environment, ACI SP -65, American Concrete Institute, pp 169-204 BS1881:Part 124:1988

Brough, AR & Atkinson, A 2002, 'Sodium silicate-based, alkali-activated slag mortars: part 1: strength, hydration and microstructure', Cement and Concrete Research, vol.32, pp.865-79.

Buenfeld, N.R., Shurafa-Dauoudi M.T. and McLoughlin, I.L (1997) "Chloride Transport due to Wick Action in Concrete". In "Chloride penetration into concrete" Nilsson, L.O and Oliver, J.P. eds (RILEM, Paris) 1997, pp. 315-324

Carroll, John J. and Mather, Alan E. 1992, "The System Carbon Dioxide-Water and the Krichevsky-Kasarnovsky Equation," Journal of Solution Chemistry, vol. 21, pp. 607-621, 1992.

Cheema, D.S., Lloyd, NA., & Rangan, BV., 2008. Durability of Geopolymer Concrete Box Culverts-A Green Alternative, 34th Conference on Our World in Concrete and Structure 09, Singapore.

Cheema, D.S., 20011. Durability of Steel in Geopolymer Concrete", 18th International Corrosion Conference, Perth, Australia.

Cheema, D.S., Lloyd, NA., & Rangan, BV., 2012. "Geopolymer Concrete Sustainability Potential" presented as Poster Paper, The Twelfth International Conference on Recent Advances in Concrete Technology and Sustainability Issues 2012- Prague, Czech Republic.

Cheema, D.S., 2012. "Low Calcium Fly ash Geopolymer Concrete – A Promising Sustainable Alternative for Rigid Concrete Road Furniture", 25th ARRB Conference- Shaping the future: Linking policy, research and outcomes, Perth, Australia 2012

Cheema, D.S., 2012. "Fly Ash – A Greener Construction Material Alternative", International Conference on Advancements in Mechanical and Materials Engineering (AFTMME-2012), Punjab Technical University, Kapurthala Jallandhar, India. Peer Reviewed Paper Presented.

Cheema, D.S. and Lloyd, NA., 2013. 'Low Calcium Fly Ash Geopolymer Concrete Sustainability and Durability Potential', First International Conference on concrete Sustainability, 27-29May, Tokyo, Japan.

Cheema, D.S. and Lloyd, NA., 2014. Blended Low Calcium Fly Ash Gepolymer Concrete - Environment Friendly Construction Material, International Conference on Geological and Civil Engineering, Macau. IPVBEE vol, 62(2014) IACSIT Press, Singapore. DOI: 10.7763/IPCBEE.2014. V62.13.

Cheema, D.S., 2008. Materials Engineering, MRWA, Technical Report No 2008-12M

Chindaprasirt P, Jaturapitakkul C, Chalee W, Rattanasak U (2009). Comparative Study on the Characteristic of Fly Ash and Bottom Ash Geopolymer. Waste Management., pp. 539-543.

Cement Concrete & Aggregate Australia (2009). Chloride Resistance of Concrete,

CIA (2001) Recommended Practice - Performance Criteria for Concrete in Marine Environments.
CIA (2011) Recommended Practice – Geopolymer Concrete (Z16)

Collepardi, M., Marcialis, A. and Turriziani, R. 1972, "Penetration of Chloride Ions into Concrete", J. Am. Ceramic Soc., Vol. 55, No. 10, pp 16-21

Crank,J., 1975, The Mathematics of Diffusion, 2nd Edition., Oxford University Press.

CRC Handbook of Chemistry and Physics, 76th Edition (1995-1996)

Daimond, S., 1986. ‘ The microstructure of cement paste in concrete’, Proc, 8th ICCC, P122-147 Re de Janderio, 1986.

Davidovits, J. (1982). Mineral Polymers and Methods of Making Them. United States Patent: 4,349,386. USA.

Davidovits, J. 1988. Geopolymer chemistry and properties. *In World Congress of Geopolymer 1988.* Davidovits, J. (ed). Institute of Geopolymer, Saint Quentin, France.

Davidovits, J. (1991). "Geopolymers: Inorganic Polymeric New Materials." Journal of Thermal Analysis 37: 1633-1656.

Davidovits, J. 1994. Properties of Geopolymer Cements. First International Conference on Alkaline Cement and Concretes, Kiev, Ukraine, 1994, SRIBM, Kiev State Technical University.

Davidovits, J. 1994. High alkali cements for 21st century concretes. In Concrete Technology, Past, Present and Future. Proceedings of V Mohan Malhotra Symposium. Mehta, K. (ed.). ACI SP.

Davidovits, J. (1994c). Global Warming Impact on the Cement and Aggregates Industries. World Resource Review, 6(2), 263-278.

Davidovits, J. 1999, ‘Chemistry of Geopolymeric Systems, Terminology. Geopolymer ‘99 International Conference, France.

Davidovits, J. 2002, ‘Environmentally Driven Geopolymer Cement Application’, Geopolymer Conference, Melbourne.

Davidovits, J 2002, ‘30 years of successes and failures in geopolymer applications: market trends and potential breakthroughs’, *Geopolymer 2002: international geopolymer conference, Melbourne, Australia*, in G Lukey (ed), *Geopolymer 2002 : turn potential into profit*, Geopolymer Institute, Saint-Quentin, France.

Davidovits J. 2008, “Geopolymer Chemistry & Applications. Saint-Quentin: Institute Geopolymer; 2008.

Diaz EI, Allouche EN, Eklund S. Factors affecting the suitability of fly ash as source material for geopolymers. Fuel. 2010; 89(5):992-996.

Duxson, P, Lukey, GC, Separovic, F & van Deventer, JSJ 2005, ‘Effect of alkali cations on aluminium incorporation in geopolymeric gels’, Industrial & Engineering Chemical Research, vol.44, no.4, pp.832-9.

Duxson, P, Fernandez-Jimenez, A, Provis, JL, Lukey, GC, Palomo, A & van Deventer, JSJ 2007d, ‘Geopolymer technology: the current state of the art’, *Journal of Materials Science*, vol.42, pp.2917-33.

Erlin, B., and Jana, D., Forces of Hydration that can Cause Havoc to Concrete – May the force not be with you, Concrete International, pp 51-57, November 2003.

Espinosa, R.M. and Franke, L.(2006) ‘ Inkbottle Pore Method: Prediction of hygroscopic water content in hardened cement paste at variable climatic conditions’, Cement and Concrete Research, 36(2006) 1956-1970.

Eur Ing R. L and Davies, K.G 1981, “ Cathodic Protection” DTI Publication.

Fawer, M., Concannon, M., Rieber, W. (1999). "Life Cycle Inventories for the Production of Sodium Silicates." International Journal of Life Cycle Assessment 4(4), 207-212.

Fernández-Jiménez A, Palomo A. Characterisation of fly ashes. Potential reactivity as alkaline cements. Fuel. 2003; 82(18):2259-2265.

Fernandez-Jimenez, A. & Palomo, A. 2005. Composition and microstructure of alkali-activated fly ash binder: effect of the activator. *Cement & Concrete Research* 35: 1984-1992.

Fernandez-Jimenez A, Palomo A, Criado M. Microstructure development of alkali-activatedfly ash cement: a descriptive model. Cement and Concrete Research. 2005[cited February 19, 2007]; 35(6):1204-1209.

Fernandez-Jimenez, A., A. Palomo, *et al.* 2006. Engineering properties of alkali-activated fly ash concrete. *ACI Materials Journal* 103: 106-112.

Fernández-Jiménez, A. and A. Palomo (2003). "Characterisation of Fly Ash: Potential Reactivity as Alkaline Cements." Fuel 82(18): 2259-2265.

Gamry, *Fundamentals of electrochemical impedance spectroscopy*, www.gamry.com/App_Notes/EIS_Primer/EIS_Primer.htm, 2005.

General Corrosion Corporation, Minneapolis, MN "Corrosion and Cathodic Protection"

Gould, E.S. Inorganic reactions and Structures; Henry Holt & Company: New York, 1957.

Gjorv, O.E. and Vennesland, O. 1979, "Diffusion of chlorides from Sea Water into Concrete", Cement & Concrete Res., Vol. 9, No. 2, pp. 229-238

Gourley, J. T. (2003). *Geopolymers; Opportunities for Environmentally Friendly Construction Materials.* Paper presented at the Materials 2003 Conference: Adaptive Materials for a Modern Society, Sydney.

Greenwood, Norman N.; Earnshaw, A. (1997), *Chemistry of the Elements* (2nd ed.), Oxford: Butterworth-Heinemann, ISBN 0080379419.)

Green,W., Riordan, G, Richardson, G., Marrosszeky, A.2010, " Durability Assessment, Design and Planning- Port Botany Expansion Project" CIA Vol 36 Issue 3.

Gu, Ping., and Beaudoin, J.J. 1998. Obtaining Effective Half-Cell Potential Measurements in Reinforced Concrete Structures, Institute for Research Construction, National Research Council of Canada.

Habert, G, d'Espinose de Lacaillerie, JB & Roussel, N 2011, 'An environmental evaluation of geopolymer-based concrete production: reviewing current research trends', *Journal of Cleaner Production*, vol.19, pp.1229-38.

Hall, C. and Hoff, W.D. (2002) " Water Transport in Brick, Stone & Concrete", Taylor and Francis, London 2002.

Hamada, M. (1968). "Neutralisation (carbonation) of Concrete and Corrosion of Reinforcing Steel" Paper presented at Fifth International Symposium on the Chemistry of Cement, Tokyo, 1968, Vol.III, pp 343-369

Hansson, C.M. and Sorensen, B., 1990' The Threshold Concentration of Chloride for the Initiation of Reinforcement Corrosion" ASTM Special Tech. Publ. 1065, Aug., pp3-16

Hansson, C.M., Poursaee, A. and Jaffar, S.J. 2007. Corrosion Reinforcing Bars in Concrete. PCA R&D Seriel No 3013

Hansson,C.M., Frolund, T.H and Markussen, J.B.(1985), "Effect of Chloride Cation Type on the Corrosion of Steel in Concrete by Chloride Salts", Cement and Concrete Res., Vol 15, No.1, pp 65-72.

Hardijito, D. and Rangan, BV 2005, 'Development and Properties of Low Calcium FlyAsh- Based Geopolymer Concrete, Research Report GC1, Faculty of Engineering, Curtin University of Technology, Perth, Australia .

Hime, William *et al.* "Salt Hydration Distress," *Concrete International*, V. 23, pp. 43-50, October 2001.

Hong, F., Tie-jun, Z and Whittman, F.H.(2006), "Carbonation and Chloride Profiles of Reinforced Concrete after 26 Years of Exposure", International Conference on Pozzolan, Concrete and Geopolymer, Khan Kaen, Thailand, May 24-25.

Hussaian, S.E., Al-Gahtani, Al-Gahtani, A.S. and Rasheeduzzafar, 1996 "Chloride Threshold for Corrosion of Reinforcement in Concrete", ACI Materials J., Vol 93, No. 6, Nov-Dec., pp534-538

Hussaian, R.R. and Ishida, T. 2009. "Critical Carbonation Depth for Initiation of Steel Corrosion in Fully Carbonated Concrete and Development of Electrochemical Carbonation Induced Corrosion Model," Int Electrochemical Sc1., 4, pp 1178-1195.

Jana, Dipayan. 2007. " Concrete Scaling – A Critical Review" Proceedings of the Twenty-Ninth Conference on Cement Microscopy Quebec City PQ, Canada, May 20 -24, 2007.

Jo B-W, Park S-K, Park M-S. Strength and hardening characteristics of activated flyash mortars. Magazine of Concrete Research. 2007; 59(2):121-129.

Juanto, S., Zerbino, J.O., Miguez, M.I., Vilche, J.R., and Arvia, A.J., *Ellipsometry of polycrystalline iron electrodes in alkaline solutions containing chloride ions under different electrochemical conditions*, Electrochemical Action, 32(12), 1987, pp1743-1749.

Jumikis., A. R., 1967 ' Introduction to soil Mechanics' D Van Nostrand Company Ltd London.

Klinghoffer, O.; Rislund, E.; Frølund, T.;Elsener, B.; Schiegg, Y.; Böhni, H.:
Assessment of Reinforcement Corrosion by Galvanostatic Pulse Technique, Proc. Int.Conf. on Repair of Concrete Strictures, Svolvaer, Norway, 1997 pp 391 – 400

Kong, D.,Sanjayan, J.G.(2010) " Effect of elevated temperatures on Geopolymer past, mortar and concrete", Cement and Concrete Research, 40(2)(2010, pp.334-339.

Koulombi, N., Batis, G., and Malami, C.H. 1993. "Progress in Understanding and Prevention, Mercer AD editors, Institute of Materials, Spain: 619

Kumar, A. and Roy, D.M., Proc. 8th Intl. Congr. Chemistry of Cement, Brazil, V.V, 73-79 (1986).

Lehraman, L. (1964) 'Journal of the American Water Works Association'. 56(8), 1009.

Li, S and Roy,D.M.,1986, ' Investigation of relations between porosity, pore structure and Cl diffusion of Fly Ash and Blended Cement pastes', Cem. Concr. Res.16, 749-759.

Main Roads WA, 1998, Water permeability of hardened concrete, Test method WA 625.1, Main Roads WA, Western Australia.

Main Roads WA, 2001, Chlorides and Total Soluble salts in Soil and Water, Test method WA 910.1, Main Roads WA, Western Australia.

Maso, J.C.,1986. ' The bond between aggregates and hydrated cement paste', Proc, 8th ICCC, P1378-380 Rio de Janderio, 1986.

McCaffrey, R 2002 'Climate Change and the Cement Industry' Global Cement and Lime Magazine (Environmental Special Issue), pp. 15-19.

Millard. S and Saddowski, L., 2009. "Novel method for linear polarisation resistance corrosion measurement" NDTCE'09 Non-Destructive Testing in Civil Engineering Nantes, France, June 30th – July 3rd.

Marchand, J., Sellevold, E. J., and Pigeon, M.1994 “The Deicer Salt Scaling Deterioration of Concrete – An Overview,” *Durability of Concrete*, American Concrete Institute, SP 145-1, pp. 1-46, 1994.

Marcotte, T. D. and Hansson, C. M.1998, *A Comparison of the Chloride-Induced Corrosion Products from Steel-Reinforced Industrial Standard versus High Performance Concrete exposed to Simulated Sea Water, International Symposium on High Performance and Reactive Powder Concretes*, 1998, University of Sherbrooke, Sherbrooke, Canada.

Marcotte, T.D and Hansson, C.M. 2003. The influence of Silica Fume on the Corrosion Resistance of Steel in High Performance of Concrete exposed to Simulated Sea Water, J. Materials Science, 2003, 38, pp 4765-4776.

Mather, B. 2004. Concrete durability. *Cement & Concrete Composites* 26: 3-4.

Mario, C. Uy. Understanding Corrosion. Technical Publication, WET,USA.

Marchand, J., Sellevold, E. J., and Pigeon, M. “The Deicer Salt Scaling Deterioration of Concrete –An Overview,” *Durability of Concrete*, American Concrete Institute, SP 145-1, pp. 1-46, 1994.

McLellan, BC, Williams, RP, Lay, J, Van Riessen, A & Corder, GD 2011, ‘Costs and carbon emissions for geopolymer pastes in comparison to ordinary OPC’, Journal of Cleaner Production, vol.19, pp.1080-90.

Mehta, P.M. & Monteiro, P.J.M. 2006. *Concrete, Microstructure, Properties and Material*. Sydney: McGraw-Hill.

Mehta, P. K. (2001). "Reducing the Environmental Impact of Concrete." ACI Concrete International 23(10): 61-66.

Mehta, P. K. (2002). "Greening of the Concrete Industry for Sustainable Development." ACI Concrete International 24(7): 23-28.

Mehta, P.K. & Manmohan, D 1980 Proc. 6th Int. Congr. Chemistry of Cement, Vol. III,Theme VII, 1-5 Editions Setma, Paris

Meyer, C. (2009). “The greening of the concrete industry” Cement and Concrete Composites, 31(8), 2009, pp601-605

Meyer, A. (1968). “Investigation on the Carbonation of Concrete”, Fifth International Symposium on the Chemistry of Cement, Tokyo, 1968, Vol.III, pp 394-401

Midgley, HG. and Illston, J.M.(1984), “The penetration of Chlorides into Hardened Cement Pastes” Cement and Concrete Res., Vol 14, pp 546-558.

Michael, D.A., Thomas, Phil B. Bamforth, 1999 “Modelling Chloride Diffusion in Concrete Effect of Fly Ash and Slag”, Cement and Concrete Research, 29, 1999, pp487-495.

Mukin,V., Radhe Khatri and Ion Dumitru (2007)- some Limitation of Geopolymer Concrete, The 23rd Biennial Conference of the Concrete Institute of Australia.

Murphy, O.J., *Spectroscopic characterization of the passive film on iron before and after exposure to chloride ion*, in Electrochemistry in transition, ed. Murphy, O.J., et al., Plenum Press, New York, 1992, pp521-545

Nagayama, M., and Cohen, M., *The anodic oxidation of iron in a neutral solution I. The nature and composition of the passive film*, Journal of the Electrochemical Society, 109, 1962, pp781-790.

Nielsen, A., *Concrete Durability (in Danish), The Concrete Book (Beton Bogen)*, A.D. Herholdt, et al., Editors, 1985, Aalborg Portland.

Neville, A.M. 1995. *Properties of Concrete*. Essex: Longman.

Nillson, L.O.(1993), "Penetration of chloride into concrete- an introduction and some definitions". A paper presented in Nordic Mini-seminar on Chloride Penetration in Concrete Structure, Department of Building Materials, Chalmers University of Technology, Sweden.

Nillson, L.O. and Tang, L.(1996), ' Transport Mechanisms in Porous Materials', The modelling of microstructure and its potential for study transport pproperties and durability, Kulwer Academic, Netherlands, 289-311.

Nordtest Method NT Build 443, "Accelerated Chloride Penetration in Hardened Concrete".

Nyame, B.K., and Illston, J.M., 1980. Proc. 6th Intl. Congr. Chem.Cement, Brazil,V.III, Theme VI, 181-185, Editions Septima, Paris(1980)

Olivia., M., 2011, 'Durability Related Properties of Low Calcium Fly Ash Based Geopolymer Concrete' PhD Thesis, Curtin University Western Australia.

Olivia M, Nikraz H Wang P, Zhong S, editors. Corrosion of low calcium fly ash geopolymer concrete: a preliminary analysis. 6th Asian Symposium on Polymers in Concrete; 2009; Shanghai: Tongji University Press.

Ovchiyan,V.N., 2003 Applied Electrochemistry and Corrosion Protection of Metals - On Passivating Action of Silicate-Alkaline Solutions on Metals

Page, C.L., Treadaway, K.W.J., *Aspects of the electrochemistry of steel in concrete*, Nature, 297, 1982. pp109-115.

Palomo, A., Grutzeck, M.W. & Blanco, M.T. 1999. Alkali-activated fly ashes. A cement for the future. *Cement & Concrete Research* 29: 1323-1329.

Palomo, A, Blanco-Varela, MT, Granizo, ML, Puertas, F, Vazquez, T & Grutzeck, MW 1999b, 'Chemical stability of cementitious materials based on metakaolin', Cement and Concrete Research, vol.29, pp.997-1004.

Patrick J. Tyson 2010, The Kinetic Atmosphere, Water Molecules.

Polder,R**.,** Andrade,C., Elsener, B. Nennesland,O.E., Gulikers, J., Weidert, R., Raupach, M. 2000. Materials and Structures, 33(2000) 603.

Pourbaix, M., Atlas of Electrochemical Equilibria in Aqueous Solutions, 2nd English Edn.,Translated by Franklin, J.A., NACE, Houston, 1974.

Poursaee, A., Hansson, C.M. Reinforcing Steel Passivation in Mortar and Pore Solution. Cement and Concrete Research.

Provis, JL & van Deventer, JSJ 2010, 'What controls the durability of geopolymer binders and concretes?', *Sixth international conference on concrete under severe conditions: environment and loading*, Taylor & Francis, London, UK, pp.1535-43.

Rangan, B.V. 2007. Low calcium fly ash based geopolymer concrete. *Chapter 26 in Concrete Construction Engineering Handbook.* Nawy, E.G. (ed.). New York: CRC Press.

Rangan, B.V. 2008. Low calcium fly ash based geopolymer concrete Research Report GC4, Faculty of Engineering, Curtin University of Technology, Perth, Australia

Rangan, B.V., Studies on fly-ash based geopolymer concrete, Malaysian construction research journal, vol 3, no. 2, 2008.

Rangan, BV 2009, 'Design and manufacture of fly-ash based geopolymer concrete' Concrete in Australia Vol 34 No 2.

Rasheeduzzafar, Dakhil, F.H. and Al-Gahtani, A.S. 1984. 'Deterioration of Concrete Structures in the Environment of Middle East", J. Am. Concrete Inst., Vol. 81, No.1, pp,13-20

Ray, N.H.(1978) Inorganic Polymers, Academic Press, London.

Rodriguez,J., Ortega,L.M. and Garcia, A.M. (1994), " Assessment of Structural Elements with Corroded Reinforcement", Corrosion and Corrosion Protection of Steel in Concrete, R.N. swamy(ed.), Sheffield Academic Press, UK, PP171-185

RIELM TC 154: Electrochemical Techniques for Measuring Metallic Corrosion

RIELM Report 12 (1995) "Performance Criteria for Concrete Durability" Ed. J. Krropp and H.K. Hilsdorf, E and F.N, Spon London.

Roy, D.M., Brown, P.W., Ski, D., Scheetz , B.E.and May,W.19993 " SHRP- C-628" Materials Research Laboratory, The Pennsylvania State University, University Park, Pennsylvania1986.

Roy, D.M., 1986. Proc. Intl. Congr. Chem.Cement, Brazil,V.I, 362-380(1986)

Rosenberg, A., Hansson, C.M., and Andrade, C. 1989. Mechanisms of Corrosion of Steel in Concrete, in The Material Science of Concrete, J. Skalny, Editor, 1989, The American Ceramic Society, pp 285-313

Sagoe-Crentsil, K & Brown, T 2006, 'Some Key Materials and Process Parameters Governing Geopolymer Binder Performance', *International Conference on Pozzolan, Concrete and Geopolymer Khon Kaen, Thailand, 2006*.

Sanjayan, J 2012, 'Non-Portland based cements and concretes', Concrete in Australia, vol.38, no.1, pp.34-9.

Shayan, A., Xu, A.2008. Evaluation of Chloride Diffusion Coefficient in Concrete by the Rapid Chloride Penetration Tests: Problems and Observation, ARRB Group, Australia

Sherman M R, McDonald D B and Pfeifer D W 'Durability Aspects of Precast Prestressed Concrete. Part 2: Chloride Permeability Study,' PCI Journal, Vol. 41, No. 4, July-Aug, 1996, pp. 76–95.

Siddiqui KS (2007), Strength and durability of low –calcium fly-ash based geopolymer concrete, Final year honours dissertation, The University of Western Australia, Perth.

Sofi M, van Deventer J, Mendis P, Lukey G. Bond performance of reinforcing bars in inorganic polymer concrete (IPC). Journal of Materials Science. 2007; 42(9):3107-3116

Sofi M, van Deventer JSJ, Mendis PA, Lukey GC. Engineering properties of inorganic polymer concretes (IPCs). Cement and Concrete Research. 2007; 37(2):251-257.

Sergi, G. and Panteli F (2011) "Erratic Properties of Portland Hardened Cement Pastes from Carbonation Variable CO_2 Concentration", Proc. Int. Symp. Cement & Concrete Materials, 7-9 November 2011, Ningbo, China, pp. 328-339.

Sergi, G., Yu, S.W. and Page, C.L.(1992), "Diffusion of Chloride and Hydroxyl in Cementitious Materiarls Exposed to Saline Environments", *Mag. Concrete Res*., No 158, pp. 63-69.

Simon, Tamas K., Vass Viktoria. 2012. Electrical Resistivity of Concrete, Concrete Structures.

Skvara,F., Lubomir Kopecky, Jiri Nemecek, Zdenek Bittnar (2006)-Microstructure of Geopolymer Materials Based on Fly , Ceramics- Silikaty 50(4)208-215(2006).

Stanish, K., Thomas, M 2003 “The use of Bulk Diffusion Tests to Establish Time Dependant Concrete Chloride Diffusion Coefficients”, Cement and Concrete Research, 33, 2003 pp55-62.

Stengel, T, Reger, J & Heinz, D 2009, ‘Life cycle cost assessment of geopolymer concrete: what is the environmental benefit?’ Concrete Institute of Australia conference, 24th, 2009, Sydney, New South Wales, Concrete Institute of Australia, Sydney, NSW, paper 6a-4.

Stern, M and Geary, A.L.(1957), “ Electrochemical polarisation. I.A theoretical analysis of the shape of polarisation curves” J. Electrochem.Soc., 104:56-63

Steveson, M & Sagoe-Crentsil, K 2005a, ‘Relationships between composition, structure and strength of inorganic polymers: part 1: metakaoloin-derived inorganic polymers’, Journal of Materials Science, vol.40, pp.2023-36.

Steveson, M & Sagoe-Crentsil, K 2005b, ‘Relationships between composition, structure and strength of inorganic polymers: part 2: fly ash-derived inorganic polymers’, *Journal of Materials Science*, vol.40, pp.4247-59.

TN 024- Concrete and Moisture Sensetive Coverings, BCRC.

Tuutti, K. 1982. Corrosion of steel in concrete. CBI Research No 4.62.

Tullmin, M., 2001. Linear Polarisation Resistance, Corrosion- Club, http://www.corrosion-club.com/lpr.htm

Temuujin J, Williams RP, van Riessen A. Effect of mechanical activation of fly ash on the properties of geopolymer cured at ambient temperature. Journal of Materials Processing Technology. 2009; 209(12-13):5276-5280.

Unger,K.D., 1979, *Porous Silica*; J. Chromatogr. Liberary: Elesevier: Arsterdam, Neatherlands, p.16.

Van Deventer J, Provis J, Duxson P and Lukely ,G.C.(2007). Reaction mechanisms in the geopolymeric conversion of organic waste to useful products. Journal of Hazardous Materials A139, pp 506-513.

Van Deventer J, Provis J, Duxson P, Brice D. Chemical Research and Climate Changeas Drivers in the Commercial Adoption of Alkali Activated Materials. Waste and Biomass Valorization. 2010; 1(1):145-155.

Van Deventer, JSJ, Provis, JL & Duxson, P 2012, ‘Technical and commercial progress in the adoption of geopolymer cement’, *Minerals Engineering*, vol.29, pp.89–104.

Van Jaarsveld, J. G. S., J. S. J. van Deventer, L. Lorenzen (1997). "The Potential Use of Geopolymeric Materials to Immobilise Toxic Metals: Part I. Theory and Applications." Minerals Engineering 10(7): 659-669.

Van Jaarsveld, JGS & van Deventer, JSJ 1999a, ‘Effect of the alkali metal activator on the properties of fly ash-based geopolymers’, Industrial & Engineering Chemistry Research, vol.38, no.10, pp.3932-41.

Van Jaarsveld, J.G.S, van Deventer, J.S.J. & Lukey, G.C. 2002. The effect of composition and temperature on the properties of fly ash and kaolinite based geopolymers. *Chemical Engineering Journal* 89: 63-73.

Van Jaarsveld, J.G.S, van Deventer, J.S.J. & Lukey, G.C. 2003. The characterisation of source materials in fly ash-based geopolymers. *Material Letters2003* 57(7) : 1272-1280.

Vimal Kumar, Gulab singh, Rajendra Rai, 2005, Fly Ash India- Fly Ash Utilization Programme (FAUP), TIFAC, DST, New Delhi – 110016

Wallah, SE and Rangan, BV, 2006, 'Low Calcium Fly Ash-Based Geopolymer Concrete: Long-Term Properties', Research Report GC2, Faculty of Engineering. Curtin University of Technology, Perth, Australia.

Wenner, F. (1912) "A method of measuring earth resistivity", Bulletin of the Bureau of Standards, Vol. 12, 1912, pp.469-478.

West, R.E. and Hime, W.G. (1985) " Chloride Profiles in Salty Concrete" National association of Corrosion Engineers, July, pp, 29-35.

Yang, T., Yao, X., et al., "Mechanical property and structure of alkali-activated fly ash and slag blends", Journal of Sustainable Cement-Based Materials, 1(4), 2012, pp 167–178.

Zehang, Z, Wang, H, Provis, JL and Reid, A. (2013) "Efflorescence: A Critical Challenge for Geopolymer Applications?" Understanding Concrete, Concrete 2013, Gold Coast, QL,Australia.

APPENDIX- A

LOCATION OF FIELD & LABORATORY SIMULATED SEVERE MODELS

AND

ANNUAL AVERAGE RELATIVE HUMIDITY

Location of Field Severe Model & Simulated Severe Laboratory Model

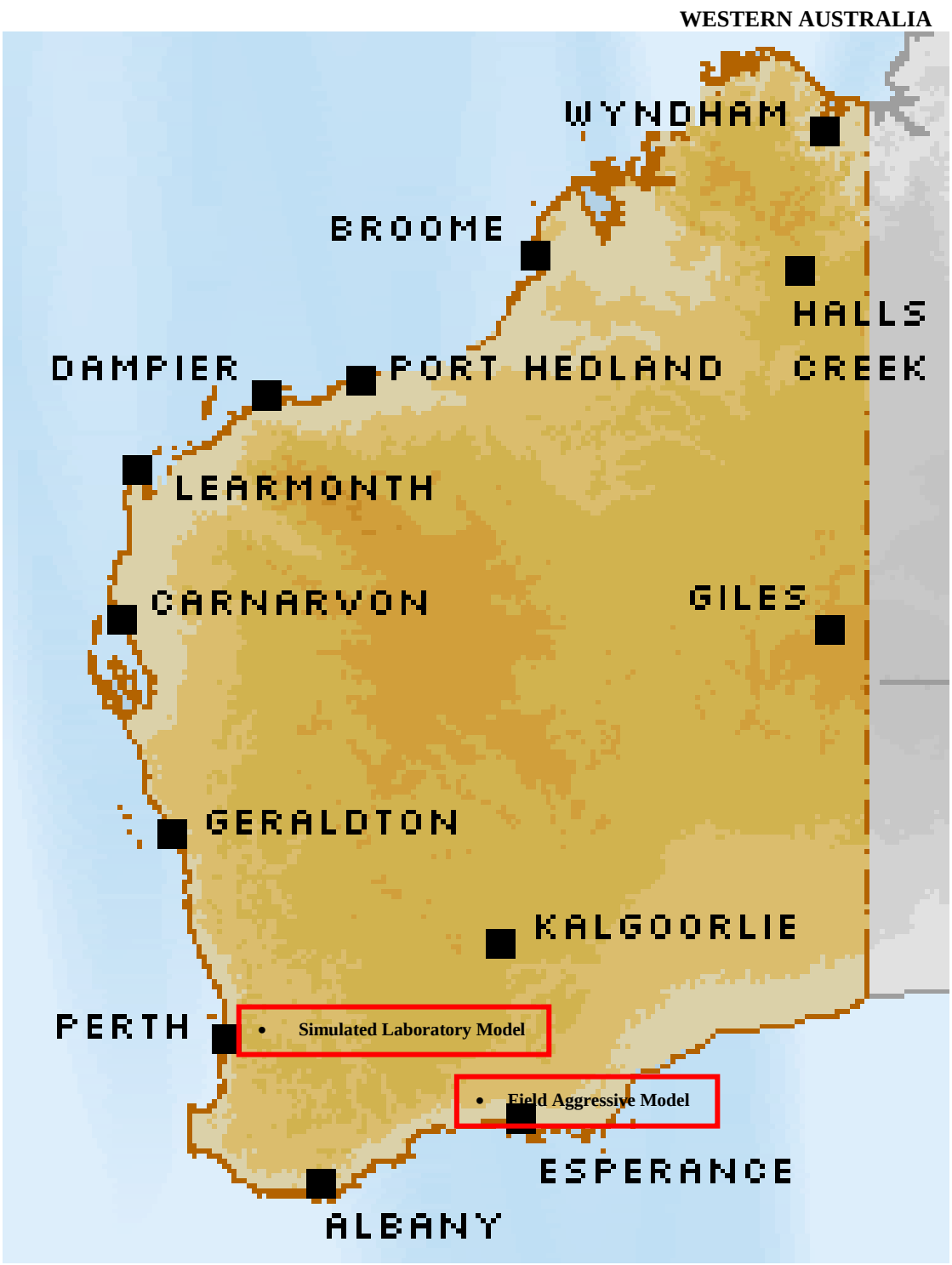

Average Annual Relative Humidityat Field and Laboratory Test Locations

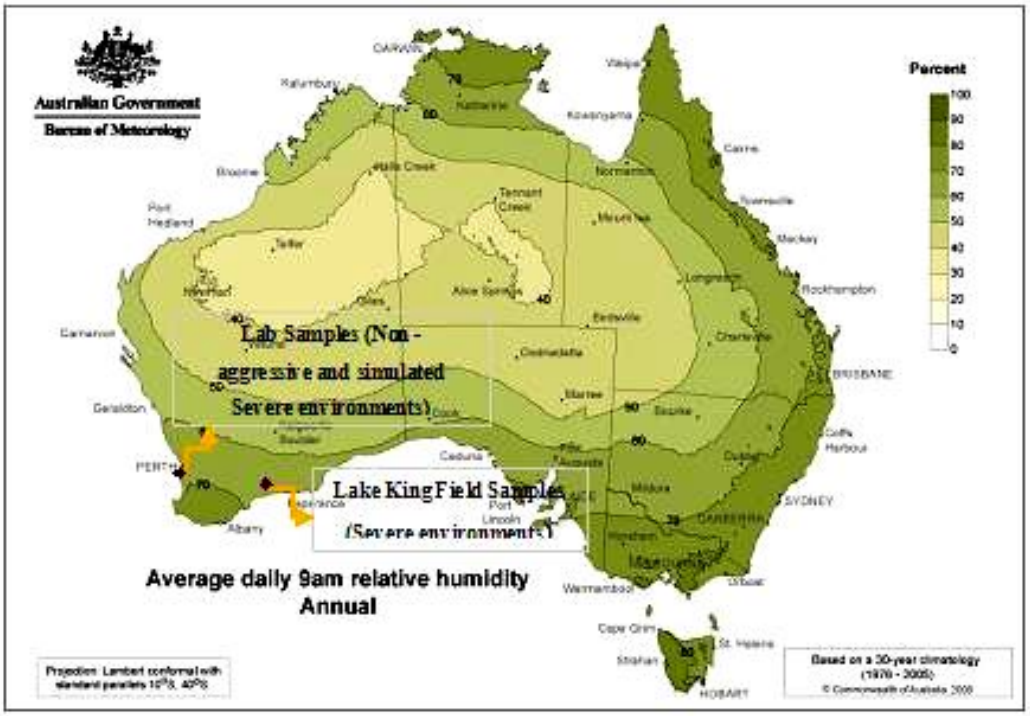

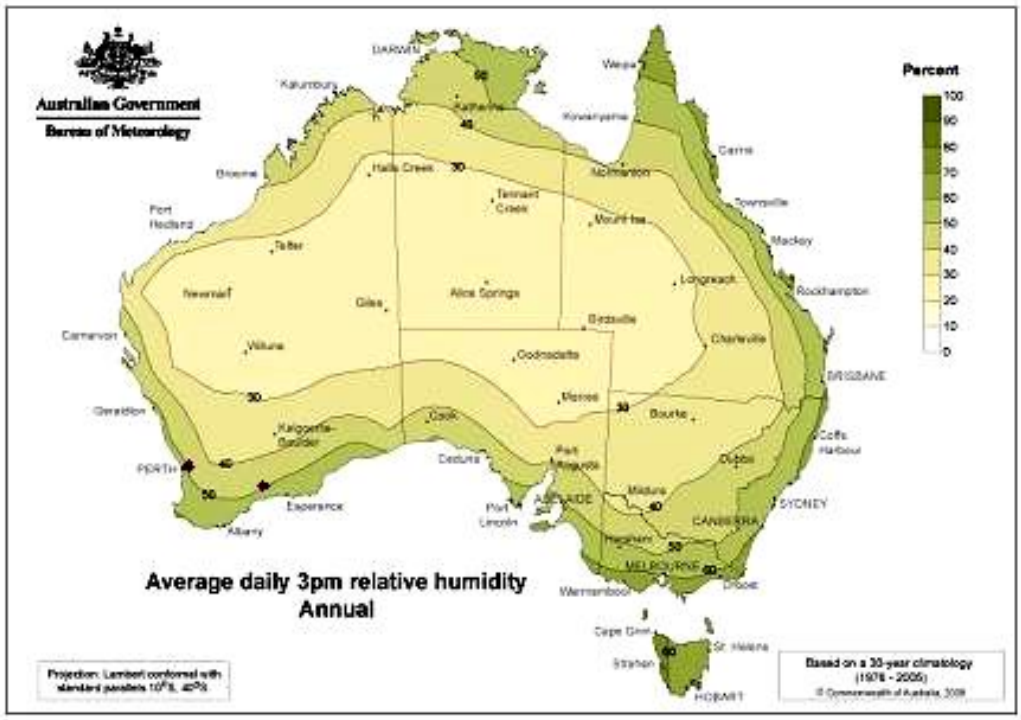

APPENDIX - B

LCFG CONCRETE & OPC CONCRETE MIX AND COMPOSITION DATA

Mixture Design Parameters and Calculations

Alkaline liquid/fly ash,	Water/geopolymer solids, by mass	Workability	Compressive strength, MPa
0.30	0.165	Stiff	58
0.35	0.190	Moderate	45
0.40	0.210	Moderate	37
0.45	0.230	High	32

The source of this Design Mix Process Example is from Chapter 26 in Concrete Construction Engineering Handbook, Editor-in-Chief: Dr. Edward G.Nawy, Second Edition, CRC Press, New York, 2007

- **LCFG Concrete Mix Design Components' Calculation (Section 4. 3)**

- **Final mass of each component Alkaline solution with 8M NaOH**

Mix Molarity	Item	Values	Unit	Remarks
8M	Fly ash	408	kg/m^3	
	Aggregate 14mm	646.8	kg/m^3	Aggregate in SSD condition
	Aggregate 10mm	646.8	kg/m^3	Aggregate in SSD condition
	Fine Aggregate	554.4	kg/m^3	Aggregate in SSD condition
	Sodium hydroxide	41	kg/m^3	26.2% solid and 68.6% water
	Sodium silicate	103	kg/m^3	
	Extra water			

- **Final mass of each component Alkaline solution with 14M NaOH**

Mix Molarity	Item	Values	Unit	Remarks
14M	Fly ash	408	kg/m^3	
	Aggregate 14mm	646.8	kg/m^3	Aggregate in SSD condition
	Aggregate 10mm	646.8	kg/m^3	Aggregate in SSD condition
	Fine Aggregate	554.4	kg/m^3	Aggregate in SSD condition
	Sodium hydroxide	41	kg/m^3	31.4% solid and 63.4% water
	Sodium silicate	103	kg/m^3	
	Extra water	10		

- **OPC Controlled Mix in the Research Study (S40 OPC Mix)**

Batch Proportions	MRWA Specification 820	Mix Design by Ready-mix
Concrete Class	S40	S40
Nominated strength (MPa)	40	40
Target strength for mix design (MPa)	48	48
Maximum aggregate size	20 mm	20 mm
Minimum aggregate/cement ratio	4.0	4.6
Maximum water/cement ratio	0.43	0.43
Minimum cement content	400 kg/m^3	400 kg/m^3
Total Alkali Content	Not exceeding 2.8 kg/m^3	
Slump(Final)	100mm Max	80 mm

- **S50 OPC Mix**

Batch Proportions	MRWA Specification 820	Mix Design by HUMES
Concrete Class	S50	S50
Nominated strength (MPa)	50	50
Target strength for mix design (MPa)	58	58
Maximum aggregate size	20 mm	14 mm
Minimum aggregate/cement ratio	3.0	4.3
Maximum water/cement ratio	0.40	0.40
Minimum cement content	420 kg/m^3	420 kg/m^3
Total Alkali Content	Not Exceeding 2.8 kg/m^3	
Slump(Final)	Maximum 100mm	80 ± 20 mm

- **Design Mix of LCFG Concrete and OPC Concrete for Laboratory Samples (Section 4.3)**

- **Aggregate Grading Envelope (Specification 820 -Concrete Structures, Main Roads, Western Australia)**

Aggregate grading envelops for S40 & S50 concrete class are as shown in figures below (Specification 820- Concrete for Structures, Document No 04/10134 Issue 23/1012).

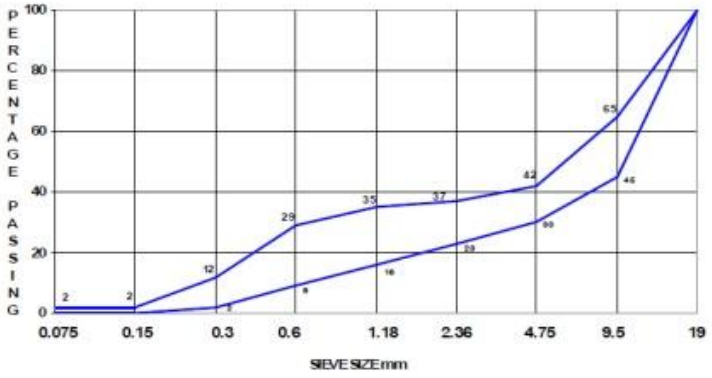

FIGURE 820.2 S40 AGGREGATE GRADING ENVELOPE 20mm

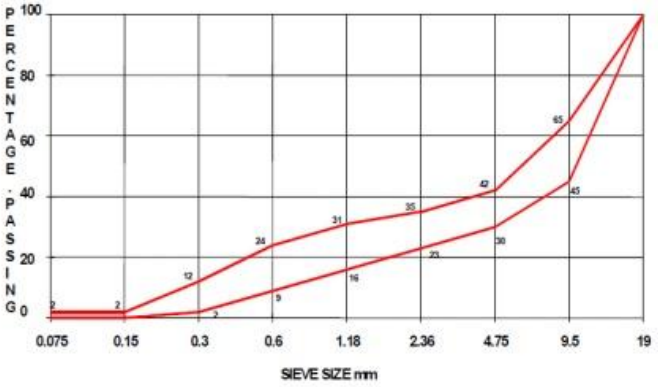

FIGURE 820.1 S50 AGGREGATE GRADING ENVELOPE 20mm

- **Main Roads Specification 404 -Combined Aggregate Grading for Box Culvert**

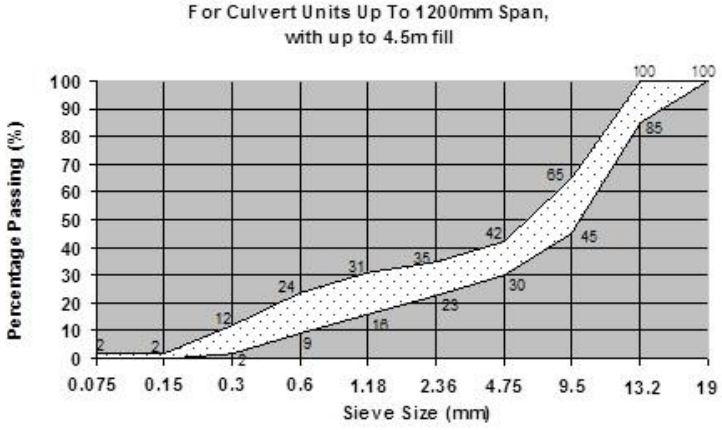

Box Culvert Combined Grading Envelope

- **ROCLA Aggregate Grading for Box Culvert**

Combined grading for small box culvert is as per Table from Concrete Technology ROCLA, 8 January 2013.

Aggregate Gradings

KEWDALE 50MPa Main Roads Approved Recipe PR022 - SCADA CP Recipe No.8

Agg. Type	14mm un-washed	10mm un-washed	Gaskell Ave Sand	Combined Grading 50MPa-0%FA
Sieve	% Passing			
19	100	100	100	100
13.2	93	100	100	96.7
9.5	17	88	100	58.8
6.7	1	13	100	40.6
4.75	1	3	100	39.2
2.36	0.9	2	100	39.0
1.18	0.5	2	100	38.8
0.6	0.5	1	85	32.9
0.3	0.5	1	27	10.7
0.15	0.5	1	2	1.1
0.075	0.4	0.6	0	0.3

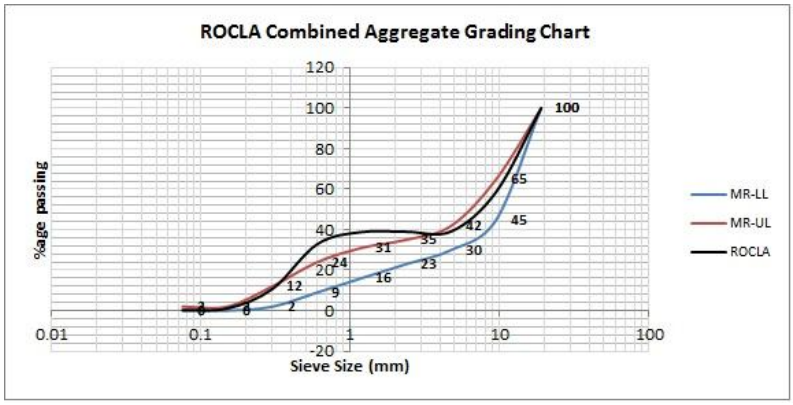

*ROCLA combined grading for box culvert has slightly higher percentage of fine aggregates passing 0.6 and 1.18mm sieve.

- **Aggregate**

Aggregate testing as per AS 1141.5

- **Fly Ash (Class- F) Composition From Various Australian Sources**

The chemical composition of Australian fly ash and general purpose cement

Compound	Fly ash				Type GP Cement
	NSW	QLD	SA	WA	
SiO_2	58-63	50-75	54	53	17-25
Al_2O_3	24-29	20-30	30	26	3-8
Fe_2O_3	3-5	1-15	4.5	1.1	0.5-6
CaO	0.5-2.5	0.1-5	5.5	1.5	60-70
*Na_2O	0.1-1	*	3	0.4	0.5-1.3
*K_2O	0.9-2	*	0.9	0.8	
TiO_2					
MgO	0.5-1.5	0.2-1.5	1.8		0.1-4.5
P_2O_5					
*SO_3	0.2-0.4	0-0.4	0.3	0.2	2.4
ZrO_2					
Cr					
MnO					
*LOI	0.7-3.0	0.2-3	0.2-3	0.9	1.1

- **Specified requirements of fly ash as per Australian Standard (AS 3582.1)**

  * LOI – Max Limit 4.0% (AS3582.1)

  *SO_3 content (% maximum) – Max 3 %(AS3582.1)

  *Boral test report for % available alkali = % Na_2O + (0.658 x % K_2O)

  (File No 126/06)

  #Based on PSD fineness (by % mass passing 45 µm sieve) – Min 75% (AS3582.1)

  # Specific Gravity 1.9-2.4 (Guide to use Coal Combustion Products - CCP, 2004, Ash Development Association of Australia)

- **Collie Power Plant Fly Ash, Western Australia Chemical Composition for LCFG Concrete from Previous Studies**

  * For batch 1 to 3, XRF (X-ray Fluorescence) analysis by the Department of Applied Chemistry, Curtin University (Hardjito & Rangan 2005) and Typical PSD (Particular Size Distribution) by CSIRO for Batch1 is shown below (Section 2.4.2).

  * XRF analysis of Batch 4 was by Cockburn Cement and Batch 5 was by CSIRO. Fly ash composition of Batch 4 & 5 was from Olivia, 2011(Section 2.4.2)

- **Particle Size Distribution (PSD) of Collie Power Plant Fly Ash**

PSD tests using the Malvern Instruments Mastersizer MS2000 document in previous research undertaken by CSIRO Minerals, Waterford Western Australia are shown in following Figures for three batches. Graph A shows the PSD in percentage by volume interval and graph B shows the PSD with percentage by volume passing size. In all batches percentage passing 45µm sieve was exceeding 75%. As per AS 3582.1 minimum requirement is 75% passing 45µm (Hardjito & Rangan 2005).

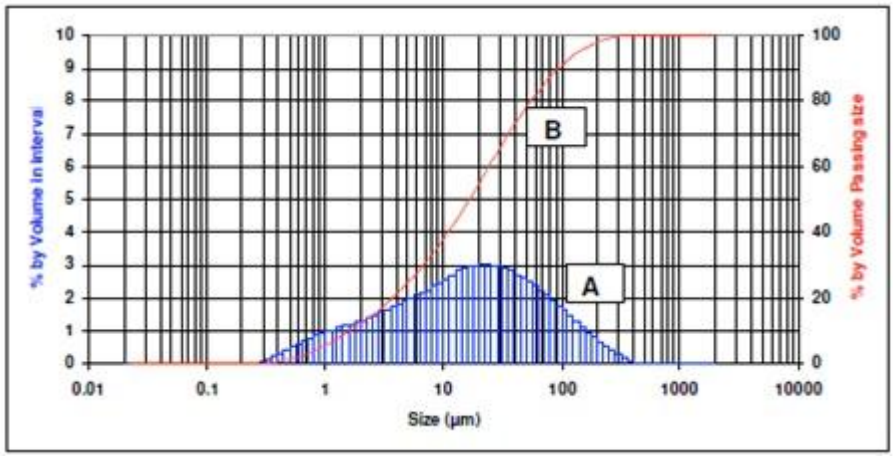

PSD – Batch 1

- **Blended LCFG Concrete (Slag Composition from Cockburn Cement, WA)**

  - Imported Raw Slag Chemical Composition

Oxides / Others	FeO	Cl	S	Al2O3	MnO	R2O	MgO	TiO2	Insol Residue	LOI (700 °C)	Basicity	Moisture	Glass content
Ave Mass %	0.40	< 0.01	0.89	14.51	0.27	0.44	6.12	0.53	0.07	0.18	1.82	7.73	99.00

Basicity = $(CaO + MgO + Al_2O_3)/SiO_2$

- Milled Slag Chemical Composition

Oxides	SiO2	Al2O3	Fe2O3	CaO	MgO	SO3	K2O	Na2O	Fineness	R332	+45µm
Ave Mass %	32.4	13	0.65	41.9	5.5	2.2	0.35	0.15	400	72.3	9.2

Milling of raw slag is energy intensive, approximately similar to clinker for GP cement (Cockburn Cement Western Australia)

- **OPC CONCRETE (General Purpose Cockburn Cement)**

Oxides	SiO_2	Al_2O_3	Fe_2O_3	CaO	MgO	SO_3	Chloride	Equivalent Na_2O	LOI
Mass %	20.7	5.2	3.1	64.1	1.9	2.3	0.01	0.5	1.4
Permissible Limits		Max. 6% ASTM C150	Max. 6% ASTM C150		Max 4.5% AS- 3972	Max 3.5% AS- 3972	Max 0.10% AS- 3972	Max 0.52% ASTM C150	Max 3% ASTM C150

Cement Specific Gravity = 3.14
Specified requirements as per AS 1379 for concrete and AS 3972 for blended cements

- **Water**

Water Corporation normal public water supply quality.

Parameters	**Content value**	**Permissible Limits**
TDS(mg/L)	463	50mg/L (AS1379-07), 50000ppm(ASTM C1602)
Chloride	N/A	500ppm (ASTM C1602)
Turbidity	0.3	
pH	7.84	>5 (AS 1379-07)
Sulphate as SO_4	N/A	3000 (ASTM C1602)

Olivia M (PhD Thesis 2012)

- **Source Material Silicate, Aluminate and Alkaline Effect on Na_2O/SiO_2 Mix Molar Ratio with NAOH of Different Molarity**

	Batch 1	**Batch 2**	**Batch 3**	**Batch 4**	**Batch 5**
SiO_2	53.36	47.8	48	50.2	50.5
Al_2O_3	26.49	29	29	26.3	26.57
Na_2O	0.37	0.31	0.39	0.36	0.45
Na_2O/SiO_2 (8M)	0.10	0.11	0.11	0.10	0.10
Na_2O/SiO_2 (10M)	0.10	0.11	0.11	0.11	0.11
Na_2O/SiO_2 (12M)	0.11	0.12	0.12	0.12	0.12
Na_2O/SiO_2 (14M)	0.12	0.13	0.13	0.12	0.12
Na_2O/SiO_2 (16M)	0.12	0.13	0.13	0.13	0.13

- **NaOH Molarity Effect on Na_2O/SiO_2 Mix Molar Ratio and Combined Alkaline Modulus**

	Na_2SiO3 Modulus (SiO_2/Na_2O)=3.2-3.3 (SiO_2 =30.1%, NaO_2= 9.4% & H_2O=60.5%)		**SiO_2/Na_2O Modulus (SiO_2/Na_2O)=2 (SiO_2 =29.7%, $NaO2$= 14.7% & H_2O=55.9%)**	
NaOH	**Na_2O/SiO_2 (Bakri)**	**Ms(Bakri)**	**Na_2O/SiO_2 (A53)**	**Ms(A53)**
8M	0.077	1.756	0.098	1.320
10M	0.083	1.619	0.104	1.239
12M	0.089	1.501	0.111	1.167
14M	0.095	1.399	0.117	1.103
16M	0.098	1.353	0.120	1.074

APPENDIX - C

LCFG CONCRETE BOX CULVERT SAMPLES MIX & STRENGTH DATA

Box Culvert Samples LCFG Concrete & OPC Concrete

- Box Culvert Reinforcement comprised of 12 mm N-bars and the clear cover to the reinforcement was 25 mm on all faces.

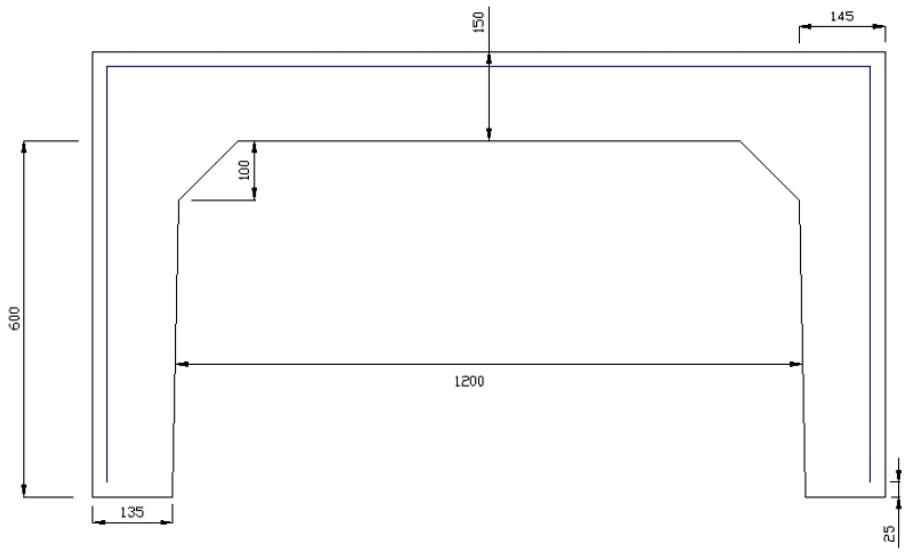

LCFG concrete box culvert samples of 40-50MPa strength as described above were prepared using local pre –cast industry plant facilities as a part of previous feasibility research study. Each mould holding two box culvert samples was steam cured in two stages for 24 hours rather than continuous one. Demoulding to free –up the box culvert moulds were carried out after initial 4 hours steam curing. Steam curing was stopped and the mould allowed cooling to room temperature and the specimens released from the mould. Followed by initial curing of 4 hours the box culvert sample specimens were steam cured for further 20 hours at temperature varying between 70- 80 ˚C by covering the box culvert mould with a polyethylene cover and inserting a steam jet under the culvert box mould as shown in Figure below.

- **Box Culvert Samples' Mix (From Previous Feasibility Study)**

Mixture No./ Casting Date	Aggregates			Fly Ash (kg)	Sodium Hydroxide Solution (8 Molar)		Sodium Silicate Solution (kg)	Super Plasticiser (kg)	Curing Temp. (°C)	Slump (mm)	Extra Water Due To Aggregates (L)
	14mm (kg)	10mm (kg)	Fine Sand (kg)		Solid (kg)	Water (kg)					
1(30/05/07)	554	702	591	409	11	30	102	6	90	220	22.5
2(19/06/07)	554	702	591	409	13	28	102	6	90	220	NA*
3(26/06/07)	554	702	591	409	13	28	102	6	80	240	NA*
4(04/07/07)	554	702	591	409	14	27	102	6	60	220	34
5(10/07/07)	554	702	591	409	14	27	102	6	90	210	19
6(11/07/07)	554	702	591	409	14	27	102	6	90	230	33

Box Culvert Samples 90 Days Ave, Compressive Strength (Cheema et al 2009)

St/ Curing Duration in Days	Mix1	Mix2	Mix3	Mix4	Mix5	Mix6
0	0.00	0.00	0.00	0.00	0.00	0.00
4	9.70	46.00	6.00	4.70	36.17	28.17
24	36.33	50.20	26.25	15.67	51.00	32.67
168	34.83	57.50	31.25	23.33	52.00	32.75
672	35.25	58.50	29.25	22.50	52.00	34.50
2160	38.50	57.75	30.00	25.25	57.25	34.75

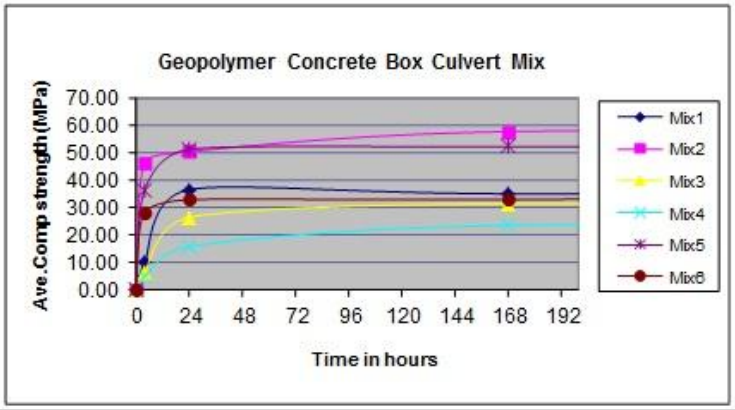

Box Culvert Samples' Mix Compressive Strength vs. Permeability Trend (Cheema et al 2009)

Mix No	90 Days Ave. Strength	Permeability		Test Data (Ave Permeability m/s)
		Specimen1	Specimen 2	
Mix1(8M)	39	9.60E-12	9.60E-12	9.60E-12
Mix2(10M)	55	4.10E-13	3.20E-13	3.65E-13
Mix3(10M)	30	1.60E-11	2.50E-11	2.05E-11
Mix4(11M)	23	5.30E-11	6.30E-11	5.80E-11
Mix5(11M)	50	8.50E-12	7.30E-12	7.90E-12
Mix6(11M)	35	2.40E-11	2.40E-11	2.40E-11

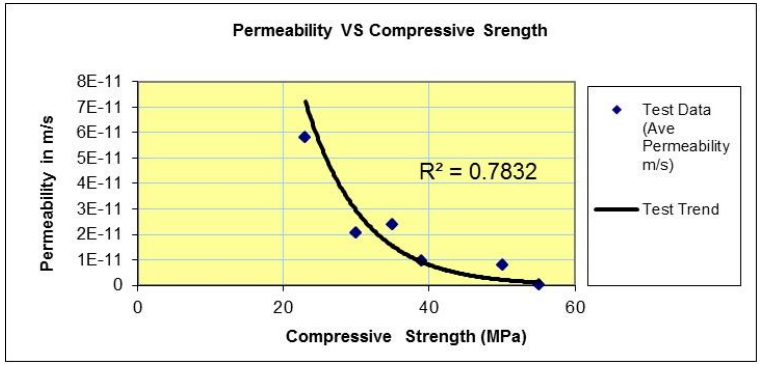

APPENDIX- D

VOLUME OF PERMEABLE VOID, CAPILLARY SUCTION, 3-D MICROTOMOGRAPHY OUTPUTS DATA AND DIFFUSION COEFFICIENT CALCULATION DATA

VPV Test Results Data

LCFG CONCRETE DURABILITY TRIALS

Density, Absorption & Voids Results: 11/5/2009 (Total Curing -4 Months) Before Severe Exposure

Mix Design	Lab No.	Specimen	Apparent Density t/m^3	Absorption %	Volume of Permeable Pore Space %
S40-14-80 Geopolymer (Cast: 11/12/08)	08C 129	Top	2.63	4.7	10.9
		Bottom	2.65	4.3	10.3
		Average	2.64	4.5	10.6
S50-14-80 Geopolymer (Cast: 15/12/08)	08C 130	Top	2.64	4.6	10.8
		Bottom	2.66	5.3	12.3
		Average	2.65	4.95	11.55
S40-14-80 GP (Cast: 17/12/08)	08C 131	Top	2.66	5.3	12.3
		Bottom	2.64	5.3	12.2
		Average	2.65	5.3	12.25
S40-14-80 GP + Xypex (Cast: 18/12/08)	08C 132	Top	2.67	4.9	11.7
		Bottom	2.66	5.3	12.3
		Average	2.665	5.1	12
S50-14-80 GP (Cast: 19/12/08)	08C 133	Top	2.68	4.9	11.6
		Bottom	2.68	4.9	11.6
		Average	2.68	4.9	11.6

LCFG CONCRETE DURABILITY TRIALS

Density, Absorption & Voids Results: 19/9/2012 (after three years of severe exposure)

Mix Design	Lab No.	Specimen	Apparent Density t/m^3	Absorption %	Volume of Permeable Pore Space %
S40-14-80 Geopolymer (Cast: 11/12/08)	08C 129	Top	2.852	2.852	6.860
		Top Middle	2.585	2.993	7.182
		Top Bottom	2.576	2.814	6.758
		Bottom	2.582	2.697	6.510
		Average	**2.649**	**2.839**	**6.828**
S50-14-80 Geopolymer (Cast: 15/12/08)	08C 130	Top	2.591	3.395	8.086
		Top Middle	2.580	3.216	7.661
		Top Bottom	2.569	3.246	7.696
		Bottom	2.533	3.654	8..533
		Average	**2.568**	**3.378**	**7.814**
S40-14-80 GP (Cast: 17/12/08)	08C 131	Top	2.616	4.657	10.858
		Top Middle	2.622	4.953	11.493
		Top Bottom	2.626	4.954	11.509
		Bottom	2.610	3.861	9.153
		Average	**2.619**	**4.606**	**10.753**
S40-14-80 GP + Xypex (Cast: 18/12/08)	08C 132	Top	2.638	4.302	10.191
		Top Middle	2.660	4.527	10.746
		Top Bottom	2.665	5.040	11.840
		Bottom	2.618	4.642	10.837
		Average	**2.645**	**4.628**	**10.904**
S50-14-80 GP (Cast: 19/12/08)	08C 133	Top	2.645	4.227	10.055
		Top Middle	2.653	4.654	10.992
		Top Bottom	2.648	4.645	10.952
		Bottom	2.556	4.697	11.137
		Average	**2.626**	**4.556**	**10.784**

Chloride & Total Soluble Salts in Soil and Water- Test Method

The procedure for measuring Chloride and Total Soluble Salts in Soil and Water is as per (MRWA910.1). Samples from field, simulated severe laboratory model and VPV test process were tested in accordance with this test method.

For chloride and sodium chloride in water, the test method procedure requires 50mL of water for determining chloride in water into 250mL conical flasks.
Add few drops of phenolphthalein indicator solution and adjust pH to 8.2 using sulphuric acid and sodium hydroxide solution drop wise as required. Brief description of the test procedure is as below.

Add 1mL potassium Chromate indicator to sample solution followed by silver nitrate from burette until the sample changes to red- brown colour. Record the total mL (T1) of silver nitrate used.

Chloride in water (mg/L) = 70.9T
Sodium Chloride in water = 116.9T where T is average number of mL of 0.1N silver nitrate used.

For total soluble salt in water take 50mL into previously dried and weighed 600mLbeaker (M1). Place the beaker in drying oven to allow the water to evaporate until the difference between successive mass readings at four intervals does not exceed 0.1 precents of the previous mass. Record the final reading of dry mass of beaker and residue to nearest 0.001g as M2.
Total soluble salt in water (mg/L) = 20,000(M2-M1)

For chloride in soil and total soluble salts in soil, soil sample of 50g passing 2.36mm sieve is added to 200ml of distilled or de-ionised water and boiled. Filter the soil after 24 hours of boiling and wash the soil thoroughly with distilled water. Make up the filtrate volume 250mL with distilled water and repeat the test procedure as for determining the chloride content of water.

Chloride content of soil (mg/kg) = 354.3T

For total soluble salt in soil, sieved sample approximately 10g in weighed 600mL beaker (M0). Add 100mL distilled water and allow 24 hours after boiling. Filter the sample into previous dried and weighed beaker and repeat the procedure in drying oven and take the final reading of beaker and the residue.

% Total soluble salts in soils = (M2-M1) (100/Mo)

Capillary Suction Test Data

	Specimen Mass with Cumulative Moisture					**Moisture gain mass**					**Absorption Volume l/m2**					**Coefficient of Capillary Suction - A**				
T0.5	G40	G50	S40	Sx40	S50	G40	G50	S40	Sx40	S50	G40	G50	S40	Sx40	S50					
T0.5	1860.60	1866.00	1862.20	1828.80	1875.20						G40	G50	S40	Sx40	S50	G40	G50	S40	Sx40	S50
1.00	1865.30	1869.70	1870.50	1836.20	1884.50	-4.70	-3.70	-8.30	-7.40	-9.30	0.60	0.47	1.06	0.94	1.18	0.60	0.47	1.06	0.94	1.18
1.73	1866.10	1871.30	1874.00	1839.00	1886.80	-5.50	-5.30	-11.80	-10.20	-11.60	0.70	0.67	1.50	1.30	1.48	0.40	0.39	0.87	0.75	0.85
2.24	1867.20	1872.60	1876.70	1841.50	1888.00	-6.60	-6.60	-14.50	-12.70	-12.80	0.84	0.84	1.85	1.62	1.63	0.38	0.38	0.83	0.72	0.73
5.00	1871.60	1879.20	1886.00	1850.50	1893.60	-11.00	-13.20	-23.80	-21.70	-18.40	1.40	1.68	3.03	2.76	2.34	0.28	0.34	0.61	0.55	0.47
7.00	1874.20	1883.20	1890.30	1854.80	1895.90	-13.60	-17.20	-28.10	-26.00	-20.70	1.73	2.19	3.58	3.31	2.64	0.25	0.31	0.51	0.47	0.38
8.72	1876.80	1886.60	1893.00	1858.00	1897.70	-16.20	-20.60	-30.80	-29.20	-22.50	2.06	2.62	3.92	3.72	2.86	0.24	0.30	0.45	0.43	0.33
10.00	1878.10	1888.40	1895.20	1859.70	1899.50	-17.50	-22.40	-33.00	-30.90	-24.30	2.23	2.85	4.20	3.93	3.09	0.22	0.29	0.42	0.39	0.31
13.00	1882.20	1889.70	1898.30	1862.30	1901.00	-21.60	-23.70	-36.10	-33.50	-25.80	2.75	3.02	4.60	4.27	3.28	0.21	0.23	0.35	0.33	0.25
19.03	1888.50	1890.30	1902.40	1866.40	1903.10	-27.90	-24.30	-40.20	-37.60	-27.90	3.55	3.09	5.12	4.79	3.55	0.19	0.16	0.27	0.25	0.19

Moisture Gained From the Environments

	G40	**G50**	**S40**	**Sx40**	**S50**
Moisture Gained After 15 days	27.9	24.3	40.2	37.6	27.9

Evaporable Moisture

Evapo-rable Water	G40	G50	S40	Sx40	S50
After 7 days	40.6	39	20.4	19.7	28.6
After 17 days	14.2	15.4	12.8	12.4	14.4

Diffusion Coefficient Calculations:

Project :	LCFG Geopolymer Concrete		
Title :	LCFG Geopolymer Concrete Durability Properties	Calc. No.	1
Job No:		Rev.	0
Spreadsheet developed by MJSD, this version chlor_2d Nov 1999.			
Prepared by:	D Cheema	Date:	

Changes from version 2c: potential failure of Solver in section 6 fixed by adding constraint to macro to prevent negative values of D.

NOTE: 1. The add-in called "Analysis ToolPak" must be enabled for this spreadsheet to work.

NOTE: 2. Recommended that Solver options "Quadratic" and "Central" are selected.

All cells available for input are highlighted. Non-highlighted cells should not be altered.

1. Input Data

Enter text for 2nd line of graph title	Title	Structure, Location		
e.g. Structure, Location				
Background Cl- concentration		Co	0.01	% by wt. of concrete
Threshold Cl- % for corrosion initiation		Ct	0.05	% by wt. of concrete
Immersion period of sample / age of structure		Td	355	days
… converted to seconds	=td*24*3600	Ts	30672000	seconds
Thickness for which profile to be plotted		Th	35	mm
Mean cover		mean	35	
Max. cover		maxc	35	
Min. cover		minc	35	

2. Enter measured Cl- concentrations and depths

Measured Cl- concentrations in % by weight of concrete

Depth Interval			Center depth (mm)	Measured Cl-	depth	Predicted Cl-	sq.error
(mm)							
0	to	0	0		0	0.543090276	

0	to	2	1	0.9	1	0.537096497	0.131699
2	to	4	3	0.43	3	0.525113698	0.0090466
4	to	6	5	0.36	5	0.513145167	0.0234534
6	to	8	7	0.41	7	0.501200379	0.0083175
8	to	10	9	0.45	9	0.489288751	0.0015436
10	to	14	12	0.49	12	0.471503889	0.0004624
14	to	20	17	0.53	17	0.442158993	0.0022888
20	to	28	24	0.5	24	0.401930884	0.0096176
28	to	32	30	0.45	30	0.368486783	0.0066444
32	to				30		

Note: if you want to delete depth intervals you must re-enter at least one value to force the recalculation

Sum of Square Errors 0.1930733

3. Calculate best fit Cs, D

This button runs the SOLVER, which iterates cs and d to minimise the sum of the square errors.

Surface Cl- concentration	Cs	0.543090276 % by wt. of concrete
Coefficient of Chloride Diffusion	D x 10-12	82.08792685 m2/s
	Do NOT delete this cell --->	8.20879E-11

NOTE: If you subsequently wish to ignore one of the measured data values from the "best fit" curve, simply 'Delete' the measured Cl- value and run the SOLVER again. Retyping the "bad" Cl- value in will reinstate the point on the curve without changing the newly fitted curve.

4. Find age at which corrosion will be initiated at cover depth

Selecting the button here runs the SOLVER to find the ages at which the threshold value of Cl- will be achieved at each of the specified cover depths.

	Depth	Calculated Cl-	Threshold Cl-	Sq. Error	Time years	Time days
Mean cover	35	0.04999477	0.05	2.73523E-11	0.074649403	27.247032
Max cover	35	0.04999477	0.05	2.73523E-11	0.074649403	27.247032
Min cover	35	0.04999477	0.05	2.73523E-11	0.074649403	27.247032

5. Results Summary

Surface Cl- concentration for "best fit" curve		Cs	0.543090276	% by wt. of concrete
Cl- diffusion coefficient for "best fit" curve		D	8.20879E-11	m2/s
Threshold Cl- for corrosion initiation		Ct	0.05	%c by wt. of concrete
Threshold will be achieved at mean cover depth of 35 mm at age			27.24703207	days
		or	years 1 months	
Threshold will be achieved at max cover depth of 35 mm at age			27.24703207	days
		or	years 1 months	
Threshold will be achieved at min cover depth of 35 mm at age			27.24703207	days
		or	years 1 months	

6. Required Diffusion coeff't for new concrete with specified age, threshold, cover depth

To find the required D click on this button ---------->

Required design life, years		years	50	
	=years*365	days	18250	
	=days*24*3600	secs	1576800000	
Specified background Cl-		Cos	0.005	%
Specified surface Cl-		Css	0.6	%
Specified depth to rebar		depth	50	mm
Specified threshold		Cts	0.05	%
		DsE12	0.251155497	
Guessed D	=DsE12/1E12	Ds	2.51155E-13	m2/s
Guessed Cl-		Cls	0.05	
	=Cos+(Css-Cos)*(1-ERF(depth/1000/(4*secs*Ds)^0.5))			
Sq. Error	=(Cls-Cts)^2	Esq	1.20371E-33	
Required D to achieve the specified age is		D =	2.51155E-13	m2/s

7. Curve at Corrosion initiation @ Mean, Max. and Min. cover depths

	Mean	Max	Min
Age at corrosion initiation from above (days)	27.24703207	27.24703207	27.247032

G40 3-D Tomography Test Outputs:

THE SIZE OF THE MODEL G40_1_A05_550-1049_200-799_1000-1499_smaller-0.0015 IS:

500 500 500

THE VOLUME FOR PROBING IS: X = (1 , 500)

Y = (1 , 500)

Z = (1 , 500)

TOTAL VOXELS OF THE VOLUME = 125000000

Voxels of target fabric in this model is: 1802899

The volume percentage of the target fabric is: 1.4423192E-02

Surface of all target fabric: 5630881

The specific surface area (SSA) is: 4.5047048E-02

50% target fabric in clusters 1 to 15916 , their voxels >= 20

60% target fabric in clusters 1 to 27006 , their voxels >= 14

70% target fabric in clusters 1 to 43294 , their voxels >= 9

80% target fabric in clusters 1 to 68122 , their voxels >= 6

90% target fabric in clusters 1 to 111525 , their voxels >= 3

95% target fabric in clusters 1 to 150560 , their voxels >= 2

99% target fabric in clusters 1 to 212220 , their voxels >= 1

Total number of clusters in this model is: 230248

The voxel-number for large cluster is truncated to: 1

Number of large clusters analysed (in .out2 & .out3) is: 230248

Percolation result in every direction:

(=0---nonpercolating, >0---number of percolating clusters)

X-direction: 0

Y-direction: 0

Z-direction: 0

Analysing all large clusters in groups of clusters .....

From cluster No. 1 to cluster No. 1276

From cluster No. 1277 to cluster No. 94733

From cluster No. 94734 to cluster No. 230248

FINISH THE CALCULATIONS !

S40 3-D Tomography Test Outputs:

THE SIZE OF THE MODEL S40_1_A09_1100-1599_400-899_0-499_smaller-0.0015 IS:

500 500 500

THE VOLUME FOR PROBING IS: X = (1 , 500)

Y = (1 , 500)

Z = (1 , 500)

TOTAL VOXELS OF THE VOLUME = 125000000

Voxels of target fabric in this model is: 2219332

The volume percentage of the target fabric is: 1.7754655E-02

Surface of all target fabric: 6899867

The specific surface area (SSA) is: 5.5198934E-02

50% target fabric in clusters 1 to 6103 , their voxels >= 55

60% target fabric in clusters 1 to 11348 , their voxels >= 33

70% target fabric in clusters 1 to 20074 , their voxels >= 20

80% target fabric in clusters 1 to 35600 , their voxels >= 11

90% target fabric in clusters 1 to 67581 , their voxels >= 5

95% target fabric in clusters 1 to 101792 , their voxels >= 2

99% target fabric in clusters 1 to 166085 , their voxels >= 1

Total number of clusters in this model is: 188278

The voxel-number for large cluster is truncated to: 1

Number of large clusters analysed (in .out2 & .out3) is: 188278

Percolation result in every direction:

(=0---nonpercolating, >0---number of percolating clusters)

X-direction: 0

Y-direction: 0

Z-direction: 0

Analysing all large clusters in groups of clusters .....

From cluster No. 1 to cluster No. 165

From cluster No. 166 to cluster No. 14410

From cluster No. 14411 to cluster No. 188278

FINISH THE CALCULATIONS !

SX40 3-D Tomography Test Outputs:

THE SIZE OF THE MODEL SX40_1_A01_500-999_500-999_500-999_small-0.00015 IS:

500 500 500

THE VOLUME FOR PROBING IS: X = (1 , 500)

Y = (1 , 500)

Z = (1 , 500)

TOTAL VOXELS OF THE VOLUME = 125000000

Voxels of target fabric in this model is: 2161766

The volume percentage of the target fabric is: 1.7294127E-02

Surface of all target fabric: 7054213

The specific surface area (SSA) is: 5.6433704E-02

50% target fabric in clusters 1 to	11405 , their voxels >=	35
60% target fabric in clusters 1 to	19045 , their voxels >=	23
70% target fabric in clusters 1 to	31023 , their voxels >=	14
80% target fabric in clusters 1 to	51170 , their voxels >=	8
90% target fabric in clusters 1 to	90670 , their voxels >=	4
95% target fabric in clusters 1 to	131415 , their voxels >=	2
99% target fabric in clusters 1 to	200932 , their voxels >=	1

Total number of clusters in this model is: 222549

The voxel-number for large cluster is truncated to: 1

Number of large clusters analysed (in .out2 & .out3) is: 222549

Percolation result in every direction:

(=0---nonpercolating, >0---number of percolating clusters)

X-direction: 0

Y-direction: 0

Z-direction: 0

Analysing all large clusters in groups of clusters .....

From cluster No. 1 to cluster No. 1238

From cluster No. 1239 to cluster No. 69265

From cluster No. 69266 to cluster No. 222549

FINISH THE CALCULATIONS !

APPENDIX – E

ELECTROCHEMICAL TESTING TECHNIQUES (RESISTIVITY, HCP &GPM) DATA

AND

SUSTAINABLE POTENTIAL ILLUSTRATION

RESIPOD Resistivity Test Outputs:

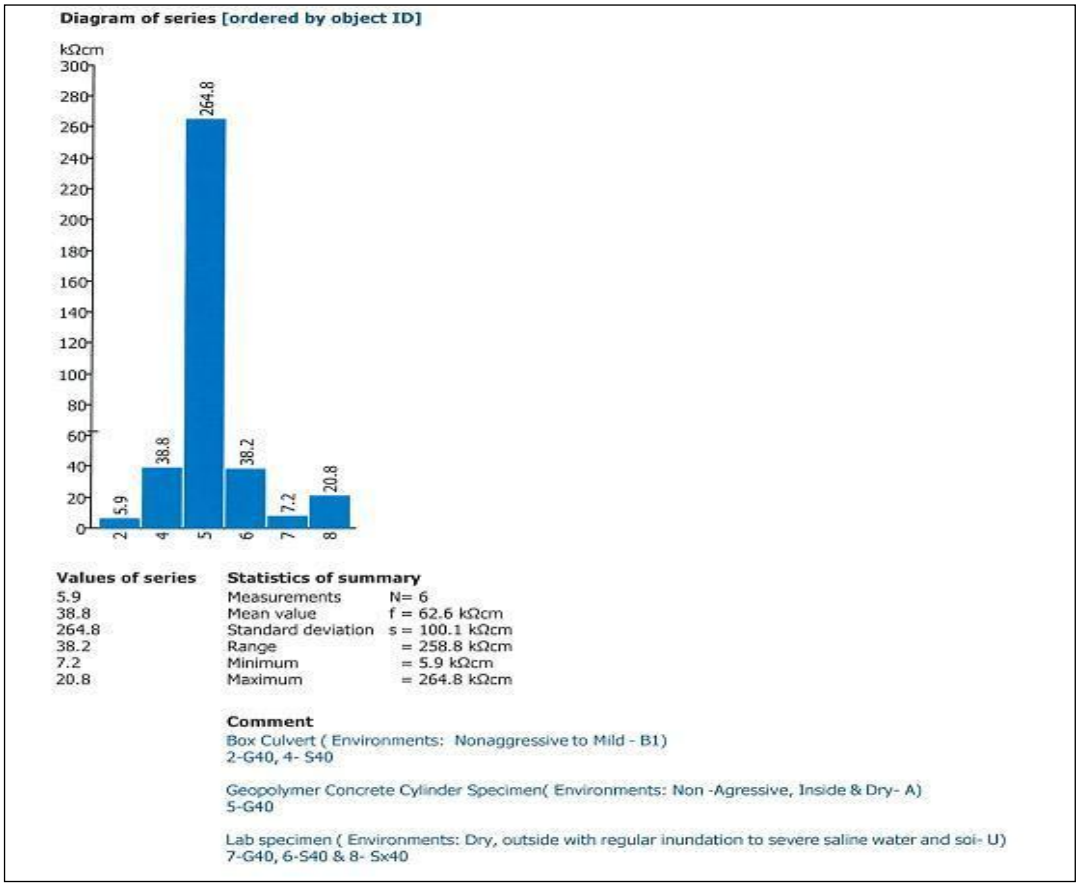

(a)

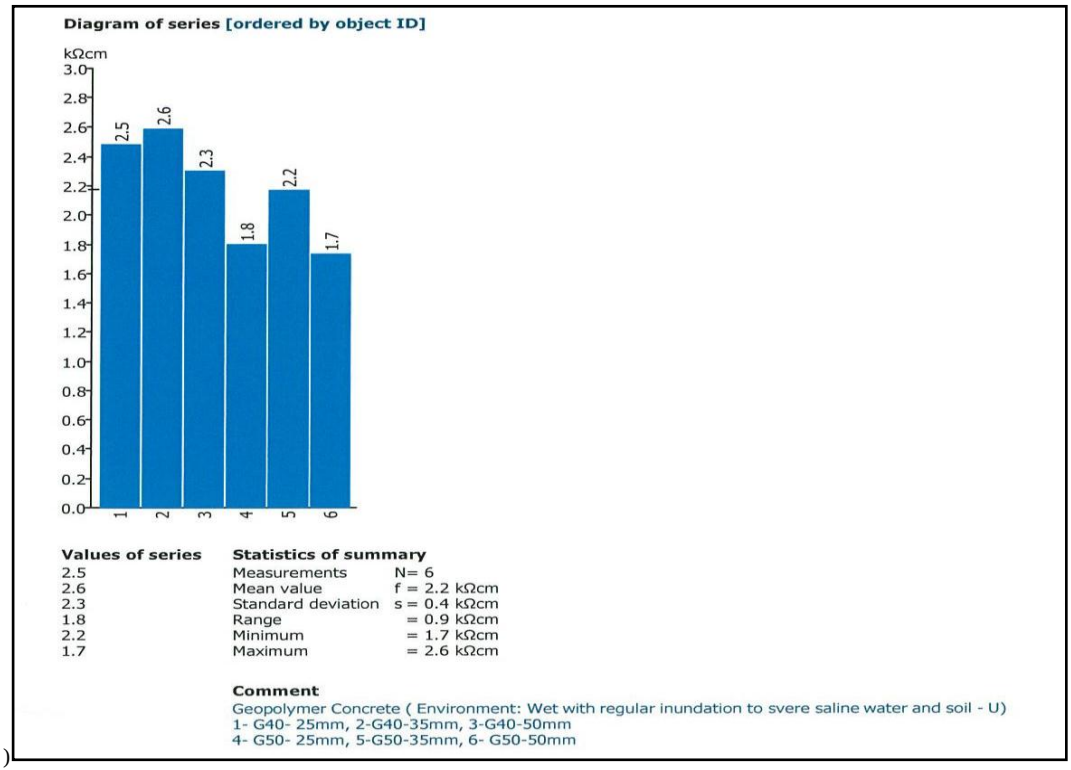

)

(b)

Diagram of series [ordered by object ID]

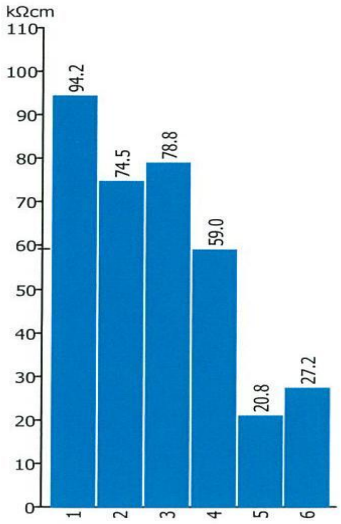

Values of series
94.2
74.5
78.8
59.0
20.8
27.2

Statistics of summary	
Measurements	N= 6
Mean value	f = 59.1 kΩcm
Standard deviation	s = 29.5 kΩcm
Range	= 73.3 kΩcm
Minimum	= 20.8 kΩcm
Maximum	= 94.2 kΩcm

Comment

OPC Concrete (Environment: Wet with regular inundation to severe saline water and soil-U)
1-S40-25mm, 2-S40-35mm, 3-S40-50mm
4-Sx40-25mm, 5-Sx40-35mm, 6-Sx40-50mm

(c)

Diagram of series [ordered by object ID]

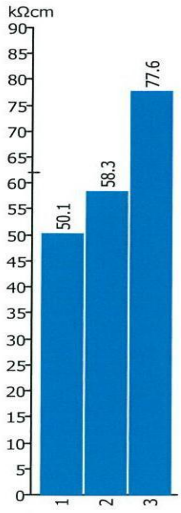

Values of series
50.1
58.3
77.6

Statistics of summary	
Measurements	N= 3
Mean value	f = 62.0 kΩcm
Standard deviation	s = 14.2 kΩcm
Range	= 27.6 kΩcm
Minimum	= 50.1 kΩcm
Maximum	= 77.6 kΩcm

Comment

OPC Concrete (Environment: Wet with regular inundation to svere saline water and soil- U)
1-S50-25mm, 2-S50-35mm, 3-S5-50mm

(d)

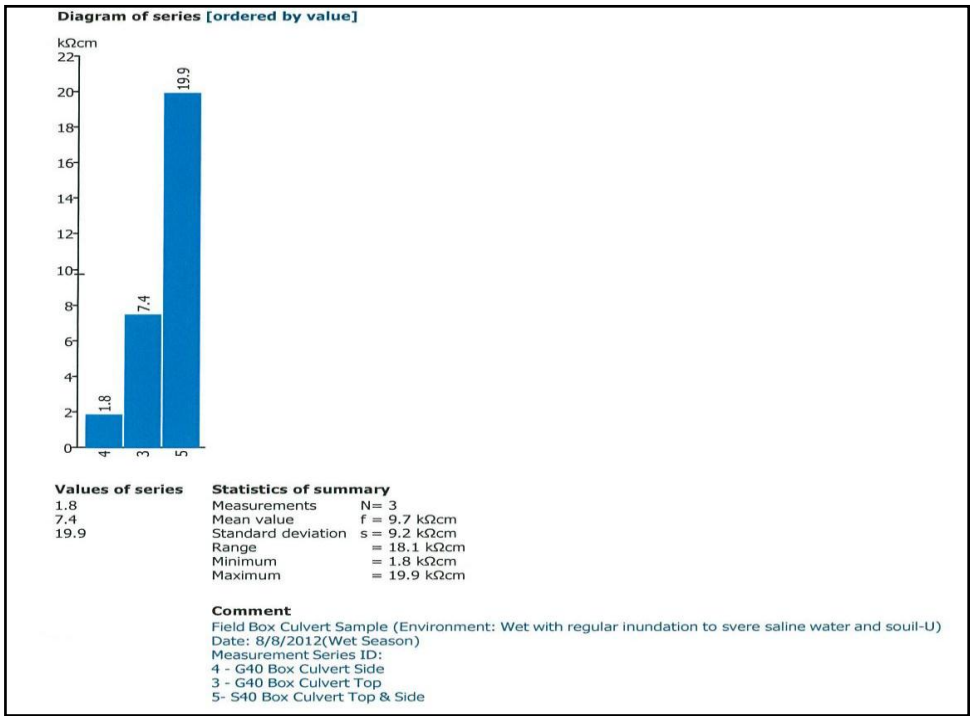

(e)

HCP Potential Data Dry (02/09) & Wet (03/09) Environments

Dry Environments

Cover	G40	G50	S40	Sx40	S50
25mm	-0.167	-0.200	-0.100	-0.120	-0.140
	-0.167	-0.200	-0.107	-0.107	-0.133
	-0.173	-0.220	-0.107	-0.093	-0.120
	-0.173	-0.233	-0.067	-0.087	-0.120
	-0.166	-0.200	-0.111	-0.125	-0.125
	-0.166	-0.202	-0.104	-0.119	-0.123
	-0.166	-0.207	-0.115	-0.119	-0.115
	-0.152	-0.203	-0.126	-0.128	-0.105
	-0.147	-0.188	-0.083	-0.115	-0.206
	-0.144	-0.195	-0.083	-0.104	-0.203
	-0.148	-0.200	-0.099	-0.114	-0.211
	-0.153	-0.204	-0.092	-0.112	-0.212
	G40	**G50**	**S40**	**Sx40**	**S50**
35mm	-0.180	-0.180	-0.113	-0.120	-0.113
	-0.180	-0.180	-0.100	-0.120	-0.120
	-0.180	-0.180	-0.120	-0.120	-0.120
	-0.180	-0.200	-0.107	-0.107	-0.107
	-0.170	-0.182	-0.116	-0.109	-0.109
	-0.172	-0.180	-0.112	-0.108	-0.114
	-0.175	-0.180	-0.140	-0.110	-0.109
	-0.176	-0.187	-0.116	-0.111	-0.106
	-0.146	-0.173	-0.103	-0.102	-0.176
	-0.153	-0.172	-0.099	-0.111	-0.173
	-0.156	-0.176	-0.098	-0.108	-0.177
	-0.158	-0.180	-0.100	-0.107	-0.182
50mm	**G40**	**G50**	**S40**	**Sx40**	**S50**
	-0.200	-0.180	-0.133	-0.107	-0.120
	-0.200	-0.187	-0.133	-0.107	-0.133
	-0.200	-0.187	-0.140	-0.107	-0.133
	-0.200	-0.187	-0.120	-0.080	-0.107
	-0.193	-0.184	-0.124	-0.113	-0.115
	-0.191	-0.184	-0.124	-0.111	-0.123
	-0.194	-0.183	-0.125	-0.110	-0.117
	-0.196	-0.184	-0.121	-0.113	-0.109
	-0.183	-0.242	-0.108	-0.112	-0.225
	-0.179	-0.240	-0.113	-0.115	-0.223
	-0.180	-0.238	-0.116	-0.110	-0.223
	-0.187	-0.239	-0.110	-0.104	-0.224

Wet Environments

Cover	G40	G50	S40	Sx40	S50
25mm	-0.397	-0.215	-0.185	-0.166	-0.141
	-0.585	-0.25	-0.191	-0.167	-0.154
	-0.674	-0.566	-0.225	-0.201	-0.159
	-0.67	-0.68	-0.261	-0.32	-0.181
	G40	**G50**	**S40**	**Sx40**	**S50**
35mm	-0.681	-0.667	-0.257	-0.173	-0.145
	-0.679	-0.668	-0.291	-0.173	-0.147
	-0.714	-0.62	-0.22	-0.121	-0.232
	-0.714	-0.693	-0.2	-0.319	-0.145
	G40	**G50**	**S40**	**Sx40**	**S50**
50mm	-0.586	-0.504	-0.185	-0.158	-0.135
	-0.587	-0.488	-0.185	-0.161	-0.16
	-0.697	-0.601	-0.212	-0.132	-0.259
	-0.682	-0.609	-0.228	-0.157	-0.258

Average HCP Results Data

Date	G40 -Ave	G50 -Ave	S40 -Ave	S40x -Ave	S50 -Ave	Cover
9/02/09	-0.167	-0.200	-0.100	-0.120	-0.140	25
9/02/09	-0.180	-0.180	-0.113	-0.120	-0.113	35
9/02/09	-0.200	-0.180	-0.133	-0.107	-0.120	50
9/02/09	-0.167	-0.200	-0.107	-0.107	-0.133	25
9/02/09	-0.180	-0.180	-0.100	-0.120	-0.120	35
9/02/09	-0.200	-0.187	-0.133	-0.107	-0.133	50
9/02/09	-0.173	-0.220	-0.107	-0.093	-0.120	25
9/02/09	-0.180	-0.180	-0.120	-0.120	-0.120	35
9/02/09	-0.200	-0.187	-0.140	-0.107	-0.133	50
9/02/09	-0.173	-0.233	-0.067	-0.087	-0.120	25
9/02/09	-0.180	-0.200	-0.107	-0.107	-0.107	35
9/02/09	-0.200	-0.187	-0.120	-0.080	-0.107	50
17/02/09	-0.166	-0.200	-0.111	-0.125	-0.125	25
17/02/09	-0.170	-0.182	-0.116	-0.109	-0.109	35
17/02/09	-0.193	-0.184	-0.124	-0.113	-0.115	50
17/02/09	-0.166	-0.202	-0.104	-0.119	-0.123	25
17/02/09	-0.172	-0.180	-0.112	-0.108	-0.114	35
17/02/09	-0.191	-0.184	-0.124	-0.111	-0.123	50
17/02/09	-0.166	-0.207	-0.115	-0.119	-0.115	25
17/02/09	-0.175	-0.180	-0.140	-0.110	-0.109	35
17/02/09	-0.194	-0.183	-0.125	-0.110	-0.117	50
17/02/09	-0.152	-0.203	-0.126	-0.128	-0.105	25
17/02/09	-0.176	-0.187	-0.116	-0.111	-0.106	35
17/02/09	-0.196	-0.184	-0.121	-0.113	-0.109	50
26/02/09	-0.147	-0.188	-0.083	-0.115	-0.206	25
26/02/09	-0.146	-0.173	-0.103	-0.102	-0.176	35
26/02/09	-0.183	-0.242	-0.108	-0.112	-0.225	50
26/02/09	-0.144	-0.195	-0.083	-0.104	-0.203	25
26/02/09	-0.153	-0.172	-0.099	-0.111	-0.173	35
26/02/09	-0.179	-0.240	-0.113	-0.115	-0.223	50

Date	G40 -Ave	G50 -Ave	S40 -Ave	S40x -Ave	S50 -Ave	Cover
26/02/09	-0.148	-0.200	-0.099	-0.114	-0.211	25
26/02/09	-0.156	-0.176	-0.098	-0.108	-0.177	35
26/02/09	-0.180	-0.238	-0.116	-0.110	-0.223	50
26/02/09	-0.153	-0.204	-0.092	-0.112	-0.212	25
26/02/09	-0.158	-0.180	-0.100	-0.107	-0.182	35
26/02/09	-0.187	-0.239	-0.110	-0.104	-0.224	50
20/03/09	-0.397	-0.215	-0.185	-0.166	-0.141	25
20/03/09	-0.681	-0.667	-0.257	-0.173	-0.145	35
20/03/09	-0.586	-0.504	-0.185	-0.158	-0.135	50
20/03/09	-0.585	-0.250	-0.191	-0.167	-0.154	25
20/03/09	-0.679	-0.668	-0.291	-0.173	-0.147	35
20/03/09	-0.587	-0.488	-0.185	-0.161	-0.160	50
27/03/09	-0.674	-0.566	-0.225	-0.201	-0.159	25
27/03/09	-0.714	-0.620	-0.220	-0.121	-0.232	35
27/03/09	-0.697	-0.601	-0.212	-0.132	-0.259	50
3/04/09	-0.670	-0.680	-0.261	-0.320	-0.181	25
3/04/09	-0.714	-0.693	-0.200	-0.319	-0.145	35
3/04/09	-0.682	-0.609	-0.228	-0.157	-0.258	50
17/04/09	-0.670	-0.600	-0.088	-0.116	-0.175	25
17/04/09	-0.678	-0.518	-0.233	-0.303	-0.154	35
17/04/09	-0.678	-0.448	-0.215	-0.230	-0.103	50
1/05/09	-0.520	-0.666	-0.277	-0.139	-0.068	25
1/05/09	-0.505	-0.629	-0.204	-0.183	-0.087	35
1/05/09	-0.532	-0.382	-0.180	-0.149	-0.036	50
18/05/09	-0.661	-0.522	-0.194	-0.198	-0.159	25
18/05/09	-0.710	-0.590	-0.252	-0.284	-0.135	35
18/05/09	-0.597	-0.487	-0.141	-0.137	-0.278	50
29/05/09	-0.395	-0.504	-0.055	-0.024	-0.073	25
29/05/09	-0.498	-0.312	-0.030	-0.132	-0.102	35
29/05/09	-0.705	-0.464	-0.062	-0.083	-0.207	50
15/06/09	-0.537	-0.518	-0.046	-0.156	-0.132	25

AVERAGE HCP RESULTS DATA Contd.

Date	G40 -Ave	G50 -Ave	S40 -Ave	S40x -Ave	S50 -Ave	Cover
15/06/09	-0.688	-0.575	-0.155	-0.180	-0.050	35
15/06/09	-0.690	-0.476	-0.176	-0.205	-0.232	50
26/06/09	-0.675	-0.641	-0.276	-0.269	-0.226	25
26/06/09	-0.706	-0.688	-0.279	-0.311	-0.170	35
26/06/09	-0.686	-0.634	-0.235	-0.282	-0.284	50
7/08/09	-0.676	-0.654	-0.235	-0.212	-0.154	25
7/08/09	-0.703	-0.683	-0.234	-0.272	-0.154	35
7/08/09	-0.672	-0.624	-0.204	-0.168	-0.173	50
1/09/09	-0.688	-0.642	-0.224	-0.204	-0.183	25
1/09/09	-0.709	-0.683	-0.178	-0.260	-0.143	35

Date	G40 -Ave	G50 -Ave	S40 -Ave	S40x -Ave	S50 -Ave	Cover
11/08/10	-0.298	-0.280	-0.124	-0.132	-0.024	25
11/08/10	-0.670	-0.660	-0.143	-0.251	-0.164	35
11/08/10	-0.351	-0.482	-0.096	-0.164	-0.257	50
11/08/10	-0.292	-0.266	-0.128	-0.132	-0.023	25
11/08/10	-0.489	-0.665	-0.140	-0.248	-0.181	35
11/08/10	-0.491	-0.482	-0.094	-0.162	-0.260	50
15/10/10	-0.682	-0.330	-0.184	-0.160	-0.040	25
15/10/10	-0.480	-0.323	-0.160	-0.180	-0.210	35
15/10/10	-0.620	-0.350	-0.151	-0.025	-0.250	50
12/11/10	-0.595	-0.780	-0.168	-0.388	-0.443	25

1/09/09	-0.671	-0.630	-0.185	-0.168	-0.211	50
2/10/09	-0.677	-0.639	-0.218	-0.193	-0.151	25
2/10/09	-0.710	-0.684	-0.198	-0.264	-0.145	35
2/10/09	-0.676	-0.631	-0.225	-0.163	-0.184	50
2/12/09	-0.523	-0.564	-0.298	-0.363	-0.302	25
2/12/09	-0.606	-0.648	-0.149	-0.337	-0.317	35
2/12/09	-0.606	-0.475	-0.219	-0.118	-0.271	50
16/03/10	-0.556	-0.557	-0.213	-0.089	-0.136	25
16/03/10	-0.561	-0.560	-0.092	-0.060	-0.126	35
16/03/10	-0.378	-0.425	-0.129	-0.016	-0.049	50
10/06/10	-0.777	-0.909	-0.325	-0.332	-0.303	25
10/06/10	-0.674	-0.742	-0.316	-0.393	-0.308	35
10/06/10	-0.641	-0.712	-0.269	-0.300	-0.269	50
10/08/10	-0.283	-0.143	-0.110	-0.171	-0.105	25
10/08/10	-0.089	-0.679	-0.155	-0.012	-0.008	35
10/08/10	-0.102	-0.684	-0.152	-0.001	-0.041	50
11/08/10	-0.316	-0.317	-0.122	-0.150	-0.033	25
11/08/10	-0.645	-0.665	-0.141	-0.262	-0.176	35
11/08/10	-0.437	-0.491	-0.097	-0.195	-0.262	50

12/11/10	-0.400	-0.785	-0.322	-0.470	-0.248	35
12/11/10	-0.660	-0.820	-0.328	-0.595	-0.245	50
9/03/11	-0.568	-0.528	-0.170	-0.187	-0.198	25
9/03/11	-0.610	-0.579	-0.305	-0.239	-0.125	35
9/03/11	-0.546	-0.570	-0.245	-0.112	-0.075	50
31/03/11	-0.461	-0.440	-0.170	-0.210	-0.106	25
31/03/11	-0.502	-0.550	-0.115	-0.065	-0.050	35
31/03/11	-0.495	-0.480	-0.090	-0.060	-0.060	50
3/06/11	-0.640	-0.730	-0.438	-0.330	-0.230	25
3/06/11	-0.682	-0.766	-0.358	-0.380	-0.302	35
3/06/11	-0.650	-0.707	-0.310	-0.258	-0.311	50
22/07/11	-0.870	-0.816	-0.297	-0.156	-0.110	25
22/07/11	-0.654	-0.699	-0.350	-0.262	-0.280	35
22/07/11	-0.647	-0.640	-0.290	-0.255	-0.185	50
4/11/11	-0.685	-0.727	-0.280	-0.215	-0.300	25
4/11/11	-0.645	-0.682	-0.220	-0.075	-0.196	35
4/11/11	-0.535	-0.685	-0.231	-0.193	-0.192	50

Rebar Cover – Wise HCP Results Data

Date	G40 -Ave	G50 -Ave	S40 -Ave	S40x -Ave	S50 -Ave	Cover
9/02/09	-0.167	-0.200	-0.100	-0.120	-0.140	25
17/02/09	-0.166	-0.200	-0.111	-0.125	-0.125	25
26/02/09	-0.147	-0.188	-0.083	-0.115	-0.206	25
20/03/09	-0.397	-0.215	-0.185	-0.166	-0.141	25
27/03/09	-0.674	-0.566	-0.225	-0.201	-0.159	25
3/04/09	-0.670	-0.680	-0.261	-0.320	-0.181	25
17/04/09	-0.670	-0.600	-0.088	-0.116	-0.175	25
1/05/09	-0.520	-0.666	-0.277	-0.139	-0.068	25
18/05/09	-0.661	-0.522	-0.194	-0.198	-0.159	25
29/05/09	-0.395	-0.504	-0.055	-0.024	-0.073	25
15/06/09	-0.537	-0.518	-0.046	-0.156	-0.132	25
26/06/09	-0.675	-0.641	-0.276	-0.269	-0.226	25
7/08/09	-0.676	-0.654	-0.235	-0.212	-0.154	25
1/09/09	-0.688	-0.642	-0.224	-0.204	-0.183	25
2/10/09	-0.677	-0.639	-0.218	-0.193	-0.151	25
2/12/09	-0.523	-0.564	-0.298	-0.363	-0.302	25
16/03/10	-0.556	-0.557	-0.213	-0.089	-0.136	25
10/06/10	-0.777	-0.909	-0.325	-0.332	-0.303	25
10/08/10	-0.283	-0.143	-0.110	-0.171	-0.105	25
11/08/10	-0.316	-0.317	-0.122	-0.150	-0.033	25
15/10/10	-0.682	-0.330	-0.184	-0.160	-0.040	25
12/11/10	-0.595	-0.780	-0.168	-0.388	-0.443	25
9/03/11	-0.568	-0.528	-0.170	-0.187	-0.198	25
31/03/11	-0.461	-0.440	-0.170	-0.210	-0.106	25
3/06/11	-0.640	-0.730	-0.438	-0.330	-0.230	25
22/07/11	-0.870	-0.816	-0.297	-0.156	-0.110	25
4/11/11	-0.685	-0.727	-0.280	-0.215	-0.300	25
9/02/09	-0.180	-0.180	-0.113	-0.120	-0.113	35
17/02/09	-0.170	-0.182	-0.116	-0.109	-0.109	35
26/02/09	-0.146	-0.173	-0.103	-0.102	-0.176	35
20/03/09	-0.681	-0.667	-0.257	-0.173	-0.145	35
27/03/09	-0.714	-0.620	-0.220	-0.121	-0.232	35
3/04/09	-0.714	-0.693	-0.200	-0.319	-0.145	35
17/04/09	-0.678	-0.518	-0.233	-0.303	-0.154	35
1/05/09	-0.505	-0.629	-0.204	-0.183	-0.087	35
18/05/09	-0.710	-0.590	-0.252	-0.284	-0.135	35
29/05/09	-0.498	-0.312	-0.030	-0.132	-0.102	35
15/06/09	-0.688	-0.575	-0.155	-0.180	-0.050	35
26/06/09	-0.706	-0.688	-0.279	-0.311	-0.170	35
7/08/09	-0.703	-0.683	-0.234	-0.272	-0.154	35
1/09/09	-0.709	-0.683	-0.178	-0.260	-0.143	35

Date	G40 -Ave	G50 -Ave	S40 -Ave	S40x -Ave	S50 -Ave	Cover
2/10/09	-0.710	-0.684	-0.198	-0.264	-0.145	35
2/12/09	-0.606	-0.648	-0.149	-0.337	-0.317	35
16/03/10	-0.561	-0.560	-0.092	-0.060	-0.126	35
10/06/10	-0.674	-0.742	-0.316	-0.393	-0.308	35
10/08/10	-0.089	-0.679	-0.155	-0.012	-0.008	35
11/08/10	-0.645	-0.665	-0.141	-0.262	-0.176	35
15/10/10	-0.480	-0.323	-0.160	-0.180	-0.210	35
12/11/10	-0.400	-0.785	-0.322	-0.470	-0.248	35
9/03/11	-0.610	-0.579	-0.305	-0.239	-0.125	35
31/3/11	-0.502	-0.550	-0.115	-0.065	-0.050	35
3/6/11	-0.682	-0.766	-0.358	-0.380	-0.302	35
22/7/11	-0.654	-0.699	-0.350	-0.262	-0.280	35
4/11/11	-0.645	-0.682	-0.220	-0.075	-0.196	35
9/02/09	-0.200	-0.180	-0.133	-0.107	-0.120	50
17/02/09	-0.193	-0.184	-0.124	-0.113	-0.115	50
26/02/09	-0.183	-0.242	-0.108	-0.112	-0.225	50
20/03/09	-0.586	-0.504	-0.185	-0.158	-0.135	50
27/03/09	-0.697	-0.601	-0.212	-0.132	-0.259	50
3/04/09	-0.682	-0.609	-0.228	-0.157	-0.258	50
17/04/09	-0.678	-0.448	-0.215	-0.230	-0.103	50
1/05/09	-0.532	-0.382	-0.180	-0.149	-0.036	50
18/05/09	-0.597	-0.487	-0.141	-0.137	-0.278	50
29/05/09	-0.705	-0.464	-0.062	-0.083	-0.207	50
15/06/09	-0.690	-0.476	-0.176	-0.205	-0.232	50
26/06/09	-0.686	-0.634	-0.235	-0.282	-0.284	50
7/08/09	-0.672	-0.624	-0.204	-0.168	-0.173	50
1/09/09	-0.671	-0.630	-0.185	-0.168	-0.211	50
2/10/09	-0.676	-0.631	-0.225	-0.163	-0.184	50
2/12/09	-0.606	-0.475	-0.219	-0.118	-0.271	50
16/03/10	-0.378	-0.425	-0.129	-0.016	-0.049	50
10/06/10	-0.641	-0.712	-0.269	-0.300	-0.269	50
10/08/10	-0.102	-0.684	-0.152	-0.001	-0.041	50
11/08/10	-0.437	-0.491	-0.097	-0.195	-0.262	50
15/10/10	-0.620	-0.350	-0.151	-0.025	-0.250	50
12/11/10	-0.660	-0.820	-0.328	-0.595	-0.245	50
9/03/11	-0.546	-0.570	-0.245	-0.112	-0.075	50
31/3/11	-0.495	-0.480	-0.090	-0.060	-0.060	50
3/6/11	-0.650	-0.707	-0.310	-0.258	-0.311	50
22/7/11	-0.647	-0.640	-0.290	-0.255	-0.185	50
4/11/11	-0.535	-0.685	-0.231	-0.193	-0.192	50

HCP Dry & Sheltered Environments in Excess of One Year

Cylinder Specimen Date Casting : 7/2/11

Environment: Dry & Sheltered for 21 Months

Date of HCP Testing 27/11/12

Obs. No	Average G40 Half Cell Negative Potential(E) in Volt	Ave. G40 HCP (Two years exposure followed by Dry & Sheltered Spill for one year)	Ave. S40 HCP (Two years exposure followed by Dry & Sheltered Spill for one year)
1	-0.433	-0.105	-0.037
2	-0.436	-0.111	-0.038
3	-0.436	-0.11	-0.036
4	-0.44	-0.138	-0.035
5	-0.43	-0.138	-0.034
6	-0.44	-0.137	-0.035
7	-0.439	-0.138	-0.036
8	-0.435	-0.137	-0.035
9	-0.438	-0.138	-0.034
10	-0.434	-0.137	-0.035
11	-0.433	-0.138	-0.034
12	-0.431	-0.138	-0.034
13	-0.429	-0.139	-0.033
14	-0.432	-0.138	-0.033
15	-0.439	-0.139	-0.035
16	-0.441	-0.138	-0.034
17	-0.437	-0.137	-0.035
18	-0.436	-0.137	-0.034
19	-0.434	-0.138	-0.034
20	-0.431	-0.137	-0.035
21	-0.432	-0.139	-0.034
22	-0.431	-0.139	-0.035
23	-0.43	-0.139	-0.034
24	-0.431	-0.139	-0.034
25	-0.43	-0.139	-0.035

Ave. HCP Dry & Sheltered Environments

Obs. No	Average G40 Half Cell Negative Potential in Volt (Dry and sheltered Environment)	Ave. G40 HCP (Two years exposure followed by Dry & Sheltered Spill for one year)	Ave. S40 HCP (Two years exposure followed by Dry & Sheltered Spill for one year)
1.000	-0.434	-0.135	-0.035

HCP Results Data on Pre-passivated Rebar with Silicate

Date	HCP
	Specimen 303 (35mm)
10/08/2010	-0.105
11/08/2010	-0.136
14/09/2010	-0.64
15/10/2010	-0.265
12/11/2010	-0.545
9/03/2011	-0.516

	Specimen 388 (35mm)
10/08/2010	-0.108
11/08/2010	-0.134
14/09/2010	-0.63
15/10/2010	-0.406
12/11/2010	-0.55
9/03/2011	-0.536

HCP & Current Density with GPM Technique

GPM (-HCP) 25mm

Date	G40	G50	S40	SX40	S50
14/07/09	830	762	309	220	224
21/10/09	806	769	302	316	201
15/01/10	835	644	224	220	166
21/04/10	611	593	208	279	157
10/08/10	720	708	206	188	157
9/11/10	659	685	192	222	152
8/03/11	590	544	254	331	238
13/07/11	706	698	207	191	182
8/11/11	774	790	183	278	282
2/04/2012	737	729	286	225	196

GPM Current Density (µA/ cm2) 25mm

Date	G40	G50	S40	SX40	S50
14/07/09			16.07	6.79	7.04
21/10/09			0.00	0.84	0.77
15/01/10			30.12	6.06	8.20
21/04/10			13.17	7.96	5.96
10/08/10			18.47	6.69	10.02
9/11/10			27.06	13.36	15.72
8/03/11			0.00	9.07	0.04
13/07/11			6.69	4.52	0.19
8/11/11			2.00	0.20	0.00
2/04/2012			0.16	2.70	1.10

GPM HCP 35mm

Date	G40	G50	S40	SX40	S50
14/07/09	844	813	245	346	195
21/10/09	844	813	264	343	218
15/01/10	689	699	181	311	179
21/04/10	606	589	223	260	152
10/08/10	722	719	193	276	151
9/11/10	685	668	164	278	151
8/03/11	598	600	313	326	192
13/07/11	714	715	192	245	148
8/11/11	800	797	175	230	183
2/04/2012	742	764	178	293	158

GPM Current Density (µA/ cm2) 35mm

Date	G40	G50	S40	SX40	S50
14/07/09			5.92	15.22	6.88
21/10/09			0.70	0.88	0.48
15/01/10			8.86	9.86	4.07
21/04/10			6.65	7.77	5.64
10/08/10			10.53	40.08	11.36
9/11/10			11.12	24.54	14.98
8/03/11			5.61	9.84	4.69
13/07/11			5.08	0.00	0.00
8/11/11			1.90	0.40	2.60
2/04/2012			8.00	1.40	1.00

GPM HCP 50mm

Date	G40	G50	S40	SX40	S50
14/07/09	801	748	204	193	274
21/10/09	801	748	228	243	252
15/01/10	660	658	175	173	182
21/04/10	610	599	157	160	158
10/08/10	722	731	188	175	159
9/11/10	675	899	251	160	157
8/03/11	624	615	182	181	272
13/07/11	710	633	154	181	165
8/11/11	794	806	208	183	203
2/04/2012	760	778	153	164	189

GPM Current Density (µA/ cm2) 50mm

	G40	G50	S40	SX40	S50
14/07/09			11.74	7.85	6.97
21/10/09			0.99	0.79	0.89
15/01/10			6.44	5.33	4.75
21/04/10			10.90	16.20	10.22
10/08/10			23.82	13.26	7.36
9/11/10			1.58	12.18	15.36
8/03/11			6.19	5.02	1.13
13/07/11			16.46	10.17	0.00
8/11/11			2.70	1.50	0.00
2/04/2012			4.00	1.80	2.80

Compressive Strength Trend after Three Years Severe Exposure

Mix	Comp St (Y0). MPa	Comp St (Y1). MPa	Comp St (Y2). MPa	Comp St (Y3). MPa
G40	54.5	59	**51.5**	**36.3**
G50	53.75	57.5	**48.5**	**34.3**
S40	55	53.75	**59**	**50.2**
SX40	56.75	58.75	**59.5**	**47.1**
S50	58.5	56.75	**54.3**	**49.3**

CO_2 Saving & Sustainable Potential Illustration

Subsequent illustration attempts to describe the sustainable potential LCFG concrete. For instance LCFG concrete applications for a project length of one kilometre of freeway having six lanes divided carriageway with a fast track for metro rail through the median island barricaded by concrete safety crash barrier as shown in Figure 5.75 will enable to cut down the CO_2 emission by 540t/km as summarised in Table below.

Illustration of Potential CO_2 Emission Saving For Road Project

Item	Design life (AS 3600) in Years	Non- Structural Concrete Class with binder content 350kg/m^3	Approx. requirement of concrete in m^3/km	OPC CO_2 emission in tonne	Geopolymer CO_2 emission in tonne @ 0.18t/ tonne of geopolymer cement	Net cut down on CO_2 emission in tonne/ km.
Concrete Safety Barrier	40-60	N32	800	280	50	
Rail Sleepers	40-60	N32	284	100	18	
Dual use path	40-60	N20	600	228	41	
Kerbing (up to 50% extent)	40-60	N20	140	50	9	
Total CO_2/km				658	118	**540**

While cutting down of CO_2 emission from climate change prospective is significant with the use of blended LCFG concrete and LCFG concrete, its potential to offer management opportunities alleviating long term negative environmental impacts of fly ash waste disposal on groundwater and resulting downstream health issues from the traces of heavy metal build-up is also significant. Investigated heavy metal and radioisotope mineral traces are summarised in Tables below (Vimal Kumar et al, 2005).

Total & Available Traces of Heavy Metals

Heavy metals in fly ash	Se	Cr	Pb	Co	Ni	Cd	As	Hg
Total	0.6-2.6	50-150	10-70	10-50	50-150	5-10	1-4	BDL
Available (ppm)	0.1-0.4	0.3-0.6	*BDL	0.05-0.15	0.15-0.25	0.03-0.7	BDL	BDL

*BDL (Below detectable limits)

Radioactivity Levels in Fly Ash

Radioactivity levels in Fly ash	226Ra	228Ac	40K
Bq/kg	30-110	30-110	180 -500

Blended LCFG concrete and LCFG concrete thus not only has the potential to raise the sustainability ranking of the project significantly and reduce CO_2 emission but will also open up the opportunities to manage the negative environmental impacts of fly ash disposal as a waste.

GPM Technique PULSE CHART DATA (291009)

Adjusted Data Report

Sample	**X,Y**	**1,1**	**1,2**	**1,3**	**1,4**	**1,5**	**2,1**	**2,2**	**2,3**	**2,4**	**2,5**	**3,1**	**3,2**	**3,3**	**3,4**	**3,5**
Pulse magnitude	**uA**	23	23	23	23	23	23	23	23	23	23	23	23	23	23	23
Measurements/sec	**#**	6	6	6	6	6	6	6	6	6	6	6	6	6	6	6
Pulse duration	**sec**	10	10	10	10	10	10	10	10	10	10	10	10	10	10	10
Rebar diameter	**mm**	8	8	8	8	8	8	8	8	8	8	8	8	8	8	8
Rebar length	**mm**	85	85	85	85	85	85	85	85	85	85	85	85	85	85	85
Rebar area	**mm2**	2136	2136	2136	2136	2136	2136	2136	2136	2136	2136	2136	2136	2136	2136	2136
Datapoints	**#**	60	60	60	60	60	60	60	60	60	60	60	60	60	60	60
Resistance	**Kohm**	**2**	**2**	**47**	**48**	**65**	**2**	**2**	**59**	**40**	**74**	**2**	**2**	**34**	**70**	**65**
Corrosion current	**uA/cm2**	**0.00**	**0.00**	**2.12**	**0.84**	**0.77**	**0.00**	**0.00**	**0.70**	**0.88**	**0.48**	**0.00**	**0.00**	**0.99**	**0.79**	**0.89**
unknown parameter		2001	1937	4060	3857	4204	1821	2164	4218	3805	4070	1817	1960	2070	3795	4022
unknown parameter		32767	32767	32767	32767	32767	32767	1935	32767	32767	32767	32767	32767	32767	32767	32767

Time (S)	**1,1**	**1,2**	**1,3**	**1,4**	**1,5**	**2,1**	**2,2**	**2,3**	**2,4**	**2,5**	**3,1**	**3,2**	**3,3**	**3,4**	**3,5**
0.0	696	659	192	206	91	734	703	154	233	108	691	638	118	133	142
0.2	697	658	191	204	94	735	699	152	234	110	689	639	117	136	140
0.3	695	658	194	206	90	735	705	154	234	109	691	637	116	134	144
0.5	697	658	193	207	93	732	702	153	235	109	691	638	116	136	139
0.7	694	656	195	205	93	735	700	153	233	104	690	637	116	134	146
0.8	695	658	194	207	93	735	706	153	236	103	687	634	116	134	142
1.0	711	671	591	612	634	740	720	645	575	723	697	651	402	718	683
1.2	712	667	599	629	645	745	723	663	581	739	698	648	410	714	688
1.3	711	669	606	639	646	745	715	665	592	743	699	653	412	722	699
1.5	712	667	612	651	647	741	719	675	595	754	699	649	418	730	700
1.7	710	665	612	658	651	743	718	682	599	762	696	649	423	735	706
1.8	710	664	616	661	654	744	717	683	603	761	698	650	425	735	700
2.0	708	662	620	667	650	746	717	691	606	762	698	652	423	739	702
2.2	710	661	620	665	656	744	719	695	610	768	698	645	430	744	703

2.3	711	659	623	666	654	745	717	696	609	769	698	650	429	747	706
2.5	707	658	625	664	658	743	719	700	611	773	700	650	433	753	706
2.7	708	655	627	667	663	744	718	704	616	773	697	650	437	756	705
2.8	709	657	630	669	661	746	717	701	618	774	696	649	437	757	708
3.0	707	661	628	670	662	744	715	703	616	777	695	648	441	759	705
3.2	708	659	630	673	664	743	720	707	617	779	697	649	439	763	709
3.3	711	655	632	678	670	742	716	711	621	781	696	651	444	768	711
3.5	709	654	628	679	671	747	717	715	624	787	698	649	444	771	713
3.7	711	653	635	685	673	745	717	714	623	787	699	647	445	774	715
3.8	713	656	638	686	675	742	718	718	627	787	699	647	446	774	715
4.0	713	655	633	687	676	741	720	718	623	791	698	648	451	775	715
4.2	708	654	635	694	677	741	721	714	624	796	698	647	453	777	719
4.3	705	654	637	696	683	745	718	717	628	799	698	652	451	778	719
4.5	704	656	637	695	681	745	718	714	628	804	696	649	453	783	722
4.7	704	651	638	700	684	745	718	711	630	807	697	647	455	784	720
4.8	709	649	639	703	686	741	721	713	630	812	700	648	459	787	721
5.0	706	653	637	703	689	744	717	713	636	806	701	645	458	791	720
5.2	704	652	640	707	690	746	719	717	636	814	701	649	461	787	723
5.3	705	653	641	709	694	744	719	717	637	817	700	649	460	789	721
5.5	707	652	639	708	693	740	718	719	638	819	699	645	463	794	718
5.7	706	653	640	713	696	746	715	726	639	825	700	646	463	792	720
5.8	708	652	641	720	697	744	718	729	640	825	700	649	463	794	719
6.0	705	653	641	723	701	741	718	729	639	830	699	648	468	794	721
6.2	705	652	643	730	701	746	716	729	643	833	699	646	470	795	721
6.3	706	650	642	726	705	744	718	732	644	832	699	648	472	794	722
6.5	704	654	642	732	703	744	717	731	645	836	698	648	470	800	728
6.7	709	650	644	735	706	744	718	739	647	837	700	648	472	802	731
6.8	706	652	642	735	707	743	720	737	650	839	700	644	472	802	731
7.0	705	647	642	735	711	741	716	743	655	839	698	643	473	802	736

7.2	708	652	641	742	710	744	716	743	658	841	698	646	477	805	737
7.3	704	653	642	767	710	744	718	742	652	842	697	649	477	802	743
7.5	705	650	641	769	713	743	717	739	651	844	700	647	477	804	742
7.7	707	653	639	684	716	747	720	744	653	847	699	647	480	805	745
7.8	704	652	642	690	718	744	717	751	658	842	698	648	483	806	744
8.0	707	646	646	691	715	743	717	755	659	845	699	648	484	807	744
8.2	707	646	645	697	716	743	717	759	660	845	701	650	482	809	755
8.3	706	651	640	704	720	746	719	760	660	847	695	645	486	805	752
8.5	704	649	641	700	720	741	720	762	662	852	697	644	484	808	760
8.7	703	647	643	703	724	744	718	766	662	850	701	642	486	811	758
8.8	704	648	644	704	720	743	719		661	852	696	649	485	812	761
9.0	706	649	646	706	722	744	722		662	853	700	647	488	813	759
9.2	704	649	643	709	724	746	719		662	854	698		490	816	761
9.3	704	649	643	710	726	744	717		662	854	700		489	817	758
9.5	706	646	646	712	727	745	719		665	856	699		497	814	

GPM Technique PULSE CHART DATA (150110)

Sample	**X,Y**	**1,1**	**1,2**	**1,3**	**1,4**	**1,5**	**2,1**	**2,2**	**2,3**	**2,4**	**2,5**	**3,1**	**3,2**	**3,3**	**3,4**	**3,5**
Pulse magnitude	**uA**	23	98	98	98	23	198	98	23	23	23	98	98	23	23	98
Measurements/sec	**#**	6	6	6	6	6	6	6	6	6	6	6	6	6	6	6
Pulse duration	**sec**	10	10	10	10	10	10	10	10	10	10	10	10	10	10	10
Rebar diameter	**mm**	8	8	8	8	8	8	8	8	8	8	8	8	8	8	8
Rebar length	**mm**	85	85	85	85	85	85	85	85	85	85	85	85	85	85	85
Rebar area	**mm2**	2136	2136	2136	2136	2136	2136	2136	2136	2136	2136	2136	2136	2136	2136	2136
Datapoints	**#**	60	60	60	60	60	60	60	60	60	60	60	60	60	60	60
Resistance	**Kohm**	**0**	**0**	**4**	**5**	**7**	**0**	**0**	**7**	**3**	**4**	**0**	**0**	**4**	**7**	**6**
Corrosion current	**uA/cm2**	**0.03**	**0.00**	**30.12**	**6.06**	**8.20**	**0.00**	**0.00**	**8.86**	**9.86**	**4.07**	**39.02**	**0.00**	**6.44**	**5.33**	**4.75**
unknown parameter		28169	2187	4194	4105	25239	2059	2011	4041	4063	4302	2057	2013	4253	3680	4237
unknown parameter		32767	32767	32767	32767	32767	32767	32767	32767	32767	32767	32767	32767	32767	32767	32767

Time (S)	1,1	1,2	1,3	1,4	1,5	2,1	2,2	2,3	2,4	2,5	3,1	3,2	3,3	3,4	3,5
0.0	725	534.3	114.1	110	55.88	578.9	588.8	70.62	200.6	68.51	550.4	547.6	65.47	62.9	72.02
0.2	725	531.3	115.1	109	54.88	579.9	591.8	66.62	199.6	69.51	555.4	547.6	65.47	67.9	69.02
0.3	725	537.3	111.1	108	53.88	580.9	588.8	70.62	195.6	65.51	549.4	546.6	65.47	62.9	75.02
0.5	725	533.3	115.1	111	56.88	575.9	590.8	77.62	200.6	71.51	551.4	546.6	64.47	57.9	70.02
0.7	725	530.3	110.1	108	52.88	580.9	579.8	66.62	204.6	67.51	549.4	550.6	65.47	63.9	76.02
0.8	725	538.3	113.1	108	56.88	579.9	591.8	68.62	198.6	68.51	552.4	551.6	67.47	64.9	69.02
1.0	725	553.3	267.1	340	122.88	602.9	596.8	140.62	232.6	103.51	565.4	552.6	108.47	131.9	309.02
1.2	725	533.3	274.1	351	112.88	578.9	592.8	144.62	202.6	106.51	545.4	544.6	102.47	131.9	309.02
1.3	725	536.3	268.1	345	114.88	577.9	582.8	148.62	201.6	108.51	551.4	548.6	118.47	134.9	304.02
1.5	725	533.3	266.1	341	116.88	578.9	590.8	145.62	203.6	103.51	549.4	546.6	102.47	131.9	304.02
1.7	725	533.3	272.1	346	109.88	578.9	589.8	139.62	198.6	100.51	550.4	550.6	105.47	130.9	306.02
1.8	725	536.3	274.1	343	110.88	581.9	588.8	144.62	200.6	105.51	548.4	545.6	111.47	136.9	304.02
2.0	725	531.3	265.1	342	114.88	577.9	589.8	139.62	200.6	103.51	551.4	552.6	104.47	132.9	304.02
2.2	725	531.3	268.1	345	108.88	575.9	590.8	144.62	202.6	108.51	550.4	544.6	108.47	129.9	310.02
2.3	725	538.3	267.1	346	108.88	585.9	580.8	142.62	201.6	98.51	553.4	547.6	103.47	131.9	302.02
2.5	725	537.3	271.1	344	113.88	571.9	594.8	144.62	195.6	104.51	551.4	542.6	108.47	126.9	306.02
2.7	725	531.3	273.1	340	113.88	583.9	587.8	144.62	205.6	103.51	547.4	546.6	104.47	135.9	307.02
2.8	725	533.3	264.1	348	113.88	573.9	587.8	141.62	198.6	105.51	550.4	546.6	109.47	132.9	304.02
3.0	725	533.3	271.1	338	109.88	575.9	591.8	137.62	201.6	104.51	553.4	551.6	104.47	131.9	301.02
3.2	725	530.3	266.1	349	115.88	585.9	585.8	147.62	203.6	100.51	549.4	548.6	112.47	123.9	310.02
3.3	725	536.3	268.1	338	104.88	580.9	589.8	143.62	198.6	105.51	550.4	549.6	104.47	134.9	306.02
3.5	725	535.3	270.1	343	117.88	574.9	592.8	141.62	199.6	101.51	549.4	546.6	108.47	130.9	304.02
3.7	725	538.3	270.1	347	106.88	577.9	585.8	143.62	200.6	103.51	548.4	543.6	110.47	130.9	311.02
3.8	725	531.3	267.1	338	117.88	579.9	589.8	142.62	205.6	106.51	549.4	548.6	100.47	133.9	308.02
4.0	725	534.3	269.1	344	113.88	578.9	584.8	141.62	193.6	103.51	553.4	551.6	103.47	131.9	301.02
4.2	725	535.3	269.1	347	107.88	576.9	595.8	143.62	208.6	107.51	546.4	541.6	108.47	129.9	303.02
4.3	725	530.3	268.1	345	111.88	578.9	580.8	140.62	194.6	103.51	557.4	549.6	106.47	131.9	306.02
4.5	725	536.3	266.1	341	115.88	577.9	586.8	148.62	205.6	101.51	544.4	545.6	111.47	129.9	303.02

4.7	725	534.3	267.1	342	107.88	581.9	594.8	141.62	203.6	103.51	554.4	552.6	98.47	131.9	305.02
4.8	725	531.3	269.1	342	107.88	578.9	590.8	140.62	198.6	105.51	545.4	542.6	114.47	130.9	302.02
5.0	725	531.3	267.1	345	113.88	574.9	585.8	142.62	198.6	102.51	550.4	550.6	105.47	135.9	305.02
5.2	725	535.3	271.1	340	113.88	583.9	588.8	143.62	199.6	105.51	552.4	547.6	105.47	129.9	306.02
5.3	725	537.3	268.1	343	111.88	574.9	592.8	143.62	205.6	103.51	551.4	545.6	108.47	126.9	301.02
5.5	725	536.3	268.1	346	115.88	580.9	581.8	142.62	197.6	103.51	549.4	548.6	107.47	139.9	304.02
5.7	725	527.3	267.1	339	105.88	581.9	596.8	140.62	200.6	106.51	549.4	551.6	107.47	124.9	304.02
5.8	725	534.3	265.1	350	111.88	574.9	583.8	145.62	197.6	100.51	556.4	546.6	105.47	128.9	306.02
6.0	725	539.3	277.1	338	114.88	584.9	590.8	143.62	204.6	103.51	545.4	546.6	102.47	136.9	303.02
6.2	725	529.3	264.1	345	110.88	575.9	593.8	140.62	196.6	104.51	551.4	548.6	109.47	129.9	306.02
6.3	725	536.3	272.1	343	111.88	577.9	578.8	147.62	201.6	103.51	551.4	543.6	108.47	133.9	305.02
6.5	725	536.3	267.1	342	113.88	574.9	593.8	139.62	200.6	105.51	552.4	549.6	105.47	124.9	304.02
6.7	725	532.3	269.1	344	112.88	580.9	588.8	142.62	204.6	101.51	544.4	548.6	107.47	135.9	303.02
6.8	725	534.3	269.1	336	112.88	576.9	589.8	141.62	197.6	102.51	553.4	541.6	104.47	129.9	309.02
7.0	725	536.3	269.1	347	109.88	576.9	590.8	144.62	201.6	102.51	551.4	552.6	104.47	129.9	300.02
7.2	725	532.3	265.1	346	109.88	584.9	588.8	142.62	200.6	110.51	548.4	545.6	111.47	129.9	306.02
7.3	725	537.3	267.1	340	112.88	578.9	583.8	142.62	203.6	98.51	555.4	547.6	103.47	129.9	298.02
7.5	725	532.3	268.1	341	111.88	577.9	589.8	142.62	203.6	107.51	548.4	547.6	105.47	132.9	308.02
7.7	725	532.3	270.1	352	112.88	574.9	591.8	146.62	194.6	101.51	549.4	549.6	112.47	129.9	305.02
7.8	725	535.3	270.1	335	109.88	582.9	585.8	140.62	197.6	107.51	550.4	546.6	107.47	134.9	303.02
8.0	725	530.3	268.1	348	115.88	581.9	590.8	143.62	202.6	102.51	550.4	550.6	103.47	127.9	302.02
8.2	725	537.3	267.1	340	111.88	574.9	588.8	134.62	201.6	105.51	545.4	545.6	107.47	136.9	299.02
8.3	725	531.3	271.1	345	113.88	579.9	586.8	148.62	207.6	101.51	552.4	542.6	106.47	125.9	308.02
8.5	725	531.3	262.1	339	110.88	581.9	591.8	141.62	195.6	105.51	550.4	552.6	106.47	133.9	308.02
8.7	725	539.3	273.1	342	108.88	571.9	585.8	142.62	198.6	97.51	549.4	545.6	106.47	128.9	301.02
8.8	725	533.3	264.1	343	110.88	582.9	585.8	140.62	202.6	108.51	549.4	551.6	106.47	131.9	304.02
9.0	725	534.3	269.1	341	114.88	574.9	591.8	149.62	199.6	101.51	554.4	543.6	108.47	127.9	301.02
9.2	725	533.3	267.1	342	111.88	580.9	593.8	138.62	200.6	103.51	552.4	549.6	101.47	130.9	305.02
9.3	725	534.3	270.1	346	114.88	576.9	581.8	142.62	203.6	107.51	547.4	550.6	110.47	129.9	307.02

9.5	725	532.3	263.1	340	110.88	579.9	592.8	142.62	198.6	102.51	547.4	544.6	106.47	132.9	297.02

GPM Technique PULSE CHART DATA (210410)

Sample	**X,Y**	**1,1**	**1,2**	**1,3**	**1,4**	**1,5**	**2,1**	**2,2**	**2,3**	**2,4**	**2,5**	**3,1**	**3,2**	**3,3**	**3,4**	**3,5**
Pulse magnitude	**uA**	21	21	21	21	21	21	21	21	21	21	21	21	21	21	21
Measurements/sec	**#**	6	6	6	6	6	6	6	6	6	6	6	6	6	6	6
Pulse duration	**sec**	10	10	10	10	10	10	10	10	10	10	10	10	10	10	10
Rebar diameter	**mm**	8	8	8	8	8	8	8	8	8	8	8	8	8	8	8
Rebar length	**mm**	85	85	85	85	85	85	85	85	85	85	85	85	85	85	85
Rebar area	**mm2**	2136	2136	2136	2136	2136	2136	2136	2136	2136	2136	2136	2136	2136	2136	2136
Datapoints	**#**	60	60	60	60	60	60	60	60	60	60	60	60	60	60	60
Resistance	**Kohm**	**0**	**1**	**8**	**20**	**10**	**0**	**-1**	**13**	**13**	**9**	**1**	**0**	**15**	**13**	**12**
Corrosion current	**uA/cm2**	**0.00**	**0.00**	**13.17**	**7.96**	**5.96**	**0.00**	**0.00**	**6.65**	**7.77**	**5.64**	**0.00**	**25.86**	**10.90**	**16.20**	**10.22**
unknown parameter		2446	2393	4123	3821	4331	2388	2446	4126	3858	4434	2412	2475	4345	4019	4335
unknown parameter		32767	32767	32767	32767	32767	32767	32767	32767	32767	32767	32767	32767	32767	32767	32767
	Time (S)	**1,1**	**1,2**	**1,3**	**1,4**	**1,5**	**2,1**	**2,2**	**2,3**	**2,4**	**2,5**	**3,1**	**3,2**	**3,3**	**3,4**	**3,5**
	0.0	501	483	98	169	47	496	479	113	150	42	500	489	47	50	48
	0.2	500	484	97	171	49	496	480	112	151	42	502	490	46	55	47
	0.3	499	486	103	169	49	498	477	117	153	43	500	489	45	45	51
	0.5	500	484	94	168	44	495	479	108	147	39	499	490	50	49	44
	0.7	504	480	101	171	52	496	479	113	149	44	497	484	45	57	49
	0.8	502	485	96	167	43	499	481	117	147	43	501	492	49	45	47
	1.0	498	496	174	347	133	496	472	228	265	125	511	488	184	169	159
	1.2	506	487	203	357	139	494	487	242	268	126	500	490	189	178	169
	1.3	498	482	202	356	136	498	476	226	267	128	503	491	190	173	159
	1.5	501	481	195	340	140	500	478	224	261	124	502	486	184	175	160
	1.7	504	488	197	357	136	496	479	227	270	125	494	489	176	172	161
	1.8	500	483	197	344	145	493	483	226	261	126	502	492	191	178	161

2.0	497	481	199	352	128	498	478	218	260	118	499	491	175	173	159
2.2	505	479	194	349	142	494	482	229	273	130	500	487	188	174	161
2.3	502	487	200	349	141	497	475	225	261	124	498	491	181	176	161
2.5	501	481	193	346	132	497	479	223	263	123	502	489	184	174	161
2.7	502	483	193	354	136	494	482	223	261	125	502	489	181	173	158
2.8	498	484	202	346	140	498	473	226	266	125	497	488	180	175	165
3.0	501	483	192	349	135	492	481	224	268	122	507	488	182	171	155
3.2	499	483	199	353	137	501	480	225	261	127	494	491	185	179	159
3.3	503	481	194	351	138	488	481	219	265	121	500	489	181	170	159
3.5	502	484	197	347	138	498	474	230	262	124	501	488	179	174	164
3.7	500	482	199	353	135	503	482	227	266	127	499	488	184	176	159
3.8	503	485	195	344	140	489	479	221	266	122	499	489	184	175	164
4.0	498	483	194	354	136	496	475	223	264	126	500	488	182	175	161
4.2	502	483	198	342	140	501	484	229	263	128	500	489	181	173	160
4.3	503	484	193	355	133	495	478	220	265	118	499	488	185	171	157
4.5	498	479	199	349	142	496	479	224	267	130	504	492	185	172	162
4.7	505	486	195	346	139	495	477	226	261	122	496	488	177	178	159
4.8	498	481	199	356	131	495	480	225	266	127	502	490	180	173	163
5.0	501	481	191	341	141	504	478	226	263	123	495	485	184	178	160
5.2	501	483	200	354	133	488	480	221	265	125	503	493	182	168	159
5.3	500	482	194	348	137	500	481	230	258	118	501	488	178	179	161
5.5	503	487	195	344	138	495	476	222	268	130	498	485	191	172	161
5.7	502	479	201	355	139	494	481	218	264	121	501	496	176	173	158
5.8	502	486	190	348	137	497	481	224	265	124	505	491	187	176	158
6.0	499	483	199	351	134	498	477	230	266	124	500	484	177	173	160
6.2	500	484	195	344	145	495	478	224	268	130	499	492	184	172	162
6.3	498	482	202	357	132	498	483	222	256	123	498	490	184	175	162
6.5	500	487	195	344	136	495	475	224	268	124	501	485	181	173	155
6.7	505	480	192	348	141	498	484	223	265	126	499	491	179	174	166

6.8	498	480	198	351	135	493	472	226	262	126	501	490	181	176	156
7.0	504	484	193	348	134	493	481	228	264	119	500	485	182	173	159
7.2	501	483	197	349	145	497	480	221	264	128	501	490	186	172	159
7.3	501	482	195	350	133	496	484	225	271	125	497	490	178	178	164
7.5	503	486	195	351	133	497	472	226	261	121	502	488	182	167	159
7.7	499	482	199	341	141	493	480	219	261	125	503	488	185	182	158
7.8	502	480	197	353	135	499	480	224	261	125	496	489	183	169	163
8.0	502	482	194	355	139	497	478	225	268	120	500	493	185	176	159
8.2	502	488	197	342	138	497	478	225	264	125	498	490	182	171	160
8.3	497	477	198	352	137	494	480	225	266	125	497	486	178	179	161
8.5	504	484	195	351	140	494	479	222	266	124	505	489	185	173	160
8.7	499	488	195	345	135	500	473	230	264	127	497	490	181	175	163
8.8	503	484	192	350	138	495	485	223	260	124	502	485	181	172	159
9.0	497	481	200	354	131	499	477	223	264	123	503	493	182	177	163
9.2	503	482	193	350	143	494	482	223	260	120	496	488	187	173	155
9.3	501	482	199	347	139	496	478	225	269	128	504	492	178	177	161
9.5	497	487	199	352	135	490	481	224	266	122	500	487	184	171	156

Not Used